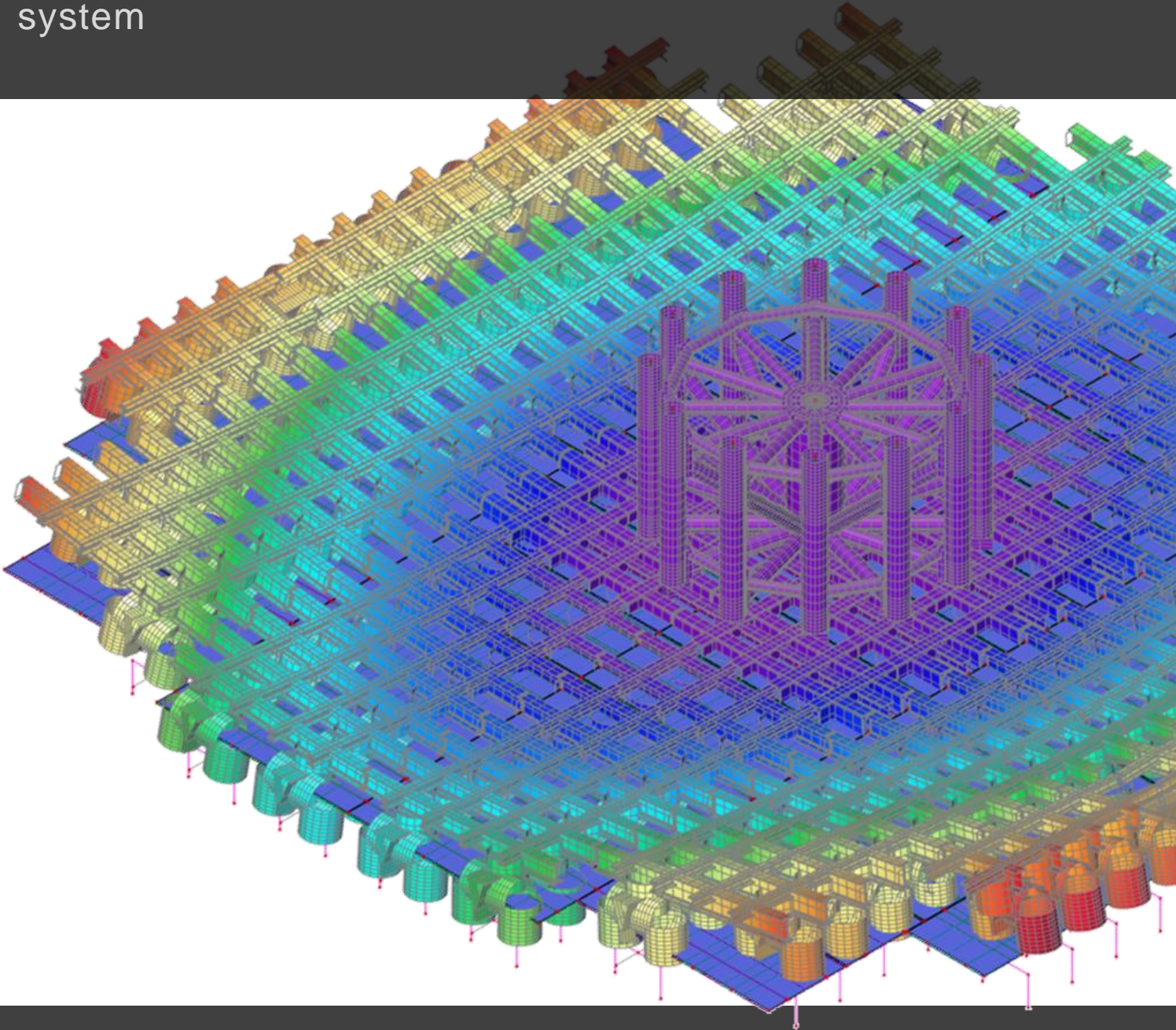


Master thesis
Bas Slingerland

An innovative way to transport and spool offshore power cables using SPMTs

Global design improvement of a containerized carousel system



An innovative way to transport offshore power cables using SPMTs

Global design improvement of a containerized carousel system

By

Bas Slingerland

Master Thesis

in partial fulfilment of the requirements for the degree of

Master of Science
in Mechanical Engineering

at the Department Maritime and Transport Technology of Faculty Mechanical, Maritime and Materials Engineering of Delft
University of Technology
to be defended publicly on Tuesday July 4, 2023, at 10:00AM

Student number:	5178754
MSc track:	Multi-Machine Engineering
Company:	Mammoet
Company department:	Structural Engineering
Report number:	2023.MME.8777
Thesis committee:	
- TU Delft committee Chair:	Prof. Dr. Ir. Dingena Schott
- TU Delft Supervisor:	Ir. Wouter van den Bos
- TU Delft committee member:	Ir. Erik Frikkee
- Mammoet Supervisor:	Ir. Ivo Harms
Date:	6/19/2023
Status:	Final

An electronic version of this thesis is available at <http://repository.tudelft.nl/>.

It may only be reproduced literally and as a whole. For commercial purposes only with written authorization of Delft University of Technology. Requests for consult are only taken into consideration under the condition that the applicant denies all legal rights on liabilities concerning the contents of the advice.

Abstract

Mammoet is developing a new type of system for the transportation of offshore power cables. With this system the cables can be spooled, stored, and transported both on land and on heavy transport vessels in a more efficient way. There are a few uncertainties for the system, mainly about the loads on the carousel and the behavior of the cable stack. These uncertainties resulted in some assumptions that have been used for the proposed design. Furthermore, there are a few challenges for the system that need to be addressed to compete with the current offshore power cable transportation methods. The main challenges include the structural strength and stability in combination with the self-weight, the used cylinder stroke of the hydraulic SPMT cylinders and other issues with the SPMTs. In this study these uncertainties and the challenges for the current design of the system are investigated, which resulted in more insight in the uncertainties and a new concept with improved performance against the challenges.

The study described in this thesis is the final part of getting my master's degree in Mechanical Engineering at the TU Delft, with the specialization in Multi-Machine Engineering. I have executed this study with great interests at the Structural Engineering department of Mammoet, located in Schiedam, where I have learned a lot. I want to thank all my supervisors for the opportunity, their guidance, and the useful feedback to carry out this study.

*Bas Slingerland
Schiedam, 6/19/2023*

Summary

Introduction

The development and installation of offshore windfarms is an increasingly growing business. These windfarms are connected by offshore power cables. A large part of the required installation time and the total costs for offshore power cables is dependent on the transport of the cable from the manufacturer to the offshore windfarm. Therefore, it is desired to increase the efficiency of the cable transportation process to save time and costs. Especially the cable transfer from one storage carousel to another carousel is very time and cost consuming. These cable transfers are needed 3 or 4 times for the current transportation process and cost multiple weeks each time.

Containerized carousel system

Based on using their Self-Propelled Modular Transporters (SPMTs), Mammoet proposed a containerized carousel system (CCS) as a possible solution for making the offshore power cable transportation more efficient. The CCS consists of a carousel in which the cable can be stored. SPMTs will be used to rotate the carousel to spool the cable out or in, and to transfer the entire carousel including the stored cable. This allows the CCS to replace some of the inefficient cable transfers by transporting the entire carousel with cable to the desired position in an efficient way. Further benefits are that the CCS is modular, containerized and that it includes sea fastening.

Research objective

For the CCS design proposed by Mammoet there are some uncertainties and challenges. The objective of this study is to acquire more insight in those uncertainties and to use this insight to improve the performance of the proposed CCS design against the challenges. For this objective the following research question has been defined: *Can the containerized carousel system improve the current offshore power cable transportation method?*

Challenges

The following challenges for the CCS design of Mammoet are defined as the result of a process analysis:

1. The loads on the CCS during the cable transportation can result in strength and/ or stability issues. Especially, the maximum load that the SPMTs can handle and the horizontal loads on the carousel due to sea transport accelerations on the full payload are governing for the strength and stability of the CCS. There are a few uncertainties for the load on the carousel. It has been estimated that the cable stack has sufficient stiffness to neglect the load on and the load transfer by the outer frame. For this it is assumed that the inner frame has sufficient stiffness and that there is some play between the cable stack and the outer frame or some flexibility of the outer frame. Furthermore, the friction between the cables, and between the cable stack and the carousel are uncertain and neglected. As a result, it is assumed that all vertical payload is uniformly distributed over the floor and all horizontal payload over the pressure side of the inner frame.
2. The used cylinder stroke of the SPMTs can reach its limits during SPMT transport. For Ro-Ro operations the SPMT cylinders have an operational stroke of 490 mm. Calculations executed for the proposed CCS design by Mammoet show that the deflection of the SPMT transport can be more than 300 mm. This leads to a reduced stroke available for the needed height difference to lift the carousel and to compensate for height differences caused by ground unevenness, camber, slopes, and RoRo ramps.
3. The high load and large operation time of the SPMTs during the spooling process can result in issues, such as wear of the SPMT tires, leakage of the hydraulic system for the cylinders and the hydraulic motors and overheating of the SPMT generator.

Concept

To lower the deflection of the SPMT transport of the CCS, such that more stroke of the SPMT cylinders is available for other height differences, it is important that most SPMT axle lines are covered by the carousel footprint. However, a larger carousel, to cover more SPMT axle lines, results in more axle lines that are needed to carry the increased weight. Many setups have been tested against performance indicators and are compared with the setup proposed by Mammoet. As a result, two new setups and the setup proposed by Mammoet have been chosen for further elaboration. Each selected setup has different main carousel dimensions, a SPMT setup, a floor plate setup, and a grillage beam setup. For the two selected setups and the setup proposed by Mammoet, a comparable FEM simulation model has been developed with identical members and connections. It follows that the best performing setup has

90 mm SPMT deflection, whereas the setup proposed by Mammoet has a deflection of 224 mm, while they have a comparable weight and size. This confirms that the SPMT setup and outer carousel dimensions are the crucial factors for the SPMT deflection. Furthermore, the more optimal setup also reduces the needed drive distance by 8%, which is beneficial for the SPMTs. This setup has been selected for further elaboration. The structural strength of the grillage, floor and inner frame of the CCS are governed by the load on the carousel due to sea transport accelerations. A more elaborated FEM simulation model has been developed for the selected setup. The inner frame of the carousel is based on the design proposed by Mammoet. To transfer the horizontal load due to roll of the vessel more effectively, extra sea fastening frames have been added at the outside of the CCS. These frames are easy to place while no extra vessel deck space is needed. For all structural components of the new concept the used cross-sections have been optimized by a few iterations of simulation and selecting other cross sections based on the unity checks according to EN1993-1-1:2005. This has led to a globally improved design where the self-weight has been reduced and the structural strength and stability is sufficient. The high occurring unity checks are acceptable as they can be solved by local reinforcement in a future detailing phase.

Cable and cable stack uncertainties

Previously it is assumed that the vertical payload has a uniform distribution on the carousel floor and that the horizontal payload is all induced by a uniform distribution on the pressure side of the inner frame. For the last assumption, the cable stack (and the inner frame) must have sufficient stiffness to neglect the load on the outer frame. To estimate the cable stack stiffness a single offshore power cable with average properties has been selected for which the axial, bending, and radial stiffness have been estimated by FEM simulations and manual calculations. With the estimated axial and radial stiffness of the cable it can be concluded that the cable stack with an average offshore power cable has enough stiffness to neglect the load on the outer frame of the carousel. Bending stiffness of the cable and thus the cable stack can have a positive influence on the SPMT deflection. Because of the low bending stiffness of a single cable, the uncertainties of the stiffness of the whole cable stack, and the spiraling orientation of the cable stack, it is defined that this effect is very uncertain and thus will be neglected.

It is assumed that the payload induces a vertical uniformly distributed load over the floor and a horizontal uniformly distributed load on the pressure side of the inner frame. To verify this load distribution, a simplified FEM model has been established. Based on multiple simulations with different inputs the following can be concluded:

- Friction between the floor and the cable stack has a beneficial effect on the load distribution as it directly lowers the load on the inner frame, which is governing for the inner frame, floor, and grillage structure.
- The assumed uniform load distribution over the parts of the inner frame which experience pressure, is a sufficient approximation. The assumed load distribution namely causes approximate equal resultant forces at comparable heights, causing a comparable bending moment on the floor structure.
- The assumed uniform load distribution on the floor is a sufficient approximation. The simulations namely show a more favorable distribution where more load is induced on places where the floor tends to bend upwards, which reduces this bending. The assumed uniform load distribution is thus a worst-case-scenario.

Conclusion and recommendation

Assuming that the SPMT issues, such as tire wear, hydraulic leakage, and generator overheating, are not problematic and can be solved by maintenance, it can be concluded from this study that the CCS is a feasible method to transport offshore power cables. It is difficult to compare the CCS with the current transportation method in terms of costs and time, as there are many parameters. Comparing the offshore power cable transportation using the CCS with the current transportation method, the main benefits include: Less cable transfers (significantly reduced costs and time), the CCS is mobile by SPMTs, easy sea fastening, the CCS is containerized, and the CCS is modular. The main disadvantage of the CCS is that the system itself is an expensive solution and that it is prone to SPMT issues. It is expected that the CCS saves time compared to the current transportation method because less cable transfers are needed. An important outcome of the study is that the performance of the system against SPMT transport deflection is dependent of the carousel main dimensions, capacity and SPMT setup. As the system is modular, every different configuration should be checked for the deflection of the SPMTs. For use of the proposed concept, further detailing and local reinforcement is needed. More research for the SPMT issues such as tire wear, hydraulic leakage and overheating of the SPMT generator is recommended for successful implementation of the CCS in the cable transportation process.

Table of Contents

Abstract	iv
Summary	v
Abbreviations	ix
List of symbols	ix
1 Introduction	1
1.1 Background	1
1.1.1 Offshore wind	1
1.1.2 Offshore power cables	1
1.1.3 Current way of transportation	1
1.1.4 Issues current way of working	3
1.1.5 Related methods	4
1.2 Motivation	5
1.2.1 Problem definition	5
1.2.2 Containerized carousel system of Mammoet	5
1.3 Research outline	6
1.3.1 Objective	6
1.3.2 Approach	6
1.3.3 Scope	7
2 Process analysis	8
2.1 Current transportation method	8
2.1.1 Process overview	8
2.1.2 General process characteristics	11
2.2 Containerized carousel system	12
2.2.1 Cable transfer	14
2.2.2 Carousel transfer	19
2.2.3 Sea transport	24
2.3 Challenges	29
2.3.1 Strength and stability	29
2.3.2 SPMT cylinder stroke	31
2.3.3 SPMT issues	34
2.4 Conclusion	35
3 Conceptual solutions	36
3.1 Boundary conditions	37
3.1.1 SPMT specification	38
3.1.2 Cable storage capacity	38
3.2 Main dimensions	39
3.2.1 Main carousel dimensions	40
3.2.2 SPMT and grillage setup	46
3.3 Structure	51
3.3.1 Outer frame	51
3.3.2 Inner frame	52
3.3.3 Floor	52
3.3.4 Grillage	53
3.4 Conclusion	54
4 Concept analysis	55
4.1 Loads	55
4.1.1 General load input	55
4.1.2 Load actions	55
4.1.3 Load factors	57
4.1.4 Load combinations	58
4.2 Setup selection	58

4.2.1	<i>Input</i>	58
4.2.2	<i>Results</i>	60
4.3	Concept elaboration.....	61
4.3.1	<i>Input</i>	61
4.3.2	<i>Concept elaboration</i>	62
4.3.3	<i>Results</i>	65
4.4	Conclusion	66
5	Influence of cable stack	67
5.1	Cable stack stiffness	67
5.1.1	<i>Cable specification</i>	67
5.1.2	<i>Cable stiffness</i>	69
5.2	Load distribution cable stack.....	74
5.2.1	<i>Cable stack description</i>	74
5.2.2	<i>Interaction forces</i>	75
5.2.3	<i>Load distribution analysis</i>	77
5.2.4	<i>Results</i>	78
5.3	Conclusion	81
6	Conclusion	82
6.1	Research questions	82
6.2	Recommendations	85
	References	86
	Appendices	89
A	Research paper	90
B	Cable stack expansion estimation	101
C	SPMT deflection study 2D	111
D	Cable stack mass and dimensions	121
E	Comparison CCS and current method	122
F	Cable analysis	124
G	Setup selection study	137
H	Analysis of elaborated concept	149
I	Load distribution study	179

Abbreviations

Abbreviation	Description
COG	Centre of Gravity
CCS	Containerized Carousel System
SPMT	Self-Propelled Modular Transporter
GBP	Ground bearing pressure
AC	Alternating Current
DC	Direct current
MBR	Minimum bend radius
XLPE	Crosslinked Polyethylene
HDPE	High Density Polyethylene
Ro-Ro	Roll-on/roll-off
SLS	Serviceability Limit State
ULS	Ultimate Limit State
FEA	Finite Element Analysis
FEM	Finite Element Method

List of symbols

Symbol	Unit	Description
L_{cable}	km	Total length of the cable stacked in the carousel
C	t	Capacity of the carousel, mass of the full cable stack
μ_{cable}	kg/m	Mass of offshore power cable per unit length
ρ_{cable}	kg/m^3	Average density of the offshore power cable
D_{cable}	mm	Diameter of the offshore power cable
V_{spool}	km/h	Spool rate, velocity of the cable during cable transfer
R_{spool}	m	Spool radius, the radius at which the cable is laid in / removed from the carousel
$V_{R,SPMT}$	m/s	Tangential velocity of SPMT axle line at radius R_{SPMT}
$S_{R,SPMT}$	km	Drive distance of an SPMT axle line at radius R_{SPMT} over entire cable transfer
R_{SPMT}	m	Radius of SPMT axle line during spooling
$V_{O,SPMT}$	m/s	Tangential velocity of the most outside SPMT axle line during spooling of the carousel
$S_{O,SPMT}$	km	Drive distance of an SPMT axle line at most outside radius over entire cable transfer
$R_{O,SPMT}$	m/s	Radius of the most outside SPMT axle line during spooling of the carousel
T_{spool}	h	Nonstop minimum spool time for spooling the entire capacity of the carousel at maximum spool rate without downtime
$L_{ct,avg}$	m	The average length of a single cable turn in the carousel
$R_{carousel}$ $D_{carousel}$	m	Respectively, the outside carousel radius and the outside carousel diameter
$r_{carousel}$ $d_{carousel}$	m	Respectively, the inside carousel radius and the inside carousel diameter
$h_{carousel}$	m	Height of the carousel
$A_{carousel}$	m^2	Area of the carousel footprint
$J_{CCS,SPMT}$	$kg \cdot m^2$	Moment of inertia of CCS loaded with full capacity during SPMT transport
$m_{carousel}$	t	Total mass of carousel (floor, inner frame, outer frame and all other component)
m_{Floor}	t	Total mass of the floor of the carousel
$m_{grillage}$	t	Total mass of the grillage frame of the carousel
m_{SPMT}	t	Total mass of the SPMT trains for the SPMT transport

$m_{CCS,SPMT,g}$	t	Total mass of the CCS for SPMT transport with grillage frame
$m_{CCS,sea}$	t	Total mass of the CCS for sea transport
m_{stack}	t	Cable stack mass
T_{SPMT}	Nm	Total torque applied to the carousel by the SPMTs for the carousel rotation
$\alpha_{CCS,SPMT}$	rad/s^2	Rotational acceleration of the carousel
F_{SPMT}	kN	The total applied drive / brake force of the SPMTs applied to the carousel
$a_{CCS,SPMT}$	m/s^2	(de-)acceleration of CCS due to SPMT drive
GPB	t/m^2	Ground bearing pressure
$a_{x,pitch}$	m/s^2	Acceleration on CCS in x direction due to vessel pitch
$a_{y,roll}$	m/s^2	Acceleration on CCS in y direction due to vessel roll
$a_{z,heave}$	m/s^2	Acceleration on CCS in z direction due to vessel heave
$E_{cable,axial}$	GPa	Elastic modulus of the cable in axial direction
$E_{cable,radial}$	GPa	Elastic modulus of the cable in radial direction
$F_{h,res}$	N	Resultant horizontal load on inner frame
$h_{h,res}$	m	Height of resultant horizontal load on inner frame
$M_{h,res}$	Nm	Resulting moment due to resultant horizontal load on inner frame
$(EI)_{cable}$	kNm^2	Bending stiffness of the cable
A_{cable}	m^2	Cross sectional area cable
s_h	mm	Distance between row centers in the cable stack
s_r	mm	Distance between cable cross sectional centers in cable stack
β	$^\circ$	Degrees on which cables are stack on each other
$a_{x,pitch}$	m/s^2	Acceleration in carousel in x direction due to pitch of vessel during sea transport
$a_{y,roll}$	m/s^2	Acceleration in carousel in y direction due to roll of vessel during sea transport
$a_{z,heave}$	m/s^2	Acceleration in carousel in z direction due to heave of vessel during sea transport
F_{res}	kN/m	Resultant distributed load on outer wall due to vertical acceleration on cable stack
δ	mm	Axial deformation of cable
N	kN	Normal force in cable
A	m^2	Cross sectional area
E	GPa	Elastic modulus
F_{rad}	kN/m	Uniformly distributed radial load on cable
Δw	mm	Horizontal deformation of cable under radial loading
M	Nm	Bending moment on cable
κ	$1/m$	Curvature of cable
w	m	Vertical displacement of cable
$((EI)_{cable\ stack})_{fixed}$	kNm^2	Bending stiffness of cable stack where cables are fixed to each other
$((EI)_{cable\ stack})_{free}$	kNm^2	Bending stiffness of cable stack where the cables don't interact with each other
$I_{i,x}$	m^4	Second moment of area of component i around the global neutral axis
$I_{i,x'}$	m^4	Second moment of area of component i around components neutral axis
A_i	m^2	Cross sectional area of component i
d_i	m	Distance between global neutral axis the neutral axis of component i
I_{cable}	m^4	Second moment of area of a single cable around its neutral axis

1 Introduction

This chapter introduces the study. It starts with some background information, after which the current way of transportation will be described with the corresponding key issues. Furthermore, the problem statement and the proposed solution by Mammoet are described. Finally, general information for the study is defined, including the objective, approach, and scope.

1.1 Background

1.1.1 Offshore wind

The development and installation of offshore windfarms is an increasingly growing business as more wind energy is demanded. The installed global cumulative offshore wind capacity has grown from 4 MW to 50 GW over the past 10 years [1]. An exponential growth is observed, which is also caused by the increasing average power delivered per installed turbine, from 6.8 MW in 2018 to 8.2 MW in 2021. Looking at the future, many reports predict this exponential growth to continue. The GWEC (global offshore wind energy council) expects that the offshore wind capacity will grow to over 234 GW by 2030 [2]. All this electric wind power generated by wind turbines needs to be connected to transformer stations and the main grid by means of large submarine power cables. This often includes a few 100 km of offshore power cables in total, which need to be installed [3]. Due to the increasing demand of offshore wind energy most cable suppliers and cable handling equipment are fully booked. It therefore becomes more important that the cable installation process is time efficient.

1.1.2 Offshore power cables

In general, there are two types of offshore power cables, alternating current (AC) and direct current (DC) cables. DC cables often are used in pairs of separate cables, each with only one conductor. AC cables consist of 3 conductors within a cable and are therefore able to transport three phase AC power. The generator in a wind turbine creates three phase power such that small transformers easily can change the voltage. For this reason, AC cables can be directly connected to the main onshore grid. DC current requires a converter at each end of the DC current line which makes it more expensive. However, DC cables transport power with less losses. It therefore depends on the cable length which type of cable needs to be used. DC cables are used with longer distances and AC cables for smaller distances [3].



Figure 1-1: Three phase AC (left) and DC (right) offshore power cable [4]

1.1.3 Current way of transportation

A large part of the costs and time for the installation of the offshore wind power cables are caused by the transportation of the cable. Figure 1-2 shows an example for a typical route of the cable during its transportation from the manufacturer to the demanding offshore windfarm.

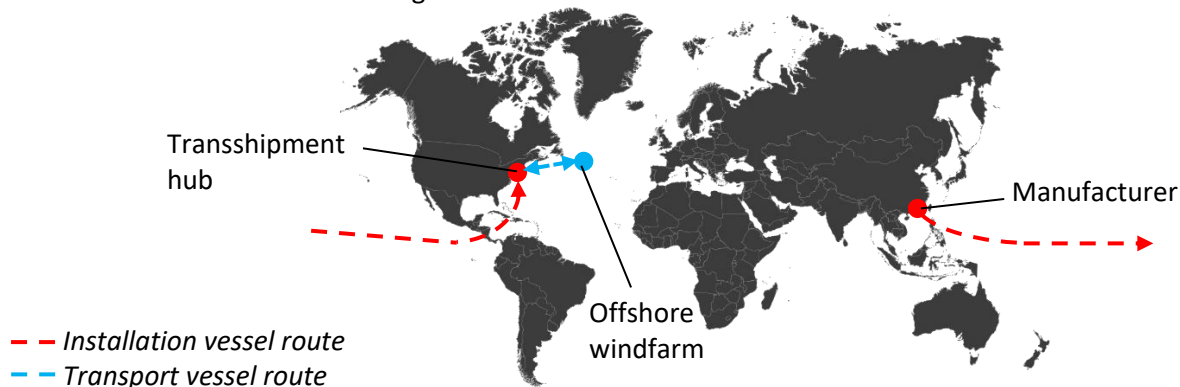


Figure 1-2: Example transportation route of offshore wind cable

Two types of vessels will be used, a transport vessel and an installation vessel. The installation vessel is very expensive and thus a cheaper transport vessel will be used to transport the cable from the manufacturer to a transshipment hub closer to the demanding offshore windfarm. At this transshipment hub the installation vessel can pick up the cable. Assuming that the average speed of a transport vessel is about 25 km/h and that the red route in the Figure 1-2 is about $10\,000 \text{ km}$, it costs the transport vessel approximate at least 3 weeks of travelling. For this reason, it is beneficial that a transport vessel less expensive than the cable installation vessel is used.

Cable storage

In all stages of the transportation process the offshore power cable will be stored in a carousel, as shown in Figure 1-3. The figure shows the general way of how cables are spooled in the carousel.



Figure 1-3: Storage of offshore power cable in carousel [5]

Cable transfer

Most carousels are fixed by their drive system to their position on the ground or on a vessel. A cable transfer is thus needed to get the cable from one carousel to the other. A typical setup for (un)spooling a cable from/to a carousel is shown in Figure 1-4.



Figure 1-4: General cable carousel (un)spooling setup [6]

The main components for a cable transfer, as numbered in Figure 1-4, are:

1. **Tensioners:** Tensioners pull the cable through themselves to the desired velocity and direction.
2. **Cable:** Offshore power cable moving from / to another carousel
3. **Guiding system:** A guiding system will be used for placing / removing the cable on the right spot in the carousel. Multiple options are available for a guiding system.
4. **Carousel:** positioned on a drive system. In Figure 1-4 the carousel is positioned on a barge.

For the un(spooling) setup there are multiple options (quay/vessel to quay/vessel) where different equipment can be used. For the cable transfer process both carousels also need a drive system to rotate the carousel. During operation these drive systems and the tensioners must ensure that the cable is unspooled from one carousel and simultaneously spooled onto the other carousel at constant velocity.

The spooling process, both onshore and offshore, can be time consuming. On average, the carousel suppliers claim a maximum spool/lay rate of 1 km/h for both loading the cable in and out the carousel. Considering one of the larger found carousels [7], with a capacity of 10 000 t, and by assuming an average cable weight of 65 kg/m, it follows that this carousel can store approximately 150 km. With the average spool/lay rate of 1 km/h it thus takes at least 150 hours of nonstop spooling to (un)load the full capacity. Due to all kinds of reasons downtime can occur and some other actions can be required before or after the spooling process. As a result, the needed time for a cable transfer from carousel to carousel can be up to approximately 2-3 weeks. In this time all the needed equipment, such as vessel(s), quay(s), both carousels, crane(s), tensioner(s), etc., are also occupied. As a result, the cable transfer process is very time and cost consuming.

Current transport method

For the most common transportation methods of offshore power cables, the following cable transfers (transpoolings) from carousel to carousel are at least needed:

- Manufacturer to transport vessel
- Transport vessel to transshipment hub
- Transshipment hub to installation vessel

The resulting process overview can be schematically visualized as shown in Figure 1-5.

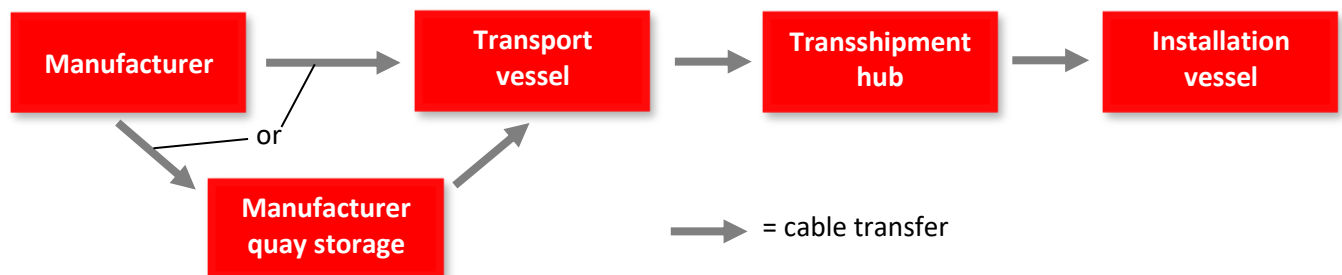


Figure 1-5: Transportation process current way

1.1.4 Issues current way of working

Below the key issues corresponding to the current way of cable transportation are listed:

- **3- or 4 times a cable transfer:** Figure 1-5 shows that at least three transfers are needed where all transfers cost approximately 2 or 3 weeks. Most of the time an extra carousel transfer is needed from the manufacturer carousel to a carousel on the manufacturer quay, which results in four cable transfers. Three or four cable transfers make the transportation process cost and time consuming.
- **No extra cable transfer possible:** Due to the reduced quality of the cable after each cable transfer, most cables are restricted to a maximum of four cable transfers. So, with the transportation method where four cable transfers are already needed, an extra transfer is not possible otherwise the cable does not satisfy its quality criteria. There can be multiple reasons why a cable must be transferred to another carousel, such as expired lease agreement, carousel is needed for other project or temporarily storage at other place.

- **Risks of project delay:** The cable occupies a carousel for a limited amount of time, defined in the lease arrangement. The carousel and equipment are fully booked due to the high demand for offshore wind, so exceedance of the agreed lease time, caused by for example by a project delay, leads to conflicts with other projects which also need the equipment or carousel.
- **Carousels in general:** Most carousels are fixed constructions and have a fixed position on their drive system, which has some disadvantages:
 - The carousel can be difficult to transport to another position. So, if the carousel must be moved, even for a small displacement on a quay, possible a cable transfer is needed.
 - Capacity is mostly fixed, so for each project another carousel can be needed
 - An empty and not used carousel still occupies a large amount of space. Because it cannot be compactly stored temporary storage is required near the expensive quay.

1.1.5 Related methods

If possible, a more efficient method is to replace the cable transfer by a carousel transfer where the loaded carousel is directly placed on its desired position. However, loaded carousels can have weights around 10 000 t, which is very hard to lift and thus lifting the carousel can only be beneficial for empty or small capacity carousels.

The offshore pipe laying industry has similarities with the cable laying industry. However, most offshore pipes are much stiffer, stronger and have a higher fatigue resistance than offshore power cables. A many used pipe laying method is the reel lay method, shown in Figure 1-6.

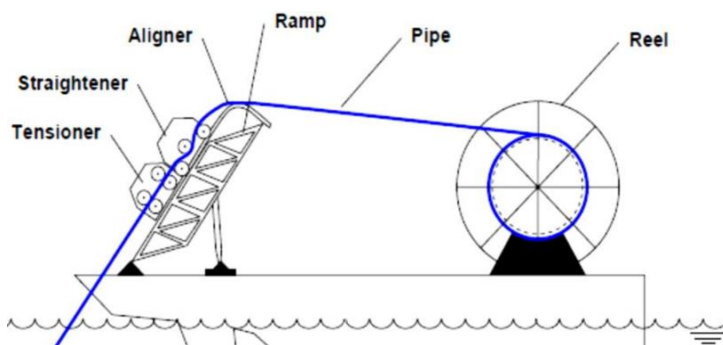


Figure 1-6: Offshore pipe reel-lay [8]



Figure 1-7: Transportation offshore power cables with reels [9]

A relative stiff offshore pipe must be spooled under tension to bend it in the right radius for storage. Using a reel is more appropriate for spooling under tension than a carousel because a reel can use its structure to bend the pipe around itself during spooling, which is not possible with a carousel. One of the larger found pipe installation vessels is the Heerema Aegir [10]. This vessel can handle reels with a capacity of 3000 t. However, this vessel is constructed for pipe laying, whereas cable installation vessels have specific equipment for offshore cable handling. Transportation and installation of offshore power cables by using reels is in practice only used for smaller offshore power cables (Figure 1-7), because of the following reasons:

- There are not much offshore power cable installation vessels using reels
- The COG is generally higher using a reel compared to a carousel with same capacity
- Heavier construction is needed for a reel compared to a carousel with same capacity
- Issues mentioned in section 1.1.4 are not solved by using a reel, so there are no direct benefits.

Another method, which has been used a few times before, is transferring the loaded carousel by means of SPMT's (Self-Propelled Modular Transporters), as shown in Figure 1-8. The SPMTs can also function as a rotational drive of the carousel for (un)spooling of the cable, as shown in Figure 1-9, by driving around to axis of the carousel. The current usage of SPMTs in the transport of offshore power cables is very limited because most carousels still need an extra operation to get the carousel on the SPMTs and the SPMTs are prone to deflection during transport when not used and checked properly for each specific transport.



Figure 1-8: 1300t capacity carousel transfer to barge [11]

Figure 1-9: 1300t capacity cable spooling using SPMTs [11]

1.2 Motivation

1.2.1 Problem definition

From the background information the following main problem is defined:

The transport of offshore power cables can be more efficient to save time and costs.

Especially the cable transfer of multiple weeks, which is needed 3 or 4 times in the entire transportation process, is very time and costs consuming. Another problem is that the current way of transportation has some risks which can cause conflicts if delay occurs in the offshore project.

1.2.2 Containerized carousel system of Mammoet

Based on using their Self-Propelled Modular Transporters (SPMTs), Mammoet proposed a containerized carousel system (CCS) as a possible solution for making the offshore power cable transportation more efficient. In this system the carousel will be optimized for the use of SPMT's. With the CCS the SPMT's of Mammoet will be used to transfer and move the carousel (carousel transfer), but they also function as a drive system to rotate the carousel during cable spooling when the cable needs to be transferred from / to the carousel. The transportation process with the CCS of Mammoet is shown in Figure 1-10.

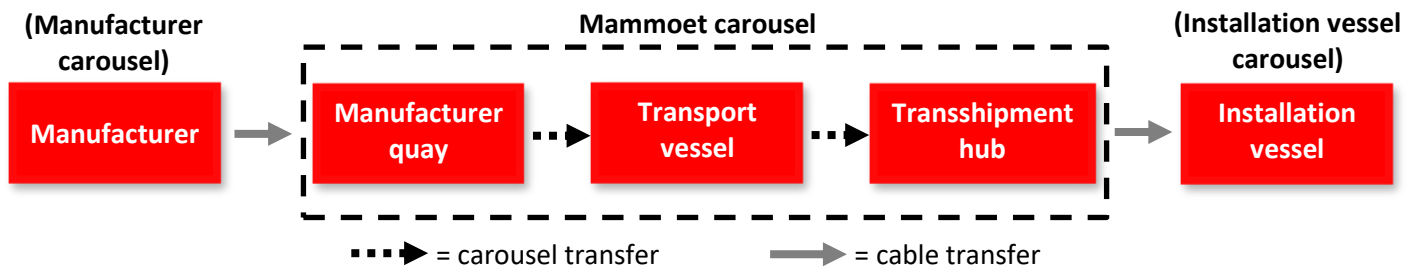


Figure 1-10: Transportation process with the CCS of Mammoet

So, for this transportation process two cable transfers have been replaced by a carousel transfer, where the entire carousel is transferred to another position instead of spooling the cable to another carousel. The proposed design of the CCS from Mammoet can be seen in Figure 1-11. The CCS of Mammoet also has included some additional functionalities:

- **Containerized:** The entire CCS (carousel, floor plates, SPMTs, structural components, grillage frame, etc.) is containerized which makes the transport of the system without the cable less expensive and more efficient. Containers are namely transported on fixed routes on a regular basis such that special vessel transport is not needed to transport the empty carousel of the CCS. Furthermore, containerization allows more compact storage of the CCS.
- **Sea fastening:** The CCS includes sea fastening, so no adjustments are needed when the carousel is placed on a vessel for sea transport
- **Easy SPMT handling:** The CCS includes space below the floor plates between the grillage beams for the SPMT's to transport the carousel without extra actions and equipment.

- **Modular:** The CCS is modular such that different sizes for the floor and outer/ inner frame of the carousel are possible. This means that the CCS could be optimized to handle different capacities.

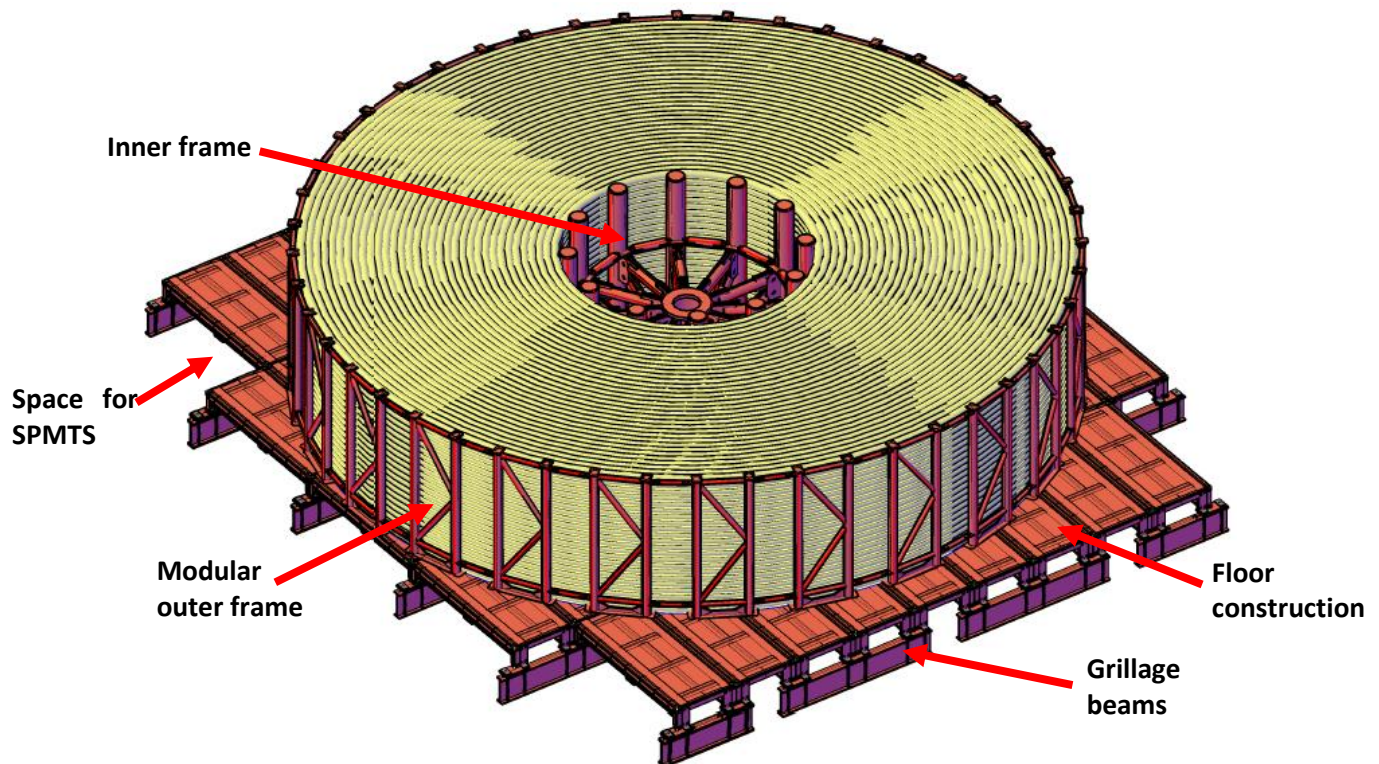


Figure 1-11: Mammoet carousel design

1.3 Research outline

1.3.1 Objective

The main challenge is that the transport of offshore power cables can be more efficient to save time and costs. Mammoet proposed its CCS and a concept design as a possible solution for a more efficient transport. For this concept there are a few uncertainties and assumptions which have been made. Therefore, the main objective of this study is to evaluate the feasibility of the CCS and determine how the CCS can be implemented to improve the current transportation method.

1.3.2 Approach

The following main research question has been defined:

Can the containerized carousel system improve the current offshore power cable transportation method?

For answering this main research question, different sub research questions are defined:

1. What are the characteristics of the current offshore power cable transportation methods?
2. Which challenges need to be addressed for the CCS?
3. Which design choices can be made for the CCS to address the challenges?
4. What design choices show the best performance against the challenges?
5. Do the properties of the cable stack have an influence on the performance of the design choices?

Answering each sub question results in a different activity, as shown in Table 1-1.

Table 1-1: Activities and results

Sub question	Activity	Result
1	Literature study and process analysis of current method (section 2.1)	Challenges
2	Process analysis of the CCS (sections 2.2 and 2.3)	
3	Defining design choices for the CCS (Chapter 3)	Conceptual solutions
4	Analysis of conceptual solutions (Chapter 4)	Concept analysis
5	Analysis of stiffness and load distribution of cable stack (Chapter 5)	Influence of cable stack

1.3.3 Scope

Multiple research boundaries have been defined, shown in Table 1-2, which form the scope of the study

Table 1-2: Scope

#	Research boundaries
1	The study focusses on improving the proposed design for the Mammoet CCS, where a general overview is given in Figure 1-11.
2	The CCS design must remain its additional functionalities as in the design proposed by Mammoet: containerized, modular, included sea fastening and easy SPMT handleability
3	The CCS in this study is dedicated to offshore power cables only. The carousel in the study must be applicable to the most common cable diameters.
4	In the CCS the Mammoet SPMT's must be used
5	Despite the modularity requirement, a capacity of 5000 t is taken for which the CCS will be elaborated. This capacity is also used in the design proposed by Mammoet and thus allows comparison between concepts
6	The CCS must be applicable to multiple transportation vessels
7	It is assumed that with the production the cable is directly loaded into the manufacturer carousel, and then to the Mammoet carousel. Usage of the Mammoet carousel in the production process or on the installation vessel for the cable installation is left out of scope.
8	Detailing of the carousel design is left out of scope, the study is only focusing on the global analysis. Only global dimensions and beam cross-sections are determined.
9	The study mainly focuses on the feasibility of the CCS and improving the CCS from a technical point of view. Most operational and financial aspects are left out of scope.

2 Process analysis

The objective of this chapter is to define the challenges for the CCS. First, a literature study and process analysis are executed to determine the characteristics of the current transportation methods with which the CCS must compete. After that, the process of the CCS will be analyzed from which challenges for the CCS are defined.

2.1 Current transportation method

2.1.1 Process overview

Previously, the process overview of the current transportation method is defined as shown in Figure 2-1.

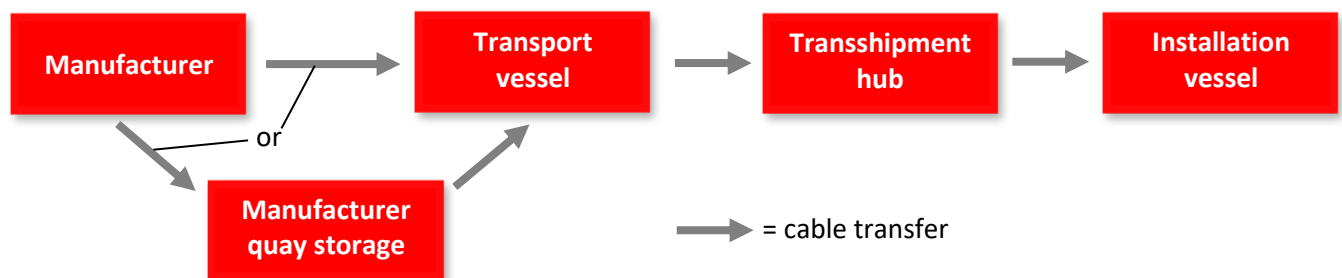


Figure 2-1: Transportation process current way

Manufacturer

The cable transportation process starts by the manufacturer which produces the cable. Each manufacturer has its own carousel(s) in which the cable is stored directly after the fabrication process. Such a carousel can be seen in Figure 2-2.

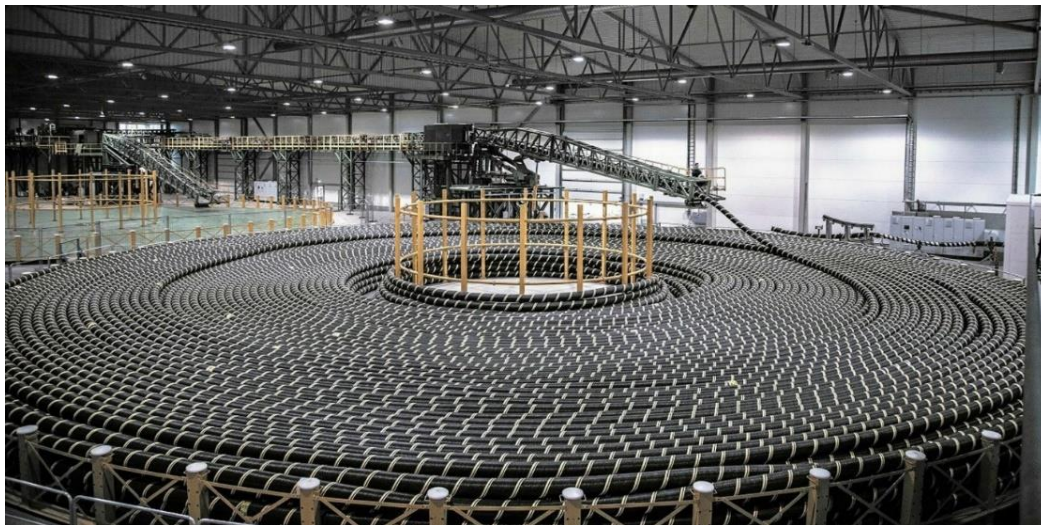


Figure 2-2: Cable storage in manufacturer carousel [12]

The manufacturer carousel is mostly fixed on its position. Due to the high demand for offshore power cables the cable needs to be removed from this carousel as fast as possible to make space for a new cable for the next customer. Therefore, the just produced cable will directly be transferred to another carousel of the customer. This new carousel can be positioned on the manufacturer quay for storage or be positioned directly on a transport vessel. In the case where the cable is transferred to a carousel on the manufacturer quay, another cable transfer is needed to get the cable in a carousel on the transportation vessel.

Cable transfer

As described previously, with a cable transfer the offshore power cable is simultaneously unspooled from one carousel and simultaneously spooled on the other carousel. The cable velocity will be kept constant by adjusting the rotational velocity of the carousels, which depends on the radius in the carousel where the cable is (un)spooled. At the start of the cable spooling one cable end needs to be positioned in the new carousel before the cable transfer can start. How this is done is left out of scope as the same principle for all other carousels can be used. In general, the cable spooling

starts at the inner wall of the carousel. Afterwards the cable is spooled in a spiral way to the outer frame of the carousel. When no cable turn fits on the ground layer anymore the cable will move one layer up and will be spiraling into the other direction as the previous layer. This will be repeated until the appropriate amount of cable is spooled. Each layer is thus alternating spiraling inward or outward. The cable won't be spooled under tension but will be laid on the right spot, guided by workers as can be seen in Figure 2-3. Each cable turn will be laid against the previous cable turn. Because the cable laying is a slow and controlled operation the cable spooling process is not governing for the strength and stiffness of the carousel.

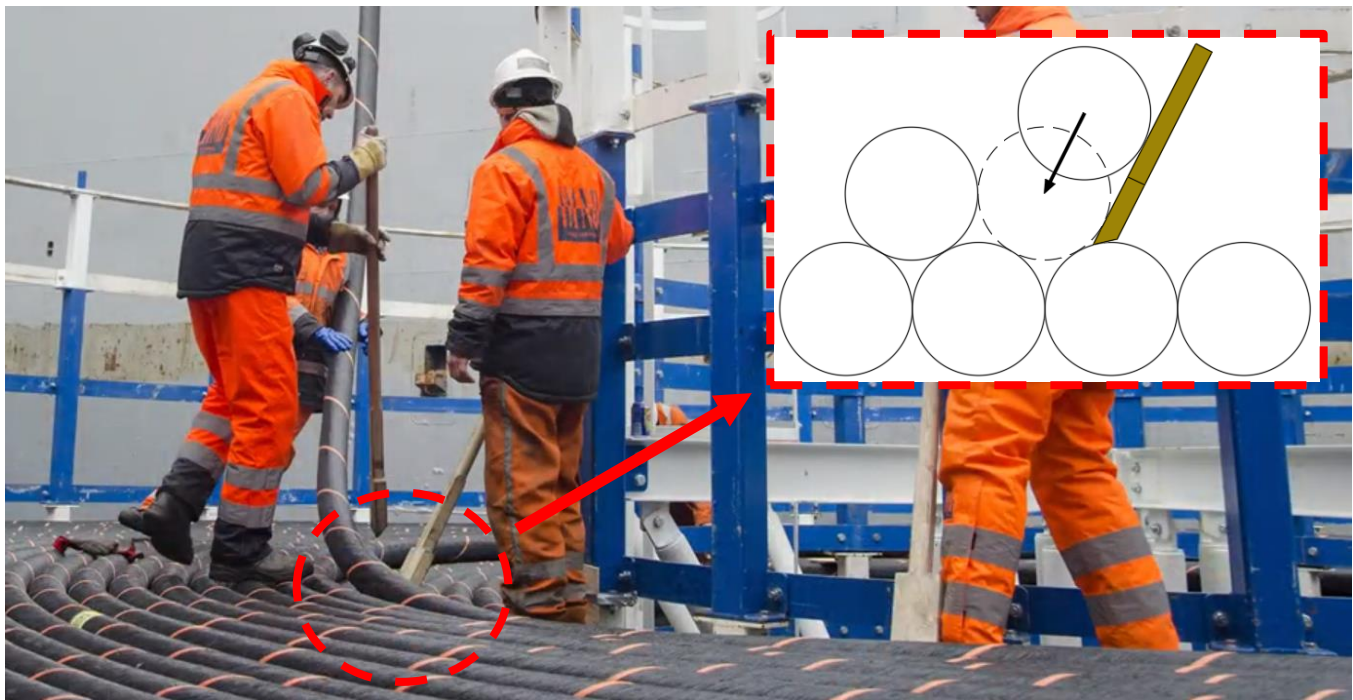


Figure 2-3: Cable placement with spooling in carousel [13]

For the drive of the carousel there are many possible solutions, where a simple solution is shown in Figure 2-4.

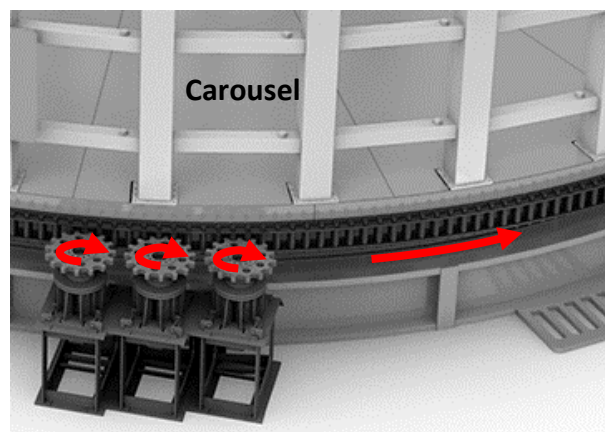


Figure 2-4: Simple carousel drive [14]

Transportation vessel

From the manufacturer carousel or another storage carousel on the manufacturer quay, the cable will be transferred to a carousel on a vessel. The installation of the cable requires a cable installation vessel (see "cable installation vessel"). However, these vessels are very expensive to hire. Thus, a less expensive vessel is needed to transport the cable to an intermediate hub closer to the demanded offshore windfarm. There are many options for transportation vessels. A general transportation vessel for offshore power cables, with two carousels fixed on their drive system, is shown in Figure 2-6.

Transshipment hub

The cable will be transferred from the carousel on the transport vessel to a carousel on the transshipment hub. The transshipment hub is an intermediate quay where the offshore power cables are stored, ready to be spooled on an installation vessel or another transport vessel for further transport. Figure 2-5 shows a transshipment hub, where the storage carousels are marked in red.

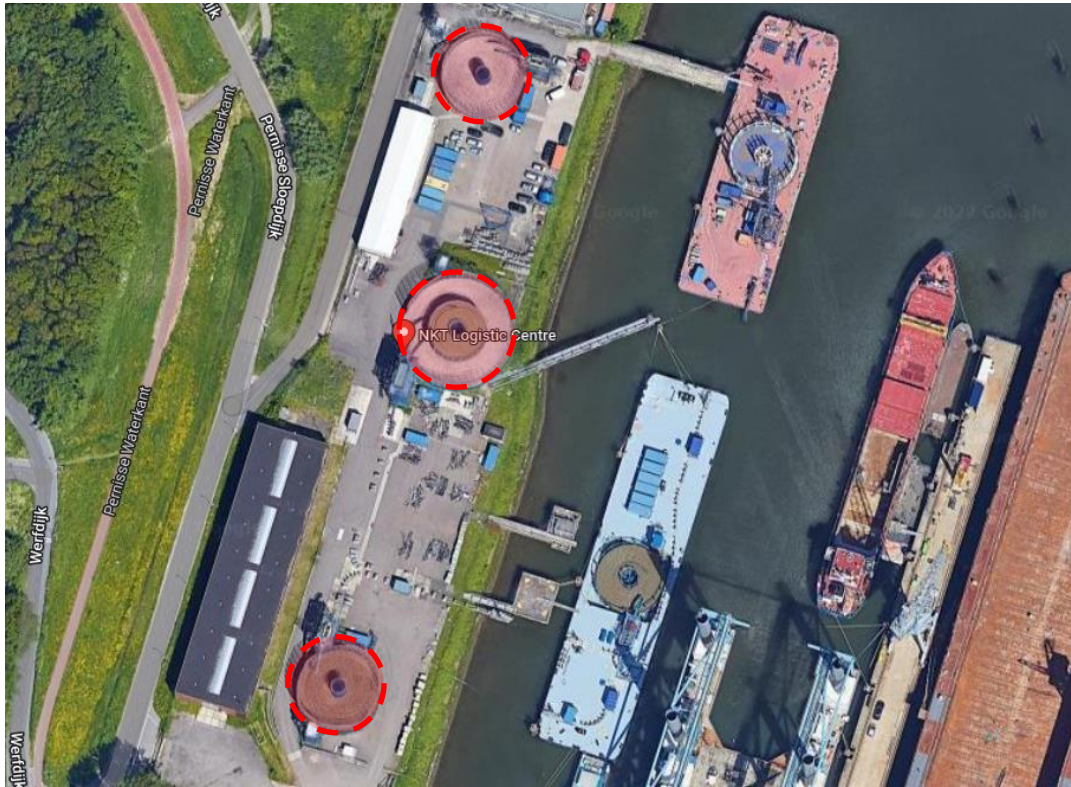


Figure 2-5: Transshipment hub [15]

Cable installation vessel

The installation of the offshore power cables is done by a cable installation vessel, which uses a cable carousel system as can be seen in the Figure 2-7. From a carousel on the transshipment hub the cable will be transferred to the cable installation vessel. Cable installation vessels are very expensive, and they control the tension and bending radius of the cable when laying it. Almost all cable installation vessels have a carousel fixed on a drive system with a usually smaller capacity. The cable installation vessel is thus possibly sailing the route transshipment hub – offshore windfarm multiple times when more cable than the capacity is stored at the transshipment hub.



Figure 2-6: Offshore power cable transport vessel [16]



Figure 2-7: Cable installation vessel [17]

2.1.2 General process characteristics

For the spooling of offshore power cables in carousels there are a few characteristics which apply for each transportation method. Some of these characteristics are described in the next paragraphs.

Cable mass

There are many different offshore power cables with many different sizes and masses. In Figure 2-8 the cable mass μ_{cable} (in kg/m) is related to the cable diameter D_{cable} for both AC and DC cables from different manufacturers [18] [19] [20] [21] [22] [23].

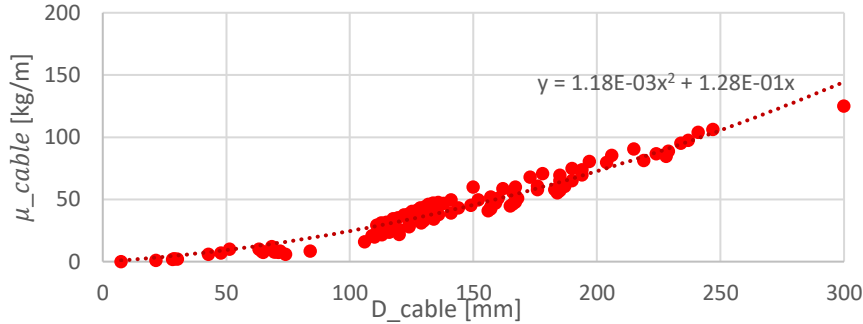


Figure 2-8: Cable mass related to cable diameter

The graph in the figure above shows that there is an approximate quadratic relation between the cable mass and the cable diameter. The approximate quadratic formula which relates the cable mass μ_{cable} [kg/m] with the cable diameter D_{cable} [mm] is given by

$$\mu_{cable} = 1.18 \cdot 10^{-3} D_{cable}^2 + 1.28 \cdot 10^{-1} D_{cable} \quad (2-1)$$

Spooling time

A few carousels have been selected to determine the rotation speed [7] [24] [14] [25]. Each carousel manufacturer specifies a maximum lay or spool rate (usually about 1 km/hour). Notice that the carousel must rotate faster when the cable is spooled at the inside for the same spool / lay rate as the cable is spooled at the outside of the carousel. Each carousel also specifies a capacity C . By assuming an average cable mass of $\mu_{cable} = 65 \text{ kg/m}$ the corresponding cable length L_{cable} in the carousel at full capacity can be determined by

$$L_{cable} = C / \mu_{cable} \quad (2-2)$$

From this, with the lay/spool rate, the minimum total non-stop spooling time T_{spool} , at maximum spool rate and without downtime, needed can be estimated. The results for the selected carousel are summarized at the red dots in Figure 2-9 for a cable mass of 65 kg/m . The red dotted line denotes the average time of non-stop spooling for the corresponding capacity. This resulting spool rate of the rate dotted line is approximated $V_{spool} \approx 0.87 \text{ km/h}$. Figure 2-9 also shows capacities for different carousel. As the CCS is modular, different capacities are possible but a capacity of 5000 t is used in this study.

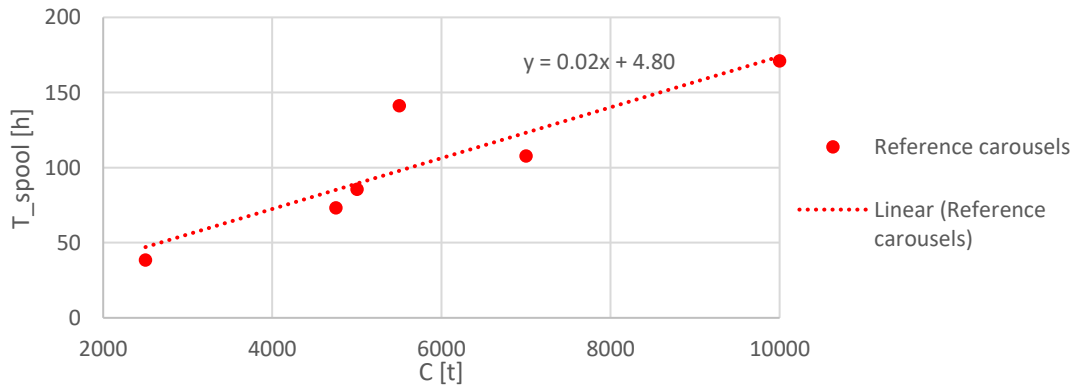


Figure 2-9: Nonstop spooling time T_{spool} related to capacity C for cable mass of 65 kg/m

Cable stack

In general, the stacking of cables starts at the lowest layer at the inside of the carousel. From the inside of the carousel the cable is spiraling outwards, until no cable turn fits between the last cable turn and the outside wall of the carousel. When no cable fits anymore on the layer the cable is laid on this layer to form a new layer, where the cable is alternating spiraling inward and outward. The cables are laid against each other by workers. What also is observed is that the cable is not spooled under tension, but it is just laid on its desired position. The general cable stack cross section is visualized in Figure 5-10.

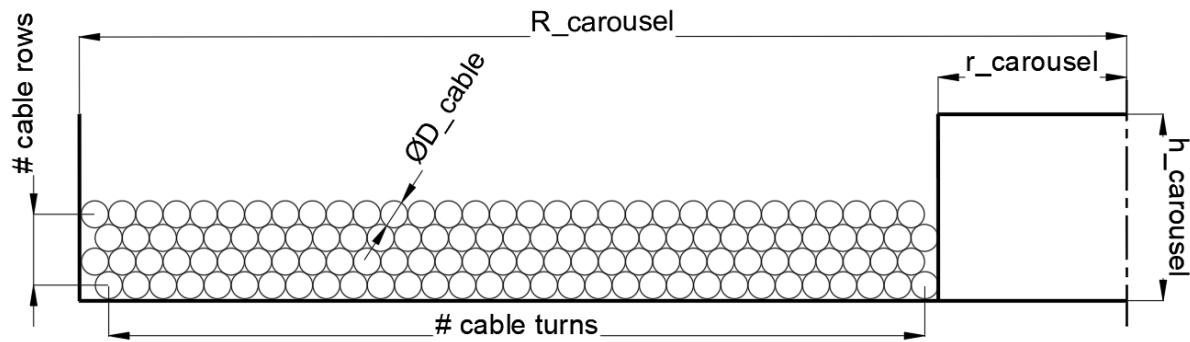


Figure 2-10: Carousel and cable stack cross section

Also the main dimensions of the carousel are shown in Figure 2-11, with inside carousel radius $r_{carousel}$, outside carousel radius $R_{carousel}$ and the height of the carousel $h_{carousel}$. In Appendix D it is defined how the carousel stack (# cable rows and #cable turns) are related to the carousel dimensions, cable diameter D_{cable} and the capacity C .

2.2 Containerized carousel system

In this section the transportation process of the CCS will be analyzed. The CCS process is divided into sub processes, which can be seen Figure 2-11. It is assumed that the governing processes for the CCS are the carousel transfer, cable transfer and sea transport. Normal storage will not be discussed as sea transport has comparable supports but higher accelerations. In the next sections each sub process is analyzed separately.

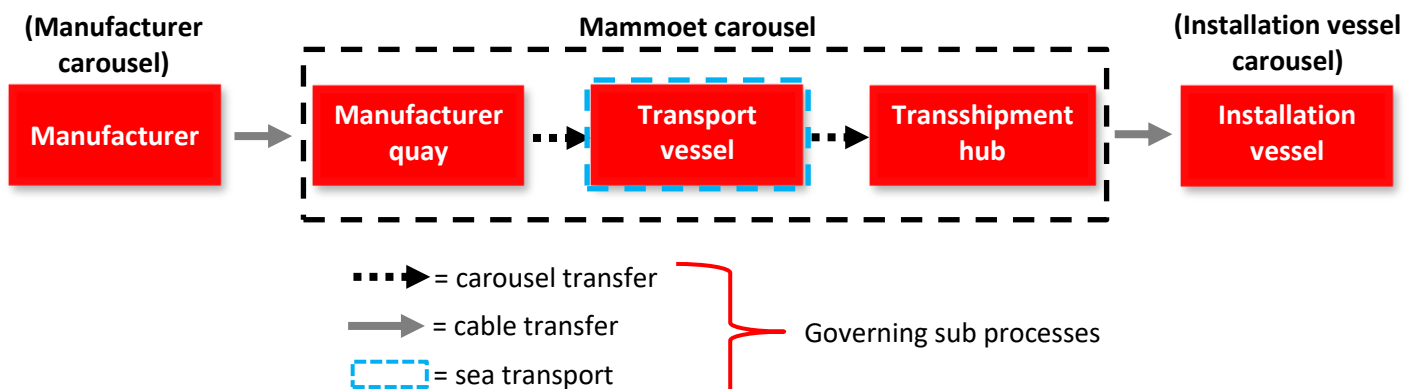


Figure 2-11: CCS process overview with governing sub processes

General input

In chapter 2, the proposed CCS design of Mammoet will be used as a reference (Research boundary 1) for the process analysis. In Table 2-1 the main properties of this design [26] [27] are summarized. The dimensions from Table 2-1 are visualized in Figure 2-12.

Table 2-1: General input CCS

Description	Abbreviation	Value	Unit
Outside carousel radius	$R_{carousel}$	13.3	m
Inside carousel radius	$r_{carousel}$	4.375	m
Carousel height	$h_{carousel}$	5.80	m
Carousel capacity	C	5000	t
Radius most outer SPMT axle line	$R_{o,SPMT}$	≈ 15.0	m
Total mass of carousel (floor, inner frame, outer frame, and all other component)	$m_{carousel}$	592	t
Total mass of the floor of the carousel	m_{Floor}	400	t
Total mass of the grillage frame of the carousel	$m_{grillage}$	127	t
Total mass of the SPMT trains for the SPMT transport	m_{SPMT}	800	t
Number of axle lines	/	184	/

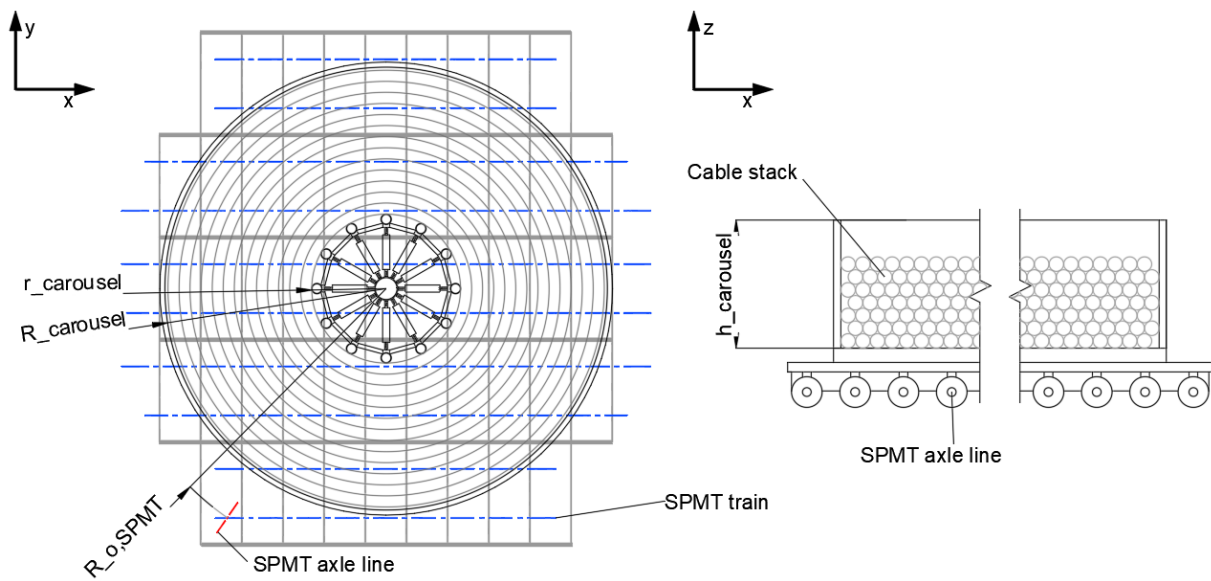


Figure 2-12: General input visualization

Use of SPMT's

As described previously, the CCS makes use of the SPMTs from Mammoet. A SPMT with 6 axle lines is shown in Figure 2-13.



Figure 2-13: Mammoet SPMT with 6 axle lines [28]

Mammoet has a fleet of 3200 axle lines, spread across the world. This makes it relatively efficient to get the SPMTs on the manufacturer quay or on the transshipment hub for usage in the cable carousel system. The SPMTs of Mammoet have a few advantages [29]:

- *Flexible and agile*: each axle can move independently such that the SPMT can be steered in almost any direction in the horizontal plane (Figure 2-14).

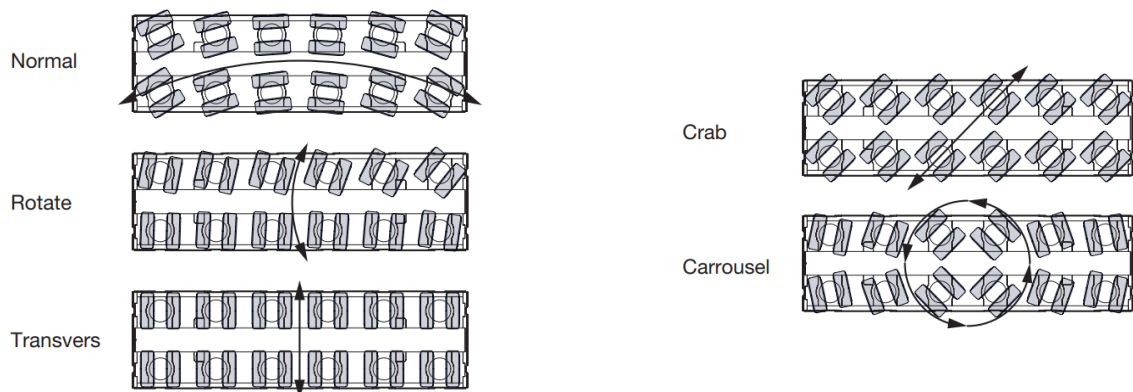


Figure 2-14: SPMT steering capabilities [30]

- *Can transport almost any object*: The SPMTs are modular, and they can be mechanically coupled in a line, side-to-side and/or head-to-tail or they can be grouped freely by data link. Multiple SPMTs coupled to each other head-to-tail is called a SPMT train.
- *Operational under the most extreme conditions*: such as extreme heat and cold climate conditions
- *Easy and swift mobilization*: SPMTs can easily transported by containers
- *Low ground bearing pressure*: usage of air-filled tires reduces the need for additional ground reinforcement.
- *Minimum environmental impact*: The SPMTs are equipped with features that help minimize the impact on the environment
- *Heavy transport*: SPMTs can be used to transport heavy objects.

2.2.1 Cable transfer

The first step of the new transportation process is to get the cable on the Mammoet carousel. For this a cable transfer is needed from the manufacturer carousel to the Mammoet carousel. In the entire process with the CCS two cable transfers are needed as marked in blue in Figure 2-15.

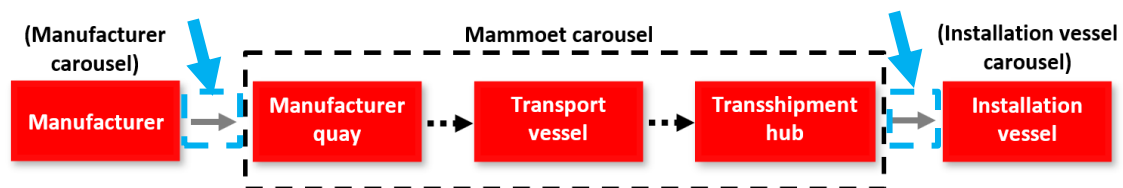


Figure 2-15: Cable transfers in the CCS of Mammoet

The general setup for a cable transfer is shown in the Figure 2-16, which shows a cable transfer by using SPMTs in a previous project with a lower capacity carousel.

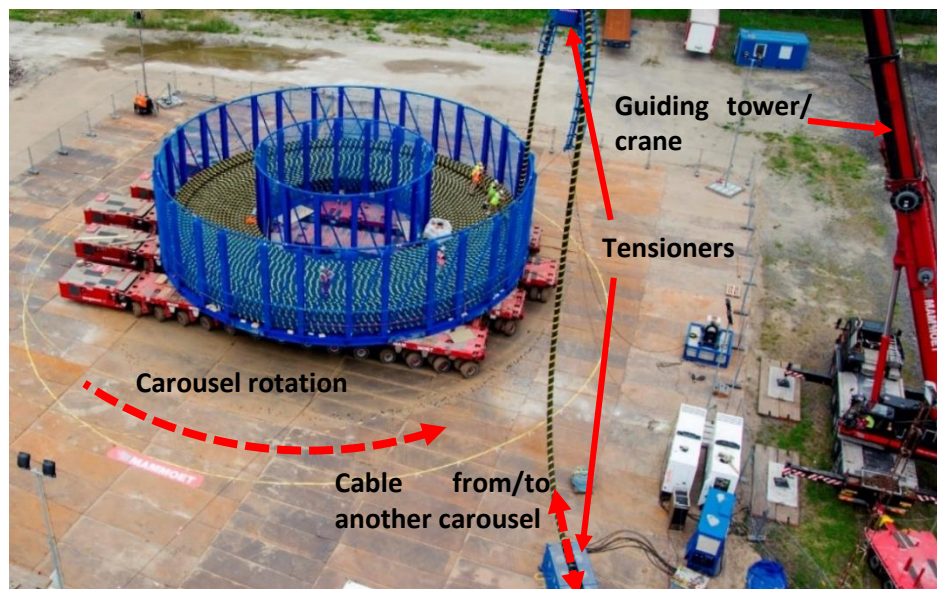


Figure 2-16: Cable transfer with carousel on SPMTs [31]

For the cable transfer the following operations are needed:

1. Preperation

- 1.1. Mobilization
- 1.2. Carousel on SPMTs
- 1.3. Carousel drive to appropriate position for cable spooling
- 1.4. Positioning of other equipment such as tensioners, crane, loading towers, vessels, and the other carousel

2. Spooling the cable: carousel rotation by SPMTs and cable throughput by tensioners from/to another carousel

3. After execution (not discussed):

- 3.1. Carousel drive to appropriate position
- 3.2. Carousel release by SPMTs
- 3.3. Removing other equipment
- 3.4. Demobilization of SPMTs, and possibly the carousel

Operations 1. and 2. are briefly discussed in the next paragraphs. Operation 3. is not discussed as it is the vice versa of operation 1.

Mobilization

The first step of the entire proposed transportation process is to mobilize the CCS to the demanding quay. The entire system (carousel, floor, SPMTs, structural components, etc.) is containerized and therefore the fixed container routes can be used to transport the carousel and SPMTs. No special transport is thus required for mobilization, which can be an advantage of the proposed transportation method. In case of spooling from the manufacturer carousel to the CCS carousel, it is important that the mobilization of the CCS is finished and assembled on manufacturer quay before the manufacturer finishes the cable production. This makes it possible to directly spool the cable on the carousel of the CCS.

For the second cable transfer on the transshipment hub, only the SPMTs need to be mobilized nearby the carousel. It is however possible that the SPMTs are already mobilized nearby the Mammoet carousel if they are also transported with the transport vessel.

Carousel lift

The carousel needs to be lifted to get it on the SPMTs. In the CCS design the carousel is supported by its grillage frame. Between the grillage frame there must be space for the SPMTs to drive below the carousel. This gives space to position the SPMTs to their appropriate position. When all the SPMTs are positioned, simultaneously the height of the SPMTs will be enlarged. At a certain height there will be contact with the carousel. A further increase of the height will lift the carousel and causes ground clearance between the carousel grillage frame and the ground (or the floor and the grillage

frame if the grillage frame is released), and the carousel will be only supported by the SPMTs. The height of the SPMTs can be regulated by the hydraulic cylinders.

The SPMTs have a limited cylinder stroke (section 2.3.2). For the lift and set down of the carousel a cylinder stroke of approximated 200-300mm is recommended for ground clearance and to overcome the ground conditions, such as, ground unevenness, slopes, and camber for the transport. The Lift operation of a single floor plate with SPMTs can be seen in Figure 2-17 (notice that the set down operation is the reversed lift operation)

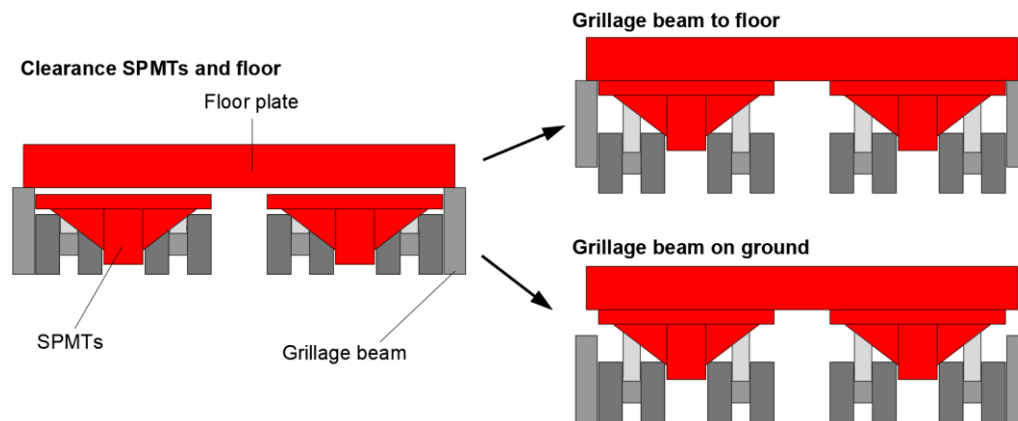


Figure 2-17: Carousel lifting by SPMTs [26]

To positioning of the carousel on the SPMTs is effectively monitored by sensors and an operator. For this reason, it is assumed that the forces corresponding to the accelerations or other impacts due to the carousel lift or set down can be neglected.

Carousel spooling position

For the spooling of the cable on the Mammoet carousel it is important that the underground has (almost) no unevenness, camber, and slopes. The Mammoet SPMTs are driven by hydraulic motors, which convert hydraulic pressure into torque and rotation, where each driven axle line has a separate motor (approximately 1/3 of the axle lines are driven). The oil that drives the hydraulic motors flows through the path with the least resistance. If there is a tire which less/no grip, possibly due to an unevenness, the torque transferred to the ground is lowered which lowers the resistance and as a result more oil will flow through the corresponding motor. This increases to angular velocity in the motor and this can cause spin/slip of the tire with respect to the ground and other tires. There are many reasons which can cause inaccuracies in the rotation of the carousel, which can result in an offset as shown in Figure 2-18.

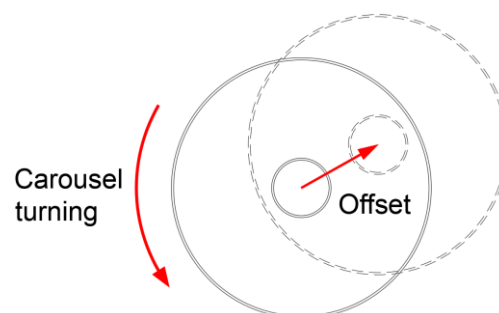


Figure 2-18: Offset with carousel turning

The possible offset requires that the turning of the carousel needs to be effectively monitored. Also, some extra space for the carousel turning must be reserved for a possible offset. If the offset is too large and the cable throughput is not aligned with the carousel anymore, to cable throughput must be paused and the carousel must be drive back to its position. This causes downtime of the process.

Other equipment

The general setup for the cable transfer and all the equipment needed is shown in Figure 2-19. This equipment must be positioned before the cable transfer can start.

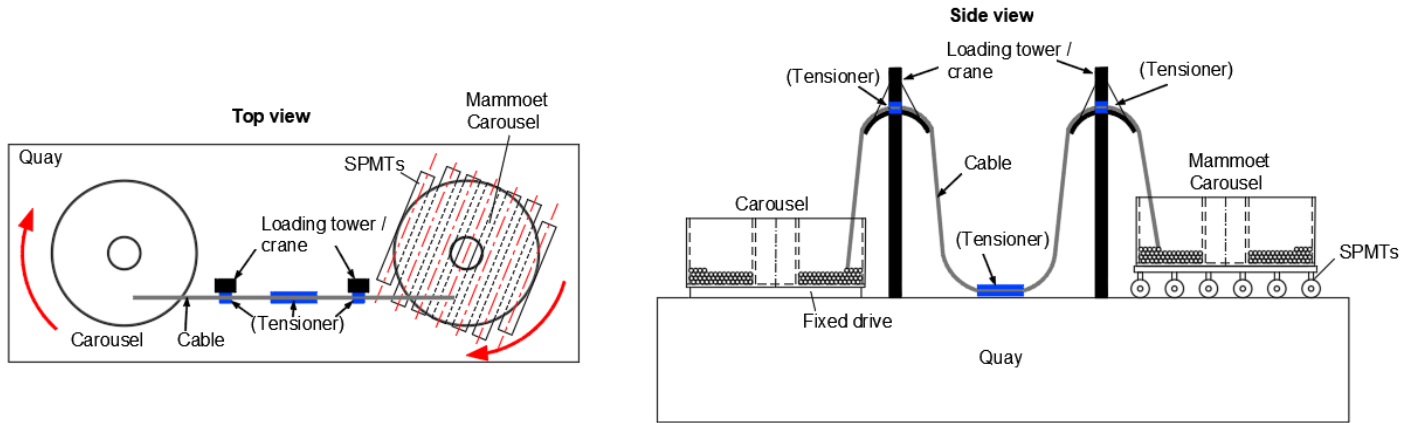


Figure 2-19: Cable transfer setup

Carousel spooling by SPMTs

The tangential speed of an SPMT axle line $V_{R,SPMT}$ is related to the spool rate V_{spool} , spool radius R_{spool} and the position radius of the concerning SPMT axle line R_{SPMT} by

$$V_{R,SPMT} = V_{spool} / R_{spool} \cdot R_{SPMT} \quad (2-3)$$

Figure 2-20 visualizes $V_{R,SPMT}$, V_{spool} , R_{spool} and R_{SPMT} .

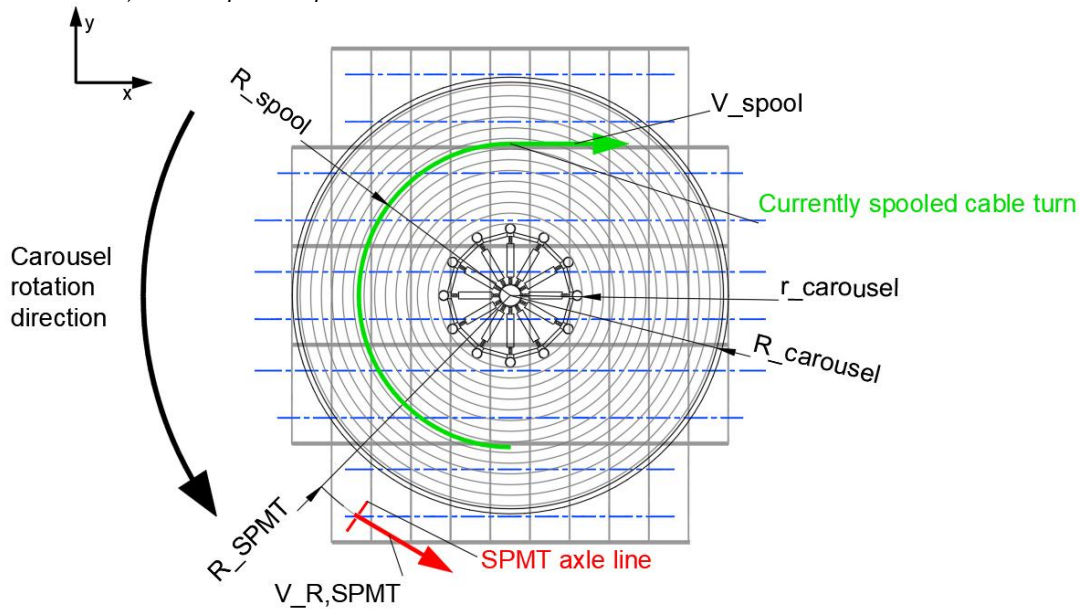


Figure 2-20: Visualization of $V_{R,SPMT}$, V_{spool} , R_{spool} and R_{SPMT}

The SPMT has a limited drive speed. For heavy loading a maximum drive speed of 4 km/h is recommended (Chapter 2.3.1). It follows that the maximum tangential velocity of the SPMT axle lines is obtained for the most outside axle line at radius $R_{O,SPMT} = \max(R_{SPMT})$, when the cable is spooled at the most inside radius $R_{spool} = r_{carousel}$, where $r_{carousel}$ is the inside carousel radius. This means that the inside carousel radius is limited by

$$r_{carousel} \geq R_{O,SPMT} \cdot \frac{V_{spool}}{V_{O,SPMT}} \quad (2-4)$$

, where the tangential velocity of the most outside SPMT axle line is defined as $V_{O,SPMT} = \max(V_{R,SPMT})$. As shown in Figure 2-9, the spool rate $V_{spool} \approx 1 \text{ km/h}$ for most carousels, and thus also an advised spool rate for the CCS.

The spool duration T_{spool} can be expressed in terms of cable mass μ_{cable} by

$$T_{spool} = \frac{L_{cable}}{V_{spool}} = \frac{C / \mu_{cable}}{V_{spool}} \quad (2-5)$$

The spool time T_{spool} for a capacity $C = 5000 \text{ t}$ and a spool rate of $V_{spool} = 0.87 \text{ km/h}$ is plotted in Figure 2-21 for the corresponding cable mass μ_{cable} . To determine the drive distance of an SPMT axle line, the average length of a single cable turn $L_{ct,avg}$ in the cable stack can be estimated by

$$L_{ct,avg} \approx \pi \cdot (R_{carousel} + r_{carousel}) \quad (2-6)$$

, where $R_{carousel}$ is the outer carousel radius and $r_{carousel}$ the inner carousel radius. From the general input (Table 2-1) it follows that $R_{carousel} = 13.3 \text{ m}$ and $r_{carousel} = 4.375 \text{ m}$. The drive distance of a SPMT axle line $S_{R,SPMT}$ at radius R_{SPMT} over the entire cable transfer process can be approximated by

$$S_{R,SPMT} \approx \frac{L_{cable}}{L_{ct,avg}} \cdot 2\pi R_{SPMT} \quad (2-7)$$

The drive distance of a SPMT axle line $S_{R,SPMT}$ with $R_{SPMT} = 15.0 \text{ m} \approx R_{o,SPMT}$ is also plotted in Figure 2-21. The figure shows that a smaller μ_{cable} results in more cable to be stored and thus a larger spooling time and SPMT drive distance.

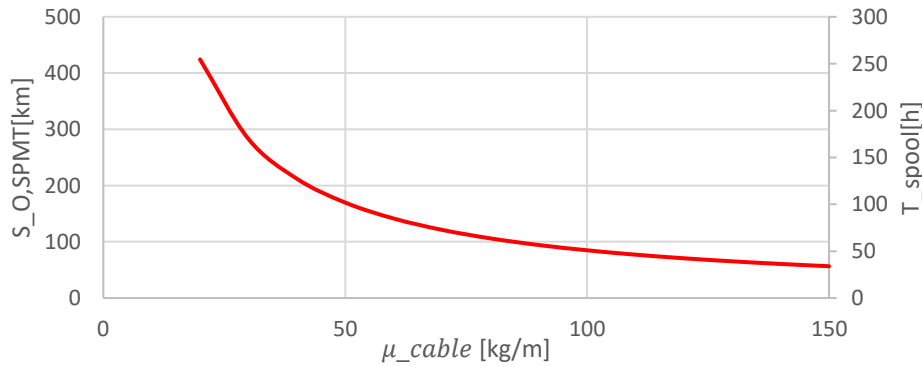


Figure 2-21: SPMT axle line at $R = 13.3$ drive time and distance travelled

Angular de-/acceleration

Each driven axle line adds a force to the carousel, where all these forces together cause a torque on the carousel during the spooling operation. From the SPMT manufacturer it follows that the brake force and both the drive force is 120 kN per drive / brake axle line. On average, $1/3$ of the total axle lines from the SPMT is driven and $1/3$ of the axle lines has a brake [32]. To estimate the rotational (de)acceleration it is assumed that the carousel filled with the cable is a homogenous cylinder as shown in Figure 2-22.

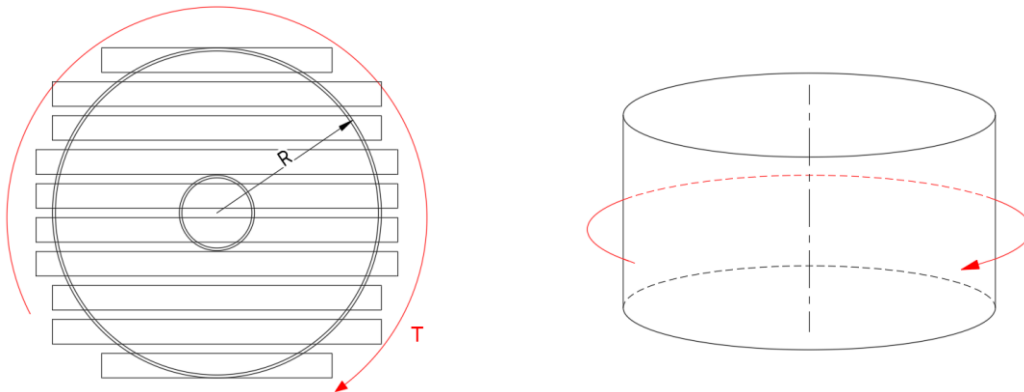


Figure 2-22: Homogeneous solid cylinder

From the general input the total mass of the CCS during SPMT transport with full capacity and the grillage frame included is given by $m_{CCS,SPMT} = m_{carousel} + m_{grillage} + m_{SPMT} + C = 592 + 127 + 800 + 5000 = 6519 \text{ t}$ (see Table 2-1). For this simplified cylinder a radius equal to the outside carousel radius $R_{carousel} = 13.3 \text{ m}$ will be used. The moment of inertia of the fully loaded CCS during SPMT transport is then estimated by

$$J_{CCS,SPMT} = \frac{1}{2} \cdot m_{CCS,SPMT} R_{carousel}^2 \quad (2-8)$$

The applied torque by the SPMTs T_{SPMT} on the CCS is related to the angular acceleration of the CCS α_{CCS} by

$$T_{SPMT} = J_{CCS,SPMT} \alpha_{CCS} \quad (2-9)$$

For the Mammoet design 184 axle lines are used. It is assumed that these are evenly distributed over the carousel area and that their average distance from the SPMT axle line to the center of the carousel $R/3$. The results for the CCS design proposed by Mammoet are given in Table 2-2.

Table 2-2: Theoretical needed SPMT drive force

Description	Abbreviation	Value	Unit
Max drive/brake torque of SPMTs	T_{SPMT}	$3.68 \cdot 10^4$	kNm
Moment of inertia of CCS during SPTM transport	$J_{CCS,SPMT}$	$7.33 \cdot 10^8$	$kg \cdot m^2$
Max angular (de)acceleration	$\alpha_{CCS,SPMT}$	0.0502	rad/s^{-2}

For an inner core with radius $r_{carousel} = 4.375$, as in the Mammoet design, a rotation speed of 0.0552 rad/s is needed for a spooling speed of $V_{spool} = 0.870 \text{ km/h}$ of cable. This means that the carousel can approximately accelerate to the needed speed or deaccelerate for an emergency stop within $0.0552/0.0502 = 1.10$ seconds.

2.2.2 Carousel transfer

For the process two carousel transfers are needed, marked blue in the process overview in Figure 2-23.

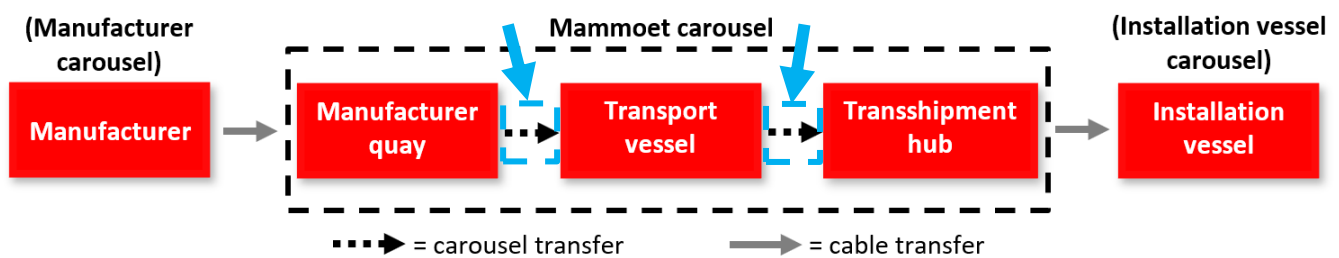


Figure 2-23: Carousel transfer in transportation process

Figure 2-24 shows a conventional cable transfer between a carousel on a barge and on the transshipment hub.

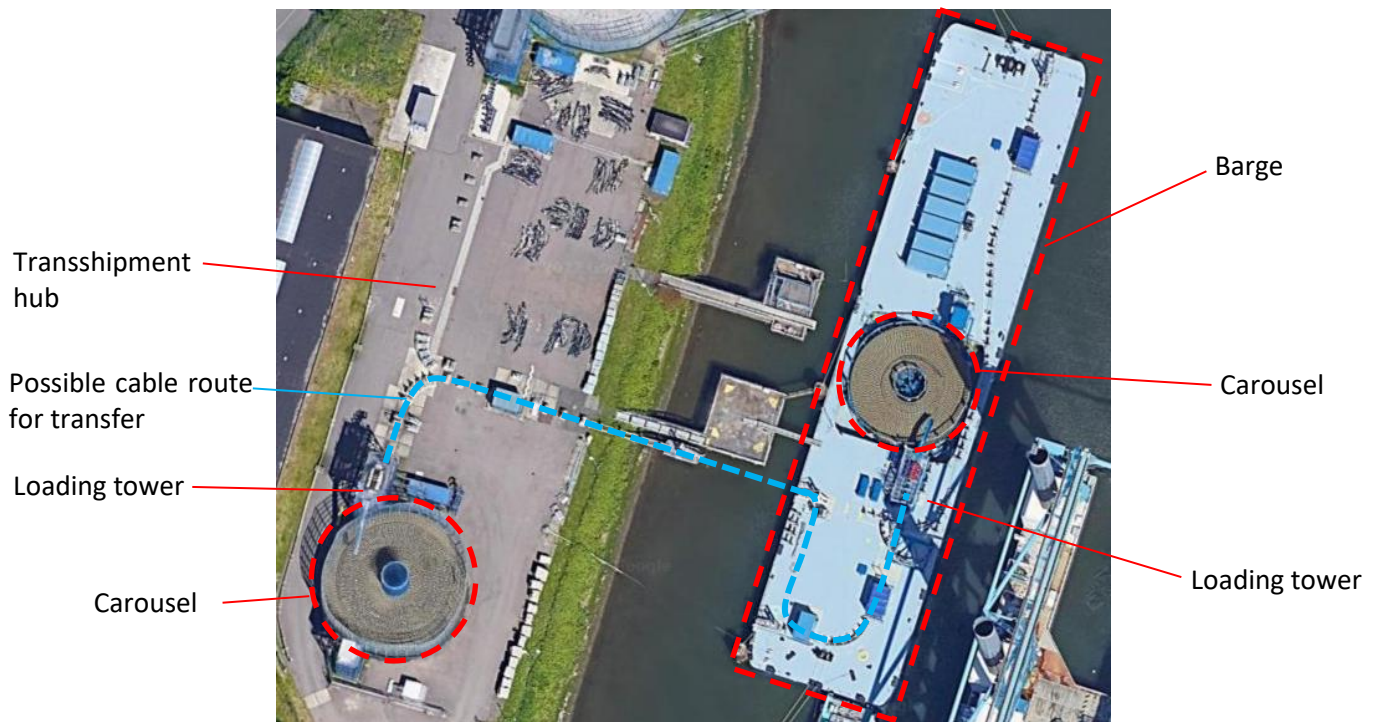


Figure 2-24: cable transfer between barge and transshipment hub [15]

For the CCS, the carousel will be transferred by means of SPMTs via a Ro-Ro ramp from the barge to the transshipment hub, or vice versa, instead of a cable transfer. A schematic overview of a carousel transfer for the CCS, from quay to vessel and vice versa, is shown in Figure 2-25.

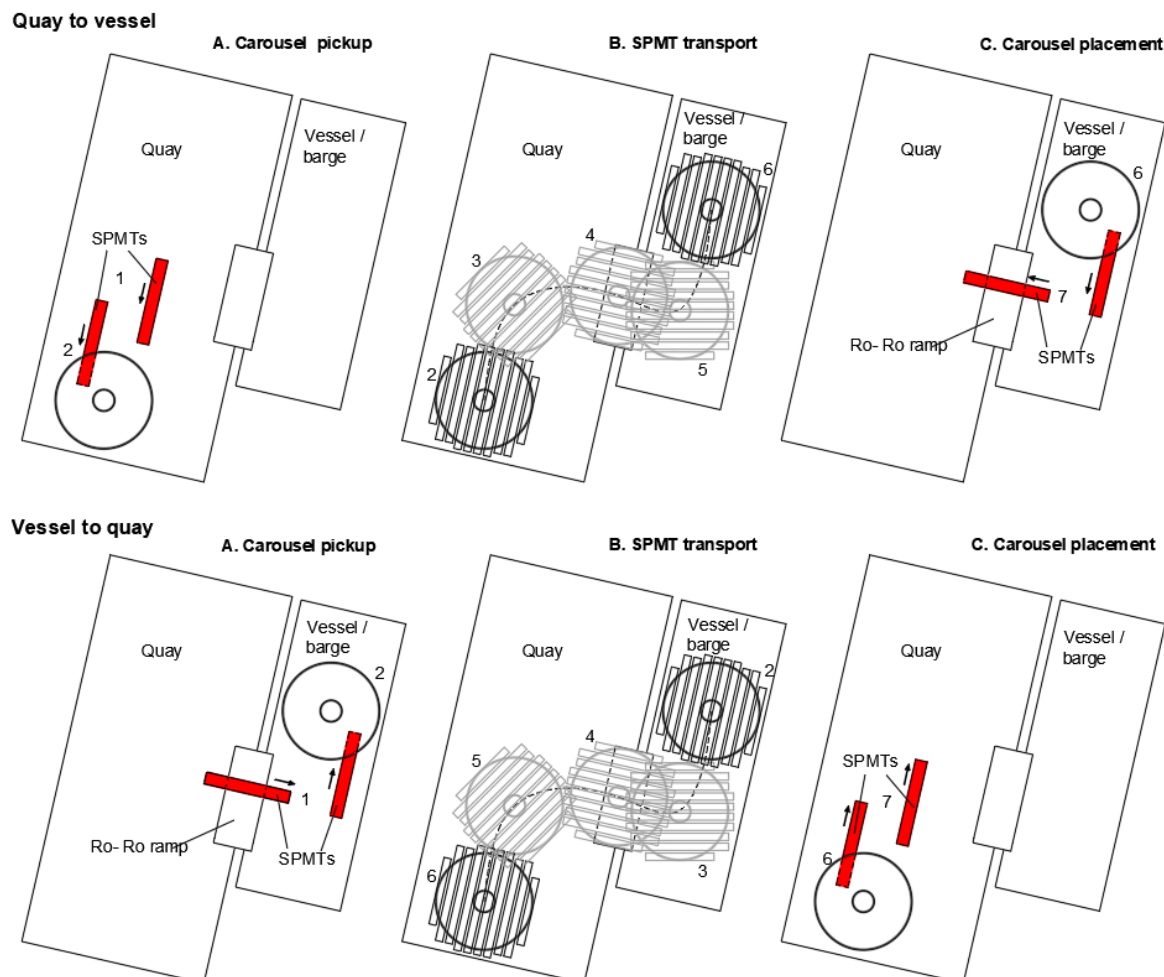


Figure 2-25: Schematic overview carousel transfer

Figure 2-25 shows that there must be maneuvering space on the vessel and the quay for the carousel and the SPMTs. The different steps of the carousel transfer operation as numbered in Figure 2-25 are given by:

1. Mobilization of SPMTs
2. Placement of carousel on SPMTs
3. SPMT transport on vessel / quay
4. SPMT transport over Ro-Ro ramp
5. SPMT transport on vessel / quay
6. Placement of carousel on vessel / quay, and removing SPMTs
7. Demobilization of SPMTs

SPMT setup and connection

Multiple SPMT trains will be used for transporting the carousel. Due to multiple reasons it is possible that transversal or longitudinal deviation between trains of SPMTs can occur during transportation, as shown in Figure 2-26 [33].

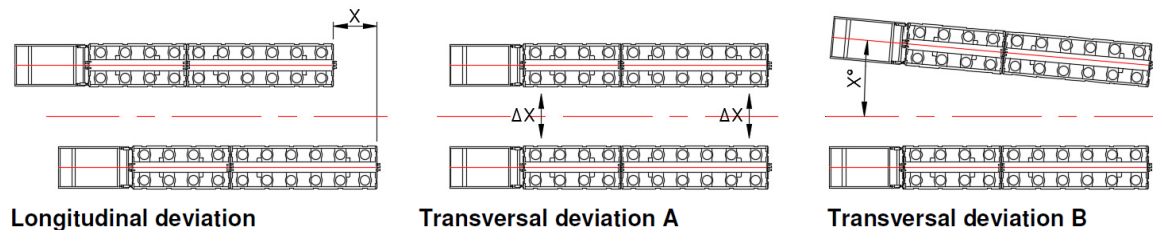


Figure 2-26: Longitudinal and transversal deviation between SPMT trains

SPMTs are generally connected by couplings. These are however not always possible such that the coupling forces need to travel through the cargo or additional couplings. If additional couplings are needed depends on the stiffness and strength of the cargo and on the connection between the cargo and the SPMTs. If the cargo is very stiff the cargo keeps the SPMTs aligned if sufficient force can be transferred from SPMT to cargo. However, if the cargo can withstand these forces is depended on its strength. If the coupling forces are too high additional couplings are needed. If the cargo is flexible the need for additional couplings is dependent on the maximum allowable deflection of the cargo and if this deflection is within the operation limits of the transport.

From Mammoet, if the SPMTs are coupled through the cargo the following loads are applied

- 50 % of the theoretical driving force from SPMT to SPMT [34]

When transporting cargo with SPMTs, possibly lashing is needed. There can be several reasons for lashing:

- Stability of the cargo on the SPMT
- Internal forces (coupling forces between SPMTs) transfer: coupling forces through the cargo require a connection between the SPMTs and cargo. This can be satisfied by friction and pressure, but sometimes additional lashing is needed
- Stability of the trailer: most of the time local stability is provided by the contact area between the SPMT and cargo. If the contact area is not sufficient to transfer moments, additional lashing is needed to provide a stabilizing moment. This can for example be needed when the cargo is support by a slender column with a small contact area on the SPMT.

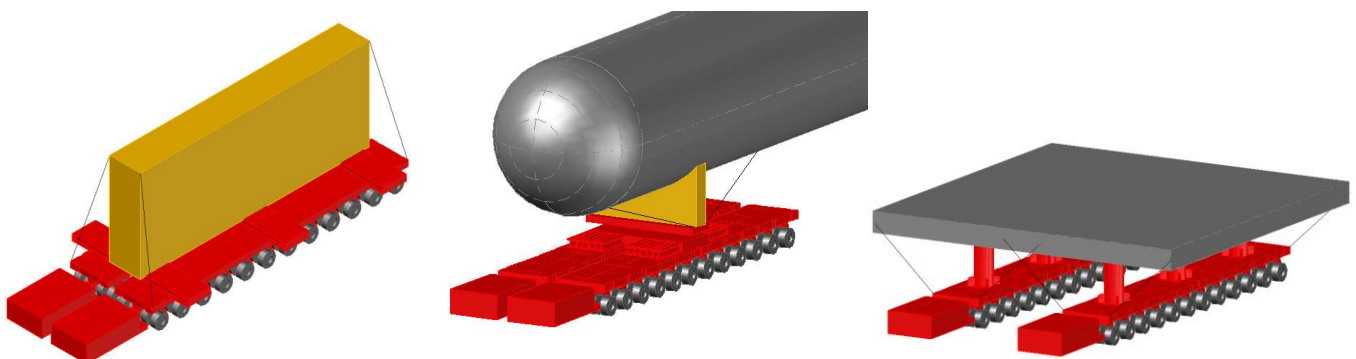


Figure 2-27: from left to right: Lashing for stability of cargo, lashing for internal forces, and lashing for stability of trailer [34]

Because of the large contact area and weight of the carousel of the CCS it is likely that no additional lashing is needed and that the connection between the SPMTs and carousel is satisfied by friction and pressure. Therefore, lashing is left out of scope of this study. For the same reasons it is assumed that no additional coupling between the SPMTs is needed and that the coupling forces travel through the carousel.

Acceleration of carousel

The main forces occurring due to driving the carousel consist of accelerating and deaccelerating the carousel. Table 2-3 shows the speeds and accelerations that are used by Mammoet based on testing for low-speed transport [34]

Table 2-3: Low speed accelerations

Speed [km/h]	Accelerations [m/s^2]	Application example
0.0 – 0.5	0.5	Ro-Ro operations
0.5 – 3.0	1.0	Site moves
3.0 – 8.0	1.5	Long distance transports

The magnitude of the accelerations in the table above are governed by the emergency breaks. From chapter 2.3.1 (SPMT strength), the maximum speed of the SPMT is limited to 4 km/h when heavily loaded. This limit can be lower if it turns out that the dynamical forces are too high. Because, for a carousel transfer the speed is expected to be lower than 4 km/h , an acceleration of 1.0 m/s^2 will be selected based on Table 2-3.

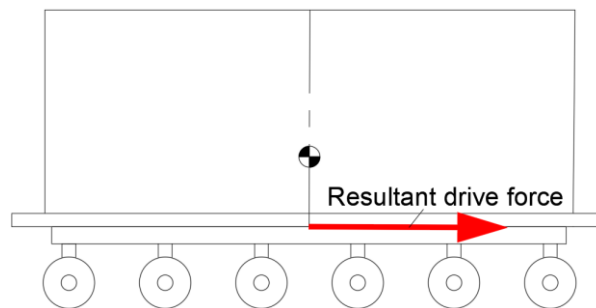


Figure 2-28: Resultant SPMT drive force on carousel

Previously the total weight of the fully loaded CCS during SPMT transport is defined to be $m_{CCS,SPMT} = 6492\text{ Ton}$. Neglecting all resistances and other effects, the needed force for the acceleration can be calculated by Newton's second law

$$F_{SPMT} = m_{CCS,SPMT} a_{CCS,SPMT} \quad (2-10)$$

The resulting drive force is given in the Table 2-4.

Table 2-4: Theoretical driving force to accelerate carousel with 0.5 m/s^2

Description	Abbreviation	Value	Unit
Approx. needed driving force for acceleration of 1.0 m/s^2	F_{SPMT}	$6.5 \cdot 10^3$	kN

As stated before, the drive or brake forces per equipped axle line is approximated 120 kN [32]. For the Mammoet design, 184 SPMT axle lines are used [26], where about 1/3 of the axle lines is driven and 1/3 is equipped with a brake. This results in a total brake / drive force of 7360 kN , which is thus enough capacity for the selected acceleration.

Transfer from/to transport vessel

For each different project multiple Ro-ro ramps are needed to drive with the SPMTs from the quay to the vessel, or from vessel to quay, as schematically visualized in Figure 2-29. There are many kinds of ro-ro ramps where each situation can result in another Ro-ro ramp. This is dependent of the quay dimensions, vessel dimensions, SPMT trains, etc.

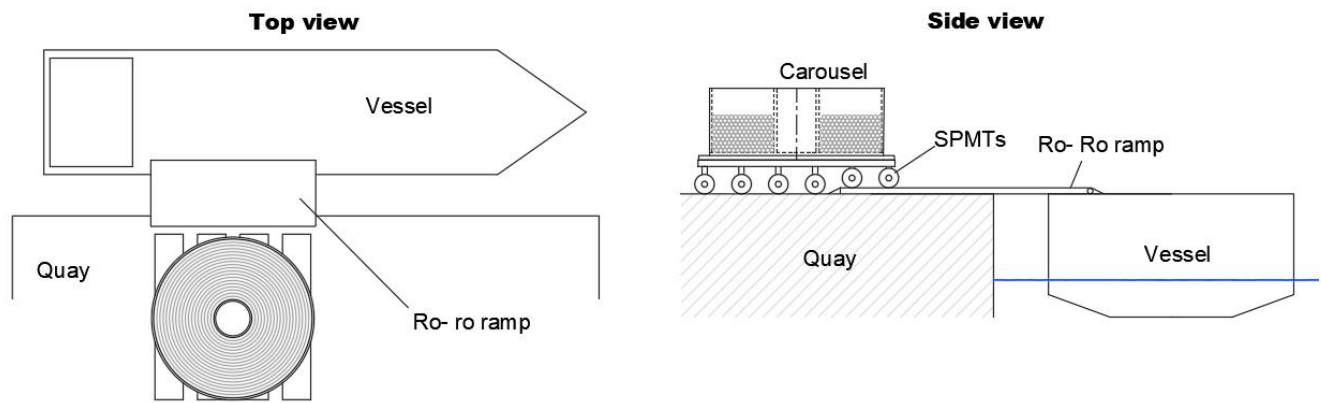


Figure 2-29: Transfer from/to transport vessel by Ro-ro ramp

Because the design of ro-ro ramps has little influence on the carousel design and SPMT setup, the ro-ro ramp is left out of scope. In the design of the ro-ro ramps it must however be included that there is a restriction on the height and slope corresponding to the SPMT cylinder stroke (section 2.3.2).



Figure 2-30: Ro-ro ramps from previous Mammoet projects

Vessel stability

When driving on or entering/leaving the vessel with the carousel, forces are induced on the vessel which influences the stability and orientation of the vessel in the water. These effects are handled by ballast tanks in the vessel where water can be pumped in and out of the vessel tanks to stabilize and control the orientation of the vessel. Some vessels with their ballast pump and tank capacity as given in Table 2-5.

Table 2-5: Transport vessel (Deck carriers) [35]

Name	Deck load [t/m ²]	Deck dimensions [m]	Ballast pump capacity [m ³ /h] ≈ [t/h]	Ballast tank capacity [m ³] ≈ [t]
Boskalis: Target	\	130.0 x 44.5	10000	\
Dong bank: Giant 1	20	113.0 x 32.0	6000	13390
Boskalis-Dockwise: swan	16	126.6 x 31.66	1000	\
ZPMC: Red box vessel 1	25	161.9 x 43.0	2000	92000
Costo: Tai An Kou	18	126.0 x 36.0	8000	\

The ballast pump capacity determines how fast the Ro-Ro operation can be performed. Taking for example the 1000 t/h capacity of the “Swan” from Table 2-5, it follows that at least 6 hours are needed for a 6000 t CCS to keep the same depth of the vessel in the water. For the “Target”, with a capacity of 10000 t/h, at least 6000/10000 = 0.6 h = 36 min are needed. Notice that the ballast pumps are also needed to overcome the tide differences. So, in practice not the entire capacity of the ballast pump can be used for ballast compensation. Also, driving over the vessel with the CCS is limited by the ballast pump capacity. For the design of the CCS the vessel stability has no influence and is thus left out of scope.

2.2.3 Sea transport

During the process, a large amount of time the cable is stored in the carousel. The carousel must resist the load from the cable stack and the load also must be transferred to the quay ground or vessel deck. Because the sea transport results in the highest accelerations on the carousel, and thus the highest loads, the sea transport is governing for the strength and stability of the carousel structure and load transfer. For that reason, the normal storage on the quay will be left out of scope. The sea transport is marked blue in Figure 2-31.

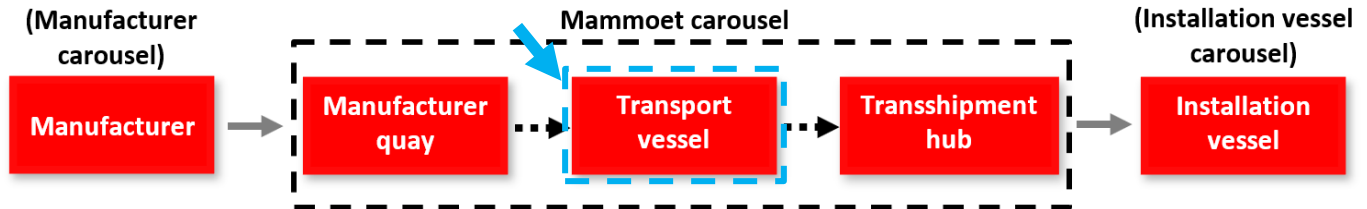


Figure 2-31: Sea transport in transportation process

The carousel will be connected to the vessel deck / quay ground by means of grillage beams (Figure 2-32). These grillage beams support the carousel structure and transfers the loads to the ground / vessel deck below. For the sea transport the grillage beams will be welded to the vessel deck.

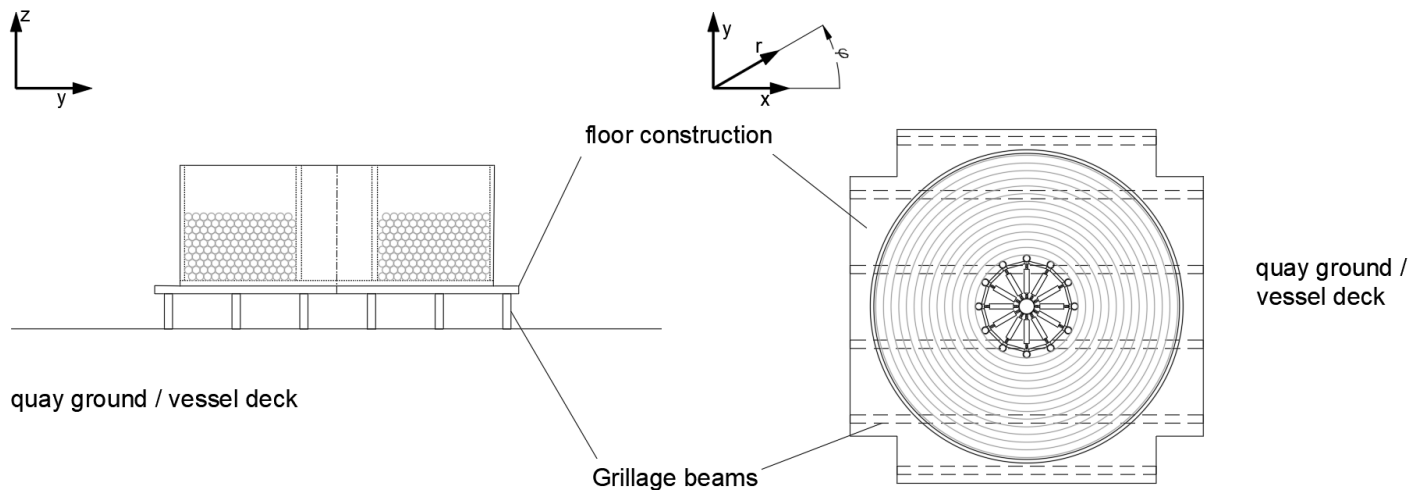


Figure 2-32: Carousel on quay or vessel deck

Sea transport accelerations

Besides gravity, the carousel will be subjected to accelerations due to the vessel motions during sea transport. The vessel motions with the most effect include the pitch, heave, and roll of the vessel, shown in Figure 2-33.

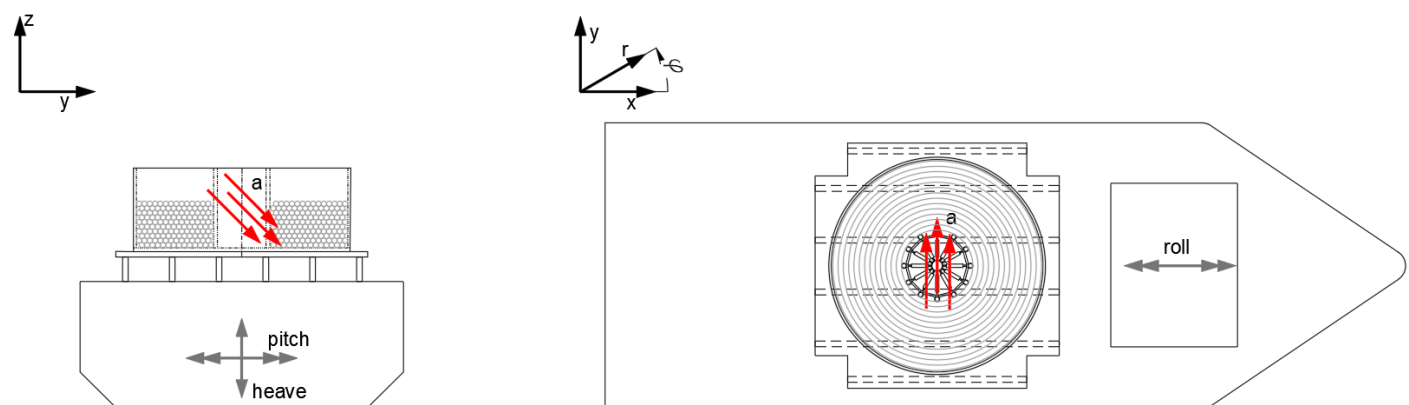


Figure 2-33: Ship motions and induced acceleration on carousel

The resulting accelerations on the carousel due to sea transport are given in Table 2-6 [26] [27]. Same accelerations as used in the design calculations proposed by Mammoet will be used for comparison.

Table 2-6: Vessel accelerations for sea transport based on current design

	$a_{x,pitch}$	$a_{y,roll}$	$a_{z,heave}$
Value	$\pm 0.20G$	$\pm 0.50G$	$\pm 0.30G$

Notice that the vessel pitch causes an acceleration in the x direction, the roll an acceleration in the y direction and the heave an acceleration in the z direction on the carousel. The accelerations are induced on the entire carousel, so on the self-weight of the carousel structure, floor, and grillage, but also on the cable stack inside the carousel. $a_{z,heave}$ should be combined with gravity as it has the same direction.

Loads on carousel

The sea transport is governing for the loads on the carousel due to the high accelerations. For the load on the carousel from the cable stack there are many uncertainties, these will be further investigated in chapter 5. For chapters 3 and 4, simplifications and assumptions regarding the load on the carousel will be made and described in this paragraph. Between the carousel and the cables, the main interaction forces consist of compression forces and frictional forces, as shown in Figure 2-34.

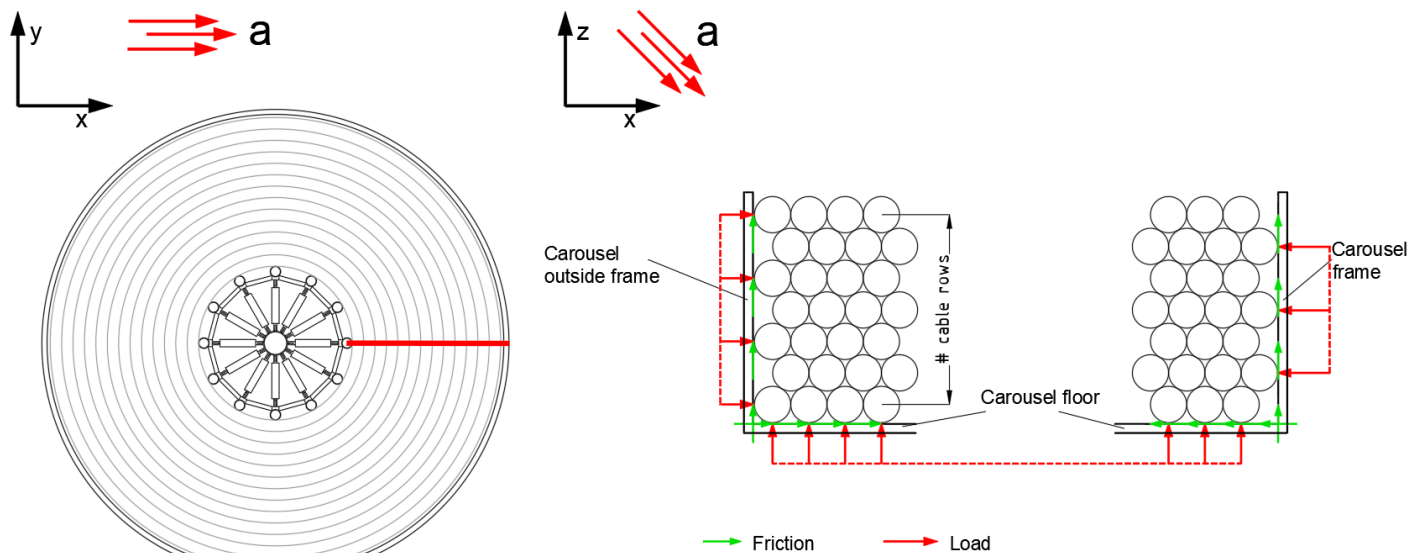


Figure 2-34: Interaction forces between cables and carousel

An overview of the made assumptions and simplifications regarding the load on the carousel is give in Table 2-7.

Table 2-7: Loads on carousel and assumptions

Load (effect)	Treatment	Description
Second order effects	Neglected	Movement of the cable stack and large deformations of the carousel are unwanted. Therefore, it is assumed that second order effect doesn't have a large influence and they will not be considered. So, the effect of the deformation of the carousel and the cable stack on the load on the carousel is not considered.
Friction walls – cable stack	Neglected	Because it is expected that there is not much tendency of the cables to move along the carousel walls it is assumed that the main interaction forces are compression forces. Furthermore, the effect of friction is difficult to determine, and its magnitude is uncertain and dependent on the conditions. As a result, it is assumed that the friction on the outside and inside frames is negligible. It is expected the neglecting the friction is worst-case-scenario, which makes it a sufficient assumption. This assumption is validated in chapter 5.
Load on floor	Uniform pressure distribution	It is assumed that the load on the floor from the cable stack has a uniform distribution, only depended on the cable stack weight and the acceleration in the z direction. The effects of the horizontal acceleration and the load distribution in the cable stack on the load on the floor neglected. These effects are further investigated in chapter 5.
Load on outer wall	Neglected	See next paragraph “ neglecting load on outer wall ”
Load on inner wall	Uniform distribution on pressure side	See next paragraph “ load on inner wall ” Uniform distribution on poles where pressure occurs. The magnitude is only dependent on the cable stack weight and horizontal acceleration. The direction of the load is towards the axis of the carousel. Effect of vertical acceleration and load distribution in the cable stack are neglected. These effects are further investigated in chapter 5.
Friction floor – cable stack	Neglected	Due to the high uncertainty of the magnitude of the friction and because friction causes a more favorable load distribution on the carousel (partly transfer of horizontal load to the floor instead of all horizontal loads to the inner frame), friction is neglected for chapters 3 and 4. Friction between the floor and the cable stack will be further investigated in chapter 5.

Neglecting load on outer wall

The load on the outer wall is caused by the cable stack pressing on the outer wall. This load from the cable stack on the outer wall causes deformation of the outer wall and as a result, the cable stack can deform as well. If the cable stack can't deform further due to its own stiffness, the load on the outer wall is also reduced. In Appendix B rough estimations have been done to determine the expansion of the cable stack if the outer wall is neglected. The input for this study is shown in Table 2-8.

Table 2-8: Input cable stack expansion study

Description	Abbreviation	Value	Unit
Outside carousel radius	R_{carousel}	13.3	m
Inside carousel radius	r_{carousel}	4.375	m
Carousel height	h_{carousel}	5.80	m
Carousel capacity	C	5000	t
Cable diameter	D_{cable}	190	mm
Axial elastic modulus cable	$E_{\text{cable,axial}}$	5.0	GPa
Radial elastic modulus cable	$E_{\text{cable,radial}}$	1.0	GPa
Horizontal acceleration	/	5.0	m/s^2

The results from Appendix B are summarized in Table 2-9.

Table 2-9: Results cable stack expansion study

Description	Change of radius	Unit
Cable stack expansion under self-weight and axial stiffness of cables	12	mm
Cable stack expansion under horizontal acceleration and axial stiffness of cables	0.65	mm
Cable stack expansion under radial deformation of bottom cables	0.87	mm

Notice that over for a cable stack radius of $13.3m$, a radius increase of 11.7 mm equals a cable stack expansion of 0.09% . The results in Table 2-9 thus show that the cable stack doesn't expand that much under the input from Table 2-8. This means that if the inner frame has sufficient stiffness to hold the cable stack on its place, the load from the cable stack on the outer wall is also limited and dependent on the stiffness of the outer wall. Furthermore, the outer wall can't have more deformation than the cable stack. Therefore, under the assumption that the inner frame has enough stiffness and that the outer wall has no resistance, the load on the outer wall will be neglected. This causes all the horizontal load to be transferred through the inner frame and the friction between the cable stack and floor, where the last is also neglected. Neglecting the stiffness and effect of the outer wall is a worst-case-scenario for the load distribution over the CCS and thus makes is a sufficient assumption for the design of the other components of the CCS.

Load on inner wall

It is assumed that the load on the inner wall is only caused by the horizontal acceleration on the cable stack. Because the friction with the floor and the load on the outer wall are neglected, all the horizontal load on the carousel needs to be transferred by the inner frame. The cable stack induces load on the poles of the inner frame. It is assumed that each pole under compression experiences the same uniformly distributed load at the places of contact with the cable stack in radial direction of the carousel, as shown in Figure 2-35. Notice that another direction of the acceleration in the $x - y$ plane changes the poles which experience loading. The load on the pole consists of point loads at the places where there is contact with a cable. This is simplified by assuming a uniformly distributed load over the whole pole, which is also shown in Figure 2-35.

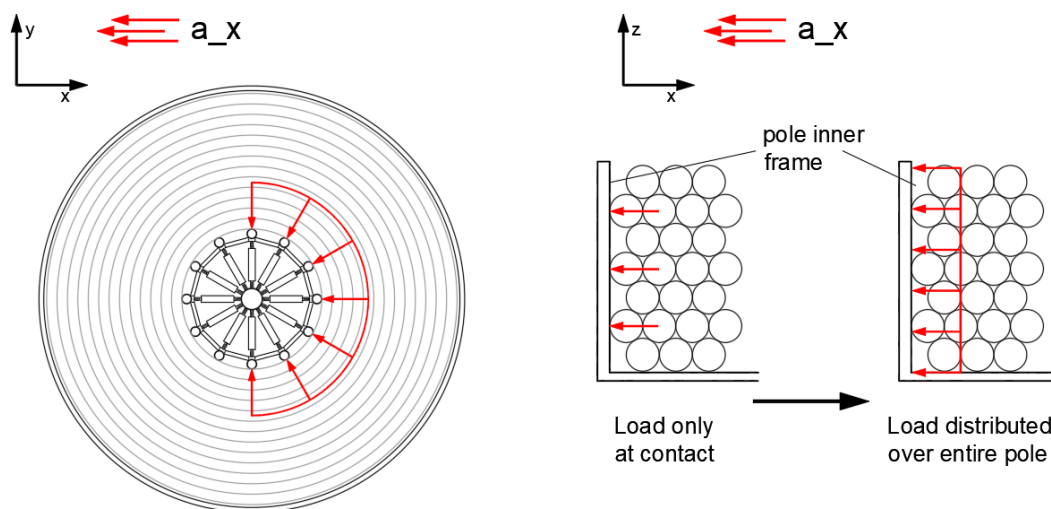


Figure 2-35: Load on inner frame

Load transfer

The loads on the CCS will be transferred through the inner frame or directly to the floor structure. For the load transfer from the carousel floor there are multiple options:

- Carousel floor → SPMTs → vessel deck
- Carousel floor → SPMTs → quay
- Carousel floor → Grillage frame → vessel deck

Other cases such as the grillage frame on the quay and driving over the Ro-Ro ramp are left out of scope as these are not governing for the CCS design. It is important that all the structural components and connections can resist the occurring loads.

Vessel deck

A vessel consists out of different compartments, separated by longitudinal and transverse bulkheads (Figure 2-36). These are the strong supports of the vessel deck, but their presence is limited (Figure 2-37). Furthermore, the deck of a vessel consists out of strong transverse web frames and less strong deck longitudinal frames, which transfer the load to the bulkheads of vessel walls. The transverse web frames will carry most of the load and thus the load mainly needs to be transferred to these frames. The distance between the transversal frames is estimated at $2m$ to $2.5m$, depending on the vessel [27].

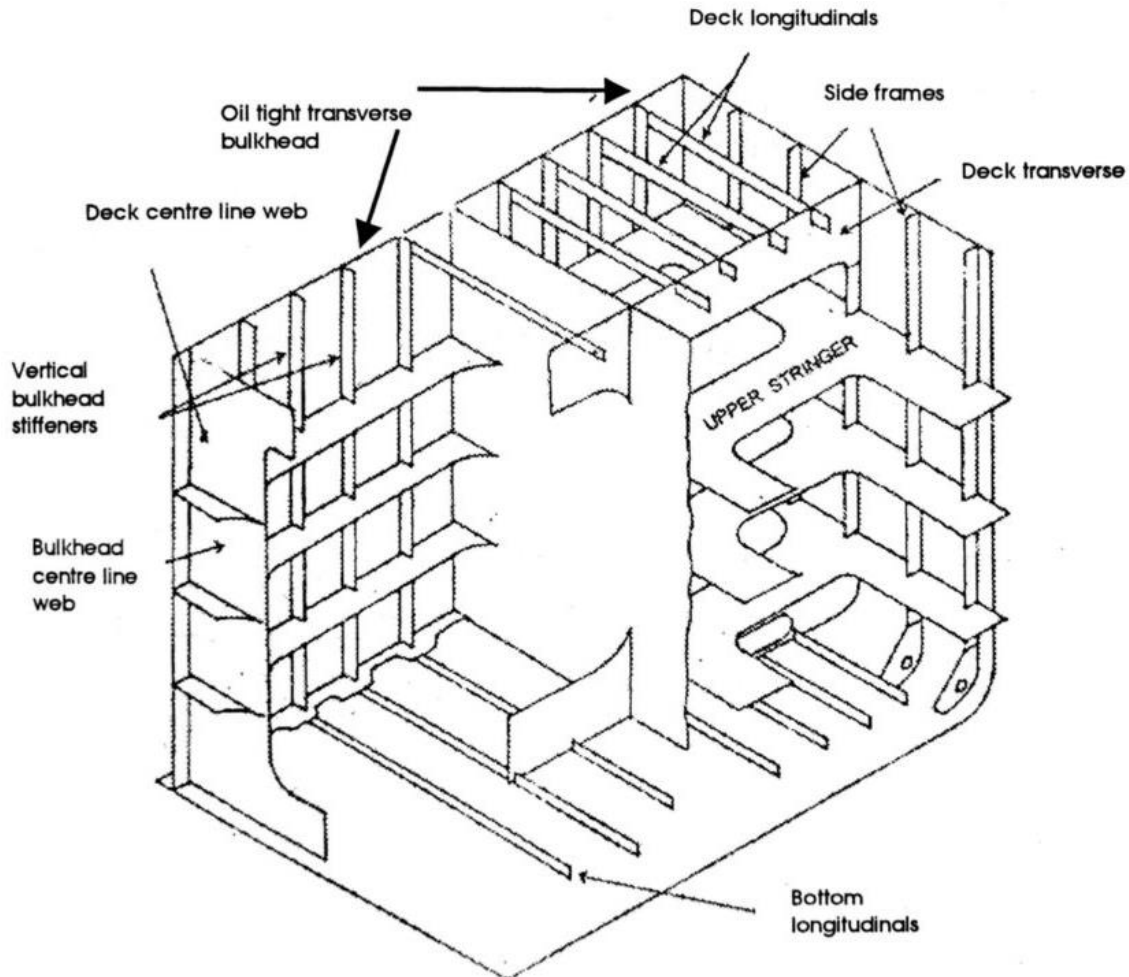


Figure 2-36: Vessel bulkheads, deck longitudinals and deck transvers frames [36]

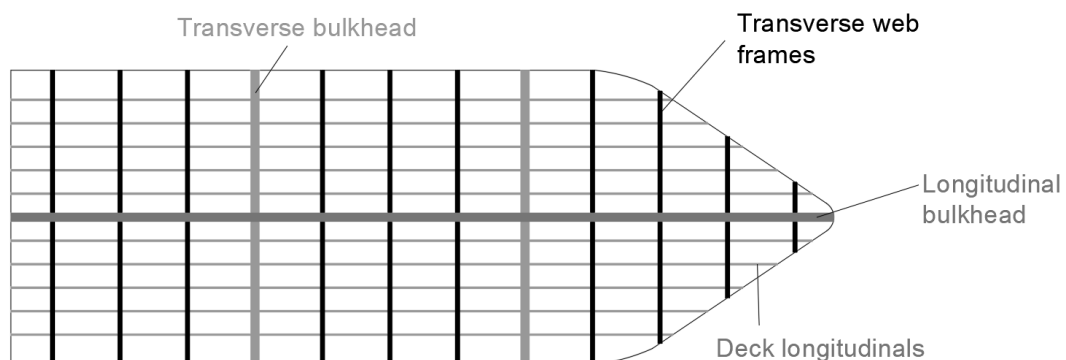


Figure 2-37: Vessel bulkheads, deck longitudinals and deck transverse frames schematic overview

2.3 Challenges

In this section the challenges and restrictions for the CCS, resulting from the process analysis, will be explained.

2.3.1 Strength and stability

Stability of SPMT support

The SPMTs have a shared hydraulic zone where there is a hydraulic connection between the cylinders in the trailer bogies / axle lines. Due to this connection the pressure in the cylinders and therefore the forces in the cylinder are equal within a hydraulic zone. Therefore, the resultant reaction force of the SPMTs on the cargo is always in the middle of the hydraulic zone, as can be seen in the 2D example in Figure 2-38 with two hydraulic zones.

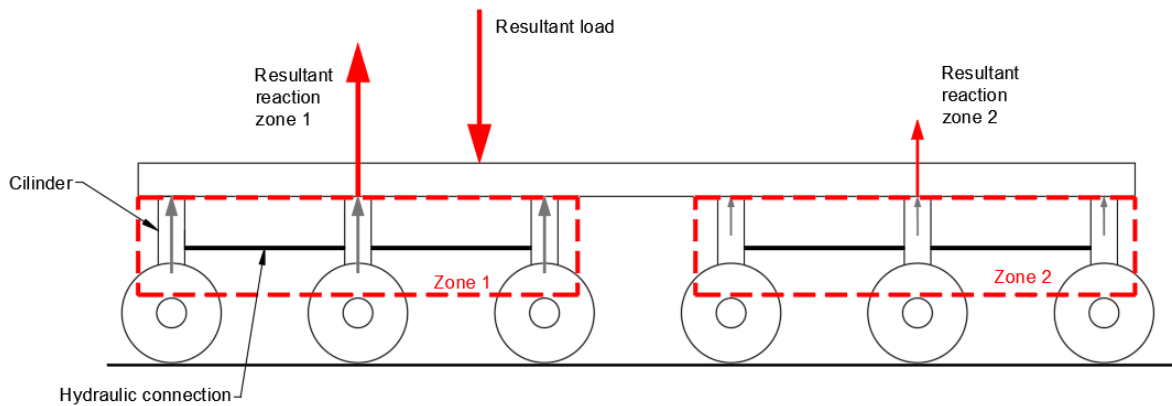


Figure 2-38: Example hydraulic zones for SPMT with 6 axle lines

The load on a hydraulic zone is thus equally spread over all the tires. To be stable in all direction at least 3 hydraulic zones are needed. The resultant reaction force from the SPMTs on the cargo, due to of all external moments, forces, and accelerations, needs to be within the virtual support area enclosed by the hydraulic zone centers. This is equal to the restriction that each SPMT must deliver a pressure to the cargo, and not pull against the cargo. For the transport of the carousel there is an option of using 3 or 4 zones (Figure 2-39). For the SPMT setup there are many options, which will be discussed later.

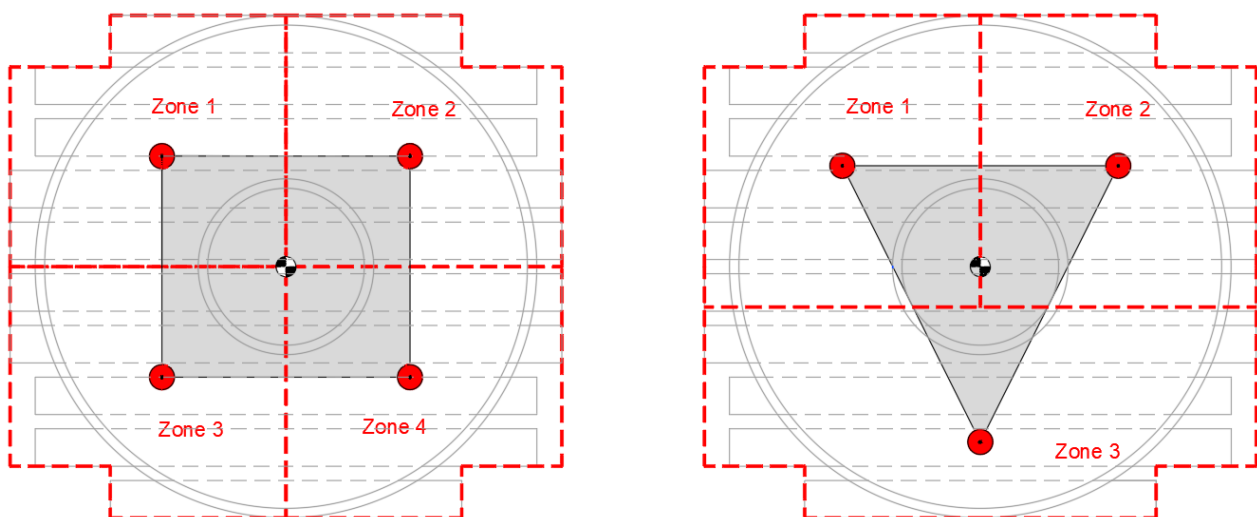


Figure 2-39: Virtual support area for stable resultant reaction force

Because the carousel has a low COG compared to the diameter, the stability of the SPMT transport is not an issue. The disadvantage of using 4 hydraulic zones is that it is statically undetermined, which makes the transport prone to differential settlements and which makes it more difficult to calculate load distribution. Using 4 hydraulic zones however leads to less deflection and stress in the transport [27]. For that reason, it is chosen to use 4 hydraulic zones.

SPMT strength [32]

It must be ensured that the occurring strength in the SPMTs is below the allowable strength. The maximum payload on the SPMT is dependent of the SPMT type and the tires used. Within Mammoet most SPMTs can handle a maximum load of 40 t per axle line (AL in Figure 2-40), including the self-weight and dynamic loads.

The self-weight of the SPMT is approximated 3 t/m, whereas the SPMT length for each axle line is 1.4m (Figure 2-40). Thus, the self-weight of the SPMT gives a load of $3 \cdot 1.4 \approx 4$ t per axle line. Because the self-weight of the SPMT is equally spread over the axle lines it has not much effect on the stress and deformation of the SPMT and therefore the self-weight of the SPMT will be neglected. The maximum payload per axle line, including dynamical effects, is thus 36 t, where the self-weight of the SPMT is already taken into account. Also, special SPMT setups applicable to higher loads can be used, but this is left out of scope because it is beneficial if all SPMTs from Mammoet can be used for the carousel transport.

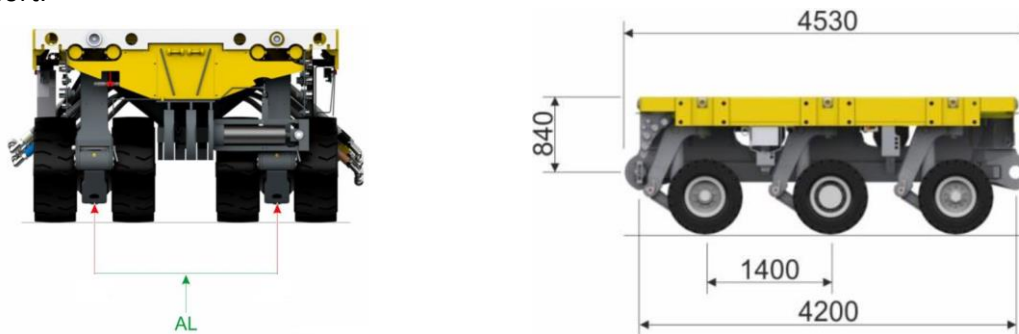


Figure 2-40: SPMT with 3 axle lines

Notice that the 4200 mm for pin-hole to pin-hole connection is a multiple of 1400 mm. Thus the SPMTs can be coupled while for each axle line in the SPMT train the axle line to axle line distance will be maintained at 1400 mm.

Because the CCS has a long travel distance for the cable spooling, air filled tires must be used. These tires of the SPMT can handle 10 t per tire, including additional dynamical effects. This thus also leads to a maximum of $4 \cdot 10 = 40$ t per axle line, including dynamical effects. The manufacturer states that under this maximum load the tire is limited to a drive speed of 4 km/h where still the load on the tire including dynamical loads may not exceed the 10 t maximum. Furthermore the manufacturer states that fully loaded to tires can drive a maximum distance of 10 km. Because more distance needs to be travelled by mostly the outer SPMTs of the CCS it is demanded not fully load the tires.

So, to satisfy the strength criteria of the SPMTs the following requirements must be satisfied as defined in Table 2-10.

Table 2-10: Requirements SPMTs

Description	Value	Units
Maximum load per axle line (including dynamic effects and self-weight SPMT)	40.0	t
Self-weight SPMT par axle line	4.0	t
Maximum load per axle line (including dynamic effects and excluding self-weight SPMT)	36.0	t
Maximum drive speed under full load	4.0	km/h

Ground pressure

The pressure from the CCS induced on the vessel deck and quay is also limited. The maximum deck load for some vessel can be found in Table 2-5, where the vessel with the least capacity has a maximum deck load of 16 t/m² on average. Locally higher pressures nearby the deck reinforcements can be induced on the deck. The Mammoet quay in Schiedam has a ground bearing capacity of 10 t/m² [37]. On both the quay and vessel the load from the CCS can be transferred to the ground by SPMTs or the grillage frame. These induce locally higher pressures on the ground. For the quays the load bearing pressure can be calculated by [38]

$$GBP = \frac{\text{Total transport load}}{\# \text{ axle lines} \cdot 1.4 \cdot 2.9} \quad (2-11)$$

Considering 1 axle line with a maximum loading of $40t$ (including the SPMT self-weight) it follows that the $GBP = 9.9 t/m^2$. This means that if the ground bearing capacity of the used quay is larger than $9.9 t/m^2$ then the maximum load on the SPMTs is governing for the pressure on the quay. Because the capacity of the Mammoet quay in Schiedam is larger than $9.9 t/m^2$, the ground bearing pressure is left out of scope for this study. When the CCS is supported by the grillage the weight of the SPMTs is not applicable and thus the load on the ground is also lowered, such that this is also not governing for the average ground bearing pressure. If the CCS with grillage support induces to large local pressure, additional load spreaders can be used, but this is also left out of scope for this study as this is not governing for the design of the CCS. Because the vessel decks have more capacity than the $10 t/m^2$, the load on the vessel deck is also neglected for the design of the CCS. Also, for the vessel deck load spreading can be used if to large local pressures occur.

Tensile stress in connections with vessel deck

Figure 2-41 shows how the horizontal acceleration a on the carousel causes a resultant horizontal force F_{res} on the inner frame. With the arm h_{res} this leads to a bending moment M_{res} on the floor structure of the CCS. Because friction with the floor and the cable stack and the outer frame are neglected, all the horizontal loads from the cable stack will be transferred through the inner frame, which causes a large M_{res} on the floor structure. The floor must have enough strength and stiffness to resist this bending moment. Furthermore, this bending moment on the floor can cause tensile in some part of the welds between the grillage frame and the vessel deck (location shown in Figure 2-41). The welds must have enough strength to resist these tensile forces.

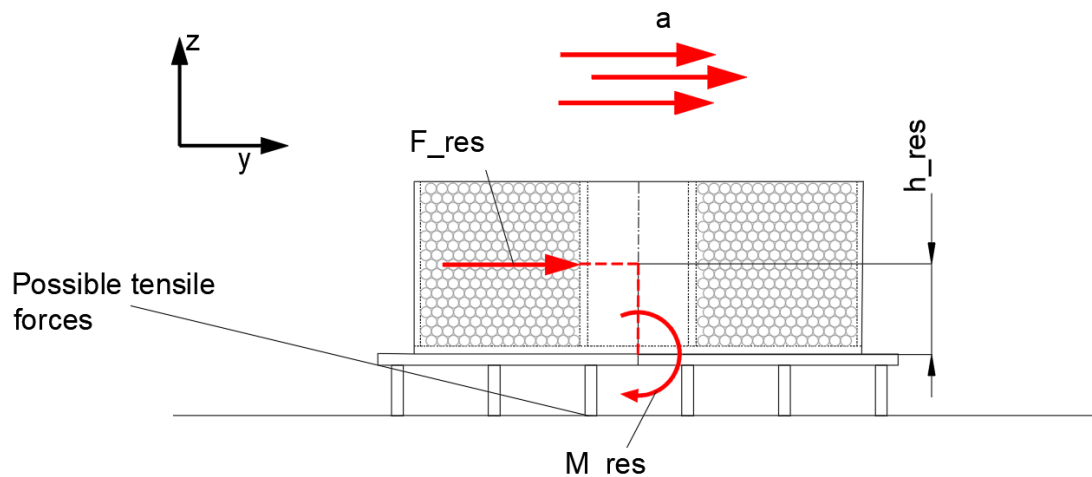


Figure 2-41: Bending moment on floor due to horizontal load

Structural strength and stability

Due to the loading on the CCS all structural components and connections must satisfy the strength and stability criteria. Connections are left out of scope for the study. The structural components are discussed in chapter 3 and the assessment against strength and stability is done in chapter 4.

2.3.2 SPMT cylinder stroke

SPMT Stroke

The SPMTs consist of coupled hydraulic cylinders. All the cylinders have an available stroke of 700 mm [32]. From Mammoet it is advised to use no more than 70% of the available stroke, and thus the operational stroke is limited to $700 \cdot 0.7 = 490\text{ mm}$ [39]. Factors which need to be considered for the available stroke are:

- Ground conditions (slopes, camber, unevenness, RoRo ramps)
- Lift and drop heights, previously assumed to be around 250 mm
- Deflection of SPMT

All factors may not exceed the available stroke of 490 mm . Due to the lift and drop height only $490 - 250 = 240\text{ mm}$ is remaining to overcome ground conditions and SPMT deflection. Stroke used to compensate for SPMT deflection can't be used for other tasks, such as to overcome the ground conditions. Figure 2-42 visualizes the effect of deflection (S1) and the effect of ground conditions (S2) on the stroke.

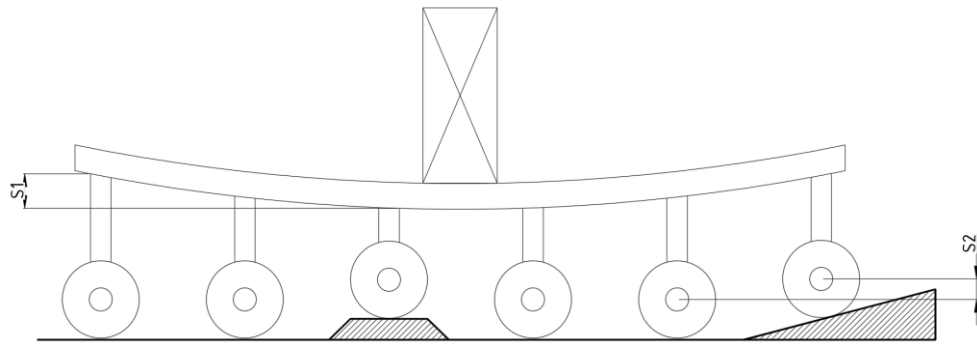


Figure 2-42: Stroke usage of SPMT where S_1 is due to SPMT deflection and S_2 due to ground conditions

Another effect of ground unevenness, also called differential settlements, is that some hydraulic zones have higher pressures than other hydraulic zones. This especially is the case when 4 hydraulic zones are used. 4 hydraulic zones are statically undetermined, and it can occur that one zone isn't loaded on its full capacity.

SPMT deflection

As discussed in the paragraph before, the deflection of the SPMTs uses a part of the cylinder stroke. It is important to have a good insight in the deflection such that it can be determined how much cylinder stroke is available to overcome the ground conditions (for example the height difference when entering / leaving the Ro-ro ramp). SPMT deflection can occur when one or both of the following holds:

- The axle load is high
- Many axle lines are unsupported

Thus, if a few axle lines of the SPMT are outside the cargo support, deflection of the SPMT can occur. This is because the axle lines will keep a constant pressure due to the hydraulic connections of the cylinder, whereas there is no load on the unsupported axle lines. An example where this effect occurs for cargo with large stiffness can be seen in Figure 2-43.

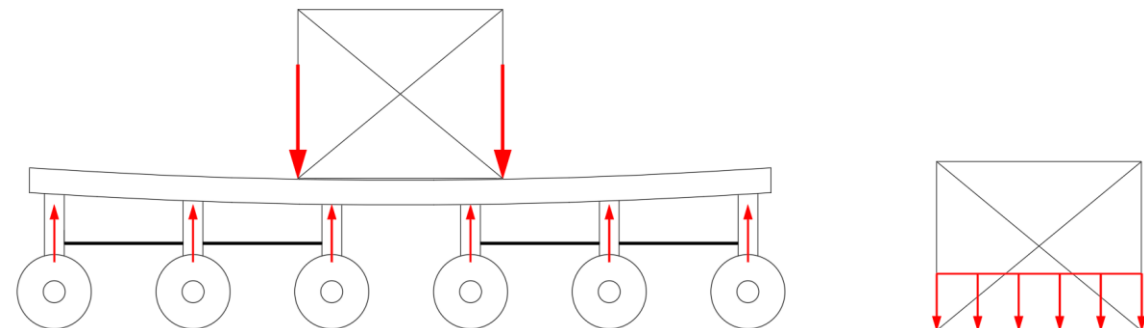


Figure 2-43: Deflection of SPMT and effect on contact area stiff cargo

The figure also shows another effect. If deflection occurs in the SPMTs and the cargo is stiff, there is possibly only contact with the SPMT at the corners of the cargo. Due to small contact areas, high pressures can occur, possibly leading to failure. A stiffer cargo however does reduce the deflection of the SPMTs which can be useful. It is thus important to also incorporate the stiffness of the carousel and the cable stack when determining the SPMT deflection. Figure 2-44 schematically visualizes these effects for a different carousel and cable stack stiffness.

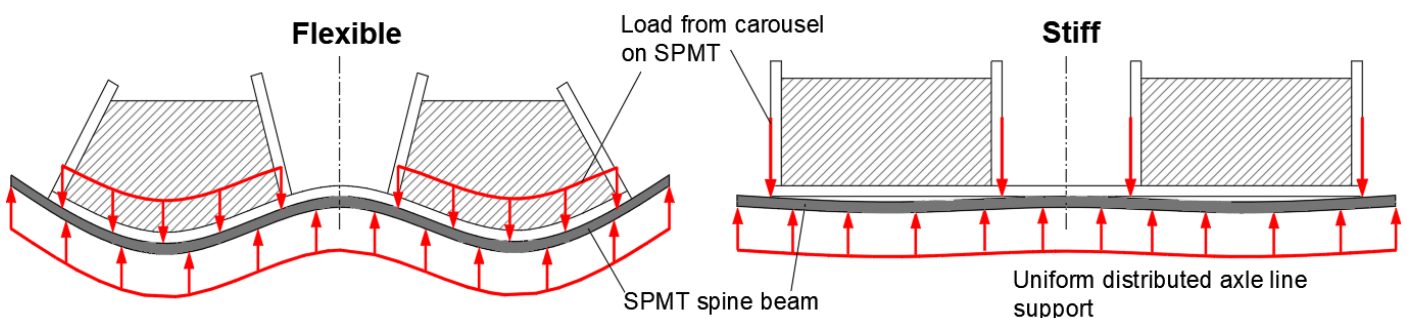


Figure 2-44: Schematic SPMT deflection for flexible and stiff carousel and cargo

As an example, a single SPMT train will be selected to investigate the effect of the carousel stiffness for the 2D case. Figure 2-45 shows the global setup and the dimensions for the selected SPMT train from the CCS design from Mammoet [26].

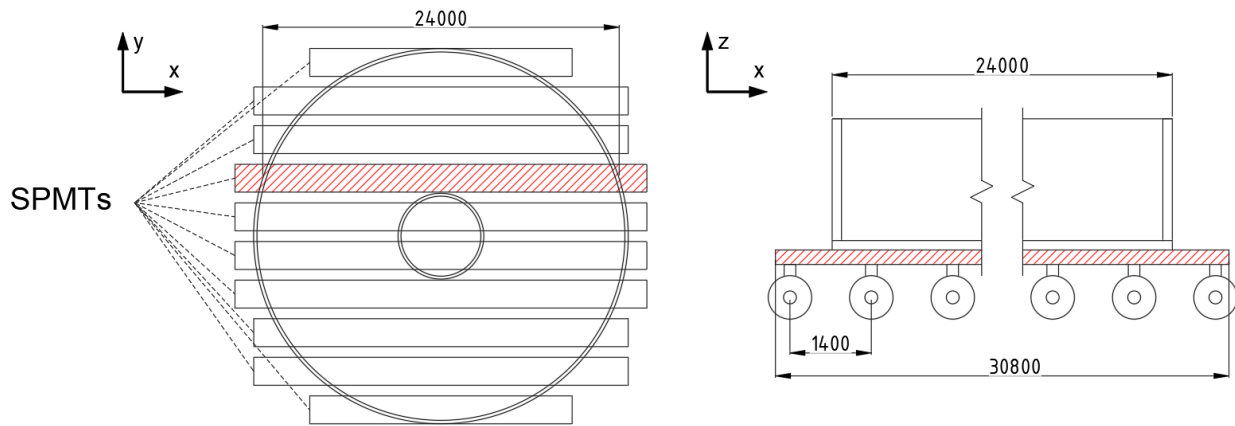


Figure 2-45: SPMT setup and dimensions for 2D deflection example

The selected SPMT has a length of 30800 mm with 22 axle lines, where it is assumed that each axle line activates 1400 mm of the SPMT, such that a uniformly distributed load over the 30800 mm can be assumed. Neglecting the self-weight of the SPMT, an axle line load 36 t per axle line is assumed for the payload on the SPMT. For the selected SPMT train it is assumed that the total magnitude of payload from the carousel on the SPMT equals the total magnitude of support load from the axle lines, such that the simplified 2D case is in equilibrium. The carousel at the selected SPMT has a width of approximated 24 m, which is thus used for the length of the payload on the SPMT. Effects of the other SPMTs and the stiffness of the carousel lateral to the SPMT is also neglected. The resulting loads on the spine beam of the SPMT are shown in Figure 2-46.

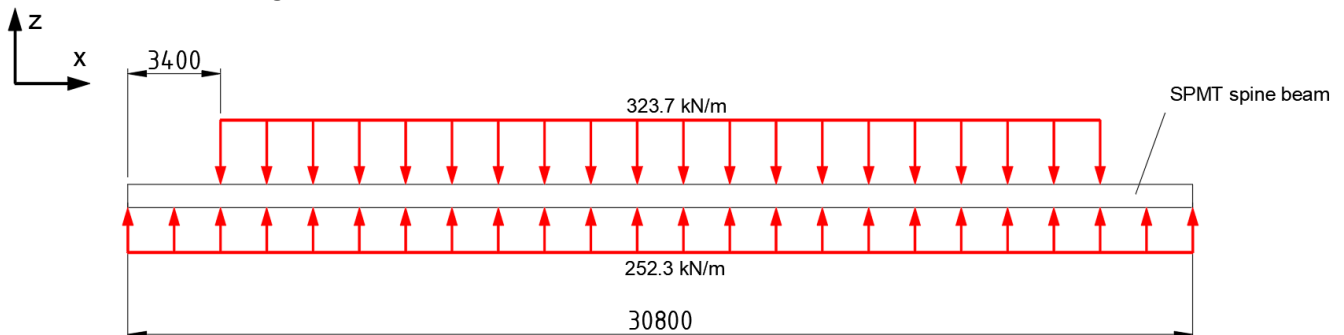


Figure 2-46: Loads on SPMT spine beam for selected SPMT train

The spine beam of the SPMT is responsible for the stiffness of the SPMT train itself. However, to incorporate stiffness for the 2D case of the carousel and cable stack an extra beam will be added, shown Figure 2-47. This beam is connected to the spine beam by dummy elements. The dummy elements have (except one dummy element) at the connection with the beam for additional stiffness a sliding support in the x direction and a free rotation around the z axis, such that clamping forces are avoided. The dummy elements are made very stiff such that then don't deform, and they have a pressure only non-linearity which allows release of the beam with additional stiffness from the spine beam.

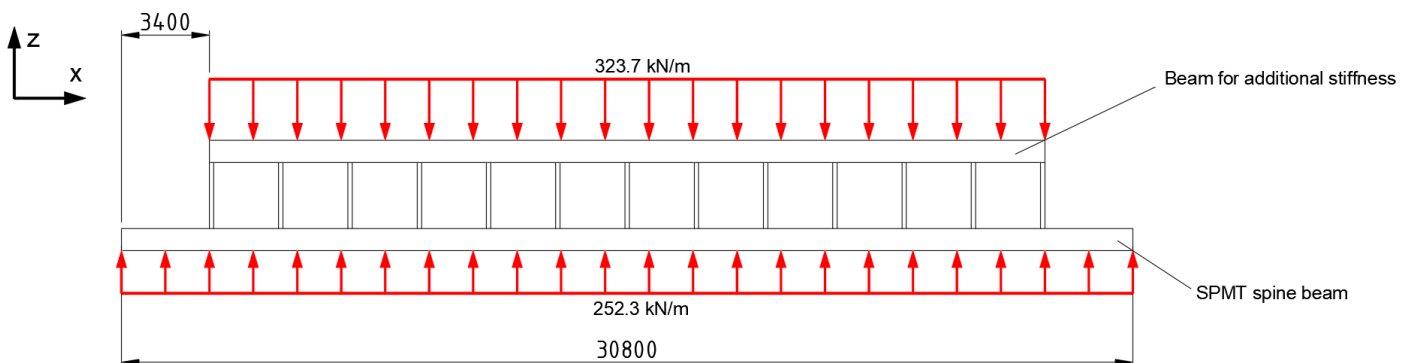


Figure 2-47: Loads on SPMT spine beam for selected SPMT train with additional stiffness

Different stiffnesses for the additional beam has been simulated for the above situation. A description of the study can be found in Appendix B.4. The results are plotted in Figure 2-48, which shows the highest deflection of the SPMT spine beam (and thus the needed stroke for the deflection of the SPMT) against the stiffness of the additional beam.

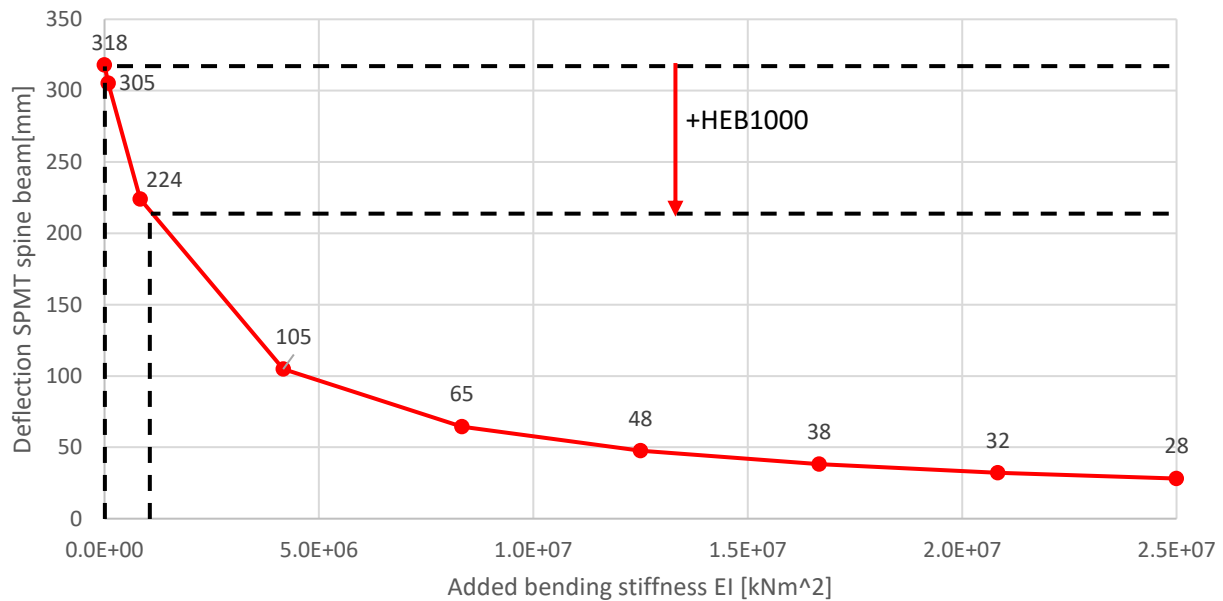


Figure 2-48: Deflection of the SPMT

A steel HEB 1000 beam has a stiffness EI of $1.0 \cdot 10^6 \text{ kNm}^2$. In the figure the deflection drop for adding a steel HEB 1000 of stiffness is shown. Figure 2-48 shows that for a low carousel stiffness and low cable stack stiffness there is a deflection of more than 300 mm for the selected input, which can be problematic.

2.3.3 SPMT issues

Figure 2-21 shows that, especially for a smaller cable diameter D_{cable} and thus a smaller cable mass μ_{cable} , the outer SPMTs need to travel large distances of a few hundred hours and kilometers with a total weight up to 6492 Ton. This is a challenging task for the SPMTs and can cause some difficulties:

- **Wear:** Due to the high load and the large distance some SPMTs (mostly at the outside) need to travel, the tires are prone to wear. The carouselling movement enlarges the wear because there is more chance that some wheels will slip compared to each other. To minimize the wear of the tires it is important to minimize the slopes and cambers and unevenness in the underground.
- **Temperature:** The motors are driven by hydraulics, where the hydraulic pressure is regulated by pumps. These pumps are driven by a generator with fuel. A lot of heat will be generated by the generator. If the environmental temperature is high, and the hydraulic motors require a lot of hydraulic power for many hours, the temperature can reach the limits. If this happens, the process needs to be paused until the temperature is low enough.
- **Hydraulic leakage:** The hydraulic cylinders of the SPMTs are heavily loaded. Along with the hydraulic motors this puts a lot of stress on the hydraulic system of the SPMTs. This makes the hydraulic system prone to leakage of oil.

Because of the issues above it is preferred that the SPMTs below the CCS are easily accessible. Also, the hydraulics and the tires must be effectively monitored because the inside carousel can't be seen by the operator(s). As discussed before, a flat ground with no unevenness minimizes the issues discussed above.

It is expected that the spooling operation by SPMTs needs to be stopped for a few times to execute maintenance for both tires and hydraulics. This extra maintenance must be considered in the spooling time. Especially if the center SPMTs have oil leakage or damaged tires, it takes some time to fix.

2.4 Conclusion

The objective of chapter 2 is to define the main challenges / problems to be addressed for the CCS. The resulting main challenges for the CCS defined by the process analysis are summarized in Table 2-11.

Table 2-11: Challenges for the CCS from the process analysis

#	Challenge for the CCS
1	The strength and stability requirements must be satisfied for the CCS. The sea transport accelerations on the full payload are governing for the needed strength and stability of the structural components. The strength and stiffness of the structural components of the CCS are however limited to the maximum SPTM load and vessel deck load. Making the CCS stronger and stiffer namely increases the weight of the CCS and thus also the load on the SPMTs and the vessel deck.
2	The total used stroke of the SPMT cylinders can reach their operational limits due to: <ul style="list-style-type: none">- Stroke needed for lifting- Stroke due to SPMT deflection- Stroke needed for ground unevenness, camber, slopes, and RoRo ramps
3	The high load and operation time of the SPMT transport can result in issues with the SPMTs: <ul style="list-style-type: none">- Tire wear- Hydraulic leakage- Overheating of generator

In objective of the following chapters is to tackle these challenges in the CCS design.

3 Conceptual solutions

The previous chapter describes the problems in general corresponding to the cable carousel system. Mammoet already proposed a concept for the CCS. This chapter describes which design choices can be made for the CCS to tackle these challenges. Also, the design choices made by Mammoet are discussed and used as a reference.

Concept proposed by Mammoet [26] [27]

From chapter 2 Table 2-1, the general input from the CCS design proposed by Mammoet is given in Table 3-1.

Table 3-1: General input CCS

Description	Abbreviation	Value	Unit
Outside carousel radius	$R_{carousel}$	13.3	m
Inside carousel radius	$r_{carousel}$	4.375	m
Carousel height	$h_{carousel}$	5.80	m
Carousel capacity	C	5000	t
Radius most outer SPMT axle line	$R_{o,SPMT}$	15.0	m
Total mass of carousel (floor, inner frame, outer frame, and all other component)	$m_{carousel}$	592	t
Total mass of the floor of the carousel	m_{Floor}	400	t
Total mass of the grillage frame of the carousel	$m_{grillage}$	127	t
Total mass of the SPMT trains for the SPMT transport	m_{SPMT}	800	t
Number of axle lines	/	184	/

The concept proposed by Mammoet is schematically visualized in Figure 3-1.

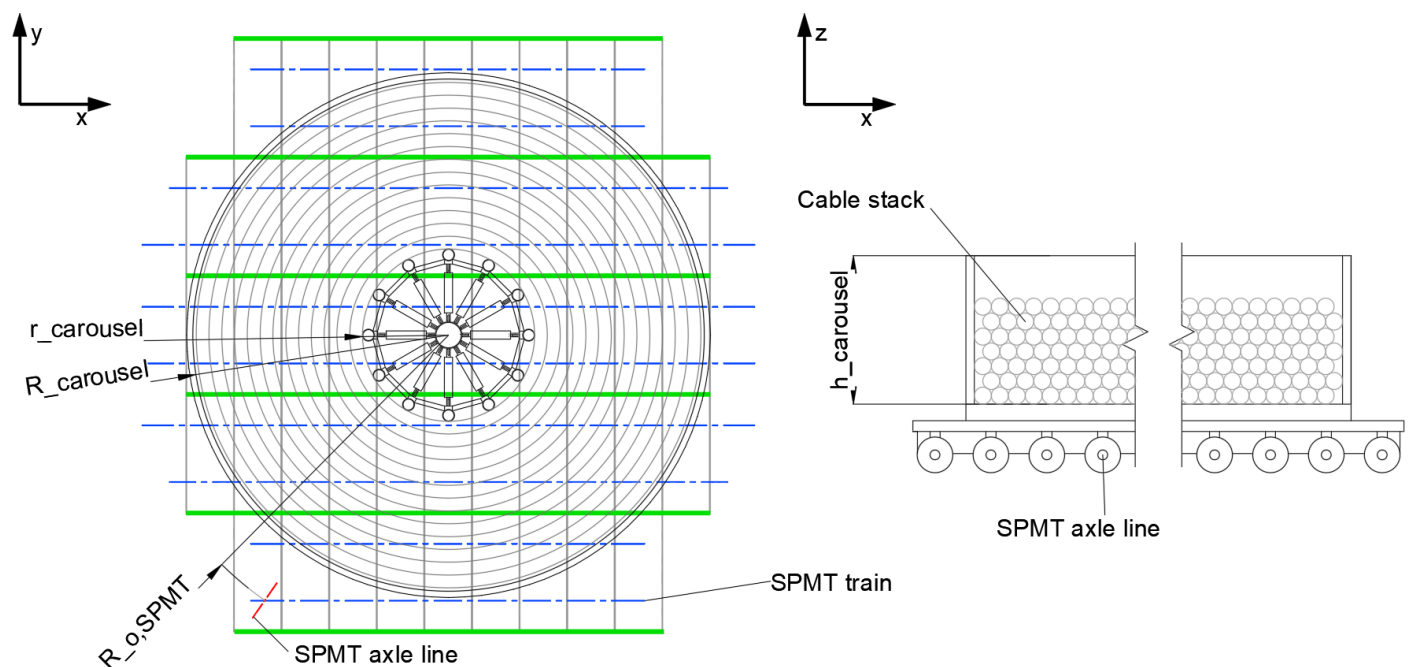


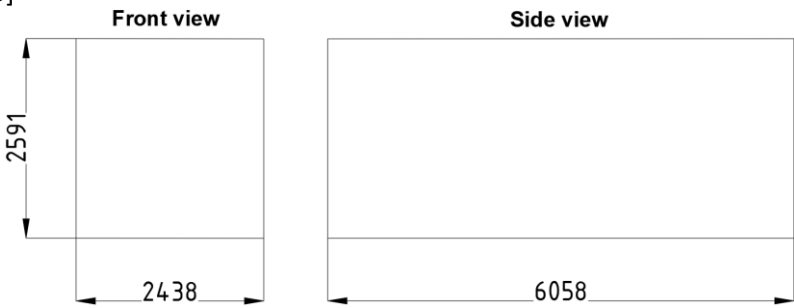
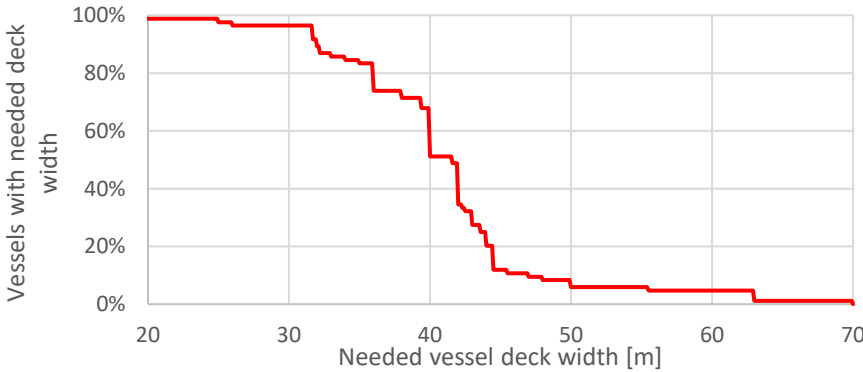
Figure 3-1: CCS concept proposed by Mammoet, schematic overview

In Figure 3-1 the grillage beams are marked **green**, the SPMT trains are marked **blue**, and the most outside SPMT axle line has been marked **red**. For the concept design by Mammoet 10 SPMT trains are used with a total of 184 axle lines. The floor construction of 51 standard 20 feet reinforced container plates (6058 · 2438 mm).

3.1 Boundary conditions

For the concept design of the CCS there are several requirements defined which must be satisfied. These are stated in the Table 3-2. Research boundaries used as reference are defined previously in Table 1-2.

Table 3-2: Requirements for the concept design of the CCS

#	Requirements	Reference
1	The CCS concept must fulfill its functions as described in chapter 2. The scope of the study is improving the concept from Mammoet	Research boundary 1
2	Carousel capacity C must be 5000 t	Research boundary 5
3	An offshore power cable with a diameter D_{cable} between 100 to 300 mm must fit in the carousel, where the total stack has a weight of 5000 t	Research boundary 7 Figure 2-8
4	CCS floor must be containerized. For the concept design the standard 20-foot container will be governing. If necessary, also other types of containers can be used. Most of the CCS parts are thus limited to the 20 feet container dimensions shown in the figure below [40]	Research boundary 2
<div style="text-align: center;">  <p>Figure 3-2: 20 feet container dimensions</p> </div>		
5	A grillage frame must be incorporated in the CCS where there is space for the SPMTs between the grillage beams	Research boundary 2
6	The load on each SPMT axle line is limited to 36 t (including dynamic loads and excluding self- weight of SPMT)	Section 2.3.1
7	Each SPMT axle lines needs a space of 2.9 · 1.4 m	Section 3.1.1
8	It must be possible to transport the CCS by multiple vessels. The database of the heavy deck carrier vessels of Mammoet is assumed to be a market average. The percentage of vessels from this database capable of transporting a certain width is plotted in the graph below [35].	Research boundary 6
<div style="text-align: center;">  <p>Figure 3-3: Vessel deck applicability</p> </div>		
9	Outer dimensions and total weight of the CCS shall be minimized	Research boundary 1
10	The design of the CCS must be modular	Research boundary 2

The requirement that for the whole CCS the stability, strength and stiffness requirements must be fulfilled is discussed in Chapter 4 and thus left out of Table 3-2 as a requirement for the concept design.

3.1.1 SPMT specification

The SPMTs consist of axle lines. Each axle line can carry a load of 36 t (including dynamic factors and excluding SPMT self-weight, Table 3-2). Each axle line also requires a certain area. From Figure 3-4 it follows that the needed area per axle line is $2.43\text{ m} \cdot 1.4\text{ m}$.

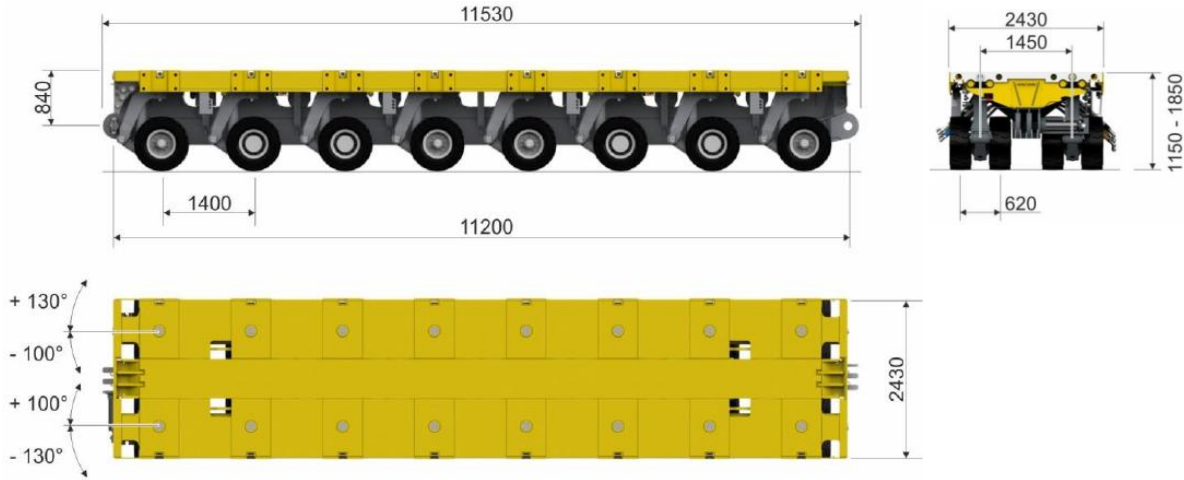


Figure 3-4: SPMT dimensions of SPMT with 8 axle lines [30]

However, the turning of the wheels and the turning of the arms holding the wheels, require more space. The design proposed by Mammoet [26] shows that a distance of 2.9 m between the centers of the SPMT trains is sufficient. This results a total area of $2.9 \cdot 1.4\text{ m}$ required per axle line.

Figure 3-4 shows a SPMT with 8 axle lines. Multiple SPMT can be coupled to form a SPMT train or more axle lines. When the SPMTs are couple the distance of 1.4 m between axle lines, and thus the boundary axle lines of two coupled SPMTs, is maintained.

3.1.2 Cable storage capacity

The volume of the carousel needed for a capacity C of 5000 t is dependent of the cable diameter D_{cable} . As defined previously in section 2.1.2, cables are stacked in the manner shown in Figure 3-5.

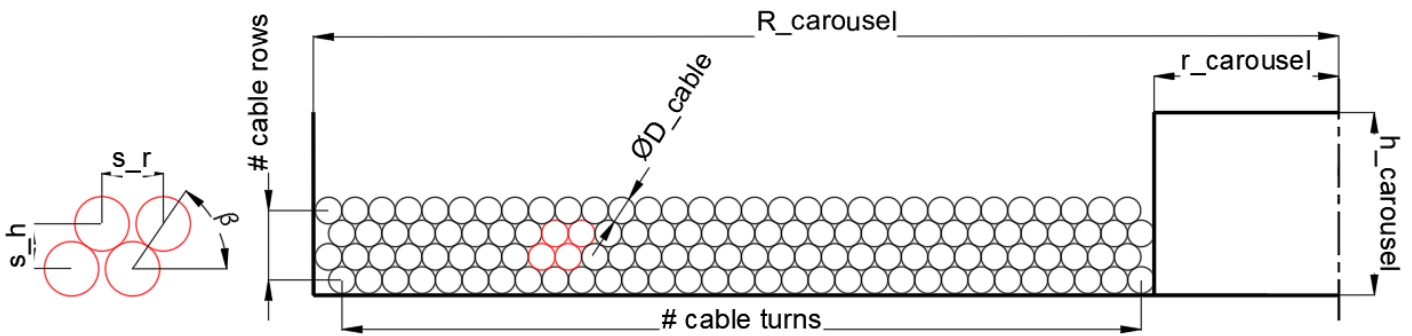


Figure 3-5: Carousel and cable stack cross section with dimensions

From Figure 2-8 and equation formula (2-1) from chapter 2.1.2 it follows that the cable mass μ_{cable} is related to the cable diameter D_{cable} by

$$\mu_{\text{cable}} = 1.18 \cdot 10^{-3} D_{\text{cable}}^2 + 1.28 \cdot 10^{-1} D_{\text{cable}} \quad (3-1)$$

The typical cable diameters for offshore power cables range from 100 to 300 mm , and thus the CCS is required to be capable of storing 5000 t of all cables within this range (Requirement 3 in Table 3-2). With the cable mass μ_{cable} the total length of the cable L_{cable} can be calculated with formula (2-2). With the cable diameter D_{cable} and carousel dimensions r_{carousel} , R_{carousel} and h_{carousel} the mass of the cable stack which fits in the carousel dimensions can be calculated according to Appendix D.

The get an insight in the needed volume and the mass of the cable stack related to the diameter of the offshore power cable D_{cable} , the cable stack mass for every cable diameter D_{cable} between 50 – 300mm has been plotted in Figure 3-6 for $r_{carousel} = 4.375m$, $R_{carousel} = 13.3m$ and $h_{carousel} = 5.80m$ as defined in Table 3-1.

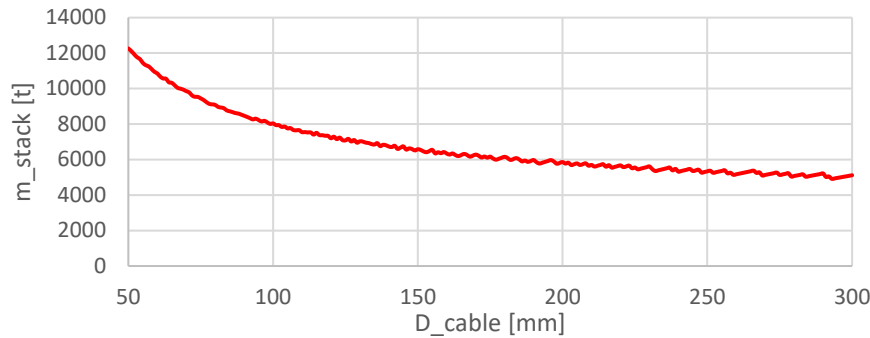


Figure 3-6: Cable stack mass per cable diameter

Figure 3-6 clearly shows that a smaller cable diameter D_{cable} results in a larger cable stack mass m_{stack} . This is mainly due to the changing cable mass dependent on the cable diameter, as defined in formula (2-1). With a constant density of the cable the cable stack should have approximately the same cable stack mass for the maximum amount of cable in the defined carousel dimensions $r_{carousel}$, $R_{carousel}$ and $h_{carousel}$ for all the cable diameters D_{cable} . In order words, Figure 3-6 shows an approximate constant m_{stack} if the cable mass density is constant. From the formulas in Appendix D, it follows that the largest cable diameter D_{cable} is governing because it gives the largest cable stack for a capacity of 5000 Ton and thus the largest cable stack height. A larger cable stack height causes more bending moment $M_{h,res} = h_{h,ref} \cdot F_{h,res}$, on the carousel floor due to a higher located $h_{h,res}$ resultant for of the horizontal load $F_{h,res}$ on the inner frame as shown in Figure 3-7. With Requirement 3 from Table 3-2 the governing cable diameter D_{cable} for the carousel dimensions is thus 300mm.

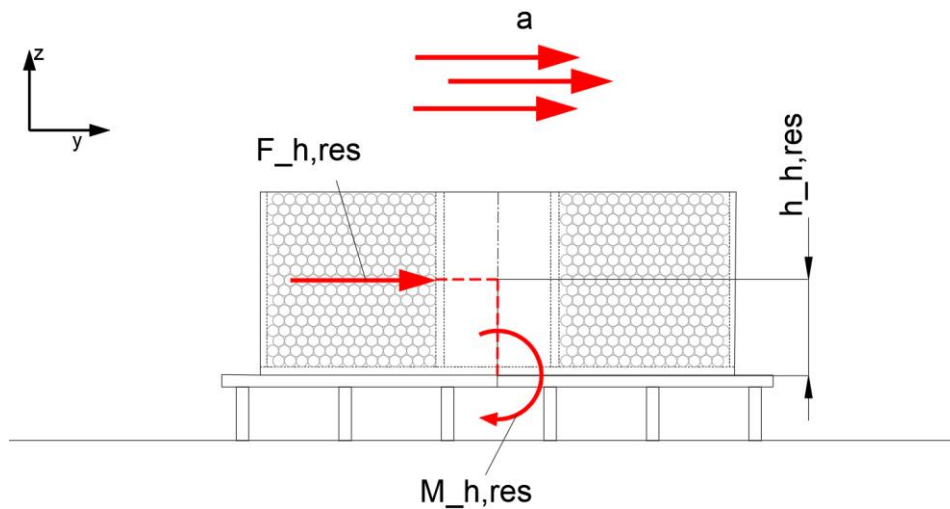


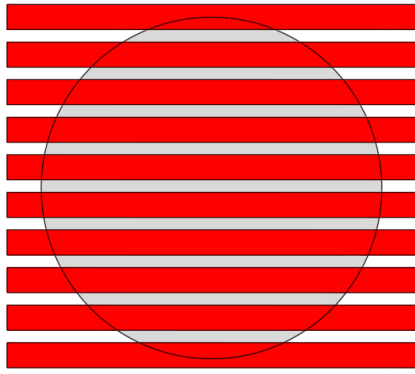
Figure 3-7: Bending moment $M_{h,res}$ on carousel floor due to resultant of horizontal load $F_{h,res}$

3.2 Main dimensions

SPMT support area and carousel footprint

The main dimensions of the CCS design proposed by Mammoet are stated in Table 3-1. One of the main challenges from chapter 2 is to doesn't exceed the available stroke of the SPMTs. Not only can the stiffness of the carousel lower the deflection, but also the SPMT setup and the dimensions of the carousel have a large influence on the deflection. From section 2.3.2 it follows that it is beneficial for the deflection of the SPMT transport that the supported area by the SPMTs equals the footprint of the carousel in shape and size (Figure 3-8). If this is the case, no SPMT axle line is unsupported, and no part of the carousel is unsupported. However, the size of the SPMT support area can't be exactly equal to carousel footprint because the SPMT trains consist of rectangles and the carousel footprint is circular, but a more improved solution improves significantly lowers the deflection of the SPMT transport.

Carousel footprint << SPMT support area



Carousel footprint >> SPMT support area

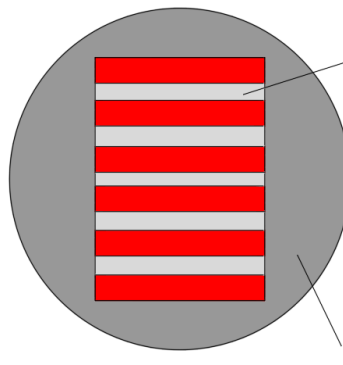
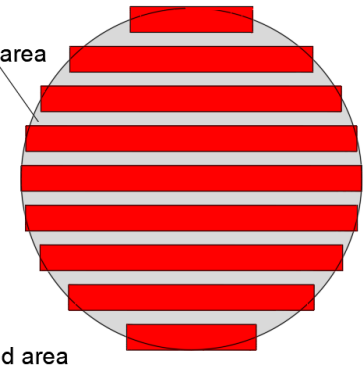
Carousel footprint \approx SPMT support area

Figure 3-8: Carousel footprint and SPMT support area

As stated in Table 3-2 requirement 4, all components of the CCS must be containerized, and so also the floor of the carousel consists of container plates. To have a good load transfer from the carousel to the SPMTs, it is desired that the whole footprint of the carousel is supported by floor plates and that all SPMT axle lines are covered by floor plates. Minimization of the carousel and floor plate dimensions is also desired, as material and production costs are lowered, less SPMTs are needed, and more vessels are enabled to transport the CCS.

3.2.1 Main carousel dimensions

Input

Table 3-3 shows the variables for determining the main carousel dimensions.

Table 3-3: Main carousel dimensions variables

Variable	Abbreviation	Unit
Outside carousel radius	$R_{carousel}$	m
Inside carousel radius	$r_{carousel}$	m
Carousel height	$h_{carousel}$	m
Number of 20 feet container plates	/	/
Number of SPMT axle lines	/	/

For the 20 feet container plates and the SPMT axle lines also the setup is variable and important. The boundary conditions for improving the main carousel dimensions are given in Table 3-4.

Table 3-4: Boundary conditions for determining main carousel dimensions

#	Boundary condition	Reference
1	Capacity of carousel $C = 5000t$	Table 3-2
2	Cable diameter $D_{cable} = 300mm$	Chapter 3.1.2
3	Maximum load per SPMT axle line is $36.0 / 1.15 = 31.3t$. For the maximum load of $31.3t$ per SPMT axle line the self-weight, dynamical effects and other SPMT loads are already implemented.	*
4	The sum of the weight of the carousel and the weight of the grillage frame $m_{carousel} + m_{grillage}$ is estimated by $1.294 t/m^2$ footprint of the carousel	**
5	The area needed per SPMT axle line is assumed to be $1.4 \cdot 2.9m$	Chapter 3.2.2
6	The area per 20-feet container plate is $6058 \times 2438 mm$	Table 3-2
7	The SPMTs have a maximum velocity of $\max(V_{o,SPMT}) = 4 km/h$. This limit applies to the most outer SPMT axle line during spooling because this axle line has a higher velocity compared to the other axle lines.	Chapter 2.3.1
8	The spool rate is assumed to be $V_{spool} = 0.90 km/h$	Chapter 2.2.1

* A safety factor is included to consider the dynamic effects and other SPMT loads. For the CCS design by Mammoet the total weight on the SPMTs is given by $m_{carousel} + m_{grillage} + C = 592 + 127 + 5000 = 5719t$. With 184 axle lines and 36t capacity per axle line, the Mammoet CCS concept can handle a maximum load of $184 \cdot 36 = 6624 t$ on the SPMTs. This means that there is $6624 - 5719 = 905t$ available for the dynamic effect and other SPMT loads, which results in a safety factor of $6624/5719 \approx 1.15$. This factor is also used to take into account the dynamical effects and other SPMT transport loads.

** A larger carousel results in a larger $m_{carousel}$ and $m_{grillage}$, and needs more SPMT capacity to transport the increased weight. The footprint of the carousel design from Mammoet equals $\pi R_{carousel}^2 = 556 m^2$. The total weight of the carousel design proposed by Mammoet is $m_{carousel} + m_{grillage} = 592 + 127 = 719t$. A rough estimation is made by assuming the weight per area carousel footprint to be $719/556 = 1.294 t/m^2$. This will be used to get an estimation of the weight of the carousel and the grillage frame depending on the size.

Carousel diameter estimation

The area of the footprint of the carousel is given by $\pi R_{carousel}^2$. Based on this area the weight of the carousel and grillage frame can be estimated by (boundary condition 4 in Table 3-4)

$$m_{carousel} + m_{grillage} = 1.294 \cdot \pi R_{carousel}^2 \quad (3-2)$$

With the needed capacity C the amount of axle lines needed can be determined by

$$\# \text{ axle lines} = \frac{m_{carousel} + m_{grillage} + C}{\text{Max axle line load}} \quad (3-3)$$

With the number of axle lines needed calculated, the total SPMT area can be estimated by using boundary condition 5 in Table 3-4, leading to

$$\text{SPMT support area} = \# \text{ axle lines} \cdot 1.4 \cdot 2.9 \quad (3-4)$$

Finally, the carousel footprint area $\pi R_{carousel}^2$ from the SPMT support area, where the absolute $|\text{SPMT support area} - \pi R_{carousel}^2|$ is plotted in Figure 3-9.

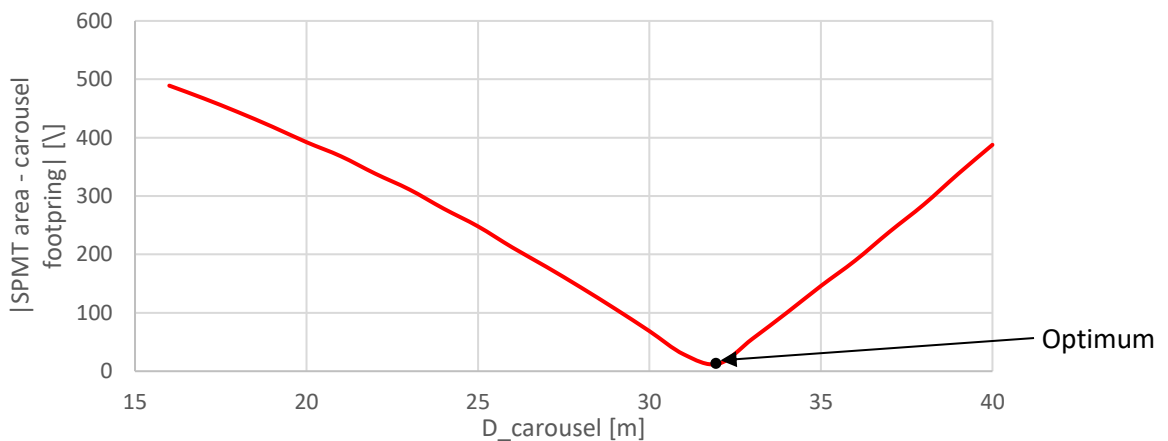


Figure 3-9: Optimal outer carousel diameter $D_{carousel}$

As discussed before, for the deflection of the SPMT transport it is most optimal if the area covered by SPMTs equals the area of the carousel footprint. This occurs when the SPMT area minus the footprint area equals 0, which from Figure 3-9 occurs when $D_{carousel} \approx 32m$. This means that for the boundary conditions in Table 3-4 an outer carousel diameter $D_{carousel}$ of approximated $32m$ is the most optimal in terms of SPMT deflection, which will be used as a starting point for determining improved setups. Notice that for this starting point a lot of factors have been neglected, such as placement of the SPMT axle lines and that the SPMT support area is not circular, which cause that the defined optimum from Figure 3-9 cannot be reached.

Proposed setups

Based on the requirement, boundary conditions, and the carousel diameter estimation $D_{carousel} \approx 32m$, the floor setups shown in Figure 3-10 have been established. Also, the footprint of the carousel which fits on the floor is shown for each setup (black circle). The larger light gray circle approximates the radius of the most outer axle line.

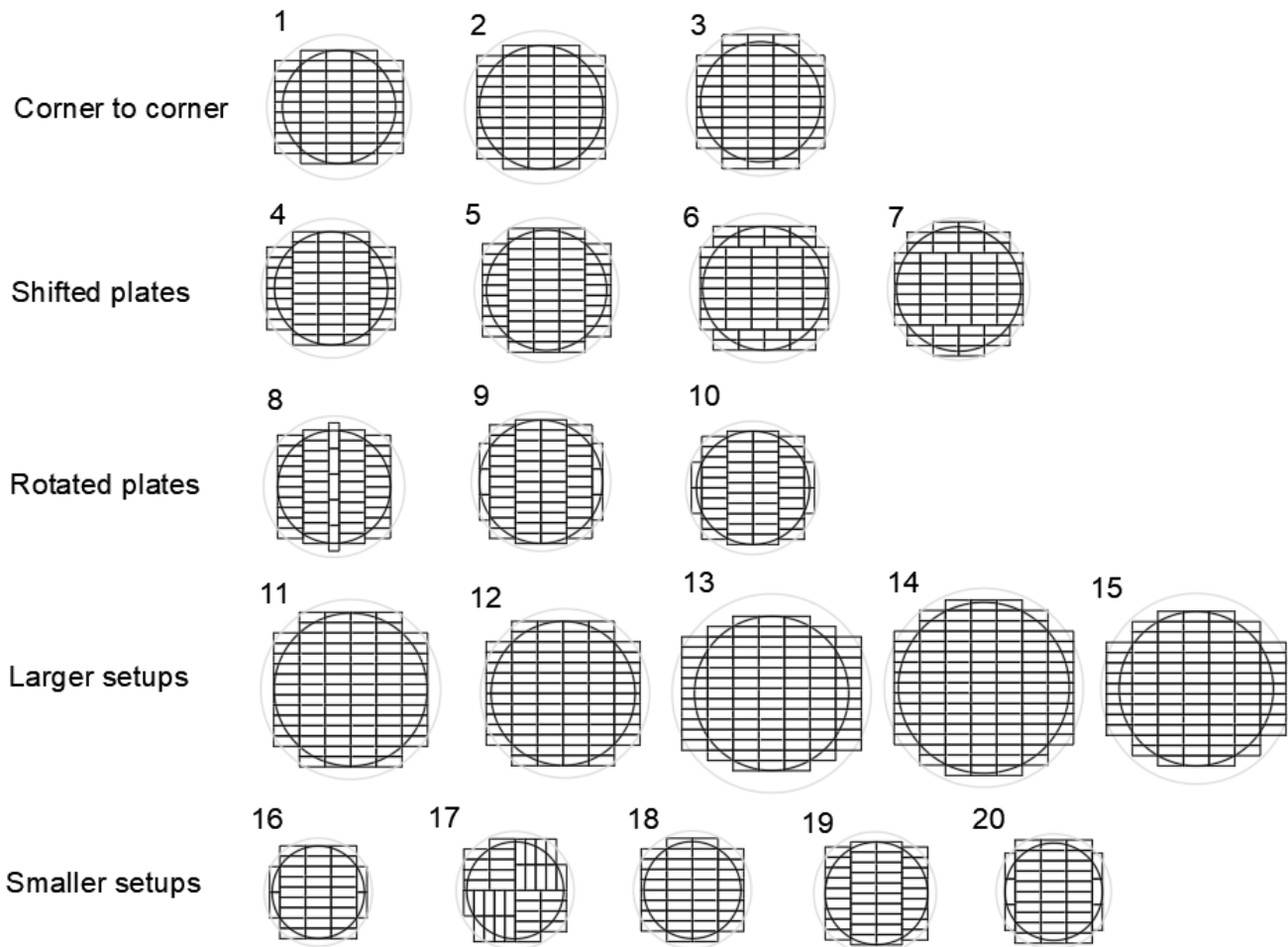


Figure 3-10: Floor setups

In Figure 3-10 the philosophy of the setups is described on the left, which is mainly about how the floor plates are connected. The connections of the plates and the setups of the SPMTs and the grillage are discussed in chapter 3.3 and 3.2.2, respectively. The amount of floor plates, the diameter of the carousel which fits on each setup, the diameter of the most outer SPMT axle line during spooling, the width and length of each setup are summarized in Table 3-5.

Performance of setups

For each setup the performance has been determined by multiple performance indicators. The results are shown in Table 3-6 and the meaning of the performance indicators is described below Table 3-6.

Table 3-5: Setup properties

Nr	Number of floor plates	Maximum carousel diameter $D_{carousel}$	Outer SPMT axle line diameter $2R_{O,SPMT}$	Setup width	Setup length
#	/	[m]	[m]	[m]	[m]
1	51	26.84	34.22	30.29	26.82
2	56	29.28	36.22	30.29	29.26
3	57	28.52	35.18	30.29	31.69
4	49	26.84	33.06	30.29	26.82
5	54	28.52	34.23	30.29	29.26
6	56	29.28	35.35	30.29	29.26
7	55	29.45	33.67	30.29	31.69
8	47	26.71	33.53	26.67	30.29
9	52	29.15	33.03	29.11	29.26
10	46	26.84	31.65	29.11	26.82
11	82	36.18	42.66	36.35	36.57
12	76	34.16	40.06	36.35	34.13
13	93	36.57	47.14	42.41	36.57
14	103	40.50	47.11	42.41	41.45
15	89	36.60	45.13	42.41	36.57
16	31	21.87	25.59	23.05	21.94
17	36	22.98	27.98	24.31	24.31
18	36	22.98	28.01	24.23	24.38
19	38	24.27	29.06	24.23	24.38
20	36	23.08	27.31	23.05	24.38

Table 3-6: Performance of setups

Nr	Factor vessel applicability	Estimated weight CCS $m_{CCS,SPMT,g}$	Needed axle lines	Factor footprint covered by SPMTs	Factor footprint covered by Floor plates	Minimum Inside carousel radius	Drive distance most outside SPMT	Needed height
#	[/]	[t]	[/]	[/]	[/]	[m]	[km]	[m]
1	0.96	5732	184	1.32	1.33	3.85	68.6	5.50
2	0.96	5871	188	1.13	1.23	4.07	67.0	4.72
3	0.96	5827	187	1.19	1.32	3.96	66.9	4.98
4	0.96	5732	184	1.32	1.28	3.72	66.8	5.50
5	0.96	5827	187	1.19	1.25	3.85	65.4	4.72
6	0.96	5871	188	1.13	1.23	3.98	65.8	4.46
7	0.96	5881	188	1.12	1.19	3.79	63.0	4.72
8	0.96	5725	183	1.33	1.24	3.77	67.8	5.50
9	0.96	5863	188	1.14	1.15	3.72	62.5	4.72
10	0.96	5732	184	1.32	1.20	3.56	64.5	5.50
11	0.74	6330	203	0.80	1.18	4.80	64.5	3.16
12	0.85	6186	198	0.88	1.22	4.51	64.3	3.42
13	0.74	6359	204	0.79	1.31	5.30	69.2	3.16
14	0.51	6667	213	0.67	1.18	5.30	63.8	2.38
15	0.74	6361	204	0.79	1.25	5.08	66.9	2.90
16	0.99	5486	176	1.90	1.22	2.88	64.1	8.09
17	0.99	5537	177	1.73	1.28	3.15	66.2	7.31
18	0.99	5537	177	1.73	1.28	3.15	66.2	7.31
19	0.99	5599	179	1.57	1.21	3.27	65.3	6.54
20	0.99	5541	178	1.73	1.27	3.07	64.7	7.31

When a setup in Table 3-6 shows good performance on a certain topic, the corresponding value has a **green front color**. If the setup has bad performance on a certain topic, or a significantly lower performance than the design proposed by Mammoet, the corresponding value has a **red front color**. The explanation of the performance indicator in each column of Table 3-6 is given below:

- **Factor vessel applicability:** Each setup requires an area on the vessel deck of at least the setup width times the setup length. Extra deck space can be needed for maneuvering space of CCS, lashing for sea transport or other possible reasons. This is however neglected for this study and the column shows the percentage of vessels from the Mammoet database [35] which have enough deck space for the width and length of the corresponding setup (requirement 7 in Table 3-2). This is calculated as the number of vessels with a larger deck width than $\min(\text{setup width}, \text{setup length})$, divided by the total number of vessels in the Mammoet database. So, a factor of 1 means that all the vessels in the Mammoet database have enough space for the setup, and a factor 0 means that no vessel in the Mammoet database has enough space (with no extra space included).
- **Estimated weight:** The footprint of the carousel which fits on each setup is given by $\pi R_{\text{carousel}}^2$, where $R_{\text{carousel}} = D_{\text{carousel}}/2$ is the maximum radius of the carousel which fits on the floor structure as defined in Table 3-5. Based on this area the weight of the corresponding carousel m_{carousel} and grillage frame m_{grillage} can be estimated by boundary condition 4 in Table 3-4, which leads to

$$m_{\text{carousel}} + m_{\text{grillage}} = 1.294 \cdot \pi R_{\text{carousel}}^2 \quad (3-5)$$

The total weight of the CCS transport by SPMTs with the carousel and the grillage frame is then given by $m_{\text{CCS,SPMT,g}} = m_{\text{carousel}} + m_{\text{grillage}} + C$

- **Needed axle lines:** Based on the estimate total weight on the SPMTs, the needed number of SPMT axle lines can be estimated. This done by dividing $m_{\text{CCS,SPMT,g}}$ by the maximum load per axle line of 31.3 t (Boundary condition 3 in Table 3-4). The results have been rounded up.
- **Factor footprint covered by SPMTs:** It has been assumed that the SPMTs are closely aligned to each other, such that the area covered by the SPMTs can be calculated by the amount of axle lines times the area needed per axle line, $1.4 \cdot 2.9\text{m}$ (boundary condition 5 in Table 3-4). The factor of the footprint covered by SPMTs can be calculated by dividing the calculated SPMT area by the area of the footprint $\pi R_{\text{carousel}}^2$. A value of 1 means that the size of the areas is equal, but this doesn't mean that the shapes of the areas are equal. The factor of footprint covered by SPMT still gives a good indication of the quality of the approximation of the carousel footprint by the SPMT support area. As shown in Figure 3-8 it is beneficial if the SPMT support area approximates the carousel footprint area. A value lower than 1 indicates that there is more space below the footprint area to store more axle lines, which also is beneficial because it allows a better distribution of SPMTs to better approximate the carousel footprint area.
- **Factor footprint covered by Floor plates:** The area covered by floor plates can be calculated by the amount of floor plates in the setup times the area of 1 floor plate, $6058 \cdot 2438\text{ mm}$ (boundary condition 6 in Table 3-4). The factor of footprint covered by floor plates can be calculated by dividing the area of the floor plates by the area of the carousel footprint $\pi R_{\text{carousel}}^2$. A value of 1 means that the size of the areas is equal, but it doesn't mean that the shapes of the areas are equal. However, the value still gives a good indication of the performance of the setups. A value lower than 1 means that the carousel footprint isn't fully covered by floor plates, which is not beneficial for the load transfer, and a value higher than 1 means that the floor is larger than necessary.
- **Minimum inside carousel radius:** The minimum inside carousel radius can be determined by formula (2-4) from section 2.2.1.

$$r_{\text{carousel}} = \max(R_{\text{O,SPMT}}) \cdot \frac{V_{\text{spool}}}{\max(V_{\text{O,SPMT}})} \quad (3-6)$$

, with the maximum outer SPMT axle line radius $\max(R_{\text{O,SPMT}})$ which has been defined for each setup in Table 3-5, the spool rate $V_{\text{spool}} = 0.9\text{ km/h}$ and the maximum velocity of the axle lines $\max(V_{\text{O,SPMT}}) = 4\text{ km/m}$. Furthermore, the inside carousel radius is also dependent of the minimum bending radius of the cables specified by the manufacturer.

- **Drive distance most outside SPMT:** How the drive distance of the most outer SPMT $S_{O,SPMT}$ can be calculated is given by formulas (2-1), (2-6) and (2-7) from section 2.2.1.
- **Needed Height:** The calculated minimum inside radius will be taken as the inside radius of the carousel $r_{carousel}$. The needed cable turns per row can be estimated by

$$\# \text{ cable turns} = \text{rounddown}\left(\frac{R_{carousel} - r_{carousel} - 0.5D_{cable}}{D_{cable}}\right) \quad (3-7)$$

The total needed cable turns can be estimated by

$$\# \text{ turns} = L_{cable} / L_{ct,avg} \quad (3-8)$$

, with the average cable turn length $L_{ct,avg}$ and cable length L_{cable} respectively calculated by

$$L_{ct,avg} = \pi(r_{carousel} + R_{carousel}) \quad \text{and} \quad L_{cable} = C / \mu_{cable} \quad (3-9)$$

μ_{cable} can be determined by formula (3-1). Under the assumption that the cables are closely packed, the needed carousel height can be estimated by

$$h_{carousel} = \text{roundup}(\# \text{ turns} / \# \text{ cable turns} - 1) \cdot \sin(60^\circ) \cdot D_{cable} + D_{cable} \quad (3-10)$$

Because the CCS must be containerized it is beneficial to keep the carousel height $h_{carousel}$ below the inside 20ft container dimensions. This ensures that every vertical column fits in a container. Therefore, the values above 5.9m (inside 20ft container length) are marked red.

Table 3-6 also contains three marked setups, namely setup 1, 9, and 11. These are the setups selected to be further elaborated. The first setup is the setup used in the design of the CCS proposed by Mammoet [26] [27]. This setup is used as a reference. All the setups where some value has a green front color, show good performance on the corresponding topic relative the setup proposed by Mammoet. As a result, setup 9 and 11 have been selected for their good performance and because they are both of another setup type (Figure 3-10).

Inside radius

Previously, a minimum inside radius has been defined for each setup. However, the inside radius effects the needed drive distance of the SPMTs and the needed height of the carousel. Figure 3-11 and Figure 3-12 show how the drive distance of the outer SPMT $S_{O,SPMT}$ and the needed carousel height $h_{carousel}$ are influenced by the inner radius of the carousel $r_{carousel}$ for setups 9 and 11 respectively. For the carousel $h_{carousel}$ formula (3-10) is used, and for the drive distance of the outer SPMT $S_{O,SPMT}$ formula (2-7).

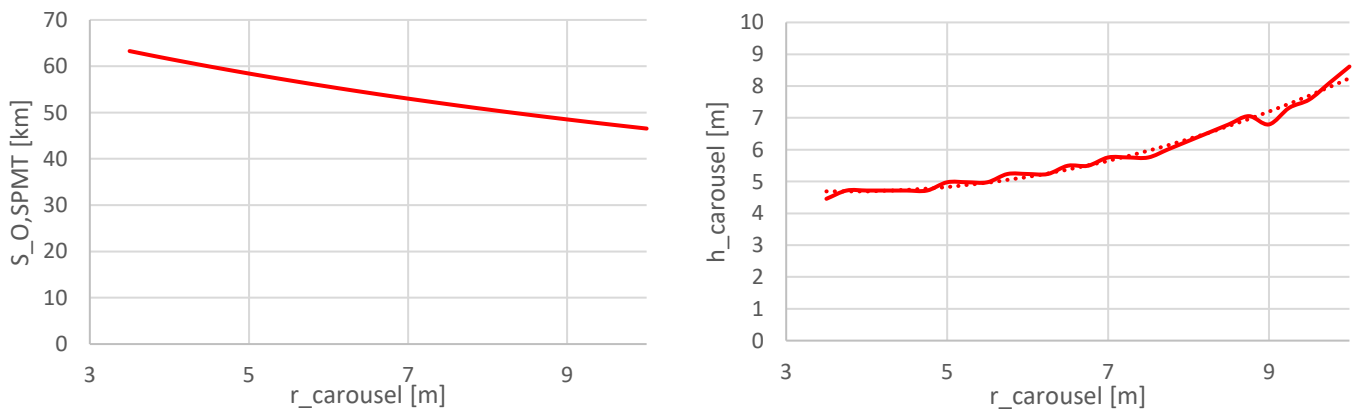
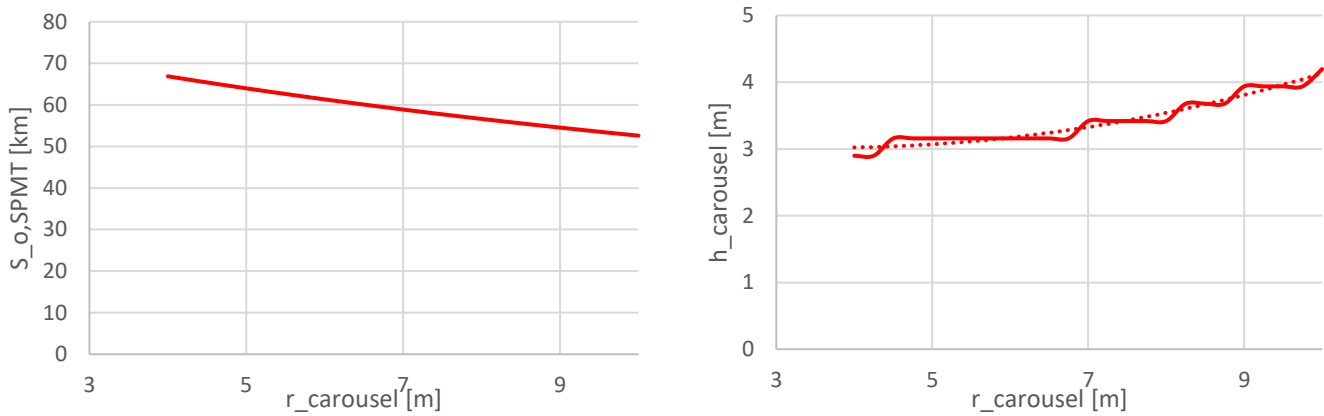


Figure 3-11: Influence of $r_{carousel}$ on $S_{O,SPMT}$ and $h_{carousel}$ for setup 9

Figure 3-12: Influence of $r_{carousel}$ on $S_{o,SPMT}$ and $h_{carousel}$ for setup 11

The fluctuations in the $h_{carousel}$ related to $r_{carousel}$ in the figures are caused by the nonlinearity that only whole cables fit on a row. If there fits one less cable turn on a single row due to the increasing $r_{carousel}$ this applies for all rows, which causes an increase in the needed carousel height $h_{carousel}$. A trend line in the figures for the needed carousel height $h_{carousel}$ shows an approximate second order relation with the inner carousel radius $r_{carousel}$.

For both setup 9 and 11 the increase of $r_{carousel}$ results in a smaller $S_{o,SPMT}$ but in a larger $h_{carousel}$. A smaller $S_{o,SPMT}$ is more beneficial for the lifetime of the SPMTs. Furthermore, the spool rate V_{spool} is kept constant, and so the spool time, this means that the average speed of the SPMTs over the entire spool process is also decreased for a larger $r_{carousel}$, which is also beneficial for the lifetime of the SPMTs. However, an increase of $r_{carousel}$ also results in an increase of the needed carousel height $h_{carousel}$ and so the cable stack height. A higher cable stack increases the bending moment on the floor and thus the CCS is heavier loaded, as shown in Figure 3-7. So, a tradeoff needs to be made between the importance of the load on the carousel and the lifetime of the SPMTs.

Conclusion

The selected setups and their properties are summarized in the Table 3-7.

Table 3-7: Selected Setups

Setup	Abbreviation	1	9	11	Unit
Outside carousel diameter	$2 \cdot R_{carousel}$	26.8	29.2	36.2	m
Calculated minimum inside carousel radius	$r_{carousel}$	3.85	3.72	4.80	m
Chosen inside carousel radius	$r_{carousel}$	4.375	4.00	5.00	m
Carousel height	$h_{carousel}$	5.50	4.72	3.16	m
Number of floor plates	/	51	52	82	/
Number of axle lines	/	185	189	204	/

For the $r_{carousel}$ of setups 9 and 11 it is chosen to use a low $r_{carousel}$ to minimize $h_{carousel}$ and the load on the carousel. A slightly higher value than the minimum inside carousel radius thus has been chosen. Furthermore, the inside radius limited by the minimum bending radius (MBR) of the cable specified by the manufacturer. The typical MBR limit of a cable is approximately $2 - 3m$ [41]. To let the CCS also be applicable to cables with a larger MBR, a minimum inside carousel radius of $4m$ is chosen. Table 3-7 shows that all the chosen inside carousel radii satisfy this requirement.

3.2.2 SPMT and grillage setup

Table 3-7 describes the selected setups and the needed axle lines. The SPMTs can be coupled to each other to form an SPMT train. The distance of $1400mm$ between the axle lines is still maintained. Figure 3-13 schematically visualizes how the SPMT trains can be modeled.

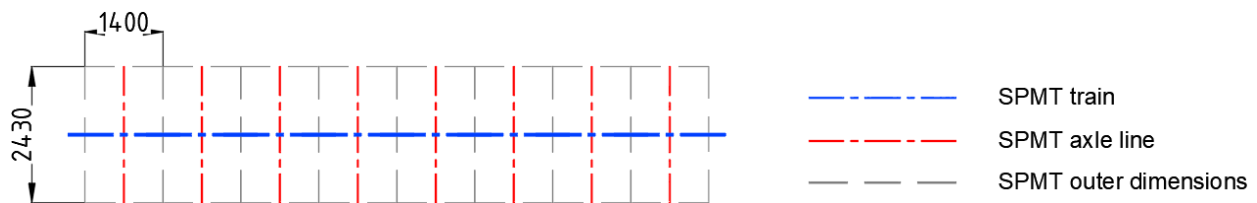


Figure 3-13: Schematic visualization of SPMT train

SPMT trains can be aligned against each other. The minimum distance between the SPMT trains is $2900 - 2430 = 470\text{mm}$ because each SPMT axle line needs a width of 2900mm . Figure 3-14 shows how the width of the SPMT trains could be fitted below the floor plates. The figure shows that two SPMT trains can be fitted under one perpendicular oriented floor plate or three parallel oriented floor plates, with an extra width of 1990mm and 740mm respectively. Furthermore, four SPMT trains can be fitted under two perpendicular oriented floor plate or 5 parallel oriented floor plates, with an extra width of 1010mm and 1070mm respectively.

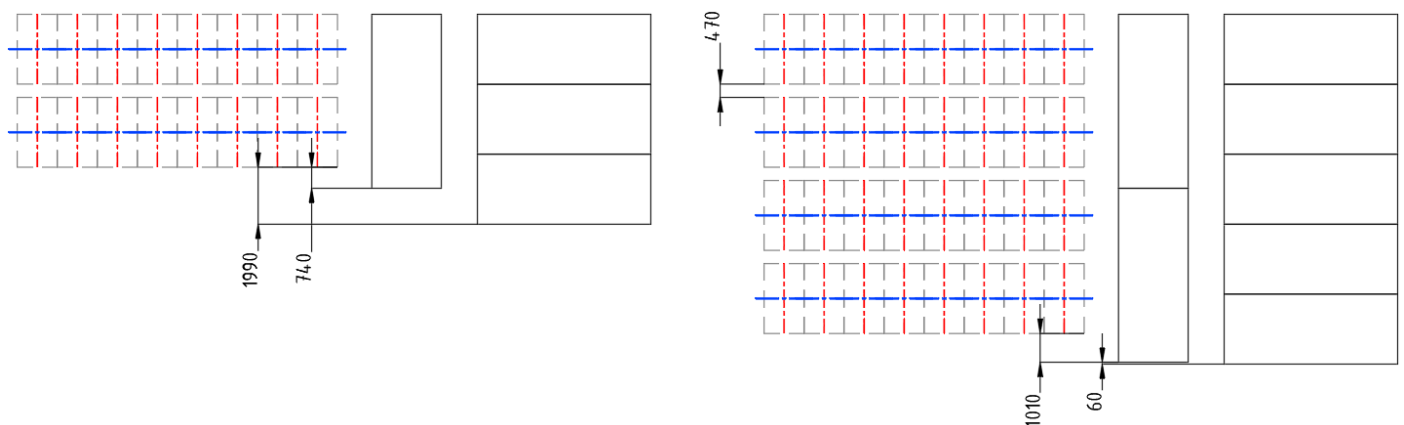


Figure 3-14: Dimensions of SPMT trains related to dimensions of container plate setups

It is important that all the SPMT trains are placed in the same direction, such that they can leave the carousel and the vessel as shown as shown schematically in Figure 3-15.

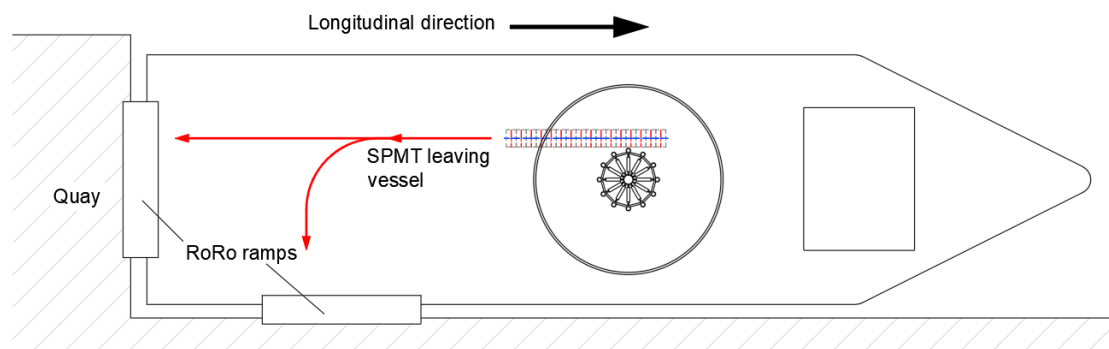


Figure 3-15: SPMT train orientation on vessel

For each of the setups 9 and 11, multiple SPMT and grillage frame setups have been established, as shown in the next paragraphs. For setup 1, the setup from the proposed design from Mammoet has been used.

Mammoet setup

Figure 3-16 shows the SPMT and grillage setup which Mammoet has used in their concept. This figure also shows the legend for the line types used in the corresponding figure and the following figures visualizing the other setups in the next paragraphs.

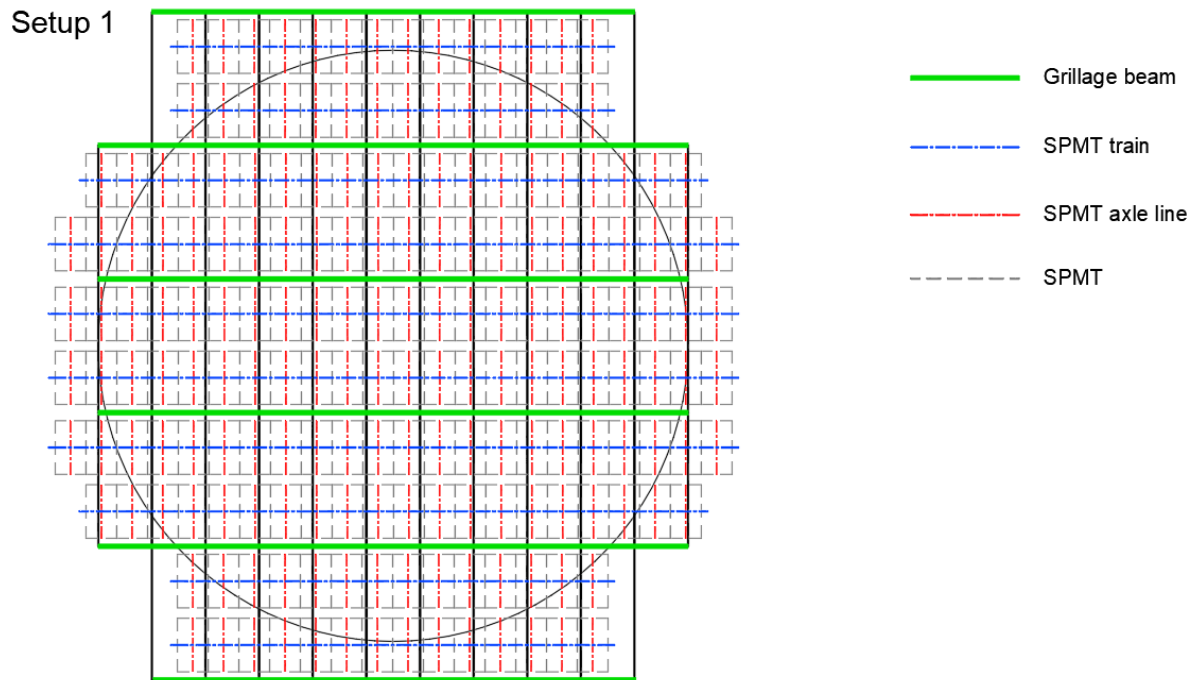


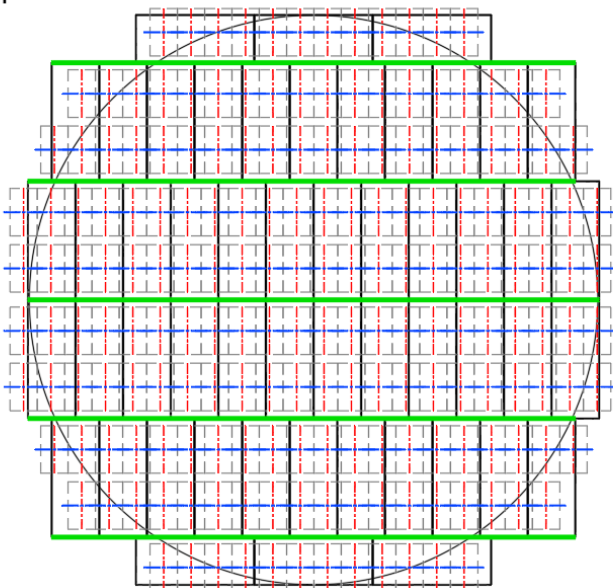
Figure 3-16: SPMT and grillage setup by proposed Mammoet design and legend

For this setup the floor plates are perpendicular aligned with the SPMT trains, and 184 axle lines have been used. Between each two SPMT trains some extra width (more than the 470mm between the SPMT trains) is applied to place a grillage beam. For this setup some of the SPMT axle lines are outside the footprint of the carousel, which causes deflection of the SPMT transport. Also, some parts of the floor structure are outside the carousel footprint, which causes extra material used which doesn't contribute to the structural strength of the CCS.

Setup 9

For setup 9 the four setups have been elaborated as shown in Figure 3-17 and Figure 3-18. All setups contain 188 axle lines.

Setup 9.1



Setup 9.2

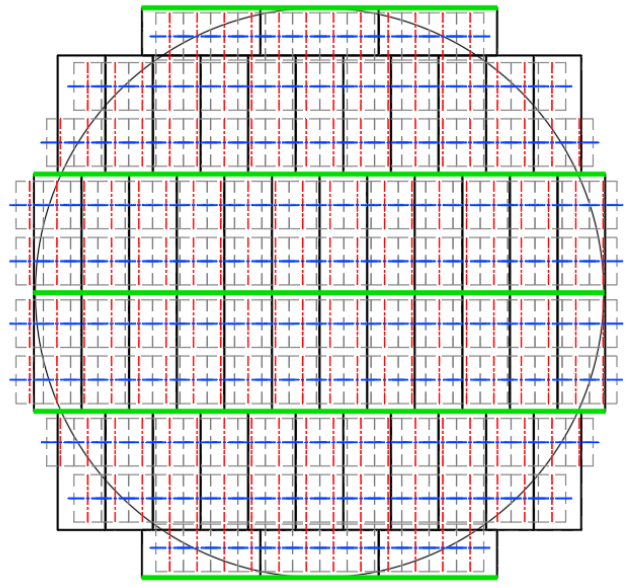
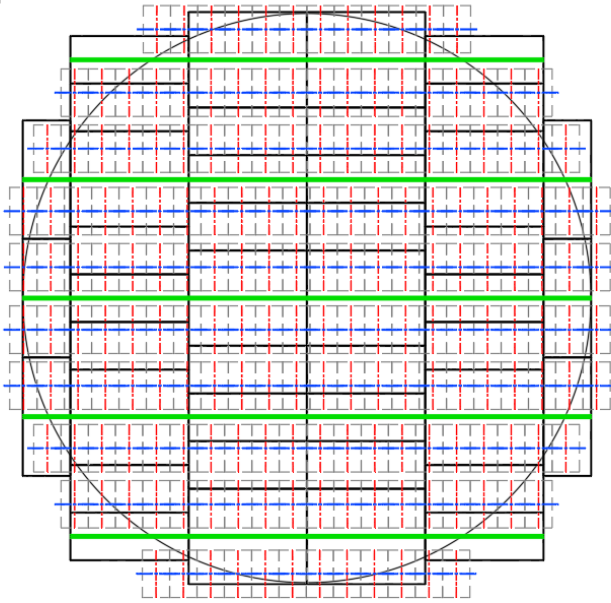


Figure 3-17: SPMT and grillage setups 9.1 and 9.2

Setup 9.3



Setup 9.4

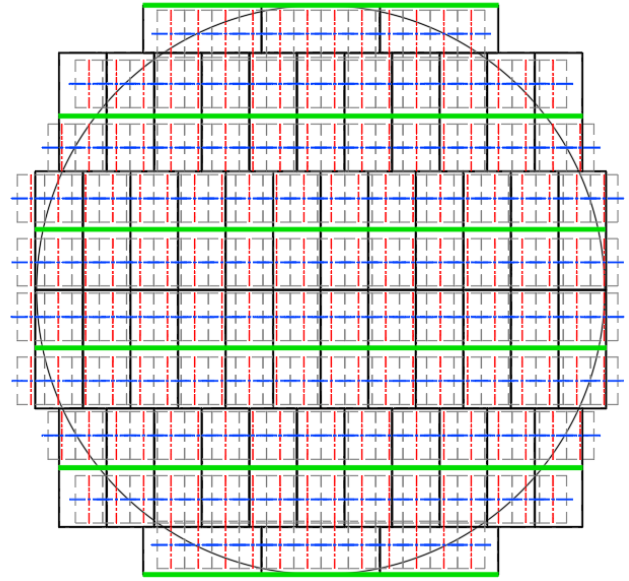


Figure 3-18: SPMT and grillage setups 9.3 and 9.4

The setups in Figure 3-17 and Figure 3-18 have the following characteristics:

- **Setup 9.1:** 5 grillage beams have been used which are aligned with the boundaries of the floor plates. Between each two grillage beams, two SPMT trains are positioned, and at each outside a single SPMT train.
- **Setup 9.2:** Compared to setup 9.1, for this setup the outer grillage beams have been shifted one SPMT train to the outside, such that all SPMT trains are between the grillage beams.
- **Setup 9.3:** For this setup the orientation of the plates is rotated 90 degrees compared to the other setups. The grillage frame is not aligned with the boundaries of the floor plates anymore. The SPMT and grillage setups are the same as for setup 9.1
- **Setup 9.4:** For this setup the floor plates again have a perpendicular orientation with respect to the grillage beams and SPMT trains. 6 grillage beams have been used, where the 4 in the middle are aligned with the center of the floor plates. Using 6 grillage beams is an advantage because the loads can be distributed over more beams, which results in lower stresses.

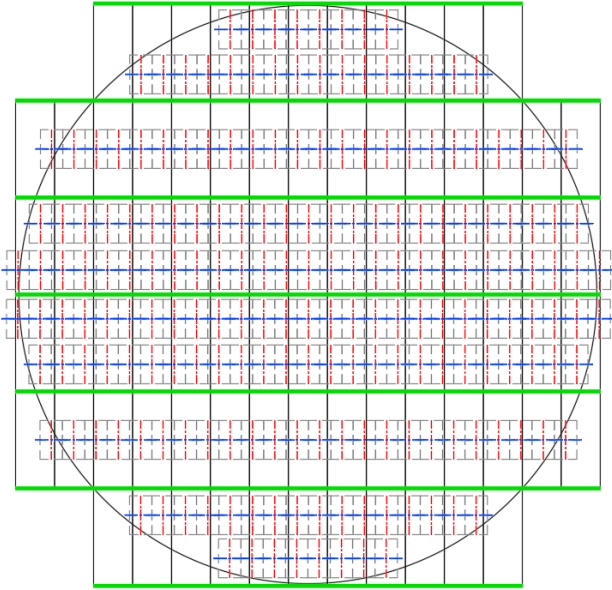
For Setup 9 in general, more SPMT axle lines fall in the footprint of the carousel compared to setup 1, which makes it more effective against SPMT transport deflection. Also, the floor plates of setup 9 form a better approximation of the carousel footprint compared to setup 1. However, the floor plates are not aligned corner to corner anymore, which makes the connections of the plates and the grillage beams to each other more difficult. For setup 9.2 and setup 9.4 the space of 470mm between the SPMT trains isn't possible for some SPMT trains due to the placement of the grillage frames. This can be solved by allowing the SPMTs to be closer packed or to enforce distance between the floor plates to create a larger setup. Furthermore, for setup 9.2, 9.3 and 9.4 the grillage frame is sometimes not aligned with the boundary of the floor plates for which other connection types are needed (section 3.3.3).

It is expected that the floor has lowered stiffness and strength at the connections of the floor plates. It therefore is beneficial to align the grillage beams to the floor plate boundaries such that some floor plate connections are above the grillage beams. Because 9.2 and 9.4 have some dimensional issues and for setup 9.1 the grillage beams are not aligned with the floor plate boundaries, it is chosen to elaborate setup 9.1.

Setup 11

Figure 3-19 shows the two SPMT and grillage setups which have been elaborated for setup 11.

Setup 11.1



Setup 11.2

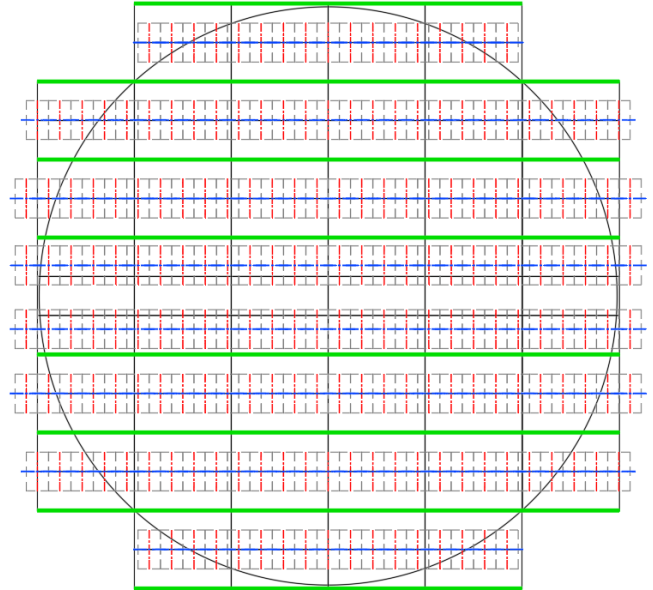


Figure 3-19: SPMT and grillage setups 11.1 and 11.2

The setups in Figure 3-19 have the following characteristics:

- **Setup 11.1:** the floor plates have a perpendicular orientation with the SPMT trains. The grillage frames are aligned with the boundaries of the floor plates. Between some grillage frames only one SPMT train is placed, but for the rest two SPMT trains are placed between the grillage frames.
- **Setup 11.2:** the floor plates are parallel oriented with respect to the SPMT trains. The main advantage of this setup is that there is much space between the SPMT trains, which increases the capability to reach the central SPMT axle lines when maintenance is needed.

Figure 3-19 and the values in Table 3-6 show that there is extra area to store more SPMT axle lines. This means that the capacity can be increased by placing more axle lines. Figure 3-20 shows a SPMT and grillage setup for setup 11 with 298 axle lines and a capacity of 8000t. For setup 11 there is thus space to use the setup then higher capacities as 5000t.

Setup 11.3

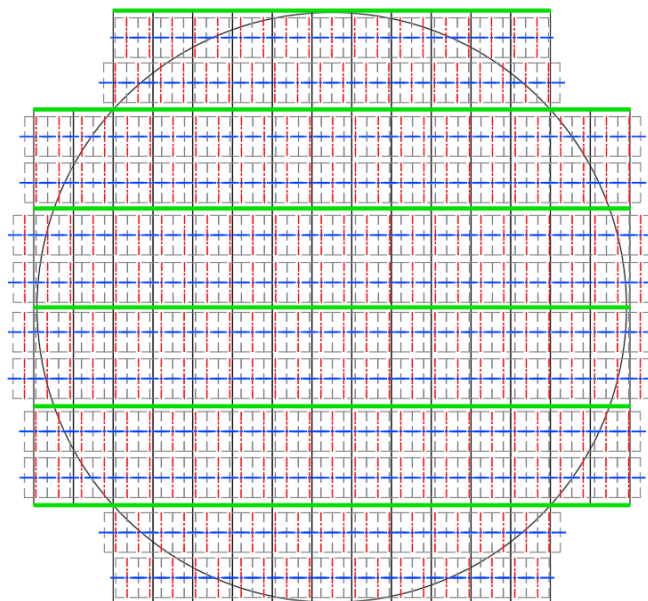


Figure 3-20: SPMT and grillage 11.3 (8000 t capacity)

Selected setups

For each of the chosen setups, one SPMT and grillage setup will be elaborated in section 4.2. The chosen setups are:

- **Setup 1:** This setup is the proposed setup by Mammoet and will be used as a reference.
- **Setup 9.1:** Very compact setup where it is expected that it has the best performance in terms of SPMT deflection. So, it is expected that setup 9.1 has the best performance against challenge 2 from Table 2-11.
- **Setup 11.2:** The main advantage for this setup is there is much space around the SPMTs for maintenance. However, as the setup is larger than setups 1 and 9.2 the CCS with setup 11.2 is more expensive, applicable to less vessels and the SPMS axle lines need to travel more distance for the cable transfer.

The main carousel dimensions, number of axle lines and the number of floor plates for each of the selected setup can be found in Table 3-8.

Table 3-8: Specification selected Setups

Setup	Abbreviation	1	9.1	11.2	Unit
Outside carousel diameter	$2 \cdot R_{carousel}$	26.8	29.2	36.2	m
Inside carousel radius	$r_{carousel}$	4.375	4.00	5.00	m
Carousel height	$h_{carousel}$	5.50	4.72	3.16	m
Number of floor plates	/	51	52	82	/
Number of axle lines	/	184	188	204	/

3.3 Structure

In this section the structural components of the carousel will globally be described, the detailing is not in the scope of this study. Assessment of the structural components against the stability and strength requirements (challenge 1 from Table 2-11) is discussed in chapter 4. Connections between the structural components is also left out of scope for this study.

3.3.1 Outer frame

As discussed in chapter 2, the structural strength of the outer frame will be neglected in the global conceptual design of the carousel because, under the assumption that inner frame is sufficiently stiff, the load on the outer frame and the deformation of the outer frame are limited by the axial stiffness of the cable stack. The outer frame however does experience load. If the outer frame is made very stiff, it will transfer much load from the cable stack to the floor and therefore must have an increased strength. Making the outer frame relatively flexible, it won't transfer much load and it therefore doesn't have to be very strong.

Because the structural strength of the outer frame will be neglected, it will not be discussed in much detail but only the global design proposed by Mammoet will be discussed [26]. The outer frame proposed by Mammoet consists of modular frames which can be connected to each other by couple pieces. This allows a changeable outer diameter of the carousel. Each modular frame has a plateau which is supported by the floor structure of the CCS, and on which the cable is stacked, as shown in Figure 3-21. The dimensions and the principle of the plateau of the outer frame are visualized in Figure 3-21.

The only horizontal connection with the floor and the outer frame is the friction with the plateau and the floor. This means that the horizontal load transferred to the floor is limited by the friction and that no bending moment can be transferred from outer frame to the floor. The outer frame is thus enabled to slide with the cable stack over the floor structure, which gives flexibility to the outer frame. The inner frame will give much resistance to the stable stack from moving, and thus most horizontal load is transferred by the inner frame.

Even though the outer frame is neglected in this study, it will mainly be used to keep the cables stacked. This will mostly cause tension in the outer frame, rather than shear and bending moment. The magnitude of this tension and the deformation of the outer frame is dependent on the axial stiffness of the cable stack. In this study it is thus assumed that the magnitude of the tension and deformation of the outer frame is negligible.

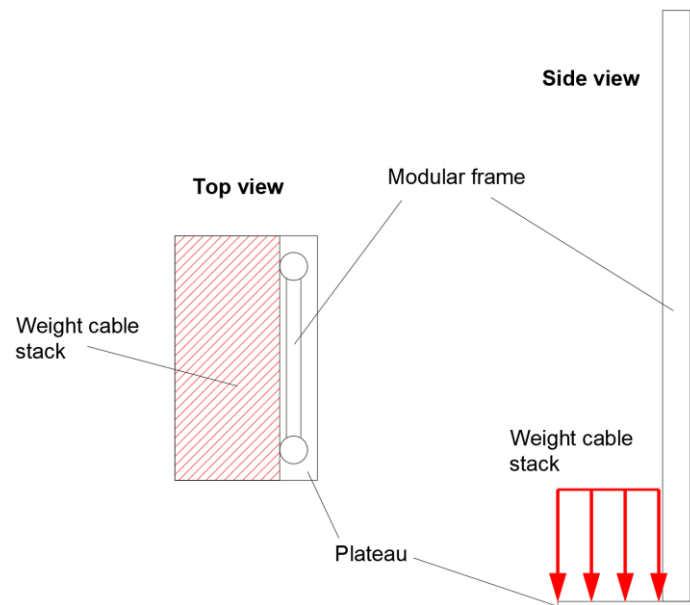


Figure 3-21: Outer frame principle

3.3.2 Inner frame

As discussed in section 2.2.3, the inner frame must be relative stiff and strong as it must transfer most of the horizontal loads from the cable stack to the floor and the other components of the CCS. The structure from the design proposed by Mammoet will be used as a starting point. This structure and the global beam dimensions are visualized in Figure 3-22. For the inner frame modularity will not be considered as the connections are left out of scope for this study. Global beam dimensions are discussed in section 4.3.2.

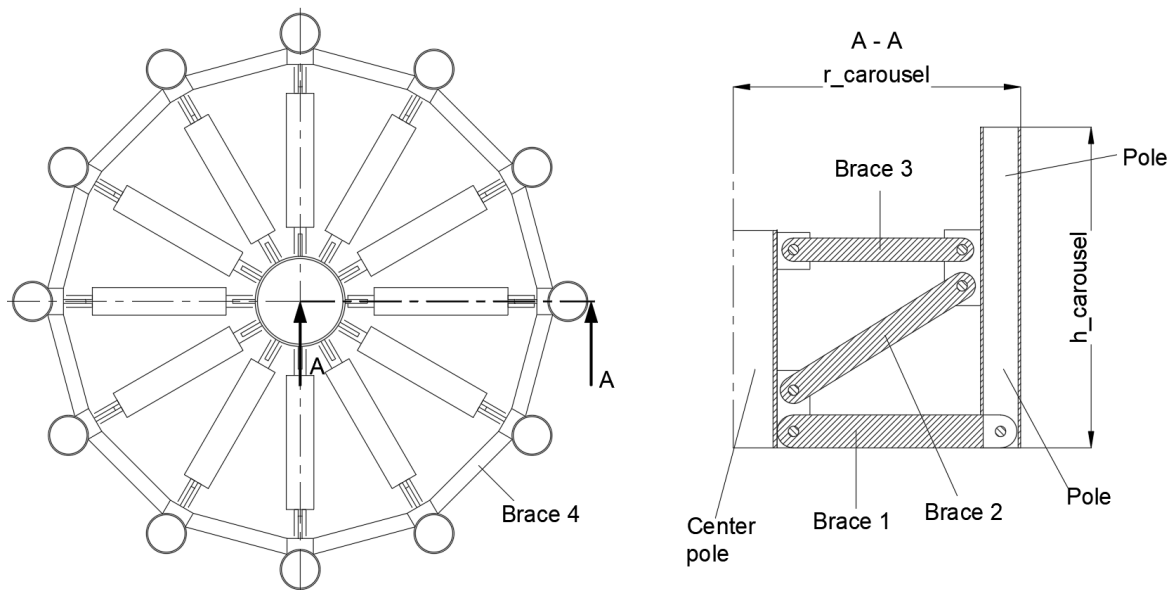


Figure 3-22: Inner frame structure and dimensions

3.3.3 Floor

As discussed before, the floor consists of floor plates with standard 20-feet container dimensions (Table 3-2 requirement 4). In the concept proposed Mammoet the floor plates are reinforced by:

- 2 longitudinal HEB 600 beams
- 4 transverse HEB 300 beams
- 1 longitudinal HEB 200 beam

Furthermore, the floor plates are aligned corner to corner. The plates are connected to each other by connecting the longitudinal beams of one plate to the other longitudinal beams for the longitudinal direction or by connecting the 2 transverse beams of one plate to the other for a transvers connection. The floor plates and their connection proposed by Mammoet are schematically visualized in Figure 3-23.

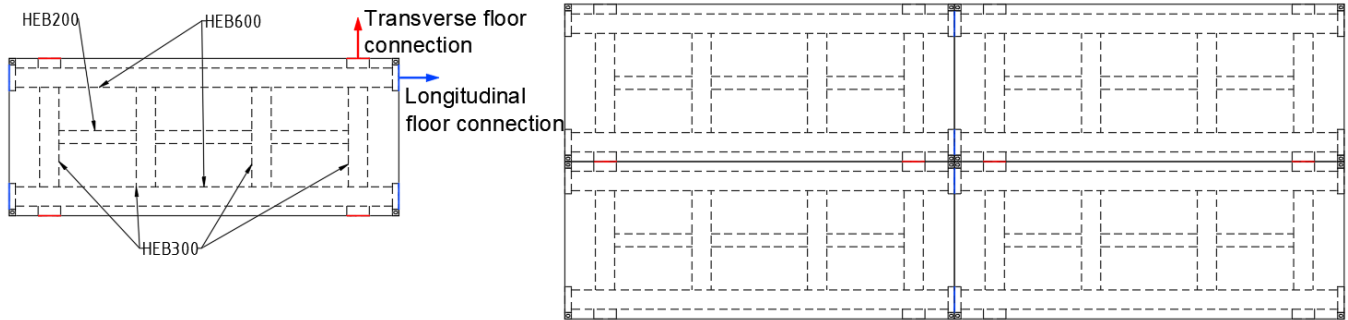


Figure 3-23: Floor plate connection in proposed design by Mammoet

For setup 9 some plates aren't aligned corner to corner to each other. To connect these plates some adjustment must be made to the floor plate. Figure 3-24 shows another principle for a new floor plate, which allows other types of connections to each other. These new floor plates also allow connection between transverse beams and longitudinal beams.

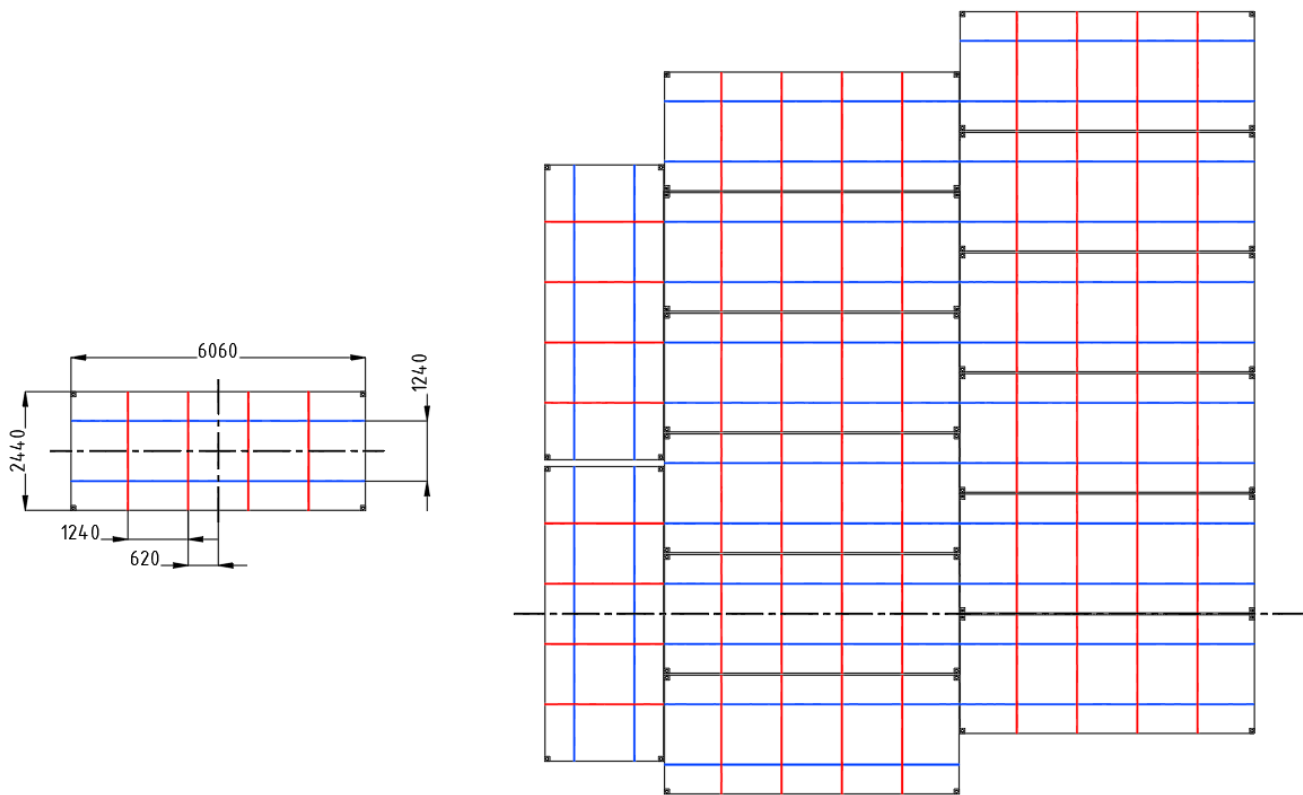


Figure 3-24: Schematic overview of new floor plate

Global beam dimensions are discussed in section 4.3.2. The SPMTs and grillage frame are placed under the floor plates. Connections are left out of scope for this study, but the floor plate must have connections between the inner frame, the SPMT trains, the grillage beams, and the outer frame.

3.3.4 Grillage

For the grillage frame a certain height is necessary to let the SPMT drive below the floor to their desired positions for transport. The SPMTs can have a height between 1150 – 1850mm [32], depending on the cylinder stroke. To overcome ground conditions, it is chosen to give the floor a height of 1350mm, such that there is 200 mm extra space between the SPMTs at lowest position and the carousel floor. As in the CCS design proposed by Mammoet, it is chosen to use reinforces HEB 1000 beams for the grillage beams. Using a HEB 1000 results in $1350 - 1000 = 350\text{mm}$ for the connection between the grillage frame and the floor of the CCS. Again, the connections are left out of scope and thus the connection between the grillage frame and the CCS floor are not considered. The heights of the CCS floor and the SPMT are visualized in Figure 3-25.

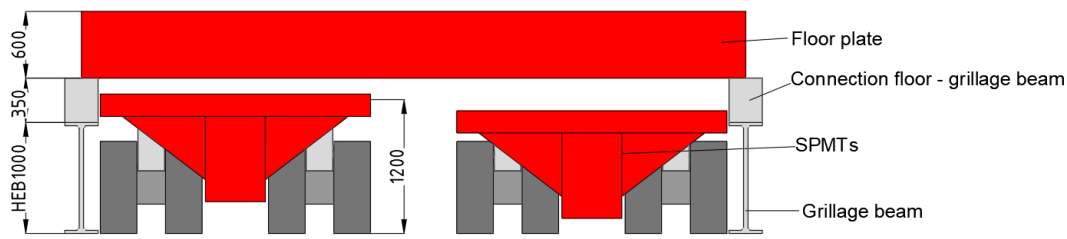


Figure 3-25: Grillage frame and SPMT heights

In the design proposed by Mammoet the grillage beams are divided into multiple pieces. The following beams are used for the grillage frame in this design:

- 4x HEB1000 x 3700mm
- 8x HEB1000 x 5600mm
- 8x HEB1000 x 6200mm
- 2x HEB1000 x 13500mm

Lengths and cross-sectional dimensions of the grillage beams will be further elaborated in section 4.3.2, where the concept will be analyzed. The overall lengths needed for each setup are determined in Section 3.2.

3.4 Conclusion

In chapter 2, multiple challenges for the CCS have been defined. In this chapter conceptual choices which can be made for the CCS have been discussed. The main design choices for the global design of the CCS include the main carousel dimensions, the SPMT setup, the grillage setup, and the floor plate setup. For the deflection of the SPMTs, and thus the used SPMT cylinder stroke, it is expected that the outer carousel dimensions and the SPMT setup are very important. Unsupported axle lines namely increase the SPMT deflection and minimizing the carousel size is beneficial for the CCS weight, costs, and vessel applicability. Three different setups for the CCS with global dimensions and a SPMT / grillage / floor setup have been selected, named setup 1, 9.1 and 11.2

Further design choices are the dimensioning and cross section selection of the structural members. These should be selected according to the strength and stability requirements where the overall CCS weight should be minimized. Minimizing the weight of the CCS is beneficial for the load on the SPMTs such that the needed SPMT axle lines and the SPMT issues as tire wear, hydraulic leakage, and generator overheating, are lowered. To lower the load on the SPMTs, also more axle lines can be used. This however increases the costs of the CCS and the needed outer carousel dimension because the SPMT deflection should be minimized. Also lowering the drive distance of the SPMTs is expected to lower the SPMT issues. This can be done by reducing the radii of the SPMT axle lines (the SPMT should be closely packed) and increasing the outer and inner radii of the carousel. All three setups have approximately equally loaded SPMT axle lines and an equal drive distance of the SPMTs. The performance against the SPMT issues (challenge 3 Table 2-11) is thus expected to be the same. The structural components of the CCS for which the cross-sections and dimensions must be selected are also defined, with the design proposed by Mammoet as a starting point and some adjustments.

4 Concept analysis

In chapter 3, three different setups are proposed, and the structural components of the CCS are defined. In this chapter it will be defined which of the proposed setups has the best performance against SPMT deflection. This setup will be further elaborated, and the structural components will be checked against stability and strength criteria for the occurring loads.

4.1 Loads

The structure will be globally checked by using EN1993-1-1:2005 Design of steel structures, general rules. The governing load cases are the sea transport and the SPMT transport. Storage and cable spooling are not considered because those are not governing for the CCS design (Chapter 2).

4.1.1 General load input

The loads are depended on the input. The general main input for the loads on the carousel is defined in Table 4-1. As described previously, a cable diameter of $D_{cable} = 300mm$ has been selected as that result in the highest cable stack height and thus the highest loads on the carousel.

Table 4-1: General load input

Distribution	Abbreviation	Value	Unit	Source
Capacity	C	5000	t	Table 3-2
Cable diameter	D_{cable}	300	mm	Section 3.1.2

4.1.2 Load actions

The following load actions are considered:

- Self-weight
- Payload
- Sea transport loads
- SPMT transport loads

Self-weight

The CCS consists of the following components: floor structure, outer frame, inner frame, grillage frame and SPMTs. The mass of the floor structure, outer frame and inner frame is referred to as $m_{carousel}$. The self-weight of the SPMTs is neglected as it is already included in the maximum load per axle line and the SPMT self-weight has only small influence on the deflections and stresses. The self-weight of the CCS is dependent on the carousel dimensions and the cross-sectional dimensions of the structure. Because many cross-sections are to be determined, the self-weight cannot be calculated. Previously, chapter 3.2.1 has made rough estimations of the self-weight of the proposed setups, shown Table 4-2.

Table 4-2: Estimated self-weight of different setups

Distribution	Abbreviation	Setup 1	Setup 9	Setup 11	Unit
Self-weight carousel and grillage frame	$m_{carousel} + m_{grillage}$	732	863	1330	t

For the unmodeled parts, reinforcement, and accessories an extra weight equal to 25% of the modelled self-weight is included for the calculations. This means that the accelerations on the self-weight, due to gravity and sea accelerations, will be multiplied by 1.25. This will not be done for the setup selection in section 4.2 as the setups are only checked for deformations in SLS, where the extra 25% self-weight doesn't change the performance of the different setups compared to each other.

Payload

The payload includes the entire cable spooled in the carousel. Under gravity of $9.81 m/s^2$ the payload results in a load of $5000 \cdot 9.81 = 49050kN$, which is uniformly distributed over the carousel footprint (section 2.2.3). Friction between the payload and the carousel floor, inner wall and outer wall is neglected (section 2.2.3).

Sea transport loads

During the sea transport the carousel is subjected to accelerations due to the vessel motion. For the elaborated concept the CCS will be checked against these loads. The carousel and vessel orientation can be seen in Figure 4-1.

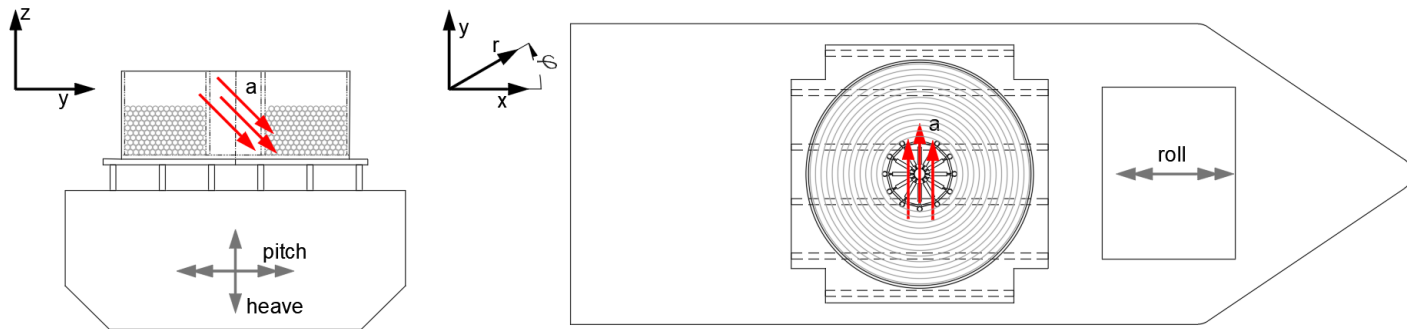


Figure 4-1: Carousel and vessel orientation

In section 2.2.3 the accelerations on the carousel due to pitch, heave and roll have been defined. These are again summarized in Table 4-4.

Table 4-3: Vessel accelerations for sea transport based on current design

	$a_{x,pitch}$	$a_{y,roll}$	$a_{z,heave}$
Value	$\pm 0.20G$	$\pm 0.50G$	$\pm 0.30G$

These accelerations are applied on both the carousel and the cable stack. The total load on the carousel due to the sea transport accelerations are given in Table 4-4. For the self-weight the load has been multiplied by 1.25 for weight of the unmodelled parts, reinforcement, and accessories.

Table 4-4: Vessel accelerations for sea transport based on current design

Resultant load	Self-weight	Pay load	Unit
F_x	$2 \cdot \text{self weight} \cdot 1.25$	$2 \cdot 5000 = 10000$	kN
F_y	$5 \cdot \text{self weight} \cdot 1.25$	$5 \cdot 5000 = 25000$	kN
F_z	$3 \cdot \text{self weight} \cdot 1.25$	$3 \cdot 5000 = 15000$	kN

According to section 2.2.3, the pay load due to the heave acceleration in the z direction is implemented in the uniformly distributed load with the payload due to gravity. The load in the horizontal direction is applied to the inner core as discussed in section 2.2.3 and shown in Figure 4-2 (example shown for acceleration in x direction). This load is validated in chapter 5.

A cable diameter D_{cable} of 300mm has been selected with a total capacity for the carousel of 5000 t (Table 4-1). The needed carousel height $h_{carousel}$ can be calculated with the formulas in Appendix D.

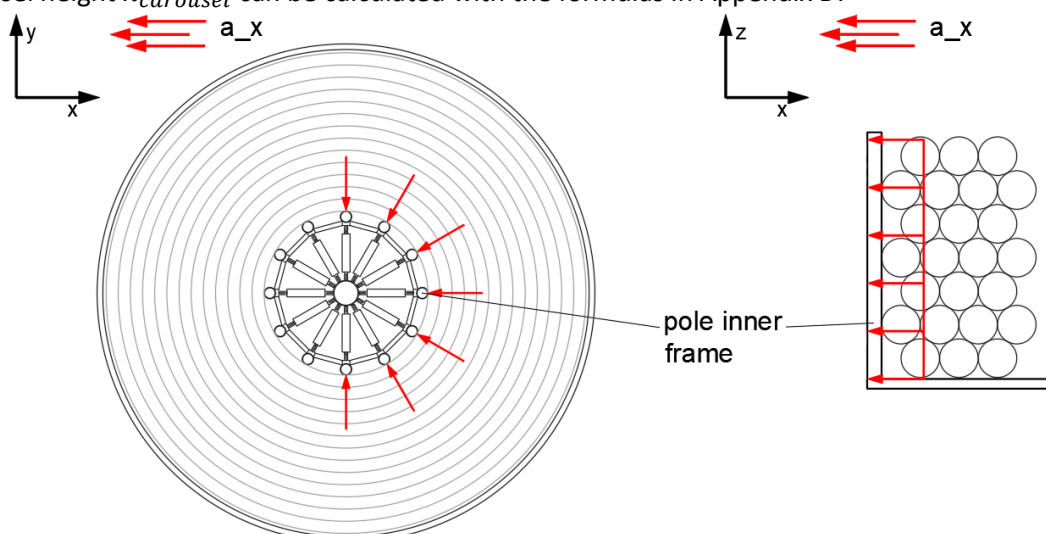


Figure 4-2: Horizontal load due to sea transport applied on inner frame

SPMT transport loads

During SPMT transport the following loads are important:

- **Dynamic SPMT loads:** the (de-)acceleration due to the drive and (emergency) brake of the SPMTs for the transport and spooling of the carousel causes load on the carousel.
- **Differential settlements:** When using 4 hydraulic zones, as is the case for the chosen concepts (Section 2.3.1), ground unevenness can cause that a hydraulic zone has a higher pressure than the other hydraulic zones. This results in higher axle loads on some parts of the CCS.
- **SPMT coupling forces:** During transport and spooling the SPMT trains are aligned with each other. Multiple reasons can cause that there is tendency of the SPMT trains to have motions relative to each other. As a result, additional coupling forces are present on the carousel to keep the SPMT trains aligned (Section 2.3.1).

For the setups defined in section 3.2 a factor of 1.15 (Table 3-4) has been used to lower the maximum load on the SPMT axle lines. This causes that more SPMT axle lines are used in each setup to have more capacity for the effects / loads listed above. From the design proposed by Mammoet [27] it follows that the sea transport loads are governing for the strength of the carousel. Considering the above reasons, the SPMT transport loads are not calculated in detail, and it is assumed the used factor for lowering the maximum axle load is sufficient to have enough capacity for the effects / loads listed above. As a result, the occurring stresses and checks must show that there is capacity left.

The needed SPMT axle loads are calculated and applied manually for each model / setup in sections 4.2 and 4.3 to simulate the effect of the hydraulic zone where all the axle loads are equal in a hydraulic zone.

Not considered

The following loads will not be considered in the calculations

- Wind loads
- Temperature loads
- Snow and ice loads
- Earthquake loads
- Vessel deck deflections
- Loads not mentioned

4.1.3 Load factors

The governing loads are thus the self-weight, pay load, sea transport loads and the SPMT transport loads. For each load defined in section 4.1.2, favorable and unfavorable load factors have been defined as shown in Table 4-5.

Table 4-5: Load factors

Load action	Unfavorable	Favorable
Self-weight carousel	1.50	1.00
Self-weight grillage	1.50	1.00
Pay load	1.50	1.00
Sea transport loads	1.50 or 0.00	1.00 or 0.00
SPMT axle loads	1.50 *	1.00 *

* The SPMT axle loads need to be calculated for each simulation to satisfy the equilibrium conditions. In general, the load factors 1.50 and 1.00 as in Table 4-5 result in equilibrium.

The heave effects are combined with the gravity loads for self-weight and the pay load, resulting in the following load factors for the payload:

- Negative heave favorable: $\gamma_f = 1.00 \cdot \frac{9.81+3}{9.81} \approx 1.31$
- Positive heave favorable: $\gamma_f = 1.00 \cdot \frac{9.81-3}{9.81} \approx 0.69$
- Negative heave unfavorable: $\gamma_f = 1.50 \cdot \frac{9.81+3}{9.81} \approx 1.96$
- Positive heave unfavorable: $\gamma_f = 1.50 \cdot \frac{9.81-3}{9.81} \approx 1.04$

4.1.4 Load combinations

For both the SPMT and sea transport, load combinations can be defined by making different combinations of load factors. Load combinations are separated into serviceability limit states (SLS) and ultimate limit states (ULS). SLS is used to check the model for stiffness / deformations in working conditions and ULS is used to determine the strength / stability of the model under the worst-case-scenario loads. For both load cases:

- **SPMT transport:** Table 4-6 shows the load combinations for the SPMT transport.

Table 4-6: Load combinations for SPMT transport

Load action	SLS	ULS *
Self-weight floor and carousel	1.00	1.50
Pay load	1.00	1.50
SPMT axle loads	1.00	1.50

* ULS checked only for elaborated concept.

The grillage frame is optionally connected with the carousel during SPMT transport. However, the grillage frame will not be included in the calculations for the SPMT transport. This is because the self-weight of the grillage frame is approximated 1% of the pay load and the grillage frame adds additional stiffness to the CCS. Therefore, it is expected that the effect is negligible and excluding the grillage frame simplifies the calculations. For the detailing of the CCS, it is advised to include the grillage frame.

- **Sea transport:** Table 4-7 shows the load combinations for the Sea transport.

Table 4-7: Load combinations for sea transport

Load action	SLS				ULS			
	1	2	3	4	1	2	3	4
Self-weight carousel	0.69	0.69	1.31	1.31	1.04	1.04	1.96	1.96
Self-weight sea fastening	0.69	0.69	1.31	1.31	1.04	1.04	1.96	1.96
Pay load	0.69	0.69	1.31	1.31	1.04	1.04	1.96	1.96
Pitch - Self-weight carousel	1.00	0.00	1.00	0.00	1.50	0.00	1.50	0.00
Pitch - Self-weight sea fastening	1.00	0.00	1.00	0.00	1.50	0.00	1.50	0.00
Pitch - Payload	1.00	0.00	1.00	0.00	1.50	0.00	1.50	0.00
Roll - Self-weight carousel	0.00	1.00	0.00	1.00	0.00	1.50	0.00	1.50
Roll - Self-weight sea fastening	0.00	1.00	0.00	1.00	0.00	1.50	0.00	1.50
Roll - Payload	0.00	1.00	0.00	1.00	0.00	1.50	0.00	1.50

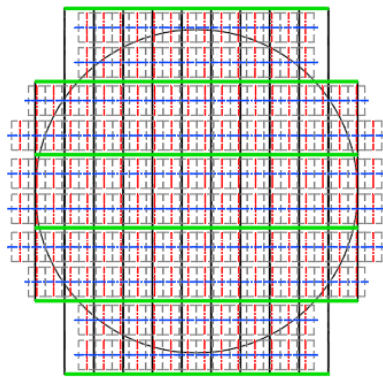
4.2 Setup selection

In section 3.2, setups 1, 9.1 and 11.2 have been selected to be further elaborated. In this section these setups checked against the SLS SPMT transport load case to define the performance against SPMT deflection, and thus challenge 2 from Table 2-11. Based on the results the setup with the best performance will be selected for further elaboration in section 4.3.

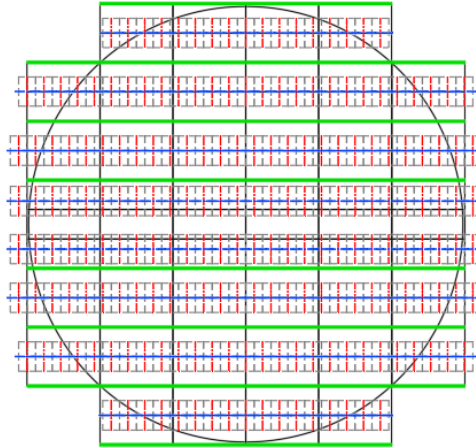
4.2.1 Input

The chosen setups are visualized in Figure 4-3.

Setup 1



Setup 11.2



Setup 9.1

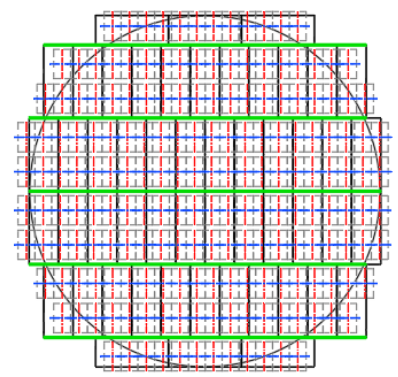


Figure 4-3: Setups 1, 9.1 and 11.2

For the setups the general input is given in Table 4-8.

Table 4-8: General input

Setup	Abbreviation	1	11.2	9.1	Unit	Source
Outside carousel radius	$R_{carousel}$	13.3	18.1	14.6	m	Table 3-7
Inside carousel radius	$r_{carousel}$	4.375	5.00	4.00	m	Table 3-7
Capacity	C	5000			t	Table 4-1
Number of floor plates	/	51	82	52	/	Table 3-7
Number of axle lines	/	185	200	188	/	Table 3-7

Each setup is modelled in the same manner as described in Table 4-9.

Table 4-9: Setup selection model description

#	Description	Source
1	Grillage frame not included in the model	Section 4.1.4
2	Inner frame not included in the model. This because its weight is approximated 1% of the pay load and its adds extra stiffness to the carousel. Therefore, it is assumed that the effect is negligible for a simplified model.	/
3	The outer frame is not included in the model	Section 3.3.1
4	SLS loads for SPMT transport from Table 4-6 are applied as described in Section 4.1	Section 4.1
5	The floor of each model consists of floor plates as described in section 3.3.3 (Figure 3-24) with HEB 600 for the longitudinal beams and HEB 300 for the transversal beams.	Section 3.3.3
6	Near the center, the model will be fixed at 1 node in all direction to prevent rigid body motion	/
7	All connections between the different structural components are modelled to be fixed. Relative stiff dummy elements have been used to transfer loads between different structural component or to figure as connections.	/

The resulting models are elaborated in Appendix G.

4.2.2 Results

The models and the results are given Appendix G. The results are summarized in Table 4-10.

Table 4-10: Results setup selection study

Setup	Weight floor [t]	Maximum deformation z direction [mm]
1	250	225
11.2	403	202
9.1	255	90

Table 4-10 shows that the setups 11.2 and 9.1 show a large improvement compared to setup 1 considering the maximum deformation in the z direction and thus the deflection of the SPMT transport is lowered. Especially setup 9.1 shows good performance as it has approximately the same weight of setup 1, but a larger outer frame diameter and significantly less deformation and SPMT transport deflection. For this reason, it is chosen to further elaborate setup 9.1. The deformation plots in the z direction of setups 1, 11.2 and 9.1 are respectively shown in Figure 4-4, Figure 4-5, and Figure 4-6. In every figure the same color scheme is used and the maximum and minimum deformations in the z direction are shown. Figure 4-5 also shows that in the middle the floor is bended upward. This results in higher maximum deformations and is caused by a too large inner carousel radius. Asymmetries in the plots are caused by an offset in the fixed point in the models. The plots in Figure 4-5 are scaled and use the same color scale.

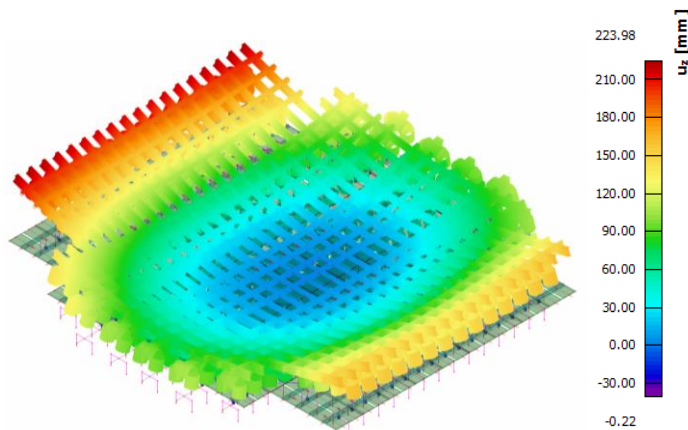


Figure 4-4: Setup 1 deformation z direction

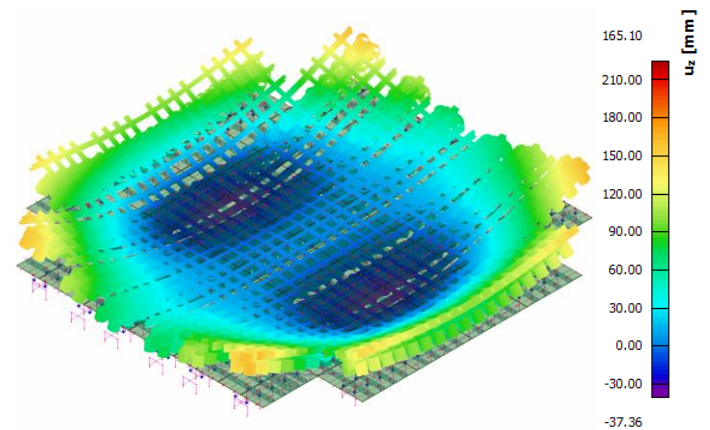


Figure 4-5: Setup 11.2 deformation z direction

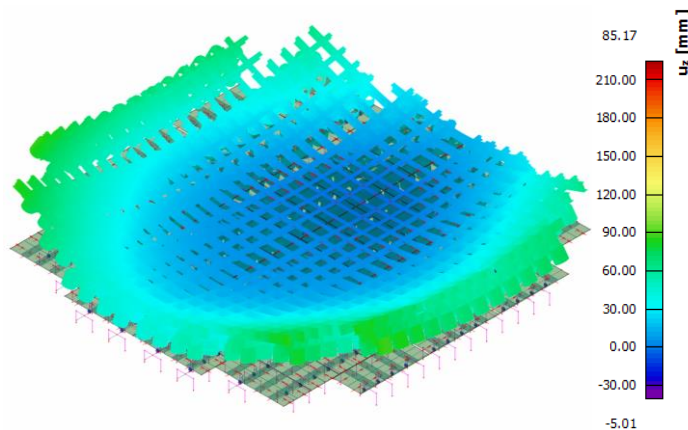


Figure 4-6: Setup 9.1 deformation z direction

4.3 Concept elaboration

In section 4.2 it is chosen to further elaborate setup 9.1. In this chapter a more accurate model of 9.1 will be made. This model will be checked for stability and strength (challenge 1 from Table 2-11)

4.3.1 Input

The general input for the model of setup 9.1 is shown in Table 4-11.

Table 4-11: General input for elaborated concept

Distribution	Abbreviation	Value	Unit	Source
Capacity	C	5000	t	Table 4-1
Cable diameter	D_{cable}	300	mm	Table 4-1
Outside carousel radius	$R_{carousel}$	14.6	m	Table 3-7
Inside carousel radius	$r_{carousel}$	4.00	m	Table 3-7
Number of floor plates		52	/	Table 3-7
Number of SPMT axle lines		188	/	Table 3-7

A model has been elaborated as described in Table 4-12.

Table 4-12: Model description for elaborated concept

#	Description	Source
1	SLS and ULS loads for both Sea and SPMT transport from Table 4-6 and Table 4-7 are applied as described in Section 4.1. For both sea and SPMT transport a different model will be made.	Section 4.1
2	A cable with a diameter $D_{carousel}$ of 300mm will be used. Using Appendix D, a carousel height of $h_{carousel} = 4.7 m$ is needed to store the corresponding cable stack based on the input from Table 4-11.	Appendix D
3	The outer frame is not included in the model	Section 3.3.1
4	The floor of consists of floor plates as described in Section 4.3.2 (Figure 3-24).	Section 4.3.2
5	For SPMT transport the model will be fixed near the center in all directions to prevent rigid body motion	/
6	<p>Connections has been implemented as follows:</p> <ul style="list-style-type: none"> - <i>Floor plate – floor plate</i>: large stiffness for rotation and translation to avoid clamping effects - <i>Floor plate – Grillage beam / sea fastening</i>: large stiffness for rotation and translation to avoid clamping effects - <i>Grillage beam / sea fastening – vessel deck</i>: at places where there is a vessel deck transverse a connection is modeled with large stiffness for rotation and translation to avoid clamping effects. - <i>Floor plate – inner frame</i>: Fixed connection is modeled, because very strong connections will be used for this connection - <i>Floor plate – SPMT</i>: pressure only and stiffness for horizontal translation as friction - <i>Inner frame connections</i>: Stiffness for rotation, translation fixed <p>All connections between structural components not mentioned above are modelled as fixed connection. Relative stiff dummy elements have been used to transfer loads between different structural components.</p>	/

The resultant model is described in Appendix H.

4.3.2 Concept elaboration

Sea fastening

One of the main problems found during the analysis is that the CCS during sea transport has difficulties with the load transfer of the load due to roll of the vessel. As shown in Figure 4-7, the horizontal load is partly transferred lateral load on the top flange of the grillage beams (the rest in tension or compression in the grillage beam). Due to the HEB1000 height of 1000mm, the webs are prone to these loads and high shear and bending moment will occur in the webs in the weak direction.

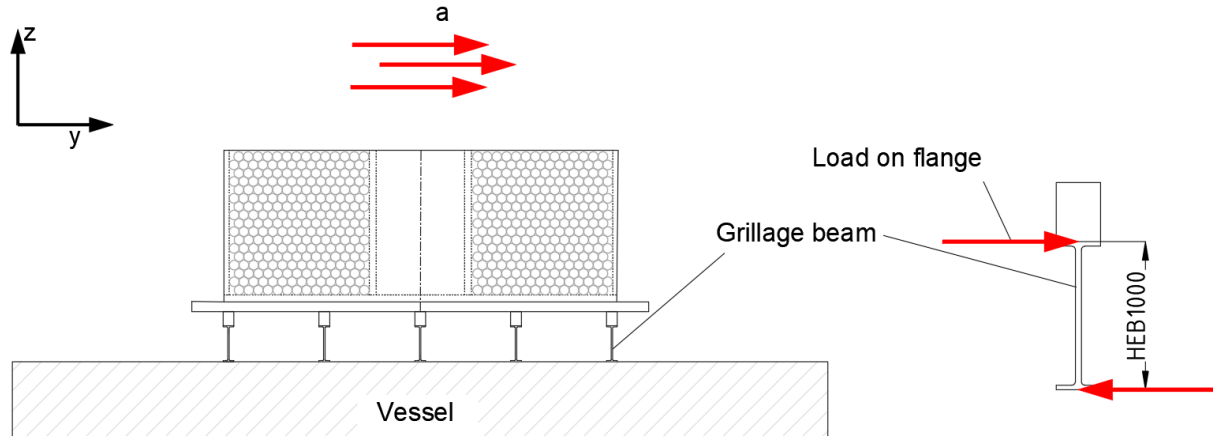


Figure 4-7: Roll acceleration on carousel

To give the webs more resistance more resistance against accelerations in y direction due to roll, stiffeners will be added to the HEB 1000 grillage beams. Furthermore, additional sea fastening will be added as shown in Figure 4-8. This sea fastening consists of very stiff frames and thus the horizontal load in the y direction will be mainly transferred through these frames. The additional sea fastening frames will be welded to the vessel deck aligned with the transverse vessel web frames, such that the high forces through these frames will be transferred to the strong parts of the vessel deck. The additional sea fastening will be inside the total width and length of the CCS on the vessel, and thus no extra vessel deck space will be needed. The percentage of horizontal load transferred through the grillage beams and additional sea fastening is dependent on their stiffnesses.

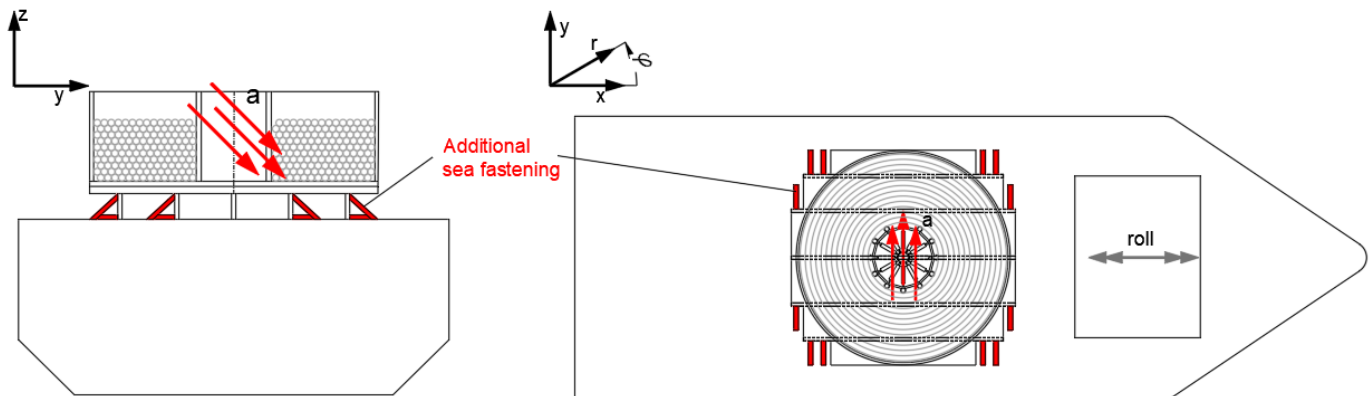


Figure 4-8: Position of extra sea fastening to transfer loads from vessel roll

The defined outer dimensions of the sea fastening are given in Figure 4-9 and the used beams are given in Table 4-14.

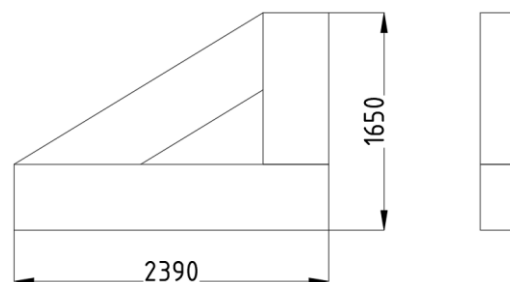


Figure 4-9: Outer dimensions of sea fastening

Figure 4-10 shows how the additional sea fastening is implemented in the calculation model.

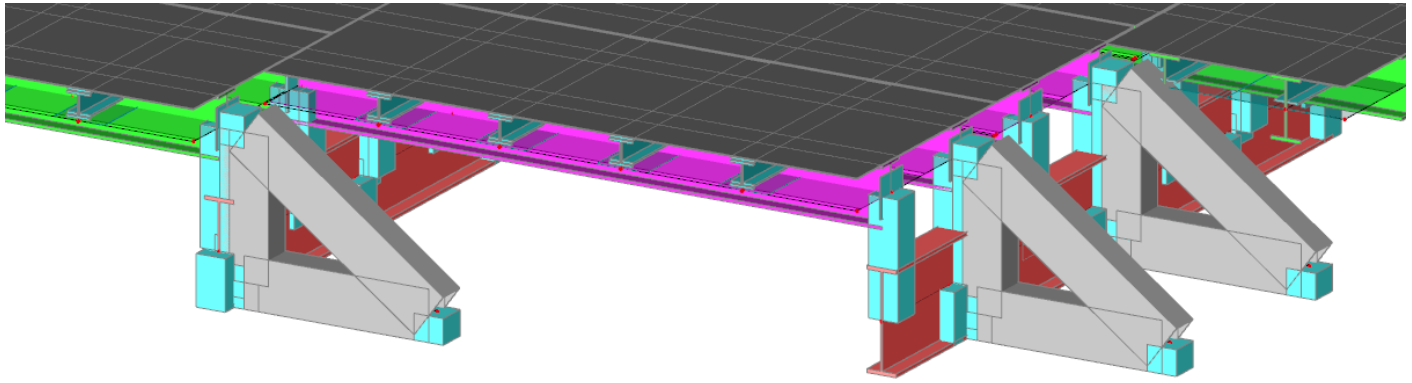


Figure 4-10: Sea fastening in calculation model

Floor

Different forces occur on different parts of the floor. To minimize the weight of the total floor, a general floor plate with less strong lateral and longitudinal beams are used. At the places where higher forces occur, the floor plate is reinforced. An overview of the different types of floor plates can be seen in Figure 4-11.

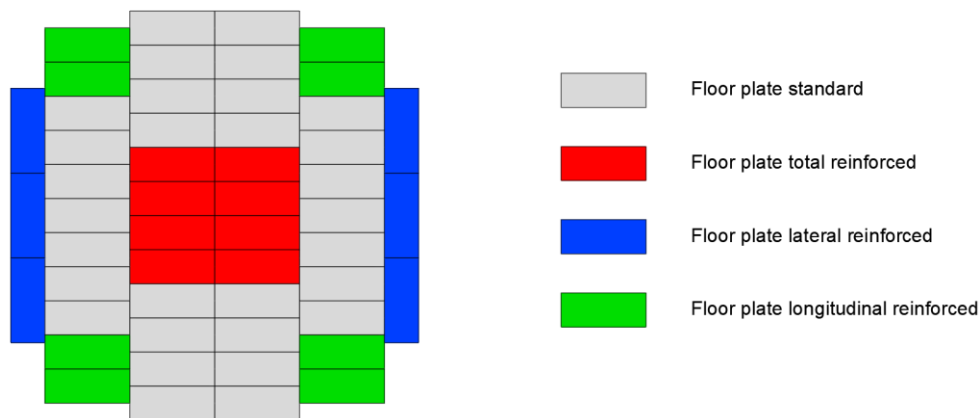


Figure 4-11: Different types of floor plates

Each floor plate has the same setup and dimensions, but other cross sections of the lateral and longitudinal beams. A general overview of a floor plate is shown in Figure 4-12.

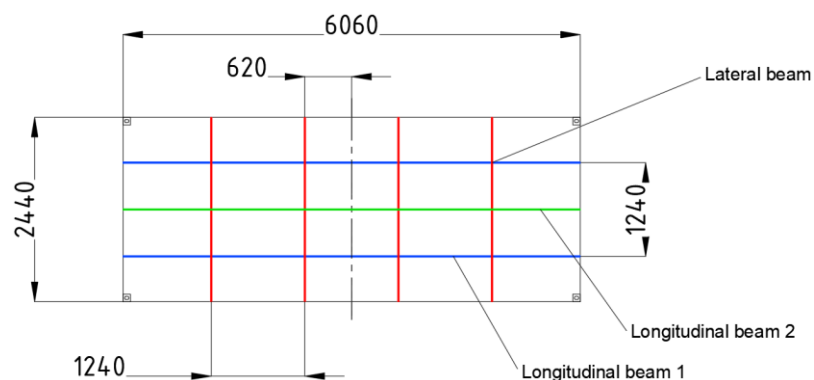


Figure 4-12: Overview of single floor plate

For the total floor, 5 different beams with different cross sections are used, as shown in Table 4-13.

Table 4-13: Beam type overview for floor structure

Floor plate	Longitudinal beam 1	Longitudinal beam 2	Lateral beam
Floor plate standard	Beam 1	/	Beam 2
Floor plate total reinforced	Beam 5	Beam 4	Beam 5
Floor plate lateral reinforced	Beam 2	/	Beam 1
Floor plate longitudinal reinforced	Beam 3	/	Beam 2

The cross sections of the beams are defined in Table 4-14. Each floor plate has the following properties:

- *Floor plate standard*: The standard plate is minimized in weight by selecting cross sections which give slightly enough stiffness, strength, and stability. The standard floor plate is mainly loaded by bending and therefore I-beams are a good choice.
- *Floor plate total reinforced*: In the center the floor must resist a large bending moment due to the horizontal load on the inner frame. This causes that the floor plate must be reinforced. Also, an additional longitudinal beam is added in the middle of the plate.
- *Floor plate lateral reinforced*: This floor plate aligned perpendicular to the other plates. As a result, the laterals are heavier loaded than the longitudinal beams and the lateral beams must be reinforced.
- *Floor plate longitudinal reinforced*: Due to the high load transfer through the sea fastening these floor plates are heavily loaded in the longitudinal direction. Therefore, the longitudinal have stronger cross sections for this floor plate.

Inner frame

The inner frame is based on the inner frame from the design proposed by Mammoet, as described in section 3.3.2. Some dimensions are updated due to another cable stack height of $h_{\text{carousel}} = 4.7\text{m}$, and the cross sections used are defined in Table 4-14. An overview of the beams and the main dimensions is given in Figure 4-13.

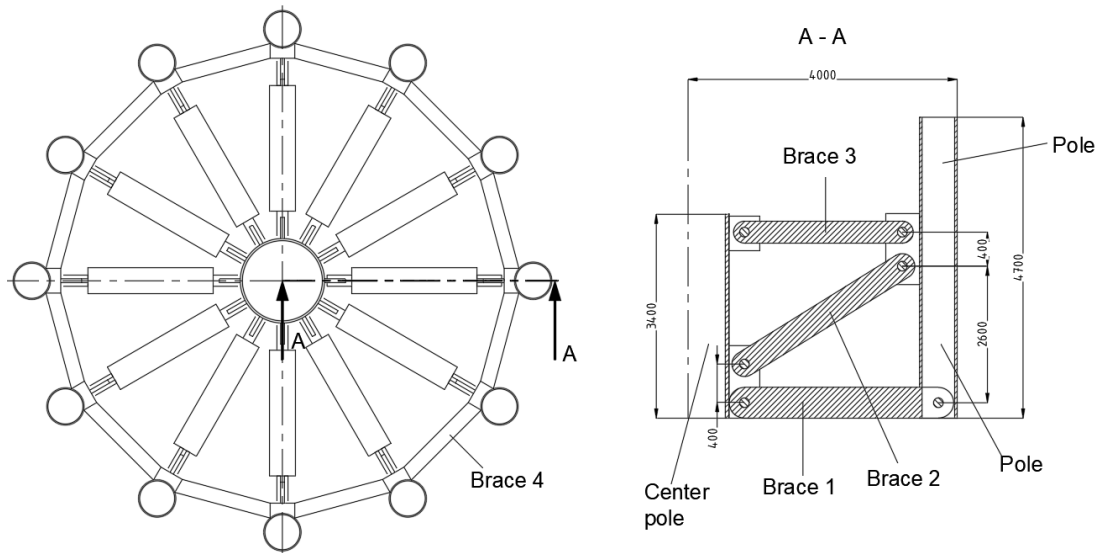


Figure 4-13: Inner frame main dimensions and overview

Grillage frame

As described in 3.3.4, it is chosen to use the HEB 1000 cross section to get the needed height difference and larger HEB beams are not standard. The grillage beams have been separated in multiple parts. 4 beams with a length of 7780mm and 11 beams with a length of 9000mm beams will be used. The setup of the grillage beams is shown in Figure 4-14.

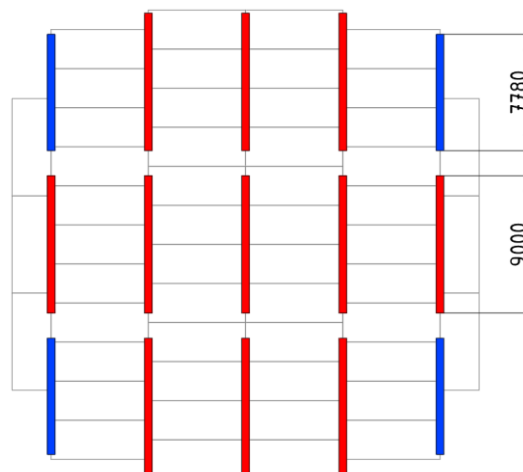


Figure 4-14: Grillage beam lengths and setup

Cross sections

In the CCS many different beam types are used for which the cross section had to be determined. The needed cross sections are dependent on the needed strength, stability, and stiffness. The cross sections are determined starting with the same cross sections as used in the concept design proposed by Mammoet. After cross sectional checks according to EN1993-1-1:2005 Design of steel structures, a stronger cross section is selected for the beams where the strength, stability or stiffness requirements aren't met. Beams for which the unity check are very low, weaker cross sections are selected. Selecting different cross sections can change the load transfer in the entire CCS, for both sea and SPMT transport. The resulting cross sections after a few iterations of simulation and changing cross sections, are summarized in Table 4-14.

Table 4-14: Resulting cross sections for elaborated concept

Structural component	Cross section description	Material	Reference
Floor – Beam 1	HEB 500	S355	Table 4-13
Floor – Beam 2	HEB 240	S355	Table 4-13
Floor – Beam 3	HEB 600	S355	Table 4-13
Floor – Beam 4	HEB 400	S355	Table 4-13
Floor – Beam 5	RHS 600 x 400 x 28	S355	Table 4-13
Inner frame – Center pole	Tube 1370 x 60	S355	Figure 4-13
Inner frame – Pole	Tube 600 x 35	S355	Figure 4-13
Inner frame – Brace 1	Tube 406.4 x 20	S355	Figure 4-13
Inner frame – Brace 2	Tube 406.4 x 25	S355	Figure 4-13
Inner frame – Brace 3	Tube 323.9 x 20	S355	Figure 4-13
Inner frame – Brace 4	Tube 273 x 16	S355	Figure 4-13
Grillage Beam	HEB 1000	S355	Figure 4-13
Sea fastening beam	RHS 500 x 300 x 16.0	S355	Figure 4-9

4.3.3 Results

The resulting structural performance of the CCS against the loads with the cross sections from Table 4-14, is summarized in Table 4-15.

Table 4-15: Results elaborated concept analysis

Description	Value	Unit
Weight floor and inner frame	417	t
Weight grillage frame	51.1	t
Largest unity-check floor (strength and stability)	1.07	/
Largest unity-check inner frame (strength and stability)	1.01	/
Largest unity-check grillage (strength and stability)	1.24	/
Largest unity-check SPMTs (strength and stability)	0.23	/
Maximum deformation z direction (SPMT deflection) without grillage	110	mm
Maximum deformation due to sea transport	36.8	mm

Table 4-15 shows that a most unity checks are slightly higher than 1. In this case these are acceptable because appendix H shows that all these high unity checks are very local and can thus be solved by local reinforcement in the detailing of the CCS. Although the stiffness of the floor is lowered, the maximum deformation of the SPMT transport is still comparable with the results from Table 4-10.

4.4 Conclusion

One of the main challenges is about the used stroke of the SPMT axle lines (challenge 2 Table 2-11). In this chapter the three selected setups from chapter 3 are elaborated to an FEM simulation model. The best performing model has on SPMT deflection of 110mm . Which is a significant improvement compared to the concept proposed by Mammoet with an estimated SPMT deflection of 224mm , while the self-weight of the CCS is approximately the same, but less SPMT axle lines are unsupported. It can thus be concluded that the main dimensions and SPMT / floor setup / grillage setup have a large influence on the SPMT deflection and thus the used cylinder stroke.

Furthermore, for this concept the structural components and the cross sections are defined such that the stability and strength requirements are satisfied for the loads as defined in section 4.1 (only local reinforcements are needed). It is determined that to satisfy strength and stability requirements (challenge 3 Table 2-11) it is beneficial to include extra sea fastening and reinforced floor plates, and that it is needed to select appropriate cross sections for the structural components.

The SPMT tire wear, hydraulic leakage, and generator overheating (Challenge 3 from Table 2-11) can be tackled by reducing the load on the axle lines and increasing the inner radius of the carousel r_{carousel} . However, reducing the load on the axle lines increases the costs and deflection of the SPMTs and increasing the inner radius enlarges the loading on the carousel. Thus, tackling the SPMT issues is not included in the elaborated concept as there are many uncertainties for the SPMT issues.

5 Influence of cable stack

In chapter 4, an improved concept of the CCS is elaborated. For the analysis of this concept, it is assumed that for the payload all the horizontal load is uniformly distributed over the inner frame on the pressure side of the inner frame and that all the vertical load is uniformly distribution over the carousel floor. For these assumptions the friction between the cable stack and the floor, and the load on and load transfer by the outer frame are neglected. To neglect the load transfer by the outer frame the cable stack must have sufficient stiffness. Furthermore, the stiffness of the cable stack can have a positive effect on the SPMT deflection during SPMT transport of the CCS (Section 2.3.2). Therefore, in this chapter the cable and cable stack will be investigated in more detail to verify the assumptions and determine the effects on the CCS. Calculations are based on elaborated concept of chapter 4. As a result, the general input is defined in Table 5-1.

Table 5-1: General input for cable stack analysis

Distribution	Abbreviation	Value	Unit	Source
Capacity	C	5000	t	Table 3-2
Carousel height	$h_{carousel}$	4.70	m	Table 4-12
Inside carousel diameter	$r_{carousel}$	4.00	m	Table 4-11
Outside carousel diameter	$R_{carousel}$	14.6	m	Table 4-11

5.1 Cable stack stiffness

In section 2.2.3 it is determined that the cable stack has enough stiffness to neglect the load on the outer frame. The input for a single cable used for the calculations in section 2.2.3 and appendix B is shown in Table 5-2.

Table 5-2: Input used in section 2.2.3 for cable stack expansion

Description	Abbreviation	Value	Unit
Cable diameter	D_{cable}	190	mm
Corresponding cable weight, equation (2-1)	μ_{cable}	66.8	kg/m
Elastic modulus cable in axial direction	$E_{cable,axial}$	5.00	GPa
Elastic modulus cable in radial direction	$E_{cable,radial}$	1.00	GPa

In this chapter a single cable is discussed to verify this input.

5.1.1 Cable specification

In Figure 5-1 and Figure 5-2 typical DC and AC cross sections are shown, respectively.

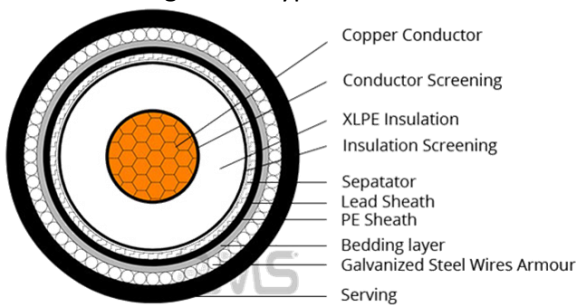


Figure 5-1: typical DC submarine cable [42]

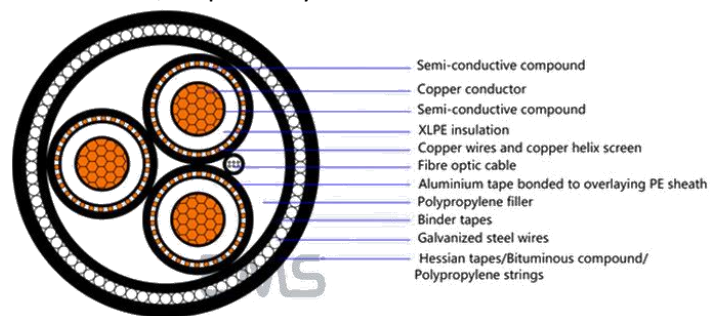


Figure 5-2: typical AC submarine cable [43]

In general, for both the DC and AC cables the same materials are used [44]:

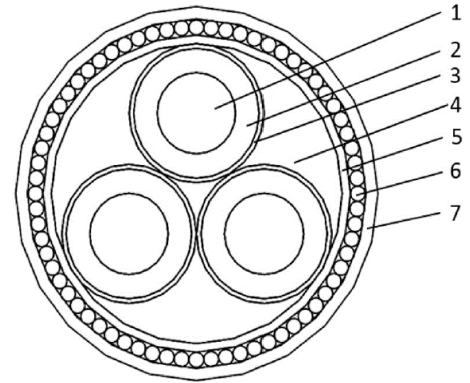
- **Conductor:** The conductor(s) are made from copper or aluminum.
- **Insulation:** The insulation is in many cases made from crosslinked Polyethylene (XLPE). For the high voltage DC cables with large capacity and distance mass-impregnated cables are used. For these cables the isolation consists of paper tapes impregnated with a viscous compound [45].
- **Cable armor:** The cable armor is made from galvanized or stainless-steel wires. This is the strongest part of the cable and is responsible for a large part of the stiffness
- **Lead sheet:** The lead sheet mostly consists of a lead alloy

- **Filler:** The filler consists mostly of a polymer
- **Inner and outer sheath:** The inner and outer sheath mostly consist of HDPE
- **Screens and other layers:** There are several screens and layers to protect the insulation from water ingress. Metallic Layers are employed to reduce the emittance of electric fields and deny Teredo-worms. Metallic layers outside of the main insulation can also be used for testing the cable insulation properties.

As described in Table 1-2: , research boundary 3, a single cable with average properties will be selected and elaborated. A cable with three conductors will be considered because the behavior of this kind of cable is more complex compared to a cable with a single core. The layers of the selected AC cable are summarized in Table 5-3.

Table 5-3: Layer thicknesses of selected cable

Layer	Component	Layer thickness [mm]	Outer diameter [mm]	Material
1	Conductor	15	30	Copper
2	Insulation	21	72	XLPE
3	Load sheath	2	76	Lead alloy
4	Filler	/	163.75	Polymer
5	Inner sheath	3.625	171	HDPE
6	Amour	5.5	182	steel
7	Outer sheath	4	190	HDPE



The poisson's ratio, elastic modulus, and the density of many used materials in offshore power cables are shown in Table 5-4.

Table 5-4: Material properties offshore power cables

Material	Usage	Poisson's ratio [λ]	Elastic modulus [GPa]	Density [kg/m ³]
Copper	Conductor	0.34	110	8900
XLPE	Insulation	0.46	1.25	955
Steel	Armor	0.33	210	7800
Lead alloy	Lead sheet	0.42	40	11340
Polymer	Filler	0.46	1.5	1000
HDPE	Inner and outer sheath	0.46	1.2	950

Cable mass

By calculating the areas and using the density of each layer, the weight per meter for each layer can be determined. Results are shown in Table 5-5.

Table 5-5: Layer weights

Layer	Component	Material	Density [kg/m ³]	Area one layer [m ²]	Area [m ²]	Mass [kg/m]
1	Conductor	Copper	8900	7.1E-04	2.1E-03	1.9E+01
2	Insulation	XLPE	955	3.4E-03	1.0E-02	9.6E+00
3	Load sheath	Lead alloy	11340	4.6E-04	1.4E-03	1.6E+01
4	Filler	Polymer	1000	\	7.5E-03	7.5E+00
5	Inner sheath	HDPE	950	\	1.9E-03	1.8E+00
6	Amour	steel	7800	\	2.4E-03	1.9E+01
7	Outer sheath	HDPE	950	\	2.3E-03	2.2E+00

Summation of all weights and areas results in the total mass per meter for the selected cable. For the average density of the cable, the mass per meter needs to be divided by the cross-sectional area of the cable. The results are shown in Table 5-6. It follows that the mass μ_{cable} is comparable as defined in Table 5-2 for $D_{cable} = 190mm$.

Table 5-6: General cable properties

Description	abbreviation	value	Unit
Cross-sectional area	A_{cable}	0.028	m^2
Average mass per meter	μ_{cable}	65	kg/m
Average cable density	ρ_{cable}	2300	kg/m^3

5.1.2 Cable stiffness

In section Appendix B it is shown that the expansion of the cable stack is dependent on the radial stiffness and axial stiffness of the cable. To determine the cable stiffness of the selected cable manual calculations and FEM simulations have been executed and compared to each other for the selected cable properties from section 5.1.1. This is described in appendix F. The FEM model is shown in Figure 5-3 and in Figure 5-4 a few parts of the model are hidden such that the helical spiraling of the cores and armor can be seen.

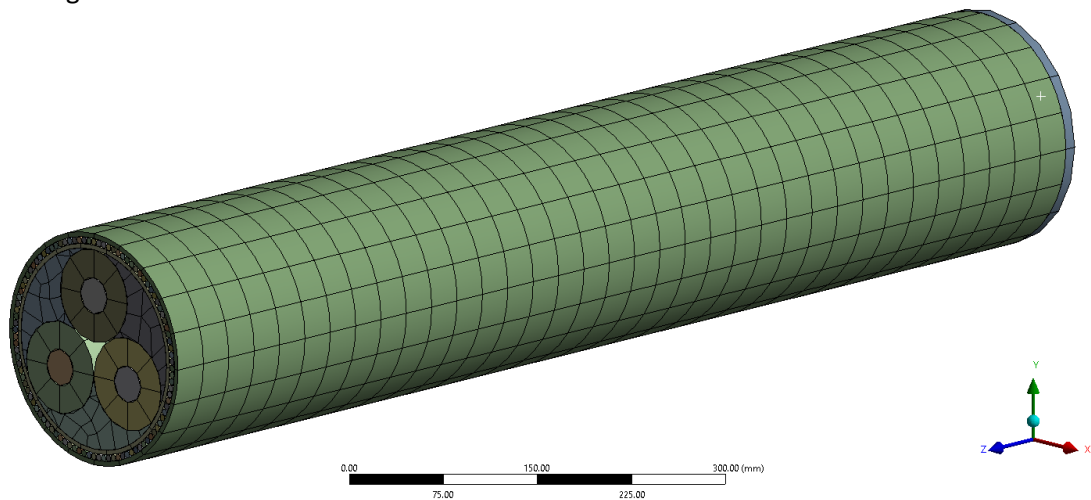


Figure 5-3: FEM simulation model for cable stiffness analysis

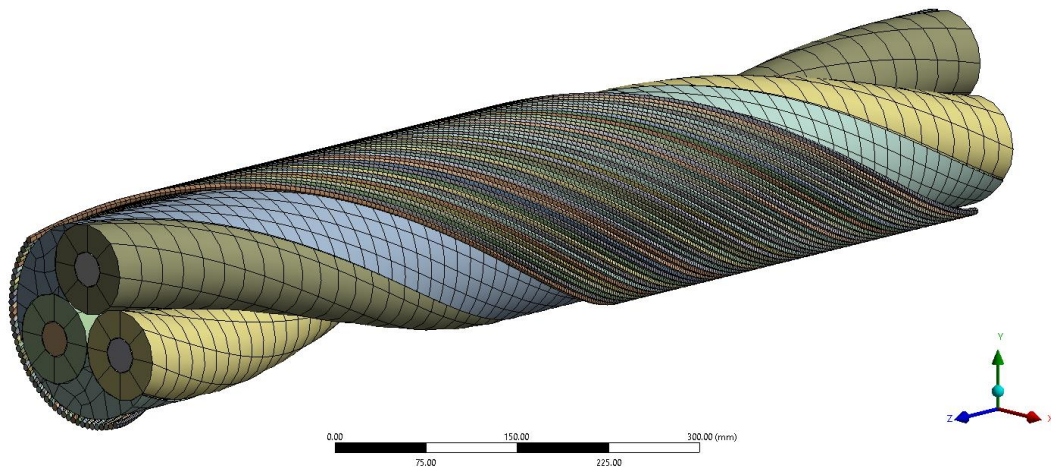


Figure 5-4: Helical spiraling in cable

The following paragraphs the axial, bending, torsional and radial stiffness are respectively discussed.

Axial stiffness

The axial stiffness of a cable is mainly determined by the conductor and the armor wires. Also, the pitch angle of the armor wires, compression of the core, and twisting of the cable have influences on the axial stiffness. For small strains it can be assumed that the offshore power cables behave linearly against tension [44]. The axial stiffness is defined as the resistance against axial deformation δ due to internal normal force $N(x)$ over the cable. For a general truss element as shown in Figure 5-5, the axial deformation against the normal force and linear axial stiffness is given by

$$\delta = \int_0^L \frac{N(x)}{E_{axial}A} dx \quad (5-1)$$

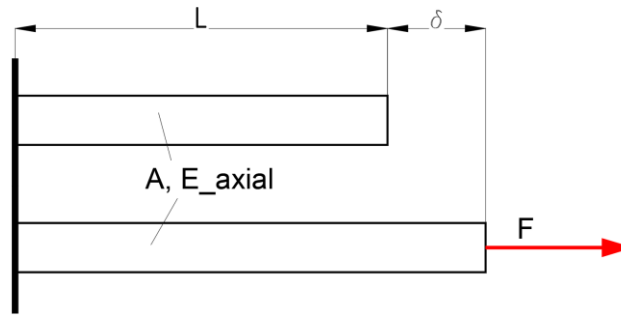


Figure 5-5: Principle of axial stiffness

, with cross sectional area A and truss length L . The main interest for the axial stiffness is to determine the axial elastic modulus E_{axial} of the cable. The results from appendix F are summarized in the Table 5-7.

Table 5-7: Axial elastic modulus results for selected cable

Description	Abbreviation	Value	Unit
Calculated elastic modulus	$E_{cable,axial}$	25.9	GPa
Elastic modulus FEM: bonded contact	$E_{cable,axial}$	21.3	GPa
Elastic modulus FEM: internal friction neglected	$E_{cable,axial}$	21.0	GPa
Elastic modulus FEM: both internal friction and wire – wire contact neglected	$E_{cable,axial}$	5.26	GPa
Elastic modulus FEM: no separation contact	$E_{cable,axial}$	6.19	GPa

The calculated elastic modulus is relatively high because the calculation only considers the elongation of average of the different layers and the straightening of the armor wires and conductors is neglected. The calculated stiffness is comparable with the FEM simulation where all the layers are bonded to each other and where internal friction is neglected. With the “no separation contact” the layers can slip relative to each other (friction is neglected), but the layers can’t separate from each other such that tension can still be transferred. The no separation contact causes that the resistance of the helical spiraled armor wires and conductor cores against straightening is lowered. This results in more cable rotation along with more elongation of the cable, which thus lowers the stiffness as shown in Table 5-7.

In the actual cable the layers can’t transfer tension and they can possibly separate, which will lower the axial stiffness. This effect is simulated by neglecting the wire – wire contact and Table 5-7 shows that allowing separation between the wires significantly decreases the axial stiffness. On the other side there is friction between the layers and Table 5-7 shows that infinity friction causes 4 times as many axial stiffness compared to zero friction. FEM simulation with frictional contacts however couldn’t converge, but it is expected that the actual axial stiffness of the cable is around 7.5 – 10 GPa. In Section 2.2.3, the expansion of the cable stack is assumed to be negligible for an axial cable stiffness of 5 GPa (Table 5-2) for a comparable cable diameter of $D_{cable} = 190 \text{ mm}$. This means that also the 7.5 – 10 GPa is sufficient axial stiffness to neglect the expansion of the cable stack and thus the load transfer by the outer frame.

Radial stiffness

In appendix B it is approximated that the cables on the bottom deform 0.01mm under the self-weight of the cable stack (Δw in Figure 5-6) with a radial stiffness of 1 GPa (Table 5-2). The radial stiffness is defined as the resistance against radial deformation against radial loading. To determine the load on the bottom cables, the amount of cable turns on the bottom row can be calculated by (see Appendix D)

$$\# \text{ cable turns} = \frac{R_{carousel} - r_{carousel} - 0.5D_{cable}}{D_{cable}} \quad (5-2)$$

The average length of a single cable turn can be calculated by (Appendix D)

$$L_{ct,avg} = \pi \cdot (r_{carousel} + R_{carousel}) \quad (5-3)$$

The total length of cable on the bottom row can then be estimated by $L_{ct,avg} \cdot \# \text{ cable turns}$. Assuming the entire capacity C induces its self-weight on the bottom row, the radial load on the cable (F in Figure 5-6) follows as

$$F_{rad} = \frac{C \cdot 9.81}{2 \cdot \sin(60^\circ) \cdot \# \text{ cable turns} \cdot L_{ct,avg}} \quad (5-4)$$

, where normal gravity is used, and other accelerations are neglected. The result is multiplied by $1/2 \sin 60^\circ$ because the load is separated over two contacts under an angle of 60° .

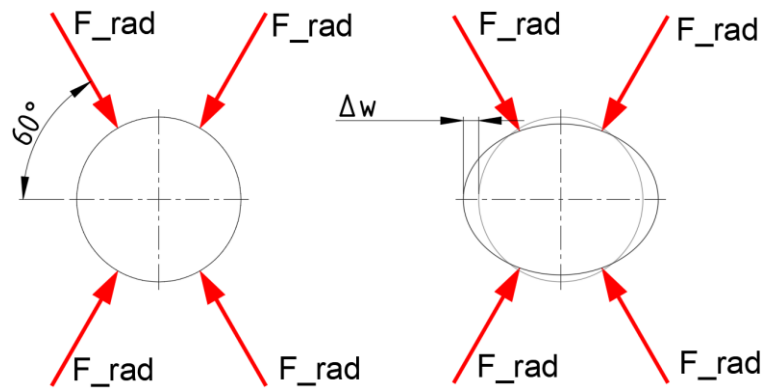


Figure 5-6: Radial stiffness principle

For C , $r_{carousel}$ and, $R_{carousel}$ as defined in Table 5-1 and $D_{cable} = 190\text{mm}$ for the selected cable (section 5.1.1) the load follows as $F = 8.8 \text{ kN/m}$. The resulting deformations for the simulations in appendix F, are shown in Table 5-8.

Table 5-8: Radial deformation in horizontal direction under cable stack self-weight

Description	Abbreviation	Value	Unit
Displacement FEM simulation no separation contact	Δw	0.0052	mm
Displacement FEM simulation bonded contact	Δw	0.0096	mm

The deformations given in Table 5-8 are relatively low compared with the cable and cable stack dimensions. In appendix B, for a comparable cable diameter $D_{cable} = 190 \text{ mm}$ and a radial stiffness of 1 GPa (Table 5-2) it is estimated that a single cable has a deformation of $\Delta w = 0.01 \text{ mm}$ under the $5000t$ self-weight of the cable stack. With this deformation the expansion of the cable stack is neglected. The results in Table 5-8 shown lower deformations, from which it can be concluded that the radial cable stiffness is sufficient to neglect the expansion of the cable stack due to radial cable deformation.

Bending stiffness

Also, the bending stiffness of the cable will be discussed to determine if it can have a large influence on the stiffness of the carousel (section 2.3.2 – ‘SPMT deflection’). The bending stiffness of offshore power cables is non-linear and influenced by the stick/slip hysteresis effects. This effect is shown in Figure 5-7.

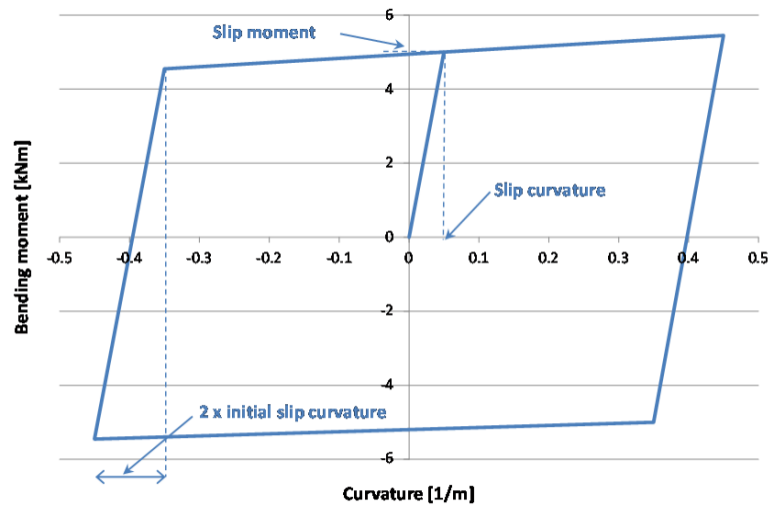


Figure 5-7: nonlinear bending moment - curvature relation of an offshore power cable [44]

The different layers in offshore power cables are mainly un-bonded and have different elastic properties. For low curvatures, the bending stiffness is approximate linear and the friction between the layer is sufficient to resist wire slippage. When the curvature increases and at a certain bending moment the friction is not high enough, some different layers start to slip. When some layers slip against each other the cable loses a large part of its stiffness. These effects are determined by many parameters [44], but are left out of scope for this study. The bending stiffness can be tested by a bending test and will be specified by the manufacturer. According to elementary beam theory, the bending stiffness is defined as the applied bending moment M and the resulting curvature κ

$$M = (EI)_{cable} \kappa = (EI)_{cable} \frac{d^2 w}{dx^2} \quad (5-5)$$

, with bending stiffness $(EI)_{cable}$ (consisting of elasticity modulus E and second moment of area I of the cable), beam displacement w and distance x along the beam. The results from appendix F for the bending stiffnesses for the selected cable are summarized in Table 5-9.

Table 5-9: Bending stiffness results

Description	Abbreviation	Value	Unit
Bending stiffness FEM simulation, no separation contact	$(EI)_{cable}$	44.7	kNm^2
Bending stiffness FEM simulation bonded contact	$(EI)_{cable}$	2150	kNm^2
Calculated bending stiffness free layers	$(EI)_{cable}$	37.8	kNm^2
Calculated bending stiffness fixed layers	$(EI)_{cable}$	1800	kNm^2
Bending stiffness from manufacturer	$(EI)_{cable}$	66.0	kNm^2

Again, the difference between no separation contacts and bonded contacts is that the friction is neglected for no separation and for bonded a friction coefficient of infinity has been used. As a result, the cable with bonded contact has a bending stiffness which is approximated 48 times higher and thus the friction is an important factor. For both contact formulations tension can still be transferred between layers, and they can't separate.

The bending stiffness of the cable also has been calculated manually in two different methods. For one method the layers are assumed to be fixed to each other, which has comparable results with the bonded contact for the FEM simulation. For the other method all the layers are considered separately and there is no interaction between the layers. For this method also the compatibility conditions are neglected between the different layers. The result for this method is a lower bound for the bending stiffness (calculated bending stiffness free layers in Table 5-9) because both friction and contact are neglected. Neglecting the contact is the main cause of the difference compared with the FEM simulation with no separation contact and the manual calculations. Finally, the bending stiffness of a cable with $D_{cable} = 190mm$ and three cores has also been defined by the manufacturer as $66 kNm^2$ [26]. The bending stiffness from the manufacturer is slightly higher than the manual calculated bending stiffness with free layers. This could mean

that the interaction and friction between the cable don't have a large effect in practice for the bending stiffness. Also, it is expected that the bending stiffness specified by the manufacturer is for the case where slip has been occurred (Figure 5-7). It finally is expected that for the curvature where no slip has occurred the stiffness is between $200 - 1000 \text{ kNm}^2$ and that the bending stiffness for higher curvatures with slip between the different layers reduces to $55 - 80 \text{ kNm}^2$.

In section 2.3.2, paragraph 'SPMT deflection' it is determined that the bending stiffness of a steel HEB1000 beam, $1.04 \cdot 10^6 \text{ kNm}^2$, lowers the SPMT deflection by approximately 100 mm . A single cable with slip with a bending stiffness of 50 kNm^2 thus has approximately 0.01% of the bending stiffness of the steel HEB1000 beam and has a negligible effect. Considering the cable stack where it is assumed that all cable turns are fixed to each other (infinite friction), the bending stiffness can be approximated by

$$((EI)_{\text{cable stack}})_{\text{fixed}} = \sum EI_{i,x} \quad (5-6)$$

, with elastic modulus E and $I_{i,x}$ the second moment of area around the neutral axis of the cable stack. The second moment of area around the neutral axis of a component can be calculated by the parallel axis theorem

$$I_{i,x} = I_{i,x'} + A_i d_i^2 \quad (5-7)$$

, with the cross-sectional area of the cable A_i , second moment of area around the cable's neutral axis $I_{i,x'}$ and the distance d_i of the neutral axis of the cable to the neutral axis of the component. Considering the cable stack where it is assumed that all the cables are free from each other and that there is not interaction (no friction and contact), the bending stiffness can be approximated by

$$((EI)_{\text{cable stack}})_{\text{free}} = \sum E_i I_{i,x} \quad (5-8)$$

The second moment of area I_{cable} of the homogeneous cable can be estimated by

$$I_{\text{cable}} = \frac{\pi}{64} D_{\text{cable}}^4 \quad (5-9)$$

As $(EI)_{\text{cable}} = 50 \text{ kNm}^2$ the elastic modulus of the cable is defined to be $E = 0.78 \text{ GPa}$. This results in the estimated bending stiffness of the cable stack as defined in Table 5-10.

Table 5-10: Cable stack bending stiffness results

Description	Abbreviation	Value	Unit
Bending stiffness of cable stack for no contact between cables	$((EI)_{\text{cable stack}})_{\text{free}}$	$8.1 \cdot 10^4$	kNm^2
Bending stiffness of cable stack for infinite friction	$((EI)_{\text{cable stack}})_{\text{fixed}}$	$9.0 \cdot 10^6$	kNm^2

Table 5-10 shows that there is a large difference between the bending stiffness of the cable stack where there is no friction between the cable compared to the stiffness where the stiffness between the cables is infinite. Furthermore, the HEB1000 in section 2.3.2 is aligned with the SPMT such that the bending stiffness can directly be added to the SPMT, while the cable stack has a donut shape causing that it is not aligned with the SPMTs. Due to this reason and the uncertainty of the friction between the cables the effect of the bending stiffness is neglected. The bending stiffness of the cable stack has a positive effect on the deflection of and the load distribution over the carousel. Neglecting the bending stiffness of the cable stack is thus a worst-case-scenario, and thus a sufficient assumption.

Torsional stiffness

The torsional stiffness of the offshore power cables is mainly depended on the armor, where there are two general options [44]:

- *Single-layer armored cables:* In case of an AC cable, the single layer armor wires are generally wrapped in the same direction as the cores. When torque is applied in the opposite direction, the armor wires will open-up, which allows the cable to absorb a certain degree of twist. When torque is applied in the armor wrapping direction the armor wires are compressed, which causes a stiffer behavior. Torsional stiffness in the armor wrapping direction can be around three- times as large as compared to the other direction.
- *Double-layer armored cables:* with double-layer armor the armor layers are counter rotating to make the torque stiffness balanced.

Because the cable is not loaded in the torsional direction, the torsional stiffness is not explicitly calculated.

5.2 Load distribution cable stack

In section 2.2.3, the following load distributions have been defined on the carousel by the accelerations on the payload due to accelerations on the payload (cable stack):

- Uniformly distributed load on floor due to gravity and vertical acceleration on payload (Figure 5-9)
- Uniformly distributed load over inner frame poles which experience pressure due to horizontal acceleration on payload (Figure 5-9). This uniformly distributed load is directed towards the center of the carousel

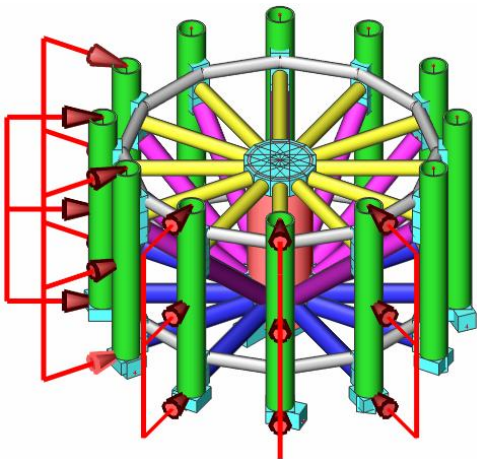


Figure 5-8: Load distribution payload inner frame

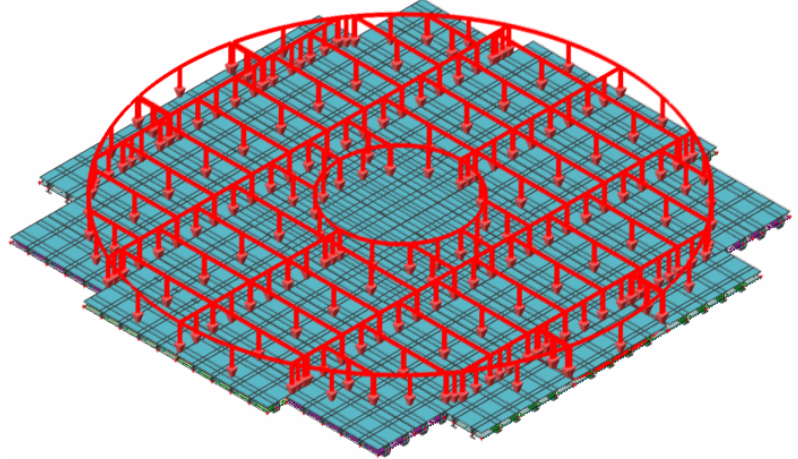


Figure 5-9: Load distribution payload on floor

These load distributions are based on assumptions and thus the reliability will be check in this section. Both loads are only consisting of compression forces and friction is neglected.

5.2.1 Cable stack description

First the description of the cable stack and the interaction forces between cables and the cables and the carousel, will be considered. Previously, the cable stack is described as shown in Figure 5-10.

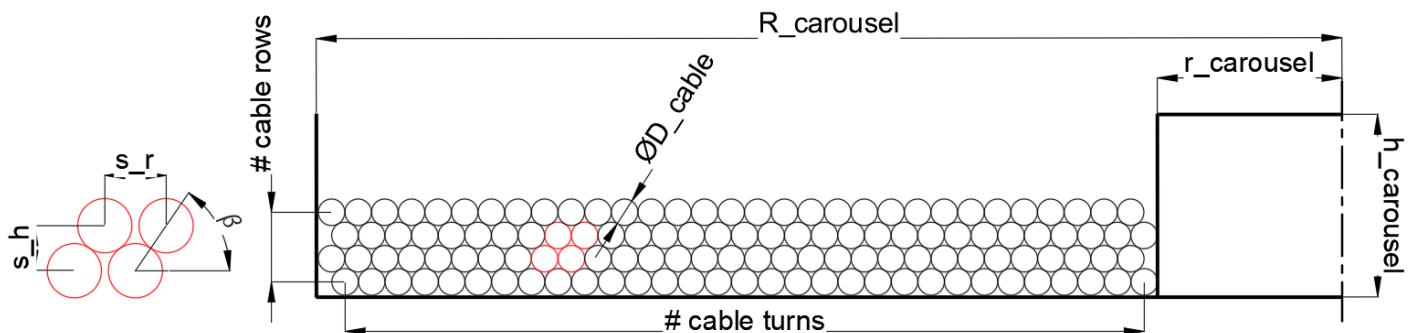


Figure 5-10: Carousel and cable stack cross section with dimensions

There are many imperfections neglected in this cable stack description:

- **Horizontal contact:** It is observed that the cables are laid against each other. However, direct contact with the neighboring horizontal cable or the carousel on the same row is not guaranteed ($s_r > D$). In the case that there is contact, it is also uncertain how large the resulting contact forces are, if two cable on the same row aren't pushed against each other due to a resultant force on the cable, the contact force can be negligible. Notice that if the cables are closely stacked that $\beta \approx 60^\circ$, $s_r \approx D_{cable}$ and $s_h \approx D_{cable} \cdot \sin(60^\circ)$.
- **Transition to next turn:** The spiraling of a single layer can be seen in Figure 5-11. Here, a cable diameter of 200mm has been used, which is an average cable diameter of offshore power cables. It can be seen there is a small transition of the cables turn radius to the radius of next cable turn. Figure 5-11 shows that the rough estimation of the needed angle for the cable transition to the next turn is only a few degrees. For this reason, the transition to the next turn will be neglected.
- **Transition to next layer:** There also is a transition of the cable from the current layer to the above layer. Because the diameter of the cable is small compared to the diameter of the carousel, also the transition from the current layer of turn to the above layer can be neglected.
- **Layer turn crossing turns in other layers:** The cable must cross another cable of the layer below and/or above each round because the layers are alternating spiraling inward and outward. Because the transition of the cable turn to the neighboring cable turn is negligible the effect of the cables crossing each other will also be neglected.

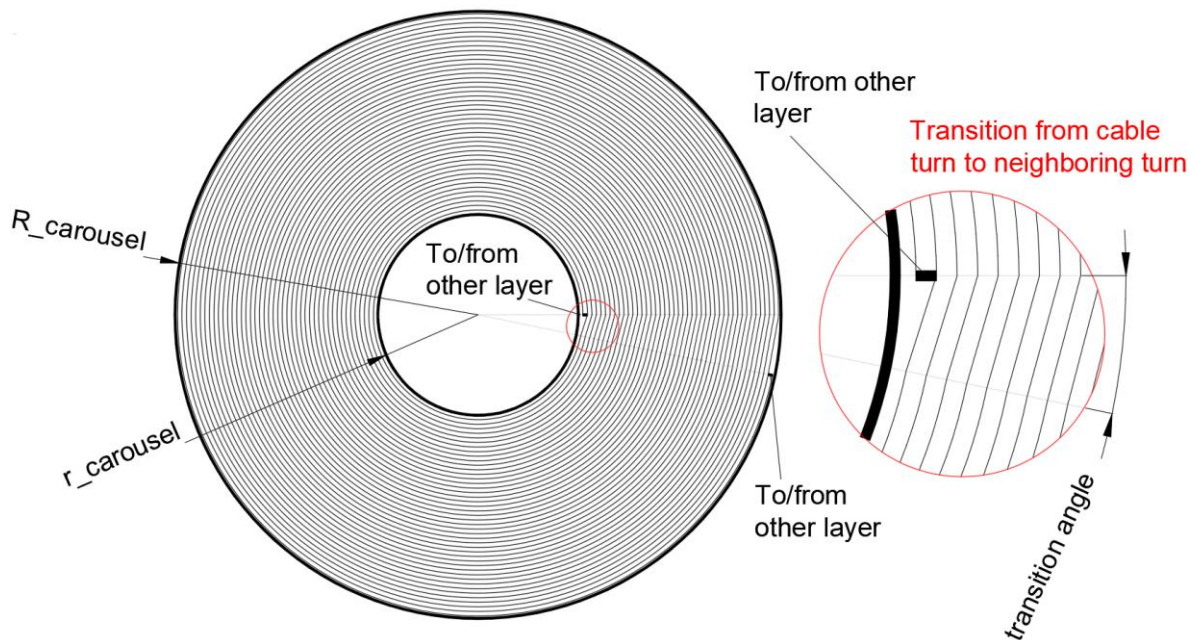


Figure 5-11: Single cable stack layer with turn transition detail

All the described imperfections for the cable stack are neglected and the general description as visualized in Figure 5-10 will be used. The calculations used in Appendix D are based on this cable stack description.

5.2.2 Interaction forces

There are many interaction forces between cables, and between cables and the carousel which influence the load distribution.

Cable - cable interaction

The interaction forces between the cables are mainly consisting of friction and compression forces. Figure 5-12 shows the radial interaction forces on a single cable in the cable stack on the left and the interaction forces on a cable in the longitudinal direction on the right.

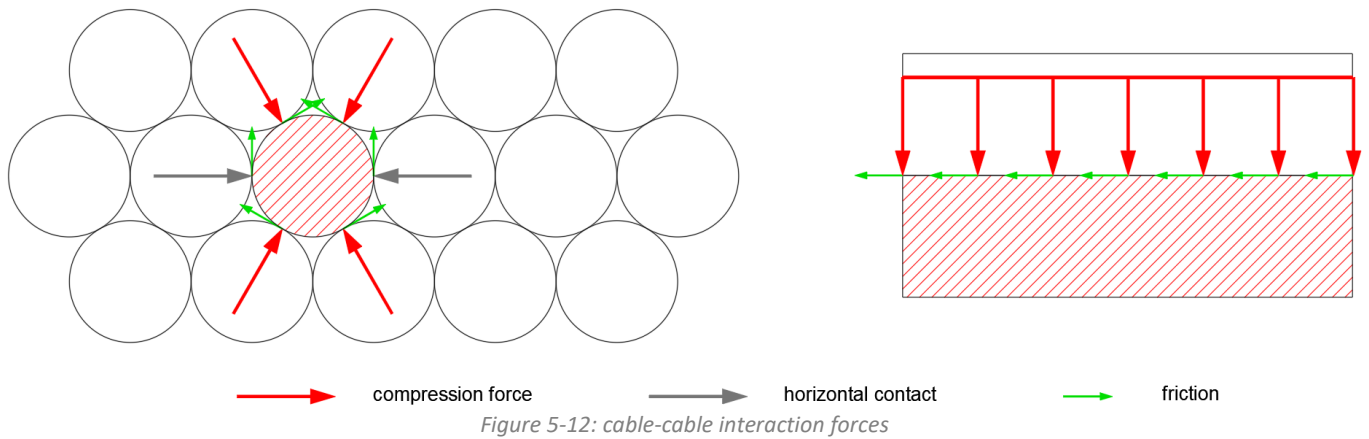


Figure 5-12: cable-cable interaction forces

Friction is the force resisting the relative motion of solid surfaces sliding against each other. Because in the stored configuration there is in general not much motion between cables it is expected that cables are more likely to press on each other than tending to slide against each other. Therefore, it is also expected that the effect of friction is not very high between cables, for both the tangential (left figure of Figure 5-12) and longitudinal friction (right figure of Figure 5-12).

Cable – carousel interaction

The main interaction forces between the carousel and the cables consist of compression forces and frictional forces, as shown in the figure below.

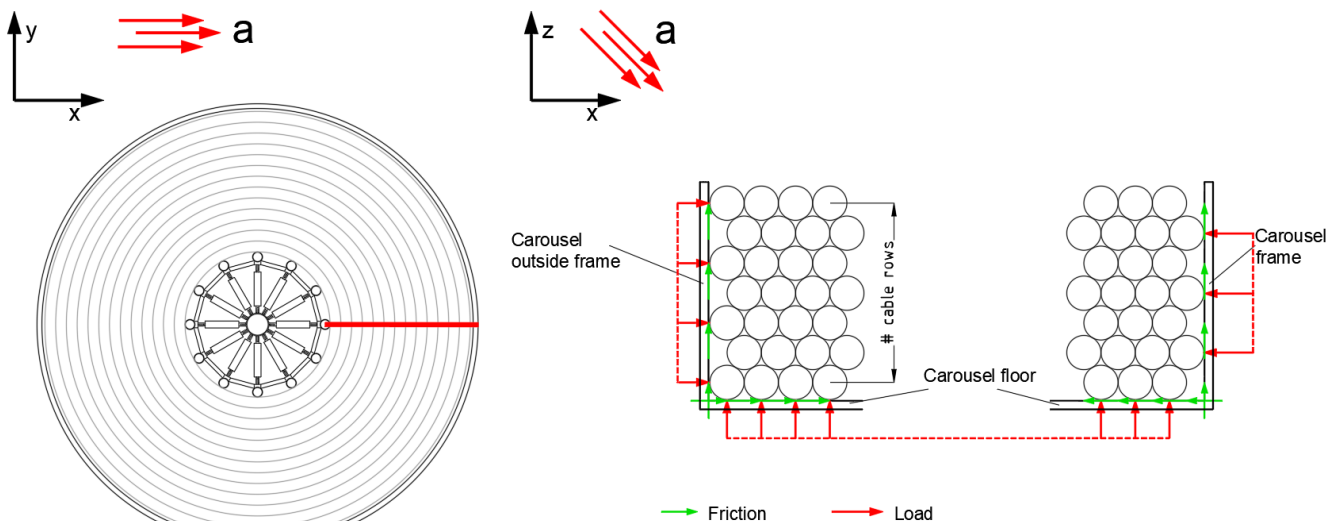


Figure 5-13: Interaction forces between cables and carousel

Because it is expected that there is not much tendency of the cables to move, it is again expected that most of the load on the carousel consist of compression forces, and not of frictional forces, especially for the outer and inner frame. Because of the high normal load on the floor, it is expected that the friction between the floor and the cable stack does play a role in the load distribution over the carousel. Previously, the effect of friction with the floor and the cable stack has been neglected because of the uncertainties of friction and because the friction with the floor has a positive effect as it lowers to horizontal load on the inner frame. This horizontal load on the inner frame causes bending moment on the floor which is governing for the floor design of the carousel.

5.2.3 Load distribution analysis

To determine the load distribution over the carousel due to the payload, a FEM model has been established based on Table 5-11.

Table 5-11: Input for load distribution study

#	Value	Reference
1	To simplify the analysis a large carousel radius of $D_{carousel} = 1.00m$ will be used	/
2	Carousel dimensions $r_{carousel}$ and $R_{carousel}$ based on the general input defined in Table 5-1 have been used	Table 5-1
3	The total mass of the cable stack will be defined as $C = 5000 Ton$. Density of the cable will be calculated according to cable stack volume and capacity C	Table 5-1
4	A horizontal acceleration of $5m/s^2$ and a vertical acceleration (gravity) of $9.81m/s^2$ will be applied.	/
5	The outer wall is neglected based on previous assumptions and for simplification of the analysis	Sections 2.2.3 and 5.1
6	The effect of the deformation of the carousel on the load distribution will not be considered and thus the inner wall and the carousel floor will both be modelled as rigid plates	/
7	For the contacts between cable – cable and cable-carousel different contact descriptions have been used for different simulations. These inputs are summarized in Table 5-12.	/
8	The cable has been modelled a homogenous with no separate layers to simplify the analysis. The elastic modulus and poison's ratio are also defined in Table 5-12.	/
9	Symmetry will be used to simplify the model	/

The resulting model is shown in Figure 5-14. Further description of the model and the analysis can be found in Appendix I.

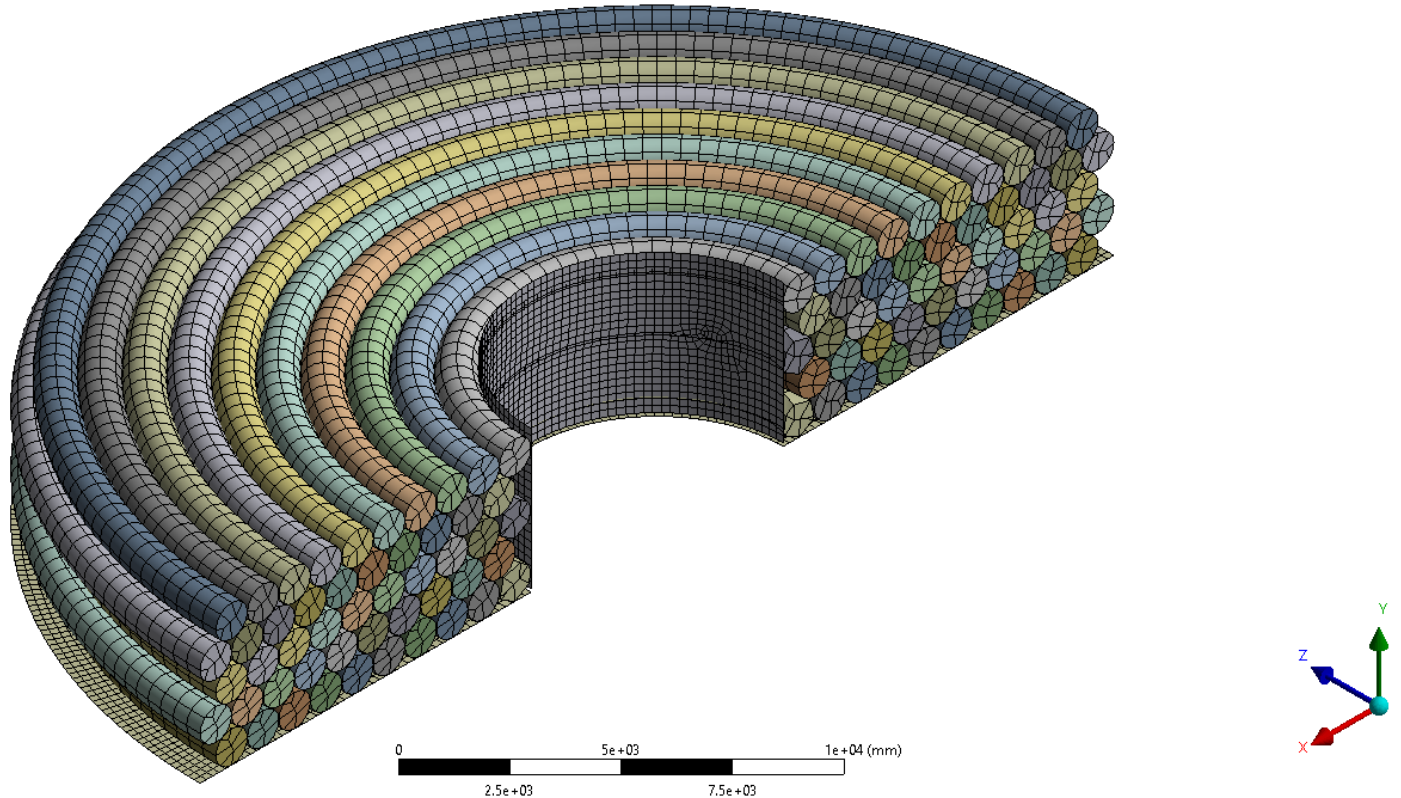


Figure 5-14: FEM model for load distribution

Multiple simulations have been executed based on different inputs. The input for each simulation can be found in Table 5-12.

Table 5-12: Simulation input

Simulation	Cable - floor	Cable - wall	Cable – cable horizontal	Cable – cable others	Elastic modulus cable	Poisson's ratio cable
	[friction coefficient / contact type]				[GPa]	[\]
1	0.2 / Pressure only	0.2 / Pressure only	0.2 / Pressure only	∞ / Bonded	1.0	0.4
2		0.0 / Pressure only			0.0 / Pressure only	1.0
3			1.0			0.4
4		0.2 / Pressure only	0.2 / Pressure only		5.0	0.4
5				0 / Bonded	5.0	0.4
6	0.1 / Pressure only				5.0	0.4

It is chosen to use the elastic modulus of the cable material as the calculated axial elastic modulus $5GPa$ from Table 5-7 and $1GPa$ to test the effect of using a less stiff cable. The Poisson's ratio has chosen to be 0.4 based on the average of the materials from Table 5-4. In Table 5-12 can be seen that four different contact types have been defined. All the contacts are in practice frictional contacts where separation is possible and where no tension but only compression can be transferred. Due to convergence issues a bonded contact has been used for the non-horizontal cable – cable contacts. Because the friction is uncertain, different frictional constant has been used to determine the influence of friction.

5.2.4 Results

The results of the simulations are summarized in Table 5-13. In this table the maximum deformation of the cable stack and the resultant reaction forces of the inner frame and the floor are shown. The corresponding load distributions can be found in Appendix I.

Table 5-13: Simulation output

#	Maximum deformation	Inner frame reaction			Floor reaction		
	[mm]	Rx [N]	Ry [N]	Rz [N]	Rx [N]	Ry [N]	Rz [N]
1	12.918	5.0824e+006	20858	3.7963e+006	7.3883e+006	2.4467e+007	2.321e+005
2	13.231	5.0543e+006	23.242	4.2138e+006	7.4124e+006	2.4487e+007	2.1821e+005
3	13.256	5.0593e+006	23.254	4.2032e+006	7.408e+006	2.4486e+007	2.0392e+005
4	2.0594	7.7698e+006	-29093	5.451e+006	4.6943e+006	2.4518e+007	-40186
5	15.435	7.9827e+006	-4.195e+005	7.0035e+006	4.4525e+006	2.4945e+007	28708
6	20.348	1.0641e+007	-8.0313e+005	8.8089e+006	2.1583e+006	2.5102e+007	-1.0165e+005

First, three simulations have been executed with a lower elastic modulus of $1GPa$. These simulations show there is a neglectable effect of the friction between the cable – inner wall and between the horizontal neighboring cables. For the 4th simulation the stiffness of the cables is increased to an elastic modulus of $5GPa$. The results show besides that expected decline in deformation, an increase in the load on the inner frame. Due to the stiffer cables less horizontal load is transferred by friction to the floor. Simulation 5 shows that the friction between cables lowers the deformation but doesn't influence the load distribution over the carousel. For simulation 6 the friction between the cable stack and the floor is lowered. This increases the load on the inner frame which makes it an important parameter as the load on the inner frame is governing for the inner frame, floor, and grillage structures. Neglecting the friction between the cable stack and the floor thus gives a worst-case-scenario.

Distribution over inner frame

All simulations show a comparable distribution (not in magnitude) over the inner frame. As shown in Figure 5-15 for the load distribution of simulation 6, the highest load is induced at middle height. Figure 5-16 shows that the assumed uniform distribution and the distribution from the simulations result in a comparable height h_{res} of the resultant force F_{res} on the inner frame. Because the resultant force F_{res} and the corresponding height h_{res} cause a bending moment M_{res} which is governing for strength of the floor and the grillage, it is important that the assumed and real h_{res} are comparable. The assumed uniform distribution is thus a good approximated of the load distribution from the simulations.

B: Load distribution model with symmetry

Pressure
Type: Pressure
Unit: MPa
Time: 1 s
Max: 8.8238
Min: 0
5/25/2023 3:27 PM

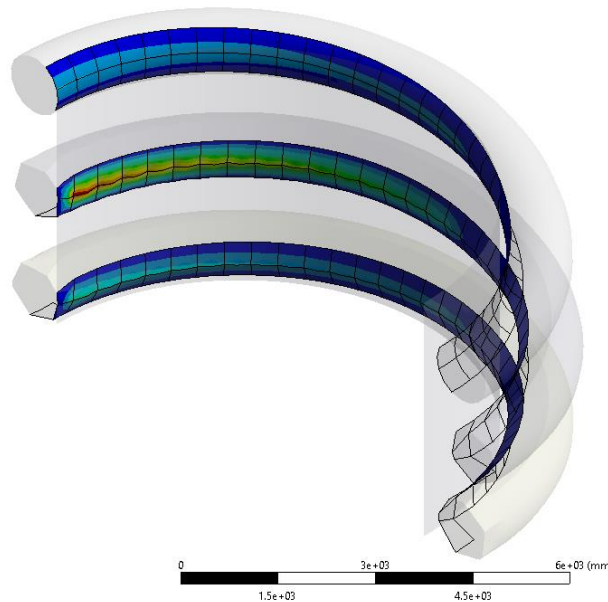
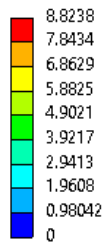


Figure 5-15: Pressure distribution inner frame simulation 6

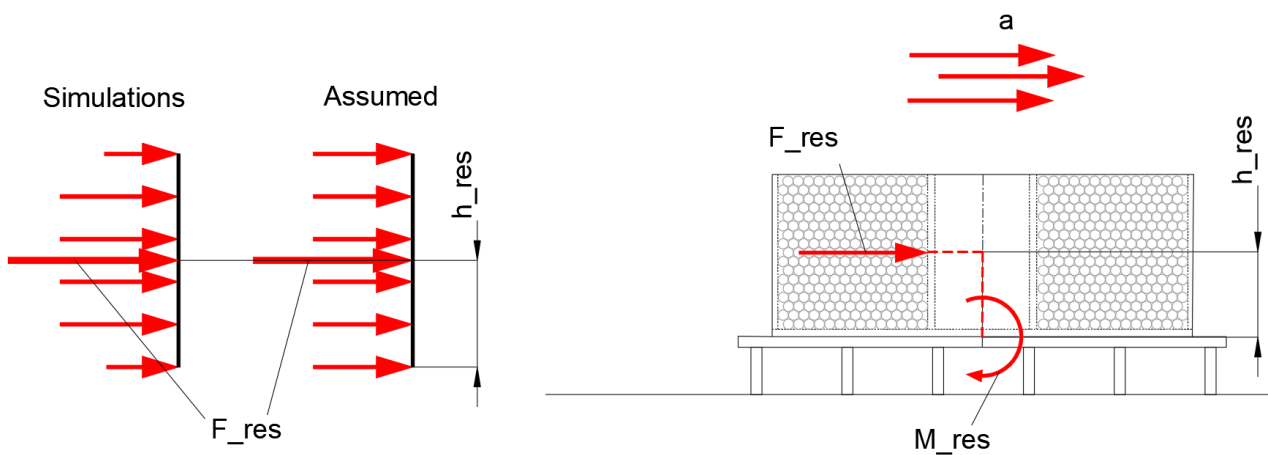


Figure 5-16: Load distribution of inner frame

In this study it is assumed that there is a uniform load distribution over the poles of the inner frame. This differs from the load distribution over the inner frame observed in the simulations, as shown in Figure 5-17. For the global load distribution the effects are expected to be comparable, but the load distribution from the simulations can result in higher local stresses at different locations. For the acceleration in Figure 5-17, the uniform distribution induces more load on the most upper and lower pole, causing more load to be transferred by those poles. The distribution from the simulations induces more load on the right pole which results in different local stresses at other positions. For the global design the assumed load distribution is sufficient but for the detailing it is necessary to apply the load distribution from the simulations for more accurate local stresses.

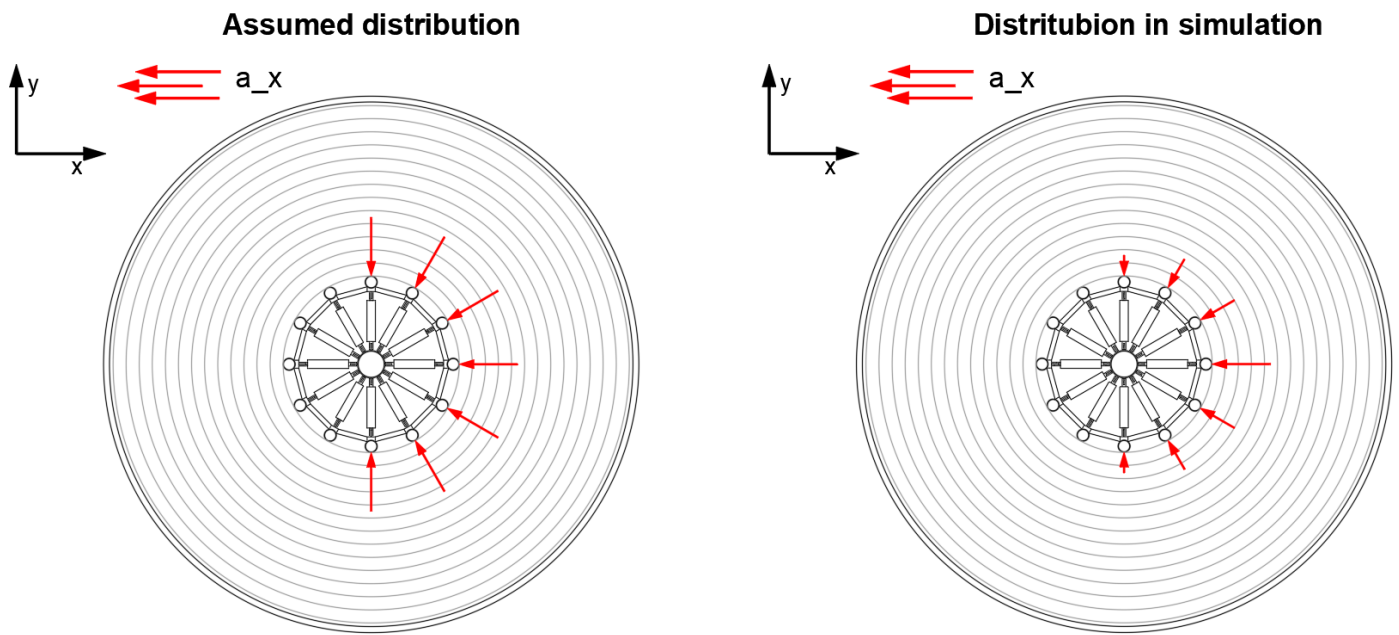


Figure 5-17: Load distribution of inner frame (top view)

Distribution over floor

All simulations show a comparable distribution (not in magnitude) over the inner frame (simulation 3 is shown in Figure 5-18). The distribution observed in the simulations is beneficial because most load is induced on the frame at the places where the floor experiences the most deformation (Figure 5-19). Assuming a uniform load distribution is also a worst-case-scenario load distribution and is thus a good approximation. Notice that the plot shown in Figure 5-18 shows scaled deformations.

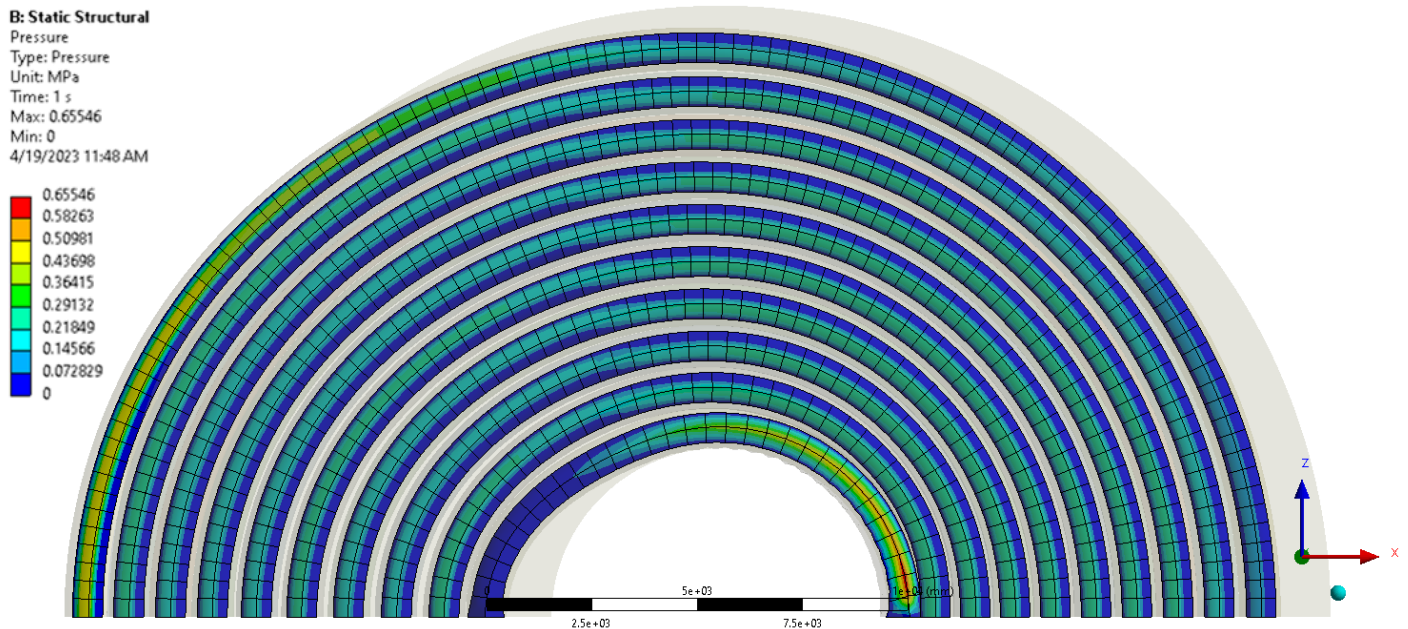


Figure 5-18: Pressure distribution floor simulation 3

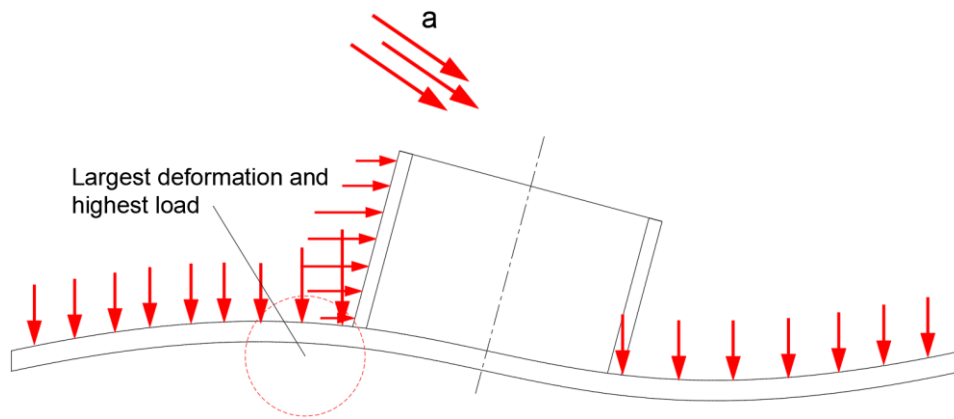


Figure 5-19: Load on floor and inner frame

5.3 Conclusion

In section 2.2.3 it has been determined that the cable stack has enough stiffness to neglect the effect and load transfer by the outer frame. For the calculations in section 2.2.3 several assumptions regarding the stiffness of a single cable have been done (Table 5-2) to estimate the expansion of the cable stack. In section 5.1 a single cable is selected for which the stiffness is determined to verify these assumptions from section 2.2.3. It follows from the calculations in section 5.1 that the cable, and thus the cable stack, have more stiffness than assumed in section 2.2.3 and thus also enough stiffness to neglect the effect and load transfer by the outer frame. Furthermore, the bending stiffness of a single cable has been determined to be 0.01% of a HEB 1000 beam. It therefore is assumed that the effect of the bending stiffness of the cable and the cable stack can be neglected.

It is assumed that the payload (cable stack) under accelerations induces a uniformly distributed compression load over half of the inner frame and the floor, where the effect of friction is neglected. In section 5.2 it is observed that the load distribution over the inner frame from the simulations has a comparable resultant force and corresponding resultant force height as the assumed uniform distribution. This causes a comparable resulted moment on the floor and grillage, which is thus sufficient for the global behavior of the CCS. However, it is observed from the calculations that the total load on each pole is not equal as assumed with the uniform distribution. This causes other local stresses and thus for further detailing of the design these stresses must be considered. It is also assumed that the load induced by the payload on the carousel floor is uniformly distributed. From section 5.2 it follows that there are regions where the cable stack induces higher pressures than other regions due to the horizontal acceleration. These higher pressures occur at beneficial regions as they have the negative direction as the direction in which the carousel floor wants to deform. This load distribution over the floor from section 5.2 is thus more favorable and causes lower deformations and stresses in the CCS floor. Also including friction with the floor and the cable stack is beneficial for the load distribution as the friction lowers the load on the inner frame. As these effects are neglected a worst-case-scenario is used for the design, which thus makes the assumptions sufficient.

6 Conclusion

This chapter describes the final conclusions of the study by answering the sub research questions and the main research question. Based on the conclusions and other finding of the study, recommendations are done for future work or studies.

6.1 Research questions

Below the sub research question for the study are answered.

1. What are the characteristics of the current offshore power cable transportation methods?

In section 2.1 it is defined that for the most common way of offshore power cable transport 4 cable transfers are used because most carousels are fixed to their positions and transferring a loaded carousel is very difficult. The following characteristics of the current transportation methods are defined to be important for the CCS to compete with the other cable carousel systems:

- Carousel capacity of 5000 *t*
- At least a spool rate of 0.87 *km/h*
- Applicable to cables with a diameter between 100 – 300 *mm*

2. Which challenges need to be addressed for the CCS?

In section 2.2 a process analysis for the CCS has been executed and in section 2.3 the resulting challenges for the CCS are described. It follows that the SPMT transport and sea transport are governing for the design of the CCS. Three main challenges have been defined for the CCS:

1. The strength and stability requirements must be satisfied for the CCS. The sea transport accelerations on the full payload are governing for the needed strength and stability of the structural components. The strength and stiffness of the structural components of the CCS are however limited to the maximum SPTM load and vessel deck load. Making the CCS stronger and stiffer namely increases the weight of the CCS and thus also increases the load on the SPMTs and the vessel deck.
2. The used cylinder strokes of the SPMTs can reach their limits during SPMT transport. The SPMT cylinders have an operational stroke of 490 *mm*. Calculations executed for the proposed CCS design by Mammoet show that the deflection of the SPMT transport can be more than 300 *mm*. This leads to a reduced stroke available for the needed height difference to lift the carousel and to compensate for height differences caused by ground unevenness, camber, slopes, and RoRo ramps.
3. The high load and large operation time of the SPMTs during the spooling process can result in issues for the SPMTs. The main issues are the wear of the SPMT tires, leakage of the hydraulic system for the cylinders and the hydraulic motors and overheating of the SPMT generator. These issues cause downtime for the operation and thus need to be prevented or the effect should be minimized.

3. Which design choices can be made for the CCS to address the challenges?

The main design choices for the global design of the CCS include the main carousel dimensions, the SPMT setup, the grillage setup, and the floor plate setup. For the deflection of the SPMTs, and thus the used SPMT cylinder stroke, it is expected that the outer carousel dimensions and the SPMT setup are very important. Unsupported axle lines namely increase the SPMT deflection and minimizing the carousel size is beneficial for the CCS weight, costs, and vessel applicability.

Further design choices are the dimensioning and cross section selection of the structural members. These should be selected according to the strength and stability requirements where the overall CCS weight should be minimized such that costs and load on the SPMTs/vessel deck are reduced.

For the SPMT issues such as tire wear, hydraulic leakage and generator overheating it is beneficial if the load on the SPMT and the drive distance of the SPMTs are minimized. To lower the load on the SPMTs, more axle lines can be used. This however increases the costs of the CCS, and the needed outer carousel dimension because the SPMT deflection should be minimized. To lower the drive distance of the SPMTs, the radii of the

SPMT axle lines should be lowered (the SPMT should be closely packed) and the outer and inner radii of the carousel should be increased.

All the above factors should be considered for selecting the main dimensions of the carousel and the floor, grillage and SPMT setups.

4. What design choices show the best performance against the challenges

In chapter 3, multiple combinations of main carousel dimensions and a floor plate setup have been proposed. For each setup the vessel applicability, estimated weight, needed axle lines, minimum inside carousel radius, need carousel height, SPMT drive distance, and the ratio of carousel footprint area related to the SPMT support area have been determined. Based on these performance indicators three different combinations have been selected for which a SPMT and grillage setup have been proposed.

One of the main challenges is about the used stroke of the SPMT axle lines (challenge 2 Table 2-11). In this chapter the three selected setups from chapter 3 are elaborated to an FEM simulation model. The best performing model has on SPMT deflection of 110mm . Which is a significant improvement compared to the concept proposed by Mammoet with an estimated SPMT deflection of 224mm , while the self-weight of the CCS is approximately the same, but less SPMT axle lines are unsupported. It can thus be concluded that the outer carousel dimension and the SPMT setup have a large influence on the SPMT deflection and thus the used cylinder stroke.

Furthermore, for this concept the structural components and the cross sections are defined such that the stability and strength requirements are satisfied for the loads as defined in section 4.1 (only local reinforcements are needed). It is determined that to satisfy strength and stability requirements (challenge 3 Table 2-11) it is beneficial to include extra sea fastening and reinforced floor plates, and that it is needed to select appropriate cross sections for the structural components.

The SPMT tire wear, hydraulic leakage, and generator overheating (Challenge 3 from Table 2-11) can be tackled by reducing the load on the axle lines and increasing the inner radius of the carousel $r_{carousel}$. However, reducing the load on the axle lines increases the costs and deflection of the SPMTs and increasing the inner radius enlarges the loading on the carousel. Thus, tackling the SPMT issues is not included in the elaborated concept as there are many uncertainties for the SPMT issues.

5. Do the properties of the cable stack have an influence on the performance of the design choices?

In section 2.2.3 it has been assumed that the offshore power cables used in the CCS have an average axial elastic modulus of 5 GPa and a radial elastic modulus of 1 GPa . Based on these values it is determined in Appendix B that the expansion of the cable stack under the accelerations is negligible. From this it is assumed that the cable stack has sufficient stiffness to neglect the load on and load transfer by the outer frame. In section 5.1 a FEM cable model has been developed with which the axial, bending and radial stiffness have been determined. As a result, the developed FEM model of a cable with average properties shows to have more axial and radial stiffness as assumed in section 2.2.3. This confirms that the cable stack has sufficient stiffness to neglect the load on and load transfer by the outer frame.

Furthermore, the bending stiffness of a single cable has been determined to be approximately 0.01% of a HEB 1000 beam. Figure 2-48 shows that a HEB1000 beam, aligned with the longitudinal direction of the SPMT, has a maximum decrease of approximately 30% of the deflection. For the cable stack the cables are spooled and not aligned with the SPMTs, which decreases the influence of the cable bending stiffness on the SPMT deflection. The entire cable stack however can have sufficient stiffness to influence the SPMT deflection and load distribution on the carousel, but because of the uncertainties and the low bending stiffness of a single cable, these effects of the cable stack stiffness are neglected.

It is assumed that the payload (cable stack) under accelerations induces a uniformly distributed compression load over half of the inner frame and the floor, where the effect of friction is neglected. In section 5.2 it is

observed that the load distribution over the inner frame from the simulations has a comparable resultant force and corresponding resultant force height as for the assumed uniform distribution. This causes a comparable resulted moment on the floor and grillage, which is thus sufficient for the global behavior of the CCS. However, it is observed from the calculations that the total load on each pole is not equal as assumed with the uniform distribution. This causes other local stresses and thus for further detailing of the design these stresses must be considered. It is also assumed that the load induced by the payload on the carousel floor is uniformly distributed. From section 5.2 it follows that there are regions where the cable stack induced higher pressures than other regions. These higher pressures occur at beneficial regions as they have the negative direction as the direction in which the carousel floor wants to deform due to the horizontal load. This load distribution over the floor from section 5.2 is thus more favorable as it causes lower deformations and stresses in the CCS floor. Furthermore, including friction with the floor and the cable stack is beneficial for the load distribution as the friction lowers the load on the inner frame.

Main research question

The main research question has been defined as:

Can the containerized carousel system improve the current offshore power cable transportation method?

Assuming that the SPMT issues, such as tire wear, hydraulic leakage, and generator overheating, are not problematic and can be solved by maintenance, it can be concluded that the CCS is a feasible method to transport offshore power cables. However, it can be concluded from the study that the SPMT setup and the main carousel dimensions need to be selected carefully to minimize the SPMT deflection. This is necessary to successfully implement the CCS, otherwise the SPMT cylinders can reach their limits.

If the CCS improves the current offshore power cable transportation method is mainly dependent of the costs and time. It is difficult to compare the costs and time for the current method and the CCS as there are many parameters which have an influence. A global comparison of the time and costs between the current methods and the transportation process using the CCS can be found in Appendix E. The following can be concluded from Appendix E:

- For the CCS a lot of time is saved by using 2 cable transfers instead of 3 or 4. As a result, the effective cable transportation time is reduced by multiple weeks for the CCS as a carousel transfer is expected to take less than a day. Furthermore, keeping all the quays, vessel and equipment occupied during the cable transfers is also very expensive. As less cable transfers are needed for the CCS these costs are also significantly reduced.
- As the CCS is mobile by the SPMTs there are many options for storage of the loaded or empty carousel. For the CCS only a quay is needed whereas for the current transportation methods a transshipment hub or manufacturer quay with a carousel are needed. This allows cheaper storage for the CCS and usage of less expensive quays at more efficient locations. More efficient locations can reduce transportation time of vessel transport, which reduces the overall transportation time and costs.
- As the CCS is completely containerized the mobilization, demobilization, and storage are relative quick and cheap compared to carousels which aren't containerized
- Cheaper transport vessel can be used for the CCS as only a deck carrier with a strong enough deck is needed instead of a vessel with a carousel
- Cons of the CCS are that carousel of the CCS is relative expensive and that the SPMTs also aren't cheap. As the CCS is an expensive solution compared to the conventional transportation methods, but it significantly decreases costs as described above, it is expected that the overall costs are comparable or lower for the CCS compared to the conventional transportation methods.
- Because less cable transfers are needed the CCS does decrease the overall effective transportation time of the cable transportation process. However, for the CCS more preparation and mobilization are needed compared to the current transportation methods.

Furthermore, based on the study described in this thesis, the following advantages of the CCS compared to the current transportation methods are defined:

- *Less cable transfers*: less cable transfers for the CCS also beneficial for the cable quality

- *Easy sea fastening*: If a conventional carousel needs to be transported by a vessel, first the sea fastening must be defined. For the CCS the sea fastening is already included in the design.
- *CCS is modular*: The modality of the CCS enables to use it for different project with different capacities. However, for each capacity, setup, and dimensioning of the structural carousel components, the CCS should carefully be checked for SPMT deflection and structural strength and stability. The concept elaborated in this study is only applicable for 5000t or lower capacities.

In summary, the CCS can improve the current transportation method and the effective cable transport is likely to be reduced. However, it is important to consider all the above where especially the SPMT setup and the outer carousel dimensions are important. It is expected that the CCS reduces the total costs of the transportation method, but this is dependent of many parameters and the exact costs should be determined in the future.

6.2 Recommendations

The following is recommended for future work or research:

- For the design of the CCS, it is recommended to apply the loads as follows:
 - o Horizontal payload distribution over inner frame as shown in Figure 6-1, where the load on each pole is uniformly distribution.
 - o Uniform distribution of the vertical payload on the carousel floor
 - o Neglecting friction
 - o Neglecting load on the outer wall for the design of the CCS. For the design of the outer wall an worst-case-scenario load on the outer wall should be determined.
- It is recommended to implemented sea fastening as globally described in section 4.3.2, namely bracing between corner floor plates and the vessel deck. This is only need in the direction perpendicular to the direction of the grillage beams. The additional sea-fastening significantly reduces the unity checks for strength and stability at the central grillage frames and floor structure.
- The study shows that the SPMT setup, capacity and carousel main dimensions have a large influence on the deflection of the SPMT transport. For further elaboration it is thus advised to use this knowledge.
- Research for possible SPMT issues such as tire wear, hydraulic leakage and generator overheating is recommended

For further usage of the concept used in this study, to following is recommended:

- In the further detailing the outer frame, connections and local reinforcements should be considered
- The neglected loads should be considered. Also, the load distribution over the inner poles from the simulations as shown in Figure 6-1, where not every pole is equally load, should be implemented.

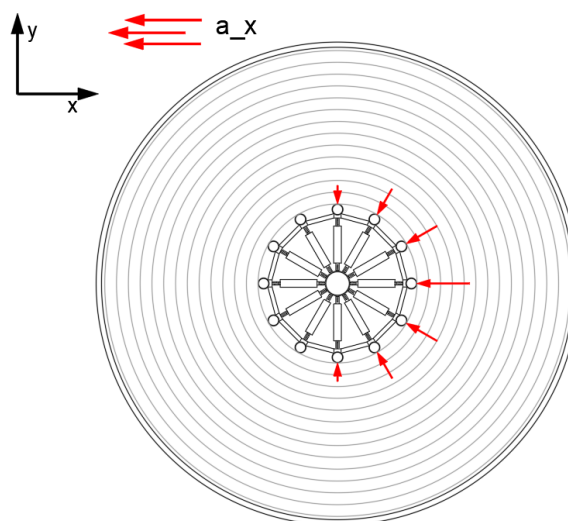


Figure 6-1: Horizontal payload distribution over inner frame

References

- [1] Wikipedia, "Offshore wind power," [Online]. Available: https://en.wikipedia.org/wiki/Offshore_wind_power.
- [2] GWEC, "GWEC: offshore wind will surge to over 234GW by 2030, led by Asia-Pacific," 5 August 2020. [Online]. Available: <https://gwec.net/gwec-offshore-wind-will-surge-to-over-234-gw-by-2030-led-by-asia-pacific>.
- [3] Wikipedia, "Submarine power cable," [Online]. Available: https://en.wikipedia.org/wiki/Submarine_power_cable.
- [4] "Submarine Cable Systems," Opnet technologies, [Online]. Available: http://www.opnet.com.tw/product_Submarine.html.
- [5] "Underground cable," Amprion, [Online]. Available: <https://www.amprion.net/Transmission-System/Technology/Underground-cable/Underground-cable.html>.
- [6] Osprey, "Cabling carousels in action," Osprey, [Online]. Available: <https://osprey.group/cabling-carousels-in-action/>.
- [7] N. americas, "Carousel-10000-spec-sheet-V.01," Neptune americas.
- [8] A. Dawood, "A study of pipeline response during reel-lay installation," Semantic scholar.
- [9] jdcon, "Installtion of four subsea power cables in the north atlantic," JD contractor, [Online]. Available: <https://www.jdcon.dk/News/Installation-of-four-subsea-power-cables-in-the-North-Atlantic>.
- [10] M. chesshrye, "Aegir's first project," Oedigital, [Online]. Available: <https://www.oedigital.com/news/453489-aegir-s-first-project>.
- [11] Mammoet, "Effecient load-in and transpooling of subsea cable for an offshore project in Saudi Arabia," 2022. [Online].
- [12] B. Radowitz, "Prysmian wins €150m offshore wind grid link project in France," Rechargenews, [Online]. Available: <https://www.rechargenews.com/wind/prysmian-wins-150m-offshore-wind-grid-link-project-in-france/2-1-769027>.
- [13] "WIND Cable transfer for the IRAQ Crude Oil Expansion Project," WIND B.V., [Online]. Available: <https://www.youtube.com/watch?v=UurKjy-9Ns>.
- [14] S. hunter, "2500 Te Basket Carousel SH-BC-2500".
- [15] "Google Maps," Google, [Online]. Available: <https://www.google.nl/maps/@51.8901129,4.398425,300m/data=!3m1!1e3?entry=ttu>.
- [16] D. o. contractors, "2x10.000T Heavy lift cable vessel," [Online]. Available: <https://www.dutchoffshorecontractors.com/media/lr1jzbe1/2-x10000t-cable-transport-vessel.pdf>.
- [17] "Kabelinstallatieschepen," Jan De Nul Group, [Online]. Available: <https://www.jandenul.com/nl/vloot/kabelinstallatieschepen>.
- [18] P. group, "66 kV Submarine Cable Systems for offshore wind," [Online]. Available: https://www.prysmiangroup.com/sites/default/files/business_markets/markets/downloads/datasheets/leaflet_submarine_epr_66%20Kv_%20final.pdf.
- [19] T. Tech, "Offshore wind submarin power cables - an introduction," 2022. [Online]. Available: <https://rodafisheries.org/wp-content/uploads/2020/11/RODA-JTF-Cabling-pres0-TtReviewed.pdf>.
- [20] C. cables, "XLPE Inulated DC High-Voltage Submarine Cable," [Online]. Available: http://www.caledonian-cables.com.tr/product/Submarine_Cables/XLPE-DC.html.
- [21] C. cables, "Lead Sheathed AC High-voltage submarine cable," [Online]. Available: <http://shipboard-cables.com/submarine-cables/Lead-Sheathed-High-voltage-Submarine-Cable.html>.
- [22] T. C. solutions, "Catalogue - Innovative cable solutions meeting international standards," [Online]. Available: https://cableconnectivitygroup.it/files/TKF-MARINE_e2857434.pdf.
- [23] O. Unosson, "Offshore cable installation - Lillgrund," [Online]. Available: <https://www.osti.gov/etdeweb/servlets/purl/979750>.

- [24] N. americas, "Carousel-5000-spec-sheet-V.01," Neptune americas.
- [25] "7000t-basket-carousel-spec-sheet," Dutch Offshore Contractors BV, Vlissingen.
- [26] I. Harms, "Basis of Design - Containerized Carousel System," Mammoet, Schiedam, 2022.
- [27] I. Harms, "Global calculations - Containerized Carousel System," Mammoet, Schiedam, 2022.
- [28] F. d. Groot, "www.flickr.com," [Online]. Available: <https://www.flickr.com/photos/71540315@N06/6476548579>.
- [29] Mammoet, "Efficient precision transport - Mammoet Self Propelled Modular Transporters," [Online]. Available: https://www.mammoet.com/siteassets/equipment/transport/self-propelled-modular-transporter/Mammoet_SPMT_brochure.pdf.
- [30] Mammoet, "SPMT Scheuerle - Dimensions and specifications," [Online]. Available: <https://www.mammoet.com/siteassets/equipment/transport/self-propelled-modular-transporter/datasheet-SPMT-Scheuerle.pdf>.
- [31] J. d. Vries, Interviewee, *SPMT usage*. [Interview]. 2023.
- [32] F. B. Andreas Köhler, "Modulaire transporter SPMT technische gegevens V1-7," Scheuerle, 2018.
- [33] Mammoet, "Best practice - Trailer synchronization," Mammoet.
- [34] Mammoet, "Best practice - Forces on cargo and lashing during transport," Mammoet.
- [35] Mammoet, "Deck Carrier Overview".
- [36] "Margin plate ship construction," [Online]. Available: <https://zaiyuniversity.amebaownd.com/posts/35759102>.
- [37] "Rotterdam, Mammoet Heavy Lift Terminal Quay 1 Details," 4C offshore, [Online]. Available: <https://www.4coffshore.com/ports/quay-details.aspx?paid=103>.
- [38] J. d. Vries, "Engineering Handbook Transport," Mammoet, Schiedam, 2023.
- [39] Mammoet, "Best Practice - Transport - Allowable deflection and camber," Mammoet, 2018.
- [40] Wikipedia, "ISO 668," [Online]. Available: https://en.wikipedia.org/wiki/ISO_668.
- [41] I. B. Ahmad, A. Schnepf and M. C. Ong, "An optimisation methodology for suspended inter-array power cable configurations between two floating offshore wind turbines," Department of Mechanical and structural Engineering and Materials Science, University of Stavanger.
- [42] Z. cable, "XLPE Insulated DC High-Voltage Submarine Cable," ZMS cable, [Online]. Available: <https://www.zmscable.com/zms-cables/Submarine-cable/XLPE-Insulated-DC-High-Voltage-Submarine-Cable>.
- [43] Z. cable, "XLPE Insulated AC Submarine Cable with fibre optical cable," ZMS cable, [Online]. Available: <https://www.xlpecable.com/ZMS-cables/ZMS-Submarine-Cable/XLPE-Insulated-AC-Submarine-Cable-with-fibre-optical-cable>.
- [44] B. Loos, "Operability limits based on vessel motions for submarine power cable installation," Delft Unisveristy of Technology, Delft, 2017.
- [45] M. Sharpless, "Offshore Electrical Cable Burial for Wind Farms: State of the Art, Standards and Guidance & Acceptable Burial Depths, Separation Distances and Sand Wave Effect," Bureau of Ocean Energy Management, Regulation & Enforcement - Department of the Interior, 2011.
- [46] Wikipedia, "Bernoulli beam theory," [Online]. Available: https://en.wikipedia.org/wiki/Euler%E2%80%93Bernoulli_beam_theory.
- [47] G. Rutgers, "Mechanical behaviour of cable in an offshore turntable," Delft University of Technology, Delft, 2016.
- [48] ynfpublishers, "Caley A-Frame for Boskalis Ndurance cable laying vessel," [Online]. Available: <https://www.ynfpublishers.com/tag/boskalis-offshore>.
- [49] "Germany: Blue Offshore to Exhibit at EWEA Offshore 2013," offshorewind.biz, 2 August 2013. [Online]. Available: <https://www.offshorewind.biz/2013/08/02/germany-blue-offshore-to-exhibiting-at-ewea-offshore-2013/>.

- [50] L. Panza, "Mechanical performance study of submarine power cables," University Politecnico di Torino, Torino, 2020.
- [51] J. Tarnowski, "Improved method of detemining bending stiffness of underground cables," Hydro-Québec (IREQ), Quebec, 2015.
- [52] P. Maioli, "Bending stiffness of submarine cables," Prysmain group, Versailles, 2015.
- [53] P. Fang, X. Jiang, H. Hopman, Y. Bai, "Mechanical responses of submarine power cables subjected to axisymmetric loadings," Delft University of Technology and Zhejiang University, Delft and Zhejiang, 2021.
- [54] Galloper, "JDR Cables," Galloper, [Online]. Available: <https://www.galloperwindfarm.com/case-study/jdr-cables/>.
- [55] J. cables, "GALLOPER," [Online]. Available: <https://www.jdrcables.com/case-studies/page/2/>.
- [56] wongship.blogspot.com, "konstruksi kapal," [Online]. Available: <http://wongship.blogspot.com/2012/04/konstruksi-kapal.html>.
- [57] Wikipedia, "Friction," Wikipedia, [Online]. Available: <https://en.wikipedia.org/wiki/Friction>.
- [58] "355/65-15 24PR N 170A5 Continental IC40 TL," Otrusa, [Online]. Available: <https://www.otrusa.com/shop/material-handling-tires/355-65-15-24pr-n-170a5-continental-ic40-tl/>.
- [59] A. M. Reda, G. L. Forbes, F. Al-Mahmoud, I. M. Howard, K. K. McKee and I. A. Sultan, "Compression limit state of HVAC submarine cables," Elsevier, 2016.

Appendices

	Page number
A Research paper	90
B Cable stack expansion estimation	101
C SPMT deflection study 2D	111
D Cable stack mass and dimensions	121
E Comparison CCS and current method	122
F Cable analysis	124
G Setup selection study	137
H Analysis of elaborated concept	149
I Load distribution study	179

A Research paper

Research paper starts on next page

An innovative way to transport and spool offshore power cables using SPMTs

Global design improvement of a containerized carousel system

C.B. Slingerland, I. Harms, W. van den Bos and D.L. Schott

Abstract - Mammoet is developing a new type of system for the transportation of offshore power cables. With this system the cables can be spooled, stored, transported both on land and on heavy transport vessels in a more efficient way. There are a few uncertainties and challenges for the system, resulting in some assumptions which have been made for the current design. In this study those uncertainties and the challenges for the current design are discussed, which results in more insights in the uncertainties and a new concept with improved performance against the challenges.

1. Introduction

The development and installation of offshore windfarms is an increasingly growing business as more wind energy is demanded. The installed global cumulative offshore wind capacity has grown from 4 MW to 50 GW over the past 10 years [1]. An exponential growth is observed. This is also caused by the increasing average power delivered per installed turbine, from 6.8 MW in 2018 to 8.2 MW in 2021. Looking at the future, many reports predict the exponential growth to continue. The GWEC (global offshore wind energy council) expects that the offshore wind capacity will grow to over 234 GW by 2030 [2]. All this electric power generated by wind turbines needs to be connected to transformer stations and the main grid by means of large submarine power cables. This requires a few 100 km of offshore power cables to be installed [3]. A large part of the required installation time and the total costs for offshore power cables is caused by the transport of the cable from the manufacturer to the offshore windfarm. It therefore is desired to minimize the costs and time for the transport of the cable from the manufacturer to the offshore windfarm.

During the entire transportation process, the offshore power cable is stored in a carousel. Most carousel are fixed on their position and thus a cable transfer is required to get the cable from one carousel to the other (Fig. 1). With a cable transfer the offshore power cable is simultaneously unspooled from one carousel and spooled on the other carousel. Such a cable transfer can take multiple weeks of non-stop spooling [4] and occupying all the equipment, vessels and quays used. This makes each cable transfer very expensive. For the current transportation process of the offshore power cables, 3 or 4 cable transfers are needed (Fig. 4).

It would be more efficient to replace some cable transfers by a carousel transfer, where the loaded carousel is directly placed

on its desired position. However, loaded carousels can have weights around 10 000t, which is very hard to lift and thus not beneficial [5]. For the offshore pipe laying industry reels are used [6] [7]. However, there are almost no cable dedicated installation vessels using reels, reels generally have lower capacities with heavier constructions and cable transfers are still needed. The center of gravity of a reel also is higher, which is unfavorable for sea transport.



Fig. 1: General cable transfer / carousel (un)spooling setup [8]

Another method, which has been used a few times before but is not fully implemented in the industry, is transferring the loaded carousel by means of SPMTs (Self-Propelled Modular Transporters), as shown in Fig. 2.

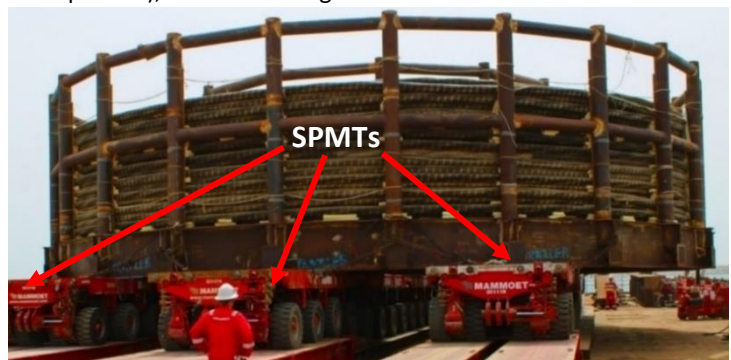


Fig. 2: 1300 Ton loaded carousel transfer to barge [9]

Based on using their SPMTs, Mammoet proposed the CCS (containerized carousel system) as a possible solution for making the offshore power cable transportation more efficient (new process overview shown in Fig. 7), where a carousel will be optimized for the use of SPMT's. With the CCS the SPMTs of

Mammoet will be used to transfer the loaded carousel, but they also function as a drive system to rotate the carousel during cable spooling when the cable needs to be transferred from / to the carousel. SPMTs can namely drive in almost any direction in the horizontal plane, and they are thus also capable of rotation the carousel around its axis. Further benefits of the CCS are that it is containerized, modular, easily to handle by SPMTs and has included sea fastening. The design for the CCS proposed by Mammoet is shown in Fig. 3.

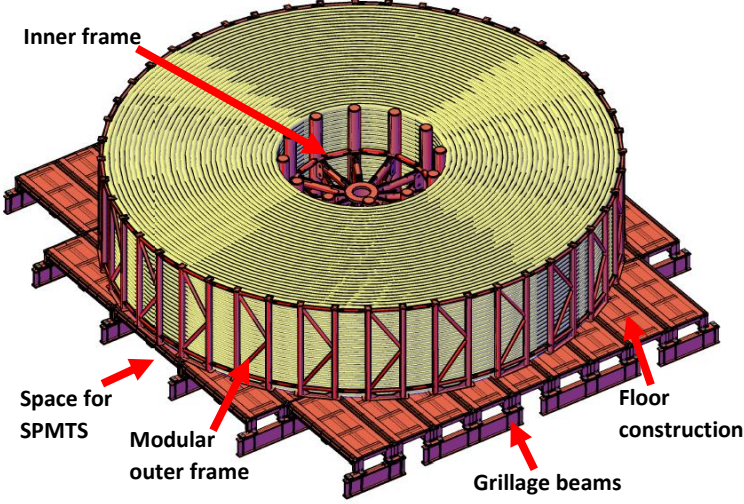


Fig. 3: CCS design proposed by Mammoet [10] [11]

There are a few uncertainties and challenges for the CCS, which resulted in some assumptions which have been made for the proposed design. Therefore, the main objective of the project is to evaluate the feasibility of the CCS and to determine with the new insights if the CCS can improve the current transportation method.

II. Process analysis

A. Current transportation method

The current transportation process of offshore power cables is shown in Fig. 4.

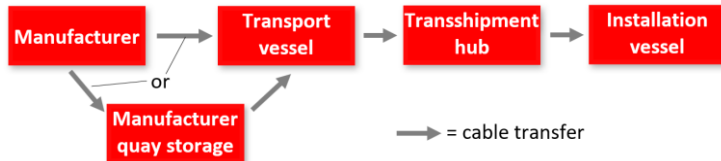


Fig. 4: Current transportation method process overview

There are many different offshore power cables with many different sizes and masses which can be transported. In Fig. 5 the cable mass μ_{cable} (in kg/m) is related to the cable diameter D_{cable} for both AC and DC cables from different manufacturers [12] [13] [14] [15] [16] [17]. A quadratic relation is observed in Fig. 5.

$$\mu_{cable} = 1.18 \cdot 10^{-3} D_{cable}^2 + 1.28 \cdot 10^{-1} D_{cable} \quad (1)$$

It is chosen that the CCS must be applicable to cables with a diameter between 100 – 300mm. Assuming a cable mass of $\mu_{cable} = 65 \text{ kg/m}$, for a few carousels [4] [18] [19] [20] the nonstop spooling time T_{spool} for spooling the full carousel capacity

with the spool rate of the carousel V_{spool} has been determined (Fig. 6). The red dotted line in Fig. 6 corresponds with a spool rate of 0.87 km/h , from which it is defined that the needed spool rate for the CCS must be $V_{spool} = 1 \text{ km/h}$ to compete with the current transportation methods. The cable spool rate will be kept constant by adjusting the rotational speed of the carousels according to the radius in the carousel where the cable is currently (un)spooled.

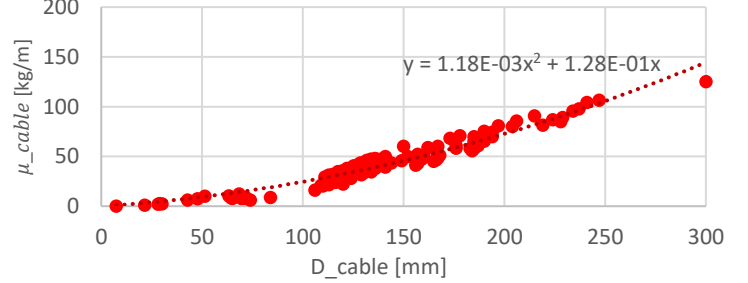


Fig. 5: cable mass related to cable diameter

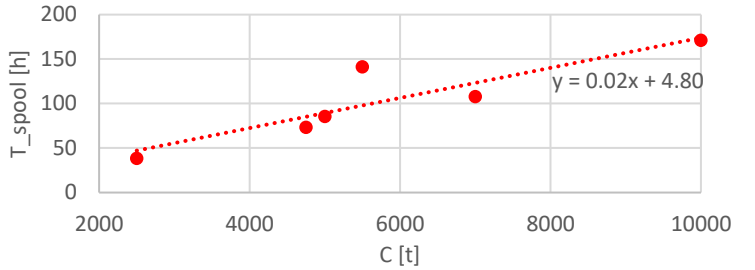


Fig. 6: Nonstop spooling time related to capacity

The stacking of cables starts at the lowest layer at the inside of the carousel. From the inside of the carousel the cable is spiraling outwards. When no cable turn fits anymore on the current layer, the cable is laid on top of this layer to form a new layer. The cable is alternating spiraling inward and outward for each layer. The cables are not spooled under tension, they are slowly and controlled laid against each other.

B. Containerized carousel system

The transportation process with using the CCS is divided into several sub processes, as shown in Fig. 7. Important characteristics of each sub process are briefly in the following paragraphs.

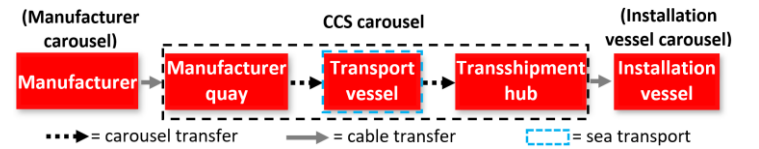


Fig. 7: Process overview of transportation with CCS

Cable transfer

The tangential speed of an SPMT axle line $V_{R,SPMT}$ at R_{SPMT} , the spool rate V_{spool} and the current spool radius R_{spool} of the current cable turn are schematically visualized in Fig. 8. The inside radius of the carousel $r_{carousel}$ must be larger than

$$r_{carousel} \geq \max(R_{SPMT}) \cdot \frac{V_{spool}}{\max(V_{R,SPMT})} \quad (2)$$

, where $\max(R_{SPMT})$ is the most outside axle line and $\max(V_{R,SPMT})$ is the corresponding tangential axle line speed. Due to the large amount of axle lines needed (184 for design proposed by Mammoet [10] [11]) there is sufficient drive and brake force to reach the needed (rotational) acceleration and deacceleration for an emergency stop.

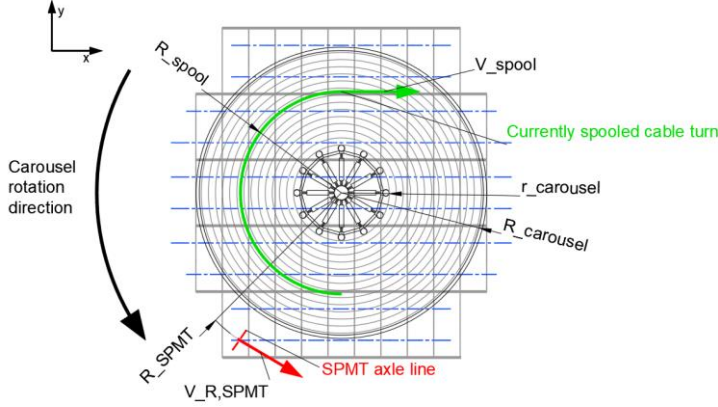


Fig. 8: Visualization of $V_{R,SPMT}$, V_{spool} , R_{spool} and R_{SPMT}

Carousel transfer

Due to large floor area of the carousel, low transport COG, and sufficient carousel stiffness, no additional couplings and lashing between the SPMTs themselves and the SPMTs and carousel is needed [21] [22]. As a result, the SPMTs and carousel are only connected by pressure and friction. For the carousel transport by SPMTs an acceleration, with the emergency stop included, of $1m/s^2$ is applicable [22].

The carousel can also be transferred from a quay to a vessel, or vice versa, by using a Ro-Ro ramp. The design of the Ro-Ro ramps is not governing for the design of the carousel, but the height difference needs to be within the remaining SPMT cylinder stroke (section III-C). For a carousel transfer over a Ro-Ro ramp a Deck carrier vessel with sufficient deck space and ballast pump/tank capacity to maintain its stability, is needed. The Mammoet database [23] shows there are multiple applicable vessels for a CCS with a capacity of 5000t.

Sea transport

The carousel must resist the load from the payload (cable stack) and transfer this load to the quay ground or vessel deck. The accelerations and the carousel, besides gravity, due to sea transport are given in Table 1 and visualized in Fig. 9 [10]. The sea transport results in the highest accelerations and the highest loads on the carousel, which makes the sea transport governing for the strength and stability of the carousel structure and load transfer.

Table 1: Sea transport accelerations on carousel ($a_{x,pitch}$ is the acceleration in x direction on the carousel due to vessel pitch)

	$a_{x,pitch}$	$a_{y,roll}$	$a_{z,heave}$
Value	$\pm 0.2G$	$\pm 0.5G$	$\pm 0.3G$

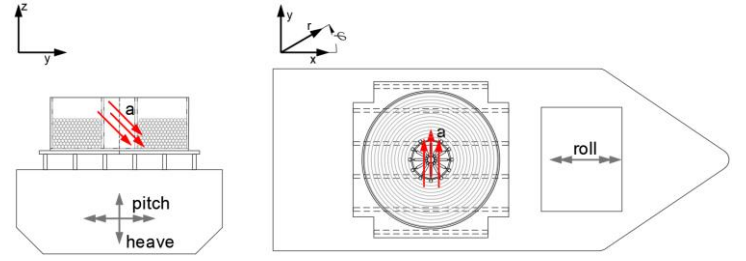


Fig. 9: Sea transport accelerations

It is assumed that all the horizontal load, due to accelerations on the payload, will be transferred to the inner frame. This means that the load on and load transfer by the outer frame and the friction between the cable stack and the floor are neglected. The cable stack and the inner frame must have sufficient stiffness to neglect the load on the outer frame. Applying all the horizontal load on the inner frame results in a worst-case-scenario loading for the inner frame, floor, and grillage of the CCS, which makes it a good approximation for the design of the CCS. The friction between cables and between the cables and inner frame and the stiffness of the cables, can result in a more favorable load distribution, but because these effects are uncertain this will be neglected.

C. Challenges

Stability and strength

The SPMTs have a shared hydraulic zone where there is a hydraulic connection between the cylinders in the axle lines (Fig. 10). Due to this connection the pressure in the cylinders and therefore the forces in the cylinder are equal within a hydraulic zone. Therefore, the resultant reaction force of the SPMTs on the cargo is always in the middle of the hydraulic zone and at least 3 hydraulic zones are needed to have a stable SPMT transport. Because the carousel occupies a large area and many axle lines are needed, stability of the SPMT transport is not a challenge for the CCS.

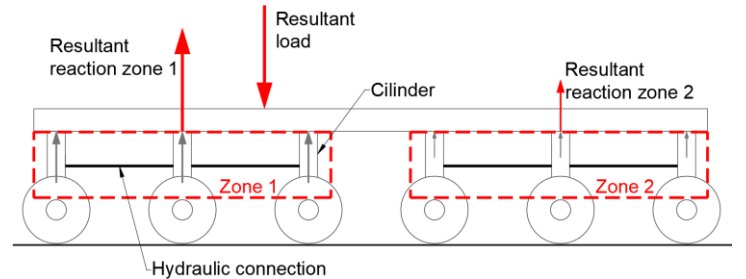


Fig. 10: Hydraulic zones of SPMT, 2D example with 6 axle lines

The maximum load, including dynamic effects and excluding the SPMT self-weight, per axle line is $36t$. With the maximum loading per axle lines the SPMT are restricted to a speed of $4m/s$ [24].

Furthermore, all structural components and connections of the CCS must satisfy the strength and stability criteria under the occurring loads, where the sea transport accelerations are governing for most structural components.

SPMT stroke

All the axle line cylinders have an available stroke of 700 mm [24]. From Mammoet it is advised to use no more than 70% of the

available stroke, and thus the stroke is limited to $700 \cdot 0.7 = 490 \text{ mm}$ [25]. Factors which need to be considered for the available stroke are (Fig. 11):

- Ground conditions (slopes, camber, unevenness, RoRo ramp heights) (S_2 in Fig. 11)
- Lift and drop heights, assumed to be 250 mm
- Deflection of SPMT (S_1 in Fig. 11)

Minimizing the SPMT deflection is thus necessary to have sufficient cylinder stroke to overcome other height differences.

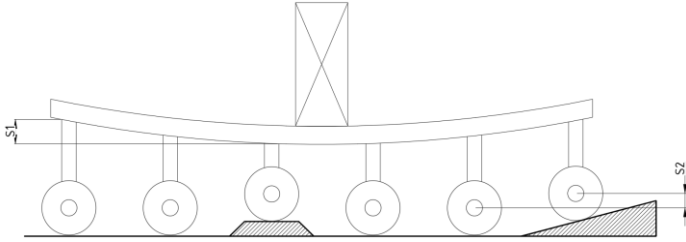


Fig. 11: Stroke usage of SPMT

SPMT issues

The SPMTs, especially the outer ones, need to travel large distances during a cable transfer while they are heavily loaded. This is a challenging task for the SPMTs and can cause some difficulties:

- **Tire wear:** Due to the high load and large travel distance of the SPMTs, the tires are prone to wear. The carouselling movement enlarges the wear because there is more chance that some wheels will slip. To lower the tire wear it is beneficial to minimize the slopes, cambers, and unevenness in the underground. During cable transfer it is expected that some tires need to be changed.
- **Overheating of generator:** The motors and cylinders are regulated by hydraulics, where the hydraulic pressure is regulated by pumps. These pumps are driven by a generator. Besides delivering enough power for a lot of hours, the generator also produces a lot of heat, which can in combination with a high environmental temperature cause overheating of the generator. Overheating requires the cable transfer to be paused to cool down the generator.
- **Hydraulic leakage:** The hydraulic motors and cylinders put a lot of stress on the hydraulic system, which make it prone to oil leakage. During cable transfer it is expected that some parts of the hydraulic system require maintenance.

III. Conceptual solutions

A. Boundary conditions

The following requirements are applicable to the CCS design:

- CCS must maintain its functions as the design proposed by Mammoet, shown in Fig. 3 [10]. The most important functions are that the CCS must be containerized, must include a grillage frame with enough space of SPMTs and it must be modular.
- The CCS must have a capacity of $5000t$, consisting of offshore cables with a maximum diameter D_{cable} of 300 mm . 300 mm is governing for the CCS design as smaller cables result in a closer packed cable stack.

- Maximum load on each SPMT axle line is $36/1.15 = 31.3t$ (section II-C) where a safety factor of 1.15 is used for dynamic effects.
- Each SPMT axle line requires a rectangular area of $2.9 \cdot 1.4 \text{ m}$ [24]
- The CCS must be applicable to multiple vessels.
- The outer dimensions and total weight of the CCS shall be minimized
- The sum of the weight of the carousel and the weight of the grillage frame $m_{carousel} + m_{grillage}$ is estimated by $1.294 t/m^2$ multiplied by the footprint area of the carousel
- SPMTs have a maximum velocity of $\max(V_{o,SPMT}) = 4 \text{ km/h}$
- The spool rate is assumed to be $V_{spool} = 1 \text{ km/h}$

B. Setups

The main design choices include the main carousel dimensions and the SPMT, floor, grillage setup. Based on the requirements several floor plate setups with the outer carousel diameter have been defined (Fig. 12).

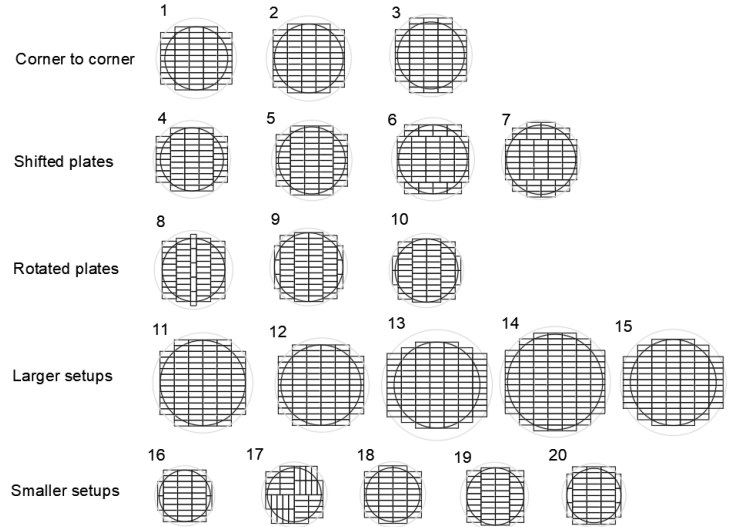
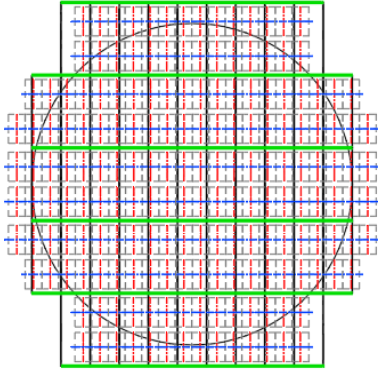


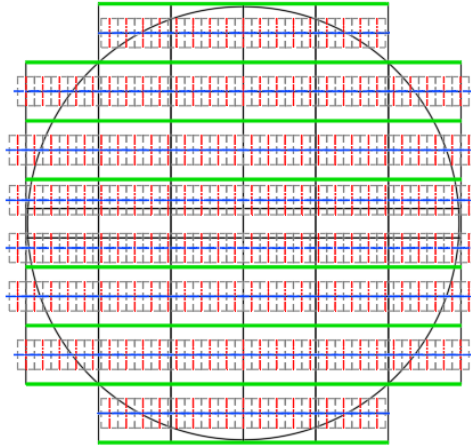
Fig. 12: Floor plate setups

For a good force transfer it is desired that the carousel is fully supported by floor plates and that these floor plates are fully covered by the SPMT axle lines. For each plate setup the vessel applicability, estimated weight, needed axle lines, inside carousel radius, need carousel height and SPMT drive distance have been determined. Furthermore, an important factor is the amount of carousel footprint covered by SPMTs. If many axle lines are unsupported the deflection of the SPMT transport is enlarged and if a large part of the carousel is unsupported the carousel is larger and heavier than needed. Setups 1, 9, 11 from Fig. 12 have been selected for further elaboration because setups 11 and 9 shown good performance, and setup 1 is the proposed setup by Mammoet. Furthermore, for the selected floor plate setups also multiple SPMT and grillage setups have been proposed. The main specifications of the chosen floor plate setups are summarized in Table 2, and the corresponding floor plate, grillage and SPMT setups are shown in Fig. 13.

Setup 1



Setup 11.2



Setup 9.1

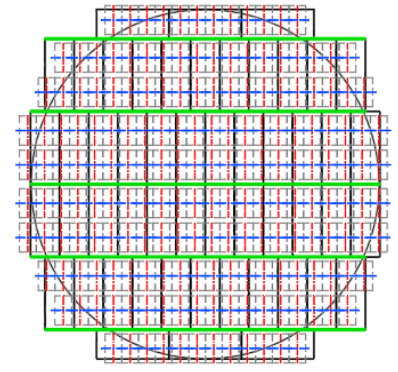


Fig. 13: Selected setups 1, 11.2 and 9.1

Table 2: Chosen setups properties

Setup	Abb.	1	9	11	Unit
Outside carousel diameter	$2R_{carousel}$	26.84	29.15	36.18	m
Minimum inside carousel radius	$r_{carousel}$	3.85	3.72	4.80	m
Chosen inside carousel radius	$r_{carousel}$	4.375	4.00	5.00	m
Carousel height	$h_{carousel}$	5.50	4.72	3.16	m
Number of floor plates	/	51	52	82	/
Number of axle lines	/	185	189	204	/

B. Structural

The dimensions and cross- sections of the different structural components are also design choices for the CCS. The structural components of the carousel will only globally be treated as the detailing is not in the scope of the project. The main structural components of the CCS are:

- **Outer frame:** not considered
- **Inner frame:** Based on the design proposed by Mammoet [10]. The cross sections and dimensions are to be determined.
- **Floor:** New proposal to allow other types of floor plate setups. With this new proposed floor plate longitudinal and transverse beams can be connected to each other. The main dimensions of the new floor plate are shown in Fig. 14 and cross sections of the longitudinal and transverse beams need to be determined.
- **Grillage:** Below the floor a height of 1350mm is needed for the SPMTs [24]. It therefore is chosen to use HEB1000 beams for the grillage, which thus leaves 350mm for the connection between the grillage and the floor

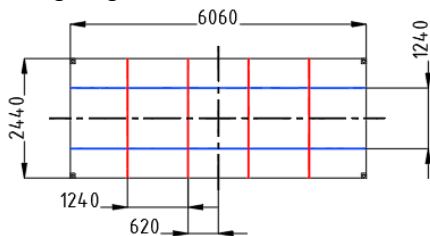


Fig. 14: New floor plate

IV. Concept analysis

A. Loads

For the CCS the SPMT transport and the Sea transport have been defined as the governing load cases. The SPMT transport will only be used to check the deflection of the transport. The sea transport load case is governing for the strength and stability of the members and connections. The following loads are applied on the CCS:

- **Self-weight:** The CCS is subjected to accelerations. For the SPMT transport only gravity is considered and for sea transport gravity and sea transport accelerations are considered.
- **Vertical payload:** For both the SPMT transport and the sea transport the vertical payload of 5000t is applied as a uniformly distributed load on the carousel footprint (Fig. 15).
- **Horizontal payload:** As described previously it is assumed that all the horizontal load is induced on the inner frame of the CCS. These horizontal loads are assumed to be uniformly distributed over the poles which are expected to experience pressure, as shown in Fig. 16.

Load factors are applied to the loads where favorable factors have been used for the Serviceability Limit State, to check deflections, and unfavorable factors have been used for the Ultimate Limit State, to check for strength and stability criteria against EN1993-1-1:2005 Design of steel structures, general rules.

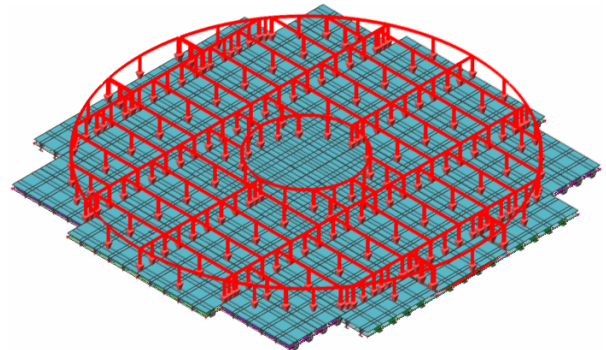


Fig. 15: Vertical payload of carousel floor

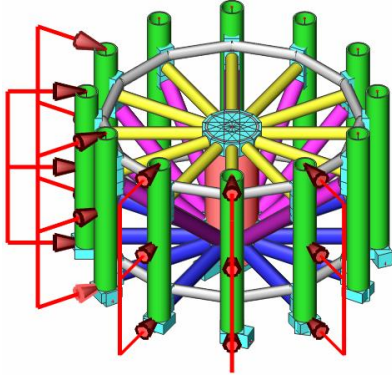


Fig. 16: Horizontal payload on inner frame

B. Concept selection

For all three selected setups (Fig. 13) a FEM model has been established to check the SLS SPMT transport deflection. The results are summarized in Table 3 and the deformation plots for setup 1 and 9.1 are shown in Fig. 17 and Fig. 18, respectively.

Table 3: Results setup selection study

Setup	Weight floor	Used cylinder stroke for deflection
1	250	225
11.2	402	202
9.1	255	90

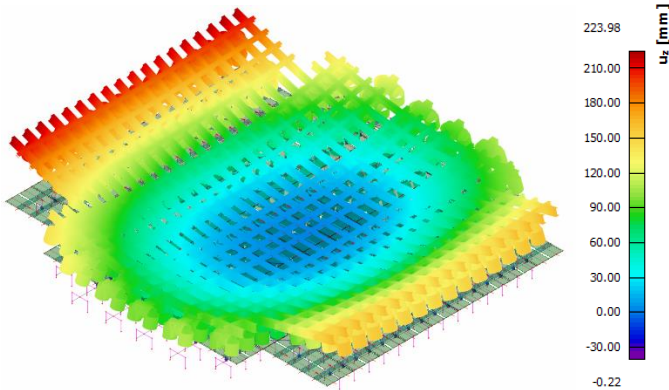


Fig. 17: SPMT transport SLS deflection Setup 1

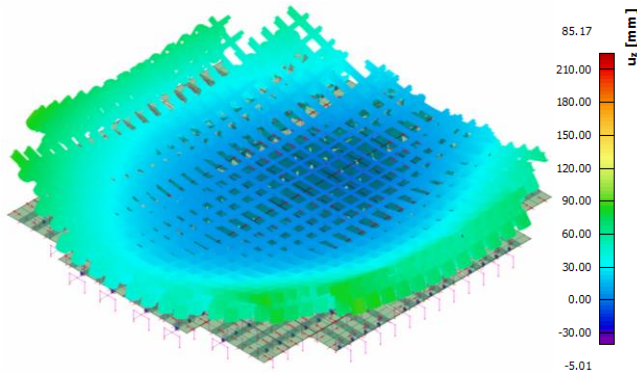


Fig. 18: SPMT transport SLS deflection Setup 9.1

Table 3 shows that setup 9.1 has a large decrease of the maximum deflection of the SPMT compared to setup 1, while they have approximately the same self-weight. A smaller deflection is beneficial for the used stroke of the SPMT and therefore setup 9.1

has been selected for further elaboration. Furthermore, the SPMTs for setup 9.1 must travel 8% less compared to setup proposed by Mammoet.

C. Concept Elaboration

For the CCS the following adjustments have been made:

- **Additional sea fastening:** Additional Sea fastening is used to transfer the horizontal loads due to roll to the vessel deck, as shown in Fig. 19.
- **Floor plate reinforcement:** To lower the weight of the floor, a general floor plate with lighter cross sections as used in Fig. 17 and Fig. 18 has been chosen. Stronger floor plates with heavier cross-sections have been used at places where needed.
- **Cross sections:** The cross sections of all structural components have been determined by a few iterations of selecting cross sections and checking the strength and stability criteria. Based on the results, stronger or weaker cross sections have been selected.

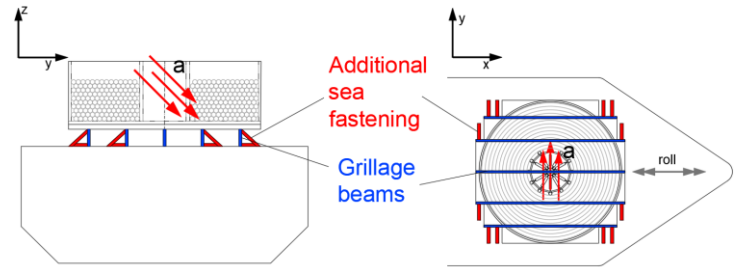


Fig. 19: Additional Sea fastening

The final FEM model is shown in Fig. 20, and the results are summarized in Table 4. For this FEM model the self-weight has been multiplied by 1.25 for the weight of unmodelled parts, reinforcement, and accessories. The overall unity checks for all members of the floor, grillage frame and inner frame are shown in Fig. 21, Fig. 22 and Fig. 23, respectively.

Table 4 shows a slightly higher SPMT deflection, which is caused by using less strong and stiff longitudinal and lateral beams in the floor plate to minimize weight. Additional stiffness thus minimizes the SPMT deflection. The stiffness and effect of the cable stack on the SPMT deflection is uncertain and thus has been neglected. Fig. 21 and Fig. 22 show that some unity checks are slightly higher than 1.00. These unity checks are however local and can thus be solved by local reinforcement, which makes the high unity check acceptable.

Table 4: Results setup selection study

Description	Type	Value	Unit
Weight floor and inner frame	/	417	t
Weight grillage frame	/	51	t
SPMT deflection	SLS	110	mm
Highest unity-check SPMT transport	ULS	0.72	/
Maximum deformation sea transport	SLS	37	mm
Highest unity-check sea transport	ULS	1.24	/

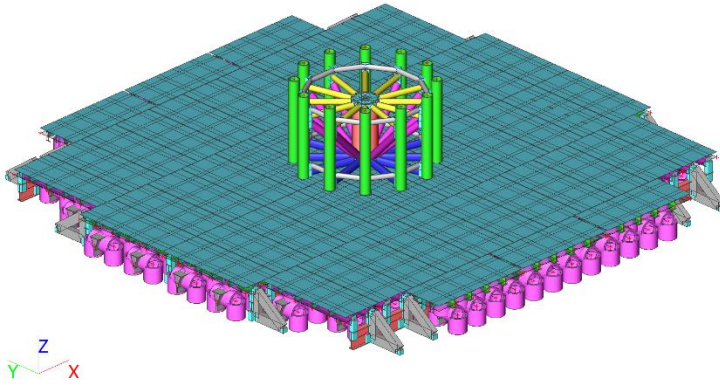


Fig. 20: Elaborated FEM model

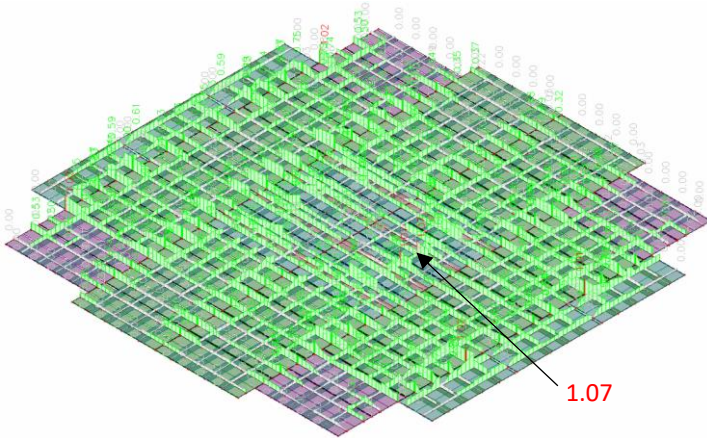


Fig. 21: Overall USL unity checks floor for sea transport

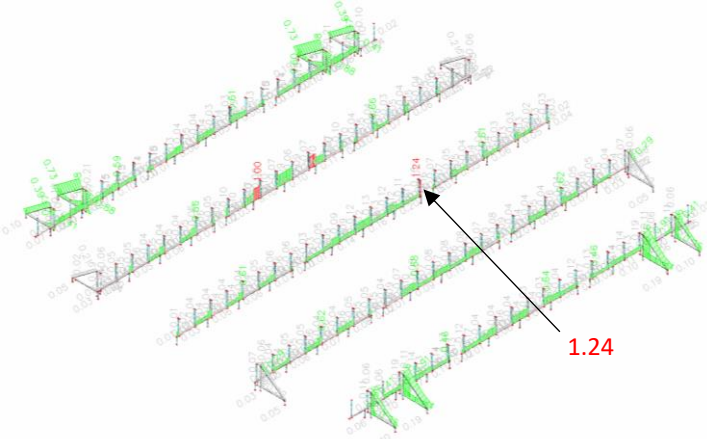


Fig. 22: Overall USL unity checks grillage frame for sea transport

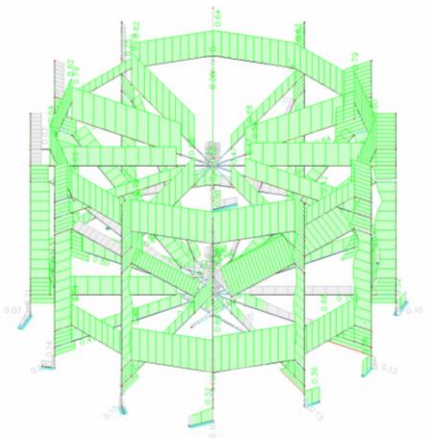


Fig. 23: Overall USL unity checks inner frame for sea transport

V. Influence of cable stack

A. Single cable

To verify that the cable stack has sufficient stiffness to neglect the load on the outer frame, a FEM model of a cable with average properties and a diameter of $D_{cable} = 190mm$ has been developed (Fig. 24). The different layers used in the model are shown in Fig. 25. The model consists of $1m$ where the conductors, insulation and armor wires are helically spiraled over the length with 360° over $1m$.

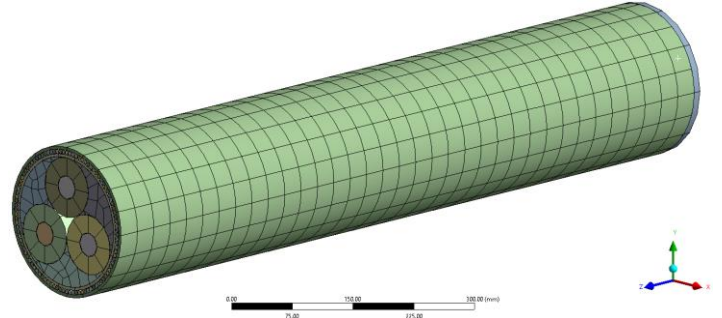


Fig. 24: Single cable FEM model

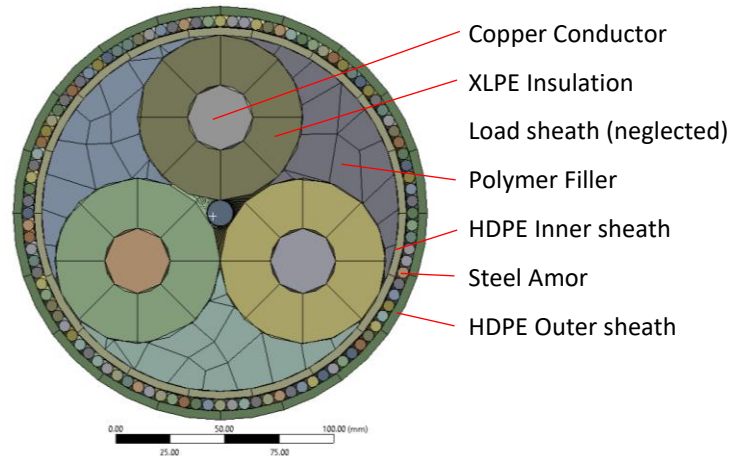


Fig. 25: Cable FEM model cross section

With simulations using the model and manual calculations, it is determined that the cable has an axial stiffness of approximated $8GPa$ and that the cable has negligible horizontal expansion under the $5000t$ cable stack. From this it can be concluded that the cable, and thus the cable stack, don't experience much deformation under the loading. This causes that if the inner frame has sufficient stiffness and if the outer frame is relatively flexible, most load is induced on the inner frame and the load on the outer frame is negligible. For the design of the CCS it therefore is a good approximation that all the load is transferred to the inner frame as load transfer by the outer frame and friction with the floor and cable stack result in a more favorable load distribution.

Friction within the cable has been neglected due to convergence issues. Multiple simulations have been executed with using different combinations of different contacts each simulation. For each contact 'no separation' (no friction) and the 'bonded' contact (infinity friction) contacts could be used. Effects of the different contacts and an estimation of the frictional effect have both been considered for the results.

B. Load distribution

Previously a load distribution of the payload on the carousel as shown in Fig. 15 and Fig. 16 has been used. To verify this load distribution, a simplified FEM model of the cable stack and the carousel has been developed, shown in Fig. 26. Symmetry and a large D_{cable} have been used to simplify the model.

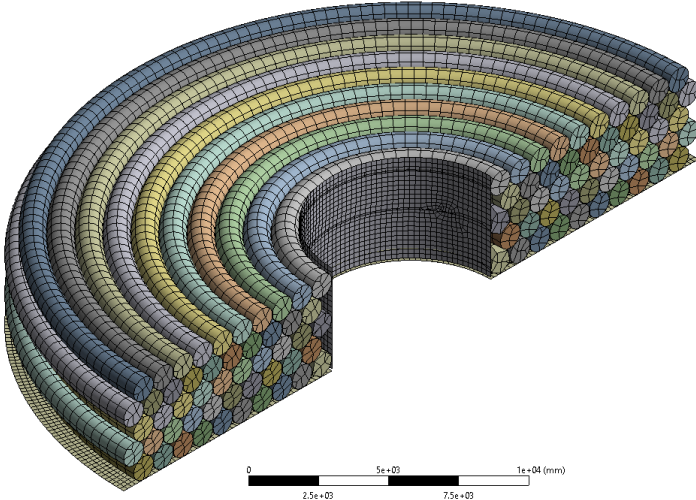


Fig. 26: Simplified FEM model for load distribution

Different simulations have been executed with different inputs for the cable stiffness and the contact types between the cables and between the cables and the carousel. Mostly frictional contacts are used for the different contacts in the simulation. All simulations show comparable load distributions, with different magnitudes. For one simulation, the load distributions on the inner frame and the floor are respectively shown in Fig. 27 and Fig. 29. It follows that the assumed uniform distribution on the inner frame and the distribution on the inner frame from the simulations, result in a comparable height and magnitude of the resultant force on the inner frame. This causes an approximately equal bending moment on the floor and grillage. Because this bending moment is governing for the design of the floor and grillage, the assumed uniform distribution is a good approximation of the load distribution which follows from the simulation for the global behavior of the CCS. From the simulations it however follows that per pole the distribution on the inner is according to Fig. 28, instead of a uniform distribution. These results in other local stresses which need to be considered in the detailing phase of the CCS.

For the load distribution of the payload on the floor, the distribution observed in the simulations is beneficial because most load is induced on the floor at the places where it tries to cancel out the floor deformation. A uniform load distribution is thus a more unfavorable load, which makes it a good approximation for the CCS design.

Friction between the cable stack and the floor shows to be beneficial as it directly lowers the load on the inner frame, which is governing for a few structural components of the CCS. Neglecting friction between the cable stack and the floor thus gives a more unfavorable load distribution and thus is a good approximation for the design of the CCS.

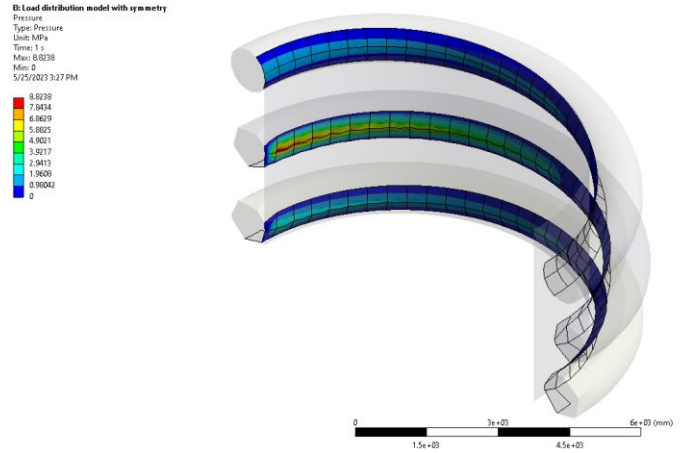


Fig. 27: Load distribution on inner frame

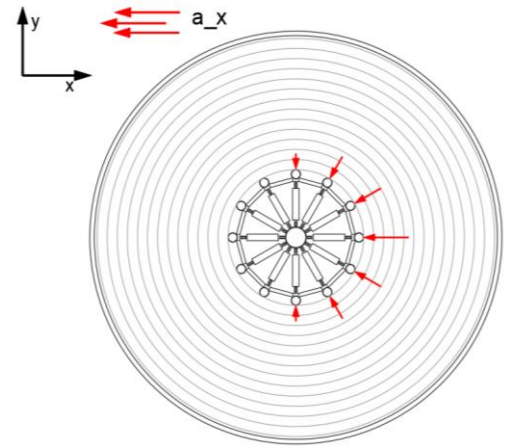


Fig. 28: Load distribution from simulations over inner frame

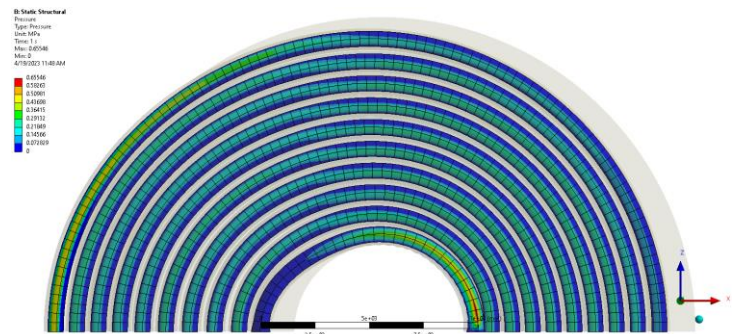


Fig. 29: Load distribution on floor

VI. Results

It follows that the SPMT deflection, CCS structural strength and stability and SPMT issues such as tire wear, overheating and hydraulic leakage, tend to be important challenges. It has been defined that the important design choices include the main carousel dimensions and the SPMT, floor and grillage setup. Furthermore, cross sections are more specific dimensions must be determined. In section IV it is shown that the appropriate choice of the carousel main dimensions and a SPMT setup can significantly decrease the SPMT deflection. As a result, a concept with a deflection of 90 mm has been elaborated, where the concept proposed by Mammoet has a deflection of 225 mm and comparable weight. For the elaborated concept the cross sections

of the structural components are improved to lower the weight and still satisfy the stability and strength requirements. For a more beneficial load transfer it is found that additional sea fastening as shown in Fig. 19 should be implemented. Due to the SPMT setup of the new concept, the SPMTs must travel 8% less compared to the Mammoet concept. This is a slight improvement corresponding to the SPMT issues such as tire wear. For the new concept it is assumed that all the load is transferred through the inner frame and that the load is uniformly distributed over the inner frame and the floor. In section V it is shown that these assumptions are good approximations as they are worst-case-scenarios considering the uncertainties.

VII. Conclusion

The other SPMT issues such as hydraulic leakage and generator overheating are still uncertain. Assuming that these issues are not problematic and can be solved by maintenance, it can be concluded that the CCS is a feasible method to transport offshore power cables. However, it can be concluded from the study that the SPMT setup and the main carousel dimensions need to be selected carefully to minimize the SPMT deflection. This is necessary to successfully implement the CCS, otherwise the SPMT cylinders can reach their limits. If the CCS improves the current offshore power cable transportation method is mainly dependent of the costs and time. It is difficult to compare the costs and time for the current method and the CCS as there are many parameters which have an influence. Comparing the offshore power cable transportation using the CCS with the current transportation method, the main benefits of the CCS include:

- *Less cable transfers*: Less cable transfer from carousel to carousel are needed. This is also beneficial for the cable quality and significantly decreases the transportation time as a cable transfer cost multiple weeks and a carousel transfer can be done in one day. Furthermore, less cable transfers lower the costs as the equipment, vessels and quays are shorter occupied.
- *CCS is mobile by the SPMTs*: Carousel and cable can be stored on much more places and the (loaded) carousel can be transferred. This allows cheaper storages.
- *Cheaper sea transport*: for the CCS only a vessel with a strong and large enough deck is needed.
- *Easy sea fastening*
- *System is containerized*: cheap and quick mobilization, demobilization, and storage
- *CCS is modular*: The modality of the CCS enables to use it for different project with different capacities. However, for each capacity, setup, and dimensioning of the structural carousel components, the CCS should carefully be checked for SPMT deflection and structural strength and stability. The concept elaborated in this study is only applicable for 5000t or lower capacities.

Cons of the CCS are that the carousel of the CCS is expensive and that also the SPMT aren't cheap. It is difficult to determine the overall costs of transportation with the CCS compared to the current transportation method. Because less cable transfers are needed the CCS does decrease the overall transportation time of the cable. However, for the CCS more preparation and mobilization are needed compared to the current transportation methods.

For future work it is recommended to apply the loads as described in Fig. 15 and Fig. 28. It is also recommended to use the sea fastening as described in Fig. 19. An important outcome of the study is that the performance of the system against SPMT transport deflection is dependent of the carousel main dimensions, capacity and SPMT setup. As the system is modular, every different configuration should be checked for the deflection of the SPMTs. For further use of the proposed concept, further detailing and local reinforcement is needed. Also, the SPMT issues such as tire wear, hydraulic leakage and overheating of the SPMT generator should be investigated for successful implementation of the CCS in the cable transportation process.

For further usage of the concept used in this study, it is further detailing the outer frame, connections and local reinforcements is recommended. Furthermore, the neglected loads should be considered.

References

- [1] Wikipedia, "Offshore wind power," [Online]. Available: https://en.wikipedia.org/wiki/Offshore_wind_power.
- [2] GWEC, "GWEC: offshore wind will surge to over 234GW by 2030, led by Asia-Pacific," 5 August 2020. [Online]. Available: <https://gwec.net/gwec-offshore-wind-will-surge-to-over-234-gw-by-2030-led-by-asia-pacific>.
- [3] Wikipedia, "Submarine power cable," [Online]. Available: https://en.wikipedia.org/wiki/Submarine_power_cable.
- [4] N. americas, "Carousel-10000-spec-sheet-V.01," Neptune americas.
- [5] jdcon, "Installation of four subsea power cables in the north atlantic," JD contractor, [Online]. Available: <https://www.jdcon.dk/News/Installation-of-four-subsea-power-cables-in-the-North-Atlantic>.
- [6] A. Dawood, "A study of pipeline response during reel-lay installation," Semantic scholar.
- [7] M. chesshrye, "Aegir's first project," Oedigital, [Online]. Available: <https://www.oedigital.com/news/453489-aegir-s-first-project>.
- [8] Osprey, "Cabling carousels in action," Osprey, [Online]. Available: <https://osprey.group/cabling-carousels-in-action/>.

- [9] Mammoet, "Efficient load-in and transpooling of subsea cable for an offshore project in Saudi Arabia," 2022. [Online].
- [10] I. Harms, "Basis of Design - Containerized Carousel System," Mammoet, Schiedam, 2022.
- [11] I. Harms, "Global calculations - Containerized Carousel System," Mammoet, Schiedam, 2022.
- [12] P. group, "66 kV Submarine Cable Systems for offshore wind," [Online]. Available: https://www.prysmiangroup.com/sites/default/files/business_markets/markets/downloads/datasheets/leaflet_submarine_epr_66%20Kv_%20final.pdf.
- [13] T. Tech, "Offshore wind submarine power cables - an introduction," 2022. [Online]. Available: <https://rodafisheries.org/wp-content/uploads/2020/11/RODA-JTF-Cabling-presottReviewed.pdf>.
- [14] C. cables, "XLPE Insulated DC High-Voltage Submarine Cable," [Online]. Available: http://www.caledonian-cables.com.tr/product/Submarine_Cables/XLPE-DC.html.
- [15] C. cables, "Lead Sheathed AC High-voltage submarine cable," [Online]. Available: <http://shipboard-cables.com/submarine-cables/Lead-Sheathed-High-voltage-Submarine-Cable.html>.
- [16] T. C. solutions, "Catalogue - Innovative cable solutions meeting international standards," [Online]. Available: https://cableconnectivitygroup.it/files/TKF-MARINE_e2857434.pdf.
- [17] O. Unosson, "Offshore cable installation - Lillgrund," [Online]. Available: <https://www.osti.gov/etdeweb/servlets/purl/979750>.
- [18] N. americas, "Carousel-5000-spec-sheet-V.01," Neptune americas.
- [19] S. hunter, "2500 Te Basket Carousel SH-BC-2500".
- [20] "7000t-basket-carousel-spec-sheet," Dutch Offshore Contractors BV, Vlissingen.
- [21] Mammoet, "Best practice - Trailer synchronization," Mammoet.
- [22] Mammoet, "Best practice - Forces on cargo and lashing during transport," Mammoet.
- [23] Mammoet, "Deck Carrier Overview".
- [24] F. B. Andreas Köhler, "Modulaire transporter SPMT technische gegevens V1-7," Scheuerle, 2018.
- [25] Mammoet, "Best Practice - Transport - Allowable deflection and camber," Mammoet, 2018.

B Cable stack expansion estimation

This appendix describes the estimation of the expansion of the cable stack.

B.1 Input

For the estimation of the cable stack expansion the input defined in Table B-1 is selected.

Table B-1: Input study cable stack expansion estimation

Description	Abbreviation	Value	Unit
Outside carousel radius	R_{carousel}	13.3	m
Inside carousel radius	r_{carousel}	4.375	m
Carousel height	h_{carousel}	5.80	m
Carousel capacity	C	5000	t
Cable diameter	D_{cable}	190	mm
Cable mass	μ_{cable}	66.8	kg/m
Axial elastic modulus cable	$E_{\text{cable,axial}}$	5.00	GPa
Radial elastic modulus cable	$E_{\text{cable,radial}}$	1.00	GPa
Horizontal acceleration	/	5.00	m/s^2

B.2 Load due to vertical acceleration

The vertical acceleration on the cable stack will be transferred to horizontal loads due to the angle of the contact of the cables from different layers. This causes a triangular distribution on the outer wall as can be seen in the figure below.

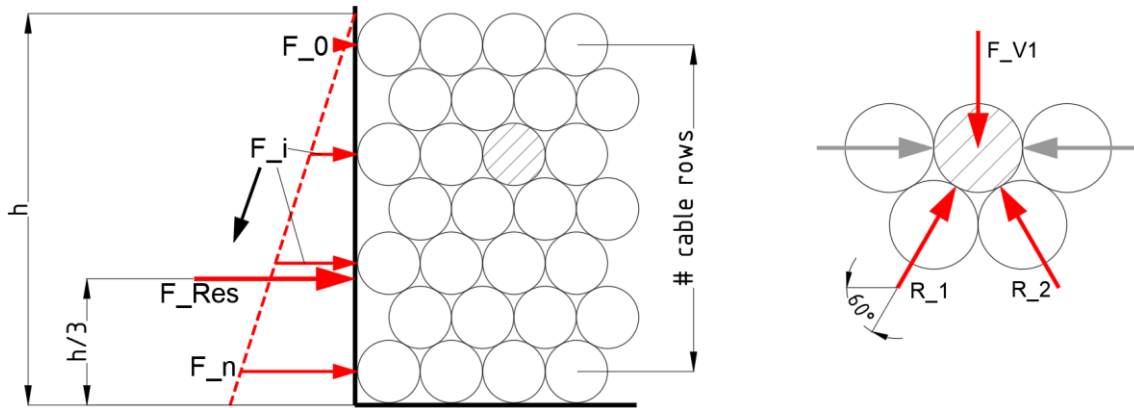


Fig. B-1: Triangular distributed load outer carousel frame and forces on one cable

Considering the force on one cable section. For this example, it is assumed that the vertical load F_{V1} is mainly transferred in R_1 and R_2 (effect horizontal forces and friction are neglected). Equilibrium for the single cross section then requires respectively that R_1 and R_2 and the magnitude of their horizontal components are given by

$$R_1 = R_2 = \frac{F_{V1}}{2 \sin(60^\circ)} \quad \text{and} \quad |R_{1x}| = |R_{2x}| = \frac{F_{V1}}{2 \tan(60^\circ)} = 0.29 \cdot F_{V1} \quad (B-1)$$

, which means that 29% of the vertical load is transferred into horizontal load to the left and 29% of the load is transferred into horizontal load to the right. It is assumed that on average roughly 1/2 of the horizontal load from each cable into the direction of the outer wall reaches the outer wall. So, summation of all cable cross sections results in 14.5% of the total capacity which is transferred into horizontal load on the outer wall. The resultant force F_{res} distributed over the outer carousel is thus given by

$$F_{res} = \frac{\text{capacity}}{4 \tan(60^\circ) L_0} \approx 0.145 \cdot \frac{\text{capacity}}{L_0} = 0.145 \cdot \frac{\text{capacity}}{2\pi R_c} \quad (B-2)$$

Notice that F_{res} is uniformly distributed over the outer wall of the carousel as shown in Fig. B-2.

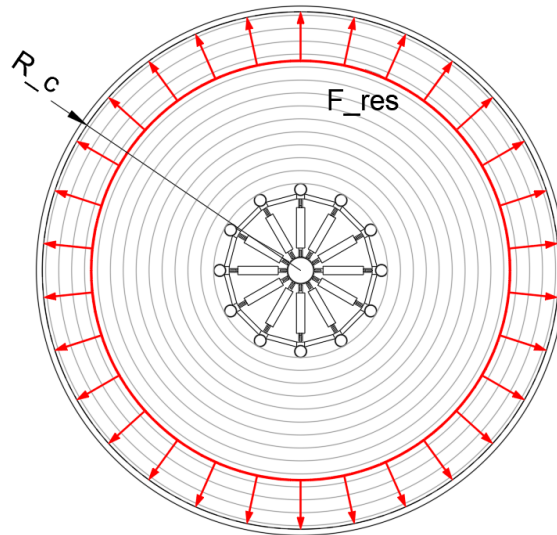
Fig. B-2: Uniformly distributed load F_{res}

Fig. B-1 shows that F_{res} is the resultant force of all contact forces between the cable stack and the outer carousel F_i over the height of the carousel. These contact forces have a triangular distribution over the height of the carousel and thus F_{res} equals

$$F_{res} = \sum_{i=0}^n F_i = \sum_{i=0}^n i \cdot \Delta F = \Delta F \sum_{i=0}^n i \quad \rightarrow \quad \Delta F = \frac{F_{res}}{\sum_{i=0}^n i} \quad (B-3)$$

, where $F_i = i \cdot \Delta F$ and n defines the number of cables which are in contact with the outer frame and i denotes the contact force F_i . From F_{res} the value of ΔF can be calculated, where ΔF denoted the decrease of the contact force for each lower contact. With ΔF , the contact force of the bottom cable to the outer wall of the carousel F_n can be calculated as

$$F_n = n \cdot \Delta F = n \cdot \frac{F_{res}}{\sum_{i=0}^n i} \quad (B-4)$$

From Fig. B-1, F_n is the highest contact force with the outer carousel. This force also results in tension in the cable instead of only pressing on the outer wall. To determine if the pressing on the outer wall can be neglected, the expansion of the cable will be calculated if the entire contact force F_n is transferred in cable tension. In Fig. B-3 a uniformly distributed load in the $x - y$ plane on a closed cable is shown, with a segment of the cable.

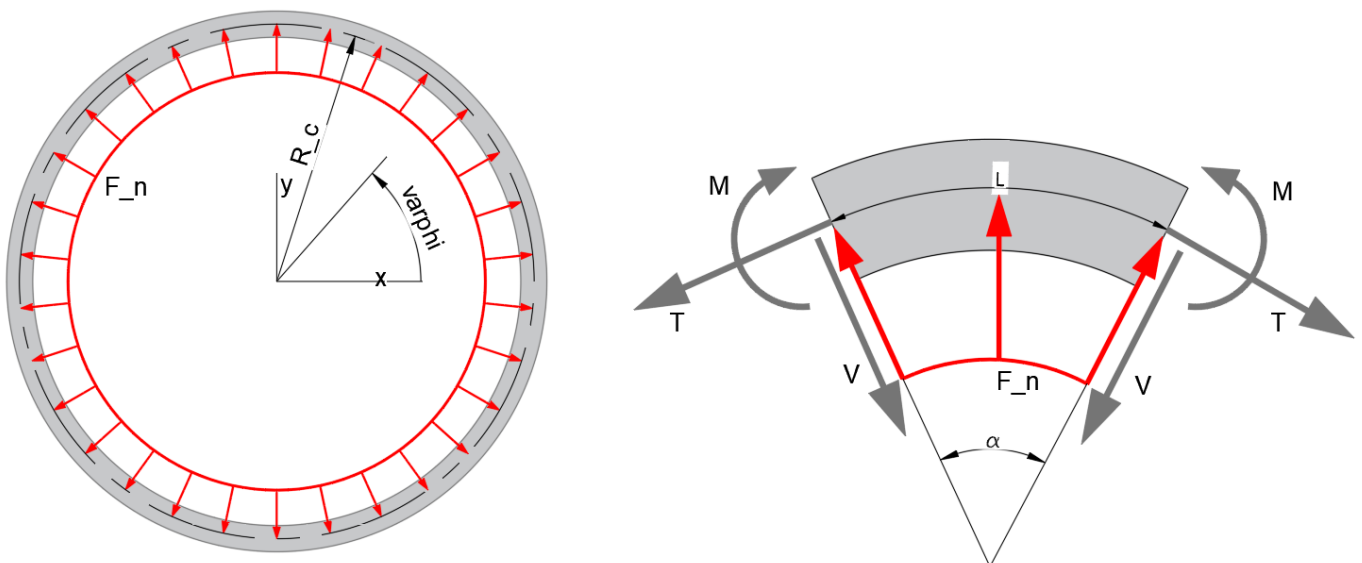


Fig. B-3: Radial uniformly distributed load on closed cable, and cable segment

Looking at a segment, as can be seen in Fig. B-3, the internal forces resisting the uniformly distributed load F are the normal force (tension) T , the shear force V and the bending moment M .

Tension force

To look at axial effect in the cable it is assumed that the load F is entirely converted into tension in the cable (bending resistance neglected), the following situation occurs. This results in the forces on the cable segment as shown in Fig. B-4.

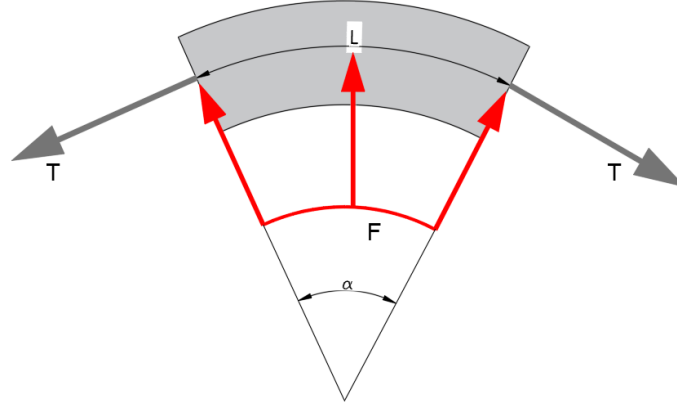


Fig. B-4: Cable segment where bending resistance is neglected

Looking at the segment, equilibrium in the y direction states

$$-2T \sin\left(\frac{\alpha}{2}\right) + \int \cos\left(\frac{\alpha}{2}\right) R_c F_n d\alpha = 0 \quad \rightarrow \quad -2T \sin\left(\frac{\alpha}{2}\right) + 2R F_n \sin\left(\frac{\alpha}{2}\right) + C = 0 \quad (B-5)$$

Notice the use of the chain rule for the integral. Because the integral must equal zero at $\alpha = 0$ it follows that for the integration constant $C = 0$. After simplification it follows that equilibrium is satisfied when

$$T = R_c F_n \quad (B-6)$$

, where T is the tension which works in the entire cable. The extension of the total cable can be calculated by

$$\delta = \frac{TL}{E_{cable,axial} A_{cable}} = \frac{8TR_c}{E_{cable,axial} D_{cable}^2} \quad (B-7)$$

With the expansion of the cable, the change of the radius R , denoted as ΔR , can be estimated by

$$\Delta R = \delta / 2\pi \quad (B-8)$$

With the assumed input from Table B-1 this leads to results shown in Table B-2.

Table B-2: Results cable expansion example

Description	Abbreviation	Value	Unit
Surface area cable cross section	A	0.028	m^2
Tension cable	T	125	kN
Cable length	L	83.6	m
Extension of cable	δ	73.8 (= 0.09%)	mm
Change of radius due to expansion cable	ΔR	11.7 (= 0.09%)	mm

FEM Simulation verification

To verify the results, a FEM model has been elaborated as shown in Fig. B-5. The dimensions are as defined in Table B-1. For the model quadratic brick elements with reduced integration have been used, with a standard size of 100mm.

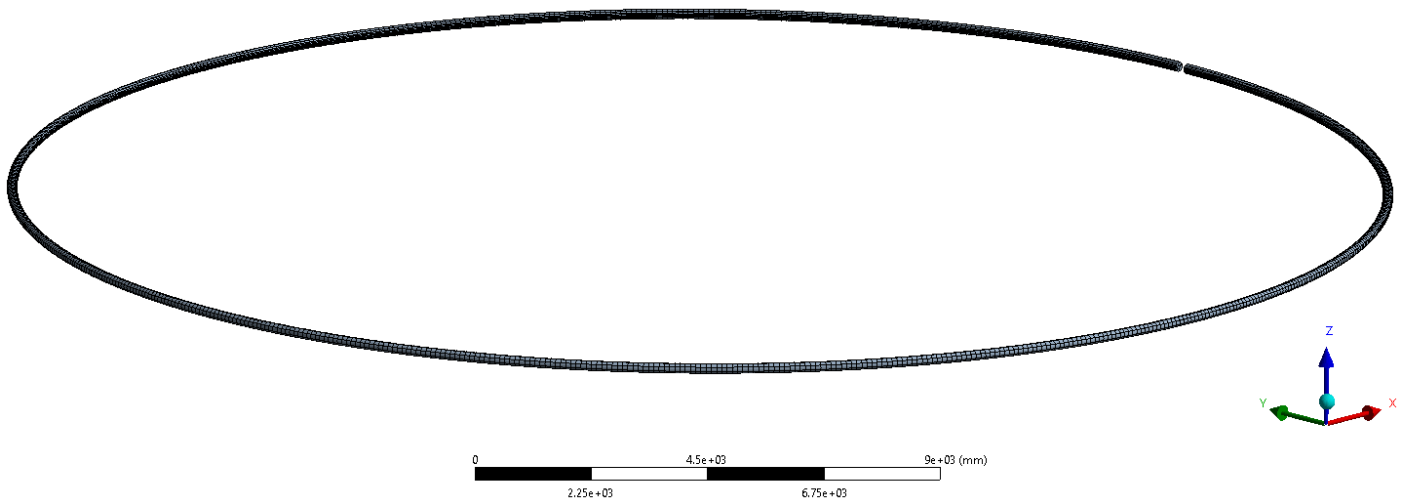


Fig. B-5: FEM model for verification

A slice in the cable has been implemented where the cable is fixed at both ends, as shown in Fig. B-6. The distributed load F_n has been implemented as a pressure on the red area in Fig. B-6.

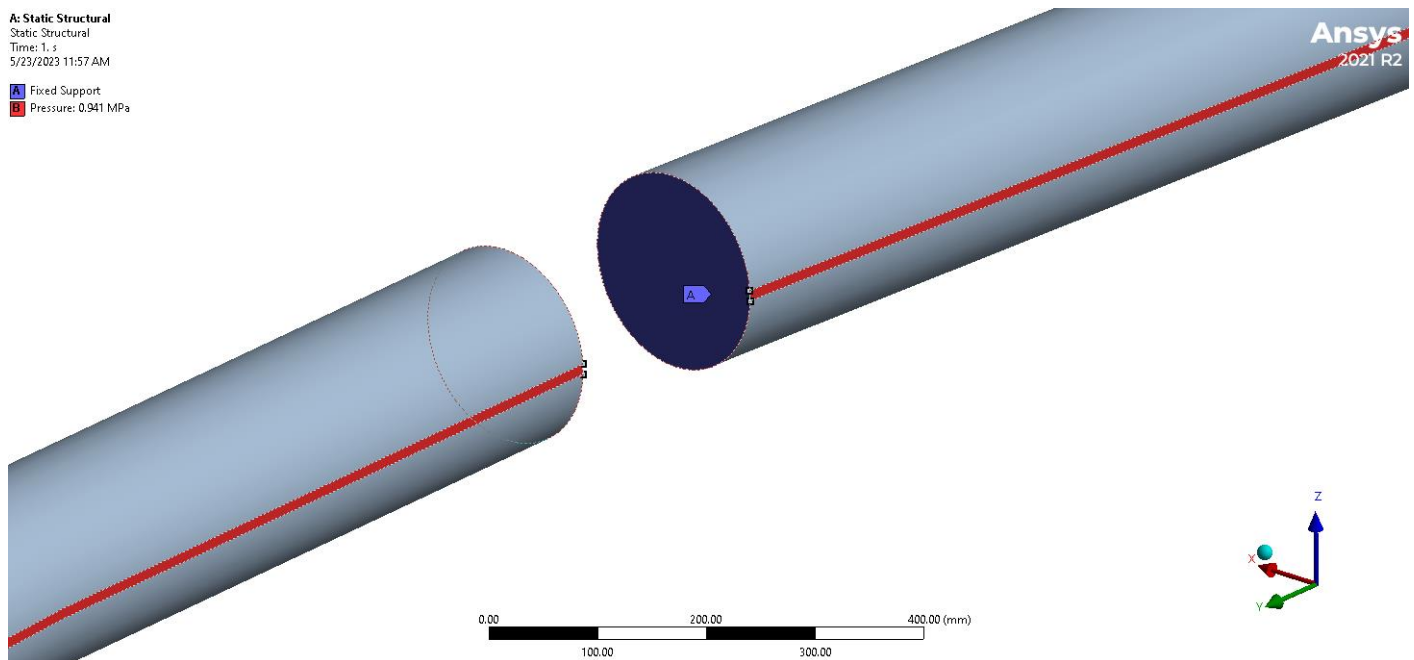


Fig. B-6: Cable segment where bending resistance is neglected

The results of the FEM simulation are shown in Fig. B-7. Notice that the 'min' probe in Fig. B-7 approximates the diameter change of the cable expansion and can thus be approximated by $2 \cdot \Delta R$. Notice that Fig. B-7 also shows the undeformed cable in gray and that the deformations in the plots are scaled.

A: Static Structural

Directional Deformation
 Type: Directional Deformation(X Axis)
 Unit: mm
 Global Coordinate System
 Time: 1 s
 Max: 0.028317
 Min: -23.388
 5/23/2023 11:51 AM

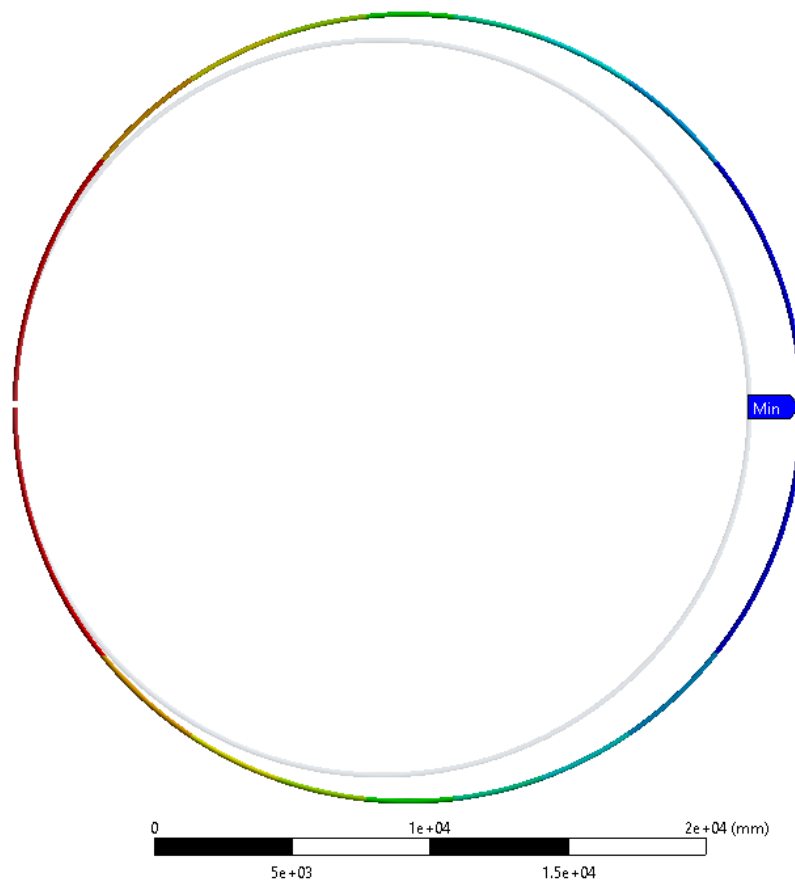
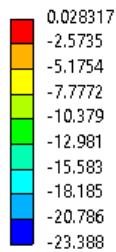


Fig. B-7: Results FEM simulation – displacement x direction

A: Static Structural

Equivalent Stress
 Type: Equivalent (von-Mises) Stress
 Unit: MPa
 Time: 1 s
 Max: 5.0012
 Min: 2.5313
 5/23/2023 1:26 PM

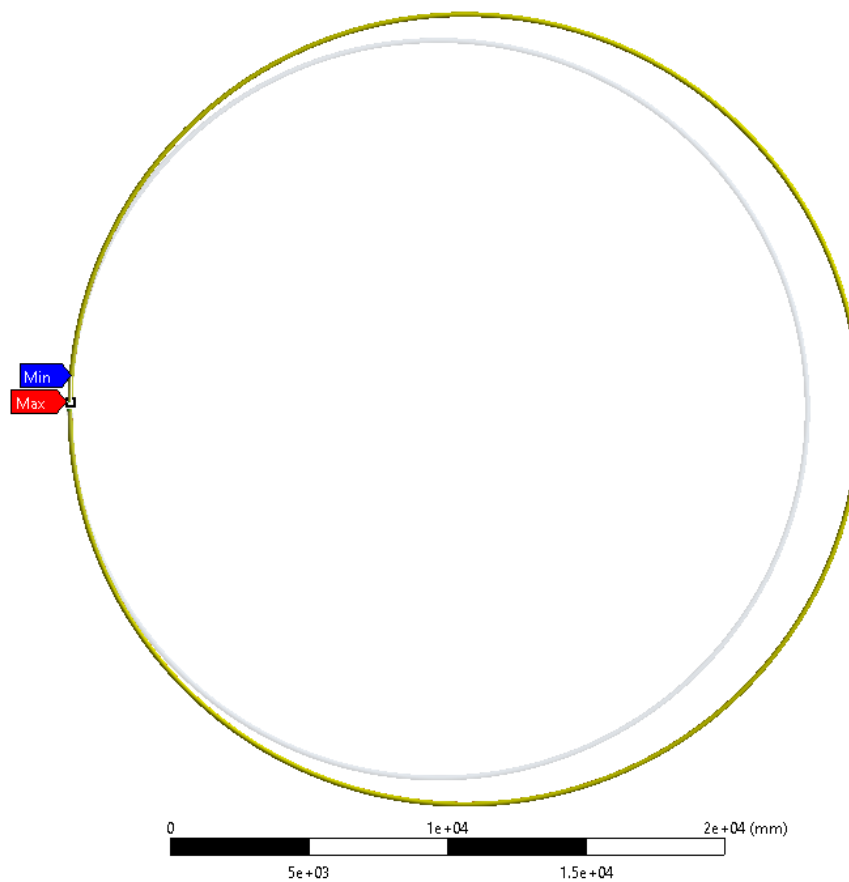
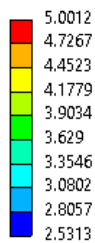


Fig. B-8: Results FEM simulation – equivalent stress

The results are summarized in Table B-3.

Table B-3: Results cable expansion by vertical acceleration

Description	Abbreviation	Value	Unit
FEM simulation result	U_x	23.4	mm
Analytical results	$U_x \approx 2\Delta R$	23.5	mm

Table B-3 shows that the results by the calculation and the FEM simulation are approximately the same. It thus can be concluded that the resistance of the cable stack expansion due to vertical acceleration comes from the axial stiffness of the cables. Fig. B-8 confirms that in the entire cable an equal tension occurs because every place in the cable has an equal equivalent stress.

B.3 Load due to horizontal acceleration

A single cable turn around a fixed wall will be considered, while an acceleration is applied as shown in Fig. B-9. This wall represents the inner frame of the carousel and possibly the part of the cable stack with a lower radius as the considered cable. The load due to the acceleration on the cable is denoted by F in the figure and the estimated reaction force from the rigid core on the cable is denoted by F_r in the figure.

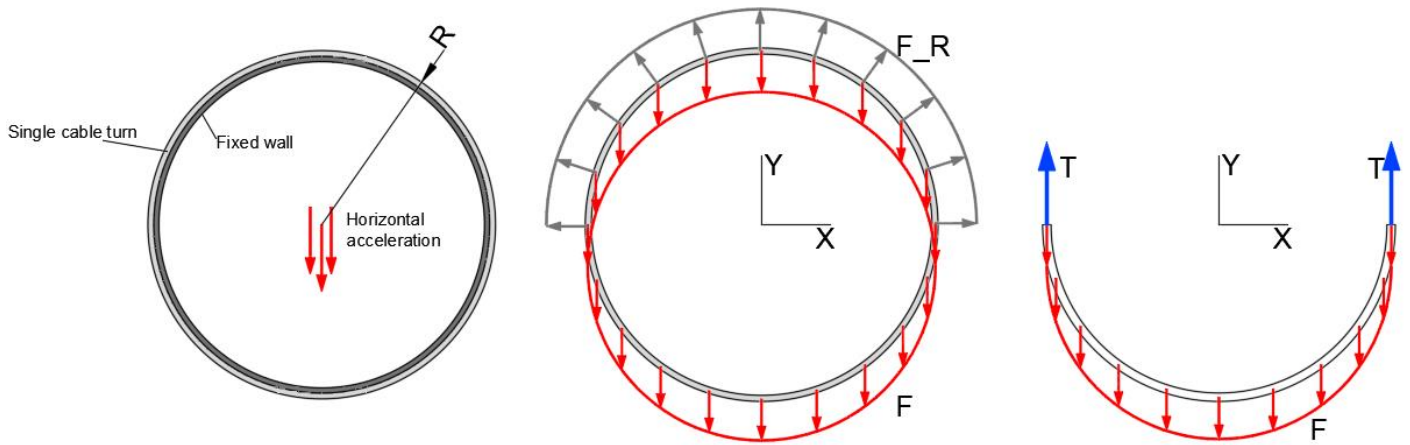


Fig. B-9: Horizontal acceleration on single cable turn

It is assumed that the entire cable is subjected to the identical tension T . Using the figure on the right in Fig. B-9s, it is determined from equilibrium in y direction that T can be calculated with

$$T = \frac{\pi R \mu_{cable} a}{2} \quad (B-9)$$

with acceleration a , cable mass per meter μ_{cable} and radius R . The elongation of the total cable due to the horizontal acceleration can be calculated with

$$\delta = \frac{TL}{E_{cable,axial} A_{cable}} = \frac{8RT}{E_{cable,axial} D_{cable}^2} = \frac{2RT}{E_{cable,axial} D_{cable}^2} \quad (B-10)$$

The horizontal displacement Δ of the cable under the horizontal acceleration is visualized in Fig. B-10.

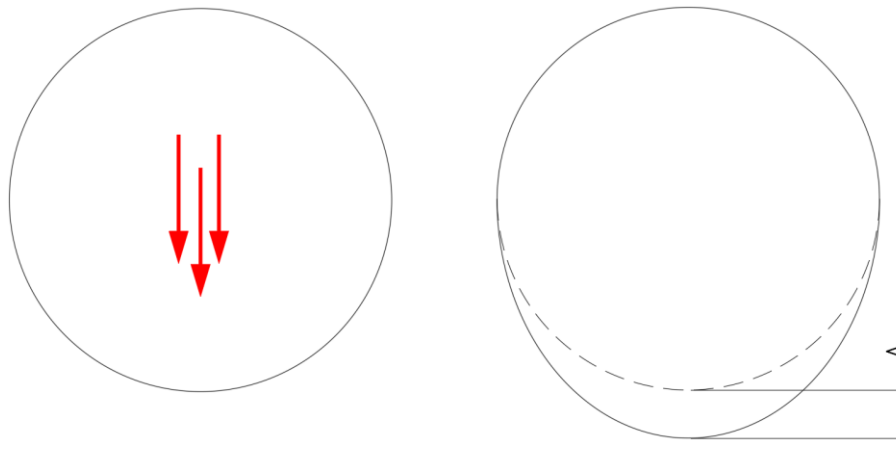


Fig. B-10: Horizontal displacement of cable under horizontal acceleration

The horizontal displacement Δ will be approximated by $\Delta = \delta/\pi$. The results for the input defined in Table B-1 and the most outside cable where $R = R_{carousel}$ are defined in Table B-4.

Table B-4: Results cable expansion due to horizontal acceleration

Description	Abbreviation	Value	Unit
Tension in entire cable	T	6978	N
Extension of cable	δ	4.11 (= 0.005%)	mm
Change of radius due to expansion of cable	ΔR	0.65 (= 0.005%)	mm
Maximum deformation	Δ	1.31	mm

FEM simulation verification

To verify the results, a FEM model has been elaborated as shown in Fig. B-11. The dimensions are as defined in Table B-1 and the most outside cable for which $R = R_{carousel}$ has been used. For the FEM model quadratic brick elements with reduced integration have been used, with a standard size of $100mm$. The rigid wall is modeled by plate elements, and it fixed.

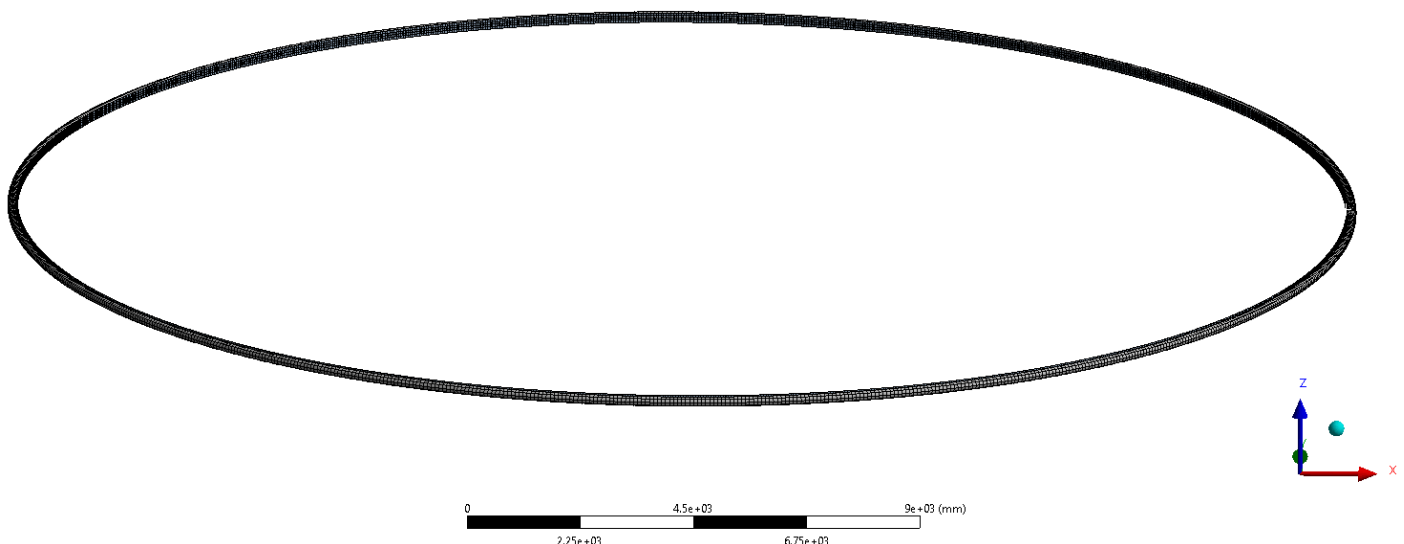


Fig. B-11: FEM model for verification

An acceleration of 5000 mm/s^2 has been applied on the model as can be seen Fig. B-12. Again, a slice has been implemented in the cable where both ends of the cable are fixed, as shown in Fig. B-13. Furthermore, the inner wall is fixed at all places. The contact between the cable and the inner wall is modelled to be frictionless.

B: Static Structural

Static Structural
Time: 1. s
5/23/2023 3:09 PM

- A Fixed Support 2
- B Acceleration: 5000. mm/s²
- C Fixed Support

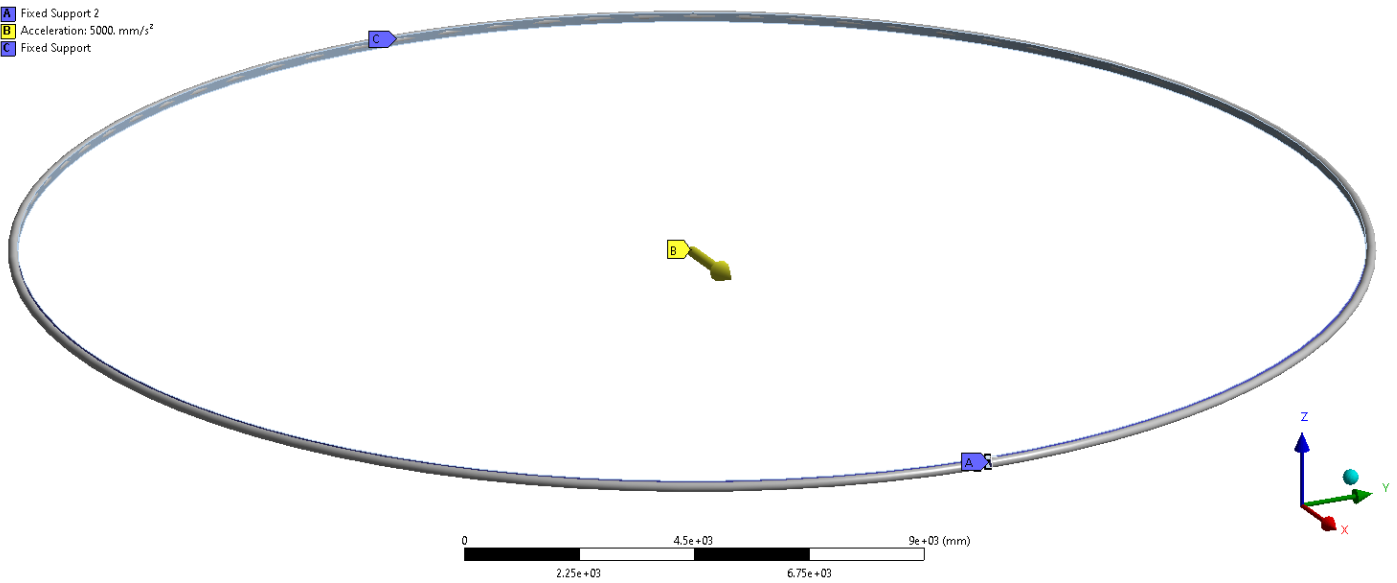


Fig. B-12: Acceleration and other boundary conditions in model

B: Static Structural

Static Structural
Time: 1. s
5/23/2023 3:09 PM

- A Fixed Support 2
- B Acceleration: 5000. mm/s²
- C Fixed Support

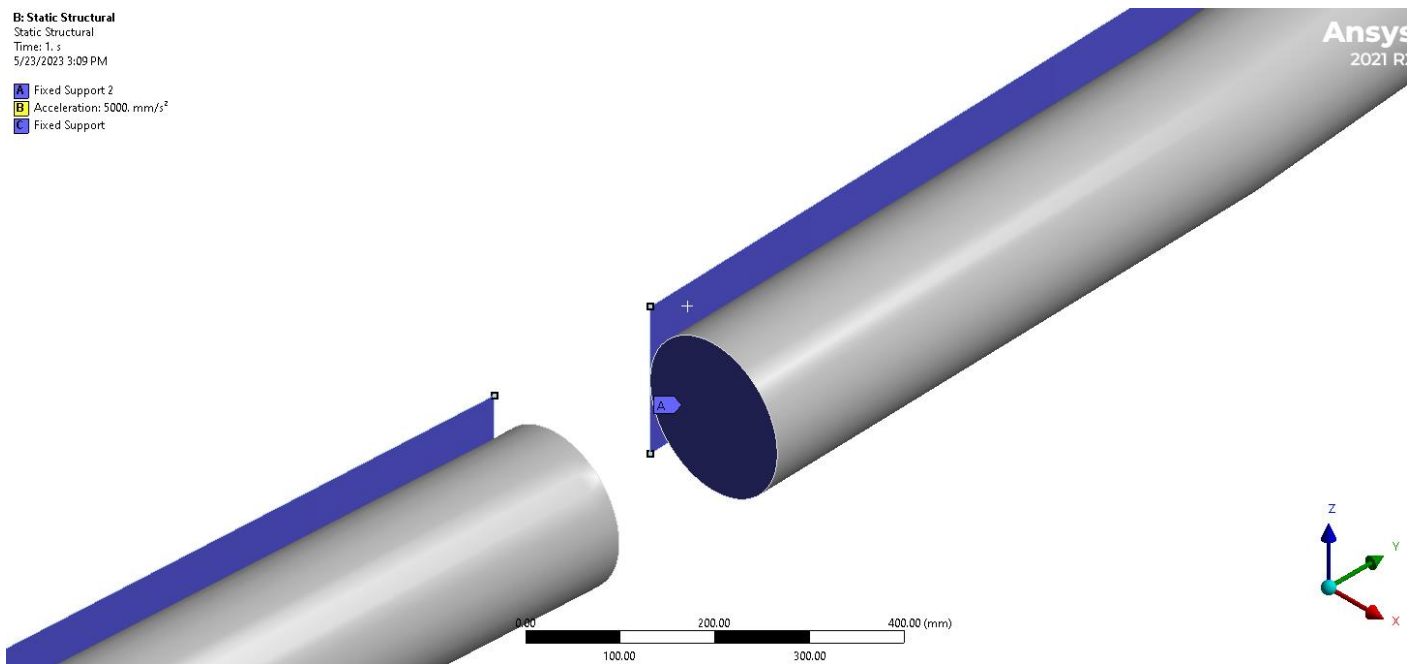


Fig. B-13: View of cable slice and fixed constraint of both cable ends

The Displacement in the x direction is shown in Fig. B-14 and the equivalent strain in the cable in Fig. B-15. The deformations in both plots are scaled.

B: Static Structural
 Directional Deformation
 Type: Directional Deformation(X Axis)
 Unit: mm
 Global Coordinate System
 Time: 1 s
 Max: 0.0017765
 Min: -8.2338
 5/23/2023 3:12 PM

0.0017765
 -0.91329
 -1.8284
 -2.7434
 -3.6585
 -4.5735
 -5.4886
 -6.4037
 -7.3187
 -8.2338

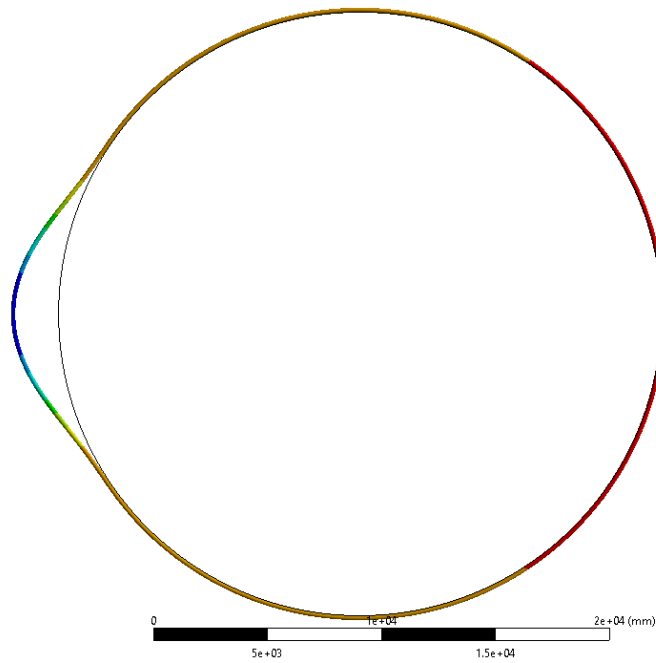


Fig. B-14: Horizontal displacement of cable under horizontal acceleration

B: Static Structural
 Equivalent Stress
 Type: Equivalent (von-Mises) Stress - Top/Bottom
 Unit: MPa
 Time: 1 s
 Max: 0.62382
 Min: 0
 5/23/2023 3:49 PM

0.62382
 0.55451
 0.4852
 0.41588
 0.34657
 0.27725
 0.20794
 0.13863
 0.069314
 0

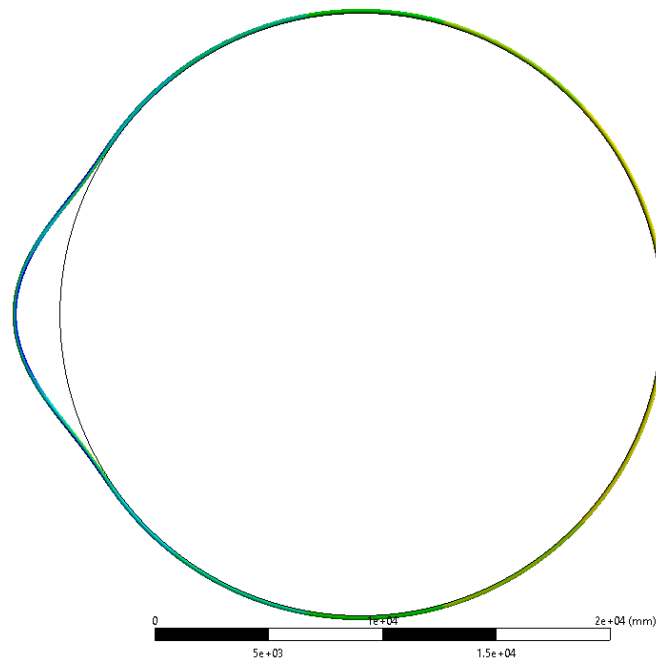


Fig. B-15: Equivalent stress in cable under horizontal acceleration

The results are summarized in Table B-3.

Table B-5: Results cable expansion by horizontal acceleration

Description	Abbreviation	Value	Unit
FEM simulation result	U_x	8.23 (= 0.06%)	mm
Analytical results	$U_x = \Delta$	1.31 (= 0.01%)	mm

Table B-3 shows that the relative error between the FEM simulation and the analytical calculation is large, but that the relative error compared to the radius of the cable turn is very low (0.06% and 0.01%). One cause of the higher results for the FEM simulation is that it has a sharper peak in its deformation pattern, where the assumed deformation pattern is more circular which gives a much lower peak deformation. Fig. B-15 shows that for this case there is no uniform stress in the cable.

B.4 Radial deformation of cables

The self-weight of the cables induces a load in the cables below, as shown in Fig. B-16.

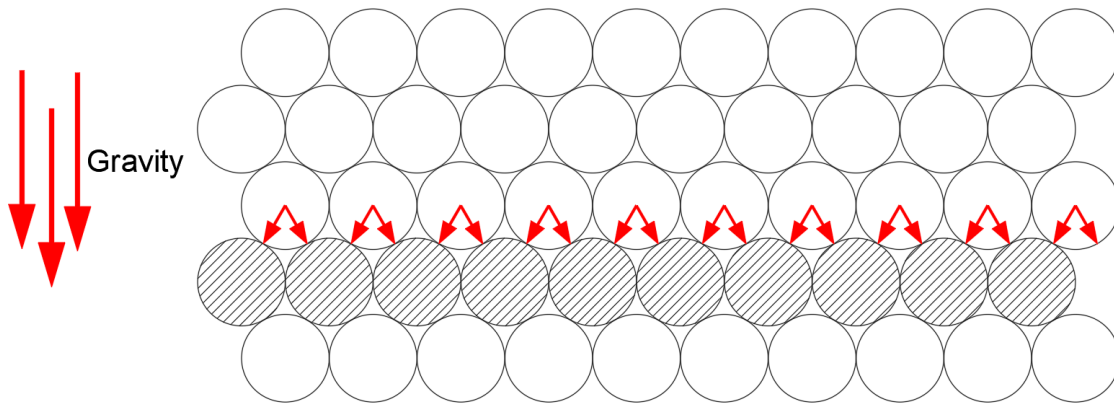


Fig. B-16: Load on cables due to self-weight cable stack

This load causes radial compression of the cable in the vertical direction and thus radial expansion of the cable in the horizontal direction. This is visualized in Fig. B-17, where the horizontal expansion of the single cable is denoted by Δw .

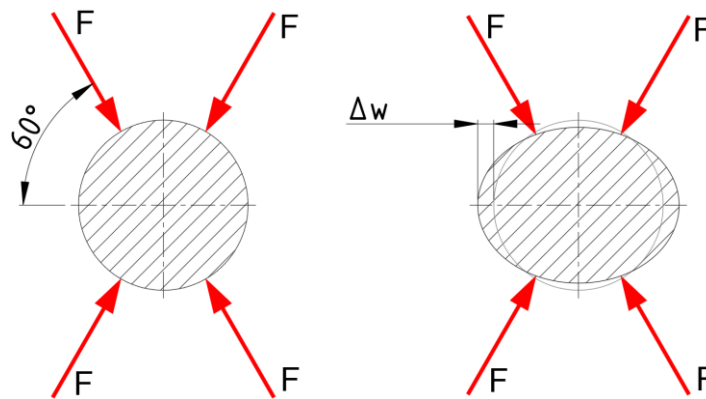


Fig. B-17: radial deformation of cable

The total load on the entire bottom row is assumed to be the entire capacity, defined as $C = 5000t$ from Table B-1, which is a load of $F_{total} = 49050kN$ under gravity of $9.81m/s^2$. The total area of the bottom row (carousel footprint) is given by

$$A_{footprint} = \pi(R_{carousel}^2 - r_{carousel}^2) \quad (B-11)$$

It is assumed that the bottom layer of the cable stack is a homogenous cylinder with the carousel footprint dimensions with the height h_{layer} equal to D_{cable} . It is assumed that the change of the height of the layer can be estimated by

$$\Delta h_{layer} = -\frac{F_{total} h_{layer}}{E_{cable,radial} A_{footprint}} \quad (B-12)$$

With this height change of the entire layer, the horizontal expansion of a single cable Δw is estimated by $\Delta w = \Delta h_{layer}/2$. The results by using the input from Table B-1 are shown in Table B-6.

Table B-6: Results radial deformation of cables

Description	Abbreviation	Value	Unit
Area bottom layer	$A_{footprint}$	496	m
Bottom layer height	h_{layer}	0.19	m
Estimated Height change of bottom layer under self-weight cable stack	Δh_{layer}	0.02	mm
Estimated expansion of single cable under self-weight cable stack	Δw	0.01	mm

C SPMT deflection study 2D

This study considers the situation in the Fig. C-1

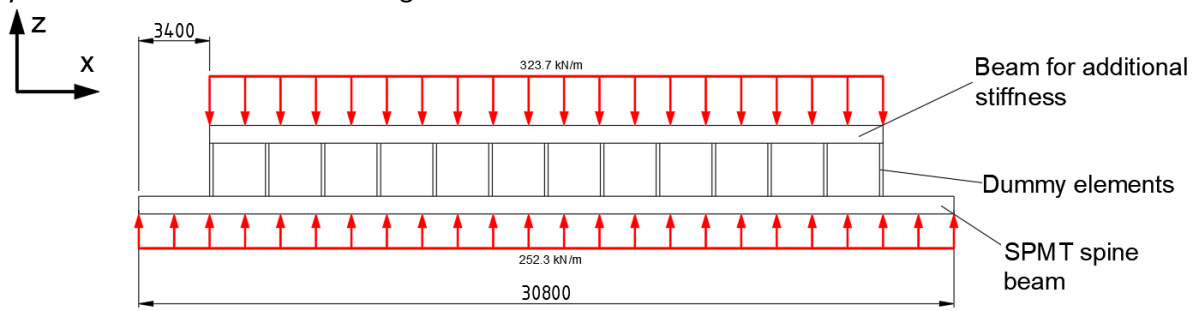


Fig. C-1: Overview SPMT deflection study in 2D

C.1 Model description

C.1.1 Overview

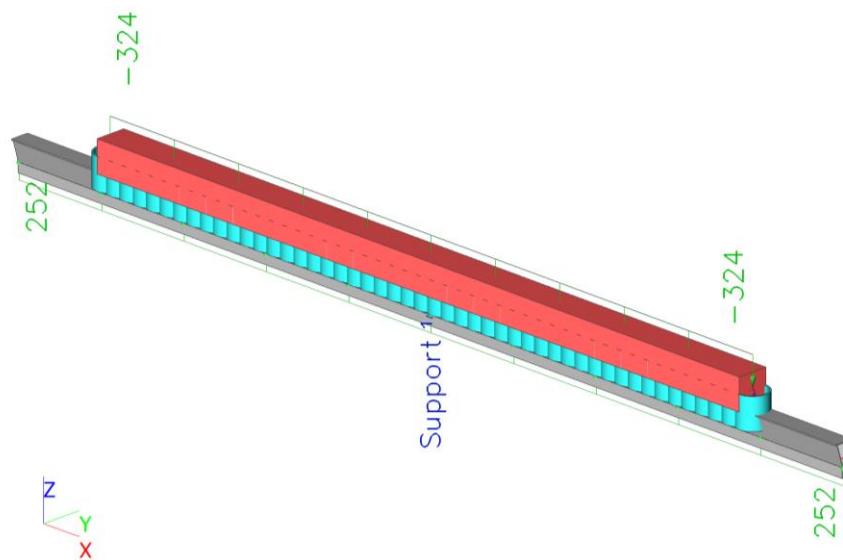

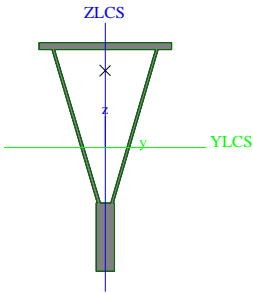

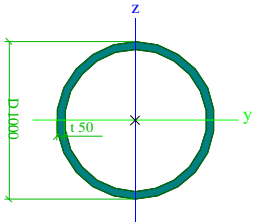



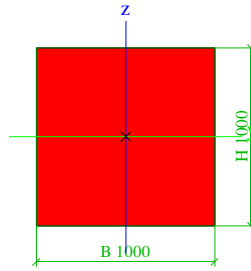
Fig. C-2: Structural model overview

C.1.2 Cross-sections

SPMT Spine beam			
Type	General cross-section		
Shape type	Thick-walled		
Item material	S 690		
Fabrication	general		
Colour			
Flexural buckling y-y, Flexural buckling z-z	d	d	
A [mm ²]	6.285e+04		
A _y [mm ²], A _z [mm ²]	5.974e+04		2.689e+04
A _L [m ² /m], A _D [m ² /m]	2.9398e+00		4.8904e+00
C _{y,UCS} [mm], C _{z,UCS} [mm]	-1		45
I _{y,LCS} [mm ⁴], I _{z,LCS} [mm ⁴]	9.362e+09		9.673e+08
I _{yz,LCS} [mm ⁴]	1.088e+07		
α [deg]	-0.07		
I _y [mm ⁴], I _z [mm ⁴]	9.362e+09		9.673e+08
i _y [mm], i _z [mm]	386		124
W _{el,y} [mm ³], W _{el,z} [mm ³]	1.664e+07		3.221e+06
W _{pl,y} [mm ³], W _{pl,z} [mm ³]	2.256e+07		5.784e+06
M _{pl,y,+} [Nmm], M _{pl,y,-} [Nmm]	1.40e+10		1.40e+10
M _{pl,z,+} [Nmm], M _{pl,z,-} [Nmm]	3.60e+09		3.60e+09
d _y [mm], d _z [mm]	-1		347
I _t [mm ⁴], I _w [mm ⁶]	1.071e+09		9.840e+12
β _y [mm], β _z [mm]	-649		4

Picture		
DUMMY		
Type	Tube	
Detailed	1000; 50	
Shape type	Thick-walled	
Item material	DUMMY	
Fabrication	general	
Colour		
Flexural buckling y-y, Flexural buckling z-z	d	d
A [mm²]	1.492e+05	
A _y [mm²], A _z [mm²]	9.983e+04	9.983e+04
A _L [m²/m], A _D [m²/m]	3.1414e+00	5.9687e+00
c _{y,UCS} [mm], c _{z,UCS} [mm]	500	500
α [deg]	0.00	
I _y [mm⁴], I _z [mm⁴]	1.688e+10	1.688e+10
i _y [mm], i _z [mm]	336	336
W _{el,y} [mm³], W _{el,z} [mm³]	3.376e+07	3.376e+07
W _{pl,y} [mm³], W _{pl,z} [mm³]	4.517e+07	4.517e+07
M _{pl,y,+} [Nmm], M _{pl,y,-} [Nmm]	1.60e+10	1.60e+10
M _{pl,z,+} [Nmm], M _{pl,z,-} [Nmm]	1.60e+10	1.60e+10
d _y [mm], d _z [mm]	0	0
I _t [mm⁴], I _w [mm⁶]	3.322e+10	1.097e+00
β _y [mm], β _z [mm]	0	0
Picture		
Beam for additional stiffness		
Type	Rectangle	
Detailed	1000; 1000	
Shape type	Thick-walled	
Item material	Added stiffness	
Fabrication	general	
Colour		
Flexural buckling y-y, Flexural buckling z-z	d	d
A [mm²]	1.000e+06	
A _y [mm²], A _z [mm²]	8.343e+05	8.343e+05
A _L [m²/m], A _D [m²/m]	4.0000e+00	4.0000e+00
c _{y,UCS} [mm], c _{z,UCS} [mm]	500	500
α [deg]	0.00	
I _y [mm⁴], I _z [mm⁴]	8.333e+10	8.333e+10
i _y [mm], i _z [mm]	289	289
W _{el,y} [mm³], W _{el,z} [mm³]	1.667e+08	1.667e+08
W _{pl,y} [mm³], W _{pl,z} [mm³]	2.500e+08	2.500e+08
M _{pl,y,+} [Nmm], M _{pl,y,-} [Nmm]	8.88e+10	8.88e+10
M _{pl,z,+} [Nmm], M _{pl,z,-} [Nmm]	8.88e+10	8.88e+10
d _y [mm], d _z [mm]	0	0
I _t [mm⁴], I _w [mm⁶]	1.404e+11	1.250e+14
β _y [mm], β _z [mm]	0	0

Picture



Explanations of symbols

A	Area
A_y	Shear Area in principal y-direction - Calculated by 2D FEM analysis
A_z	Shear Area in principal z-direction - Calculated by 2D FEM analysis
A_L	Circumference per unit length
A_D	Drying surface per unit length
$C_{Y,UCS}$	Centroid coordinate in Y-direction of Input axis system
$C_{Z,UCS}$	Centroid coordinate in Z-direction of Input axis system
$I_{Y,LCS}$	Second moment of area about the YLCS axis
$I_{Z,LCS}$	Second moment of area about the ZLCS axis
$I_{YZ,LCS}$	Product moment of area in the LCS system
α	Rotation angle of the principal axis system
I_y	Second moment of area about the principal y-axis
I_z	Second moment of area about the principal z-axis
i_y	Radius of gyration about the principal y-axis
i_z	Radius of gyration about the principal z-axis
$W_{el,y}$	Elastic section modulus about the principal y-axis
$W_{el,z}$	Elastic section modulus about the principal z-axis
$W_{pl,y}$	Plastic section modulus about the principal y-axis
$W_{pl,z}$	Plastic section modulus about the principal z-axis
$M_{pl,y,+}$	Plastic moment about the principal y-axis for a positive M_y moment
$M_{pl,y,-}$	Plastic moment about the principal y-axis for a negative M_y moment
$M_{pl,z,+}$	Plastic moment about the principal z-axis for a positive M_z moment
$M_{pl,z,-}$	Plastic moment about the principal z-axis for a negative M_z moment
d_y	Shear center coordinate in principal y-direction measured from the centroid - Calculated by 2D FEM analysis
d_z	Shear center coordinate in principal z-direction measured from the centroid - Calculated by 2D FEM analysis
I_t	Torsional constant - Calculated by 2D FEM analysis
I_w	Warping constant - Calculated by 2D FEM analysis
β_y	Mono-symmetry constant about the principal y-axis
β_z	Mono-symmetry constant about the principal z-axis

C.1.3 Materials

Name	E_{mod} [MPa]
S 690	2.1000e+05
Added stiffness	Variable
DUMMY	1.0000e+07

For the beam with the material 'Added stiffness' a variable E -modulus is used to simulate the effect of the additional stiffness from the carousel and the cable stack.

C.1.4 Analysis model

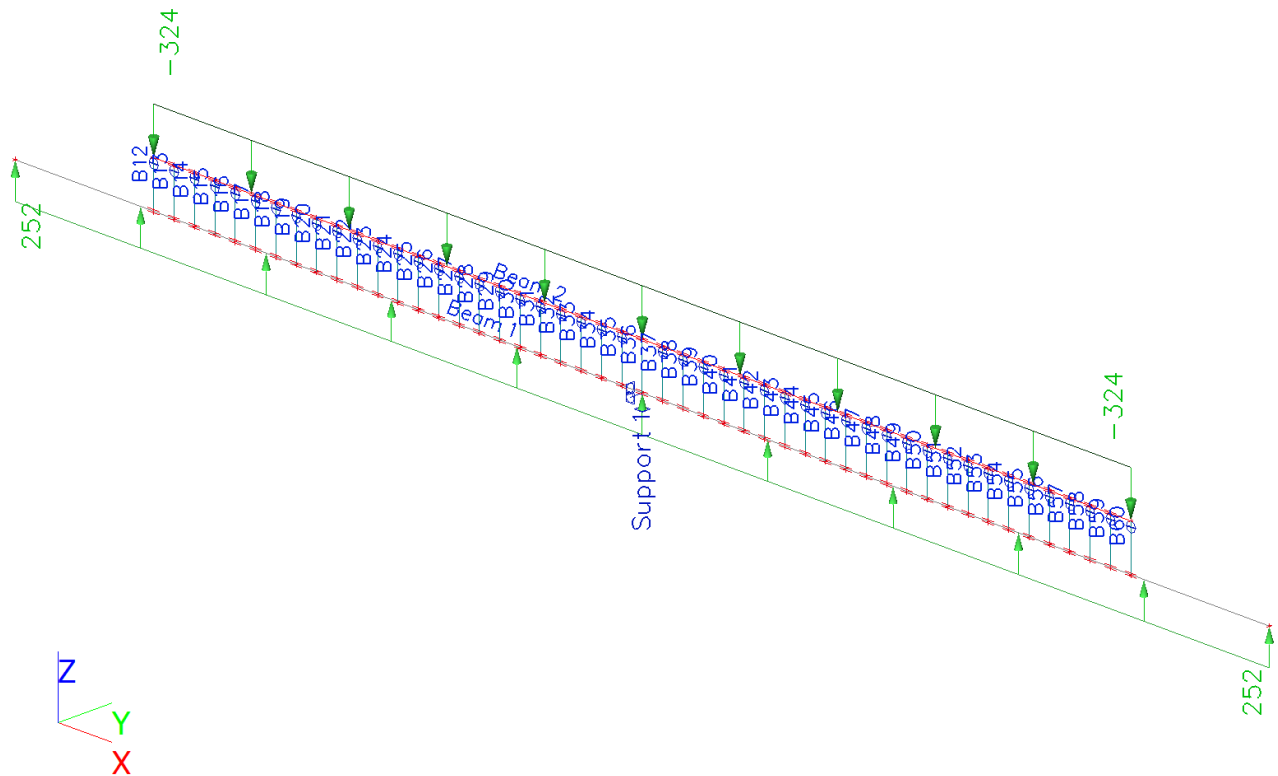


Fig. C-3: Analysis FEM model

C.1.5 Hinges

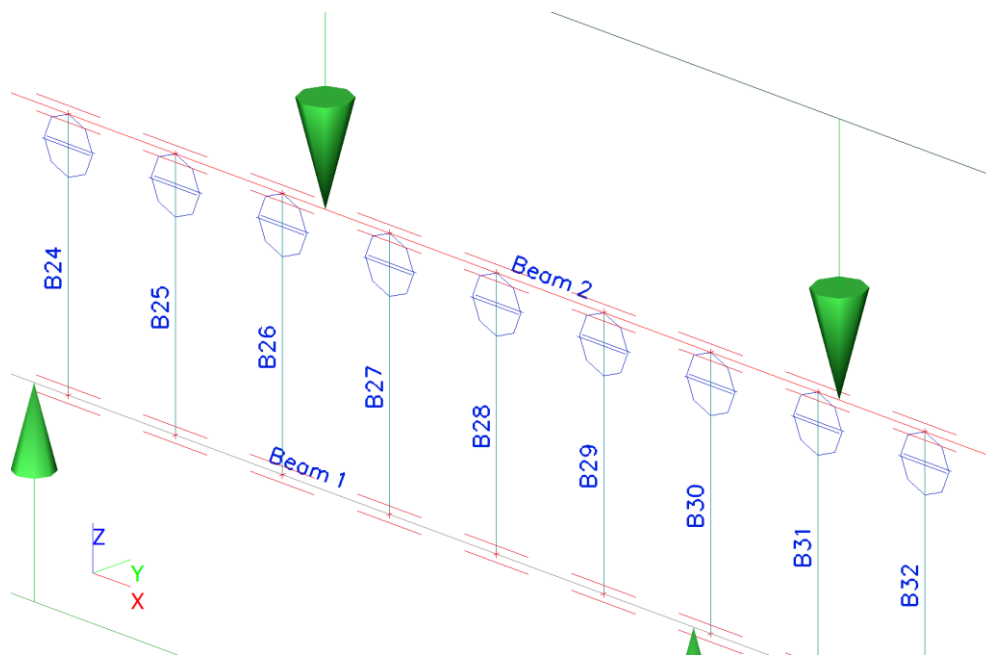


Fig. C-4: Hinges in analysis model

Name	Member	Position	ux	uy	uz	fix	fiy	fiz
H1	B12	End	Rigid	Rigid	Free	Rigid	Free	Rigid
H2	B13	End	Rigid	Rigid	Free	Rigid	Free	Rigid
H3	B14	End	Rigid	Rigid	Free	Rigid	Free	Rigid
H4	B15	End	Rigid	Rigid	Free	Rigid	Free	Rigid
H5	B16	End	Rigid	Rigid	Free	Rigid	Free	Rigid
H6	B17	End	Rigid	Rigid	Free	Rigid	Free	Rigid
H7	B18	End	Rigid	Rigid	Free	Rigid	Free	Rigid
H8	B19	End	Rigid	Rigid	Free	Rigid	Free	Rigid
H9	B20	End	Rigid	Rigid	Free	Rigid	Free	Rigid
H10	B21	End	Rigid	Rigid	Free	Rigid	Free	Rigid
H11	B22	End	Rigid	Rigid	Free	Rigid	Free	Rigid
H12	B23	End	Rigid	Rigid	Free	Rigid	Free	Rigid
H13	B24	End	Rigid	Rigid	Free	Rigid	Free	Rigid
H14	B25	End	Rigid	Rigid	Free	Rigid	Free	Rigid
H15	B26	End	Rigid	Rigid	Free	Rigid	Free	Rigid
H16	B27	End	Rigid	Rigid	Free	Rigid	Free	Rigid
H17	B28	End	Rigid	Rigid	Free	Rigid	Free	Rigid
H18	B29	End	Rigid	Rigid	Free	Rigid	Free	Rigid
H19	B30	End	Rigid	Rigid	Free	Rigid	Free	Rigid
H20	B31	End	Rigid	Rigid	Free	Rigid	Free	Rigid
H21	B32	End	Rigid	Rigid	Free	Rigid	Free	Rigid
H22	B33	End	Rigid	Rigid	Free	Rigid	Free	Rigid
H23	B34	End	Rigid	Rigid	Free	Rigid	Free	Rigid
H24	B35	End	Rigid	Rigid	Free	Rigid	Free	Rigid
H26	B37	End	Rigid	Rigid	Free	Rigid	Free	Rigid
H27	B38	End	Rigid	Rigid	Free	Rigid	Free	Rigid
H28	B39	End	Rigid	Rigid	Free	Rigid	Free	Rigid
H29	B40	End	Rigid	Rigid	Free	Rigid	Free	Rigid
H30	B41	End	Rigid	Rigid	Free	Rigid	Free	Rigid
H31	B42	End	Rigid	Rigid	Free	Rigid	Free	Rigid
H32	B43	End	Rigid	Rigid	Free	Rigid	Free	Rigid
H33	B44	End	Rigid	Rigid	Free	Rigid	Free	Rigid
H34	B45	End	Rigid	Rigid	Free	Rigid	Free	Rigid
H35	B46	End	Rigid	Rigid	Free	Rigid	Free	Rigid
H36	B47	End	Rigid	Rigid	Free	Rigid	Free	Rigid
H37	B48	End	Rigid	Rigid	Free	Rigid	Free	Rigid
H38	B49	End	Rigid	Rigid	Free	Rigid	Free	Rigid
H39	B50	End	Rigid	Rigid	Free	Rigid	Free	Rigid
H40	B51	End	Rigid	Rigid	Free	Rigid	Free	Rigid
H41	B52	End	Rigid	Rigid	Free	Rigid	Free	Rigid
H42	B53	End	Rigid	Rigid	Free	Rigid	Free	Rigid
H43	B54	End	Rigid	Rigid	Free	Rigid	Free	Rigid
H44	B55	End	Rigid	Rigid	Free	Rigid	Free	Rigid
H45	B56	End	Rigid	Rigid	Free	Rigid	Free	Rigid
H46	B57	End	Rigid	Rigid	Free	Rigid	Free	Rigid
H47	B58	End	Rigid	Rigid	Free	Rigid	Free	Rigid
H48	B59	End	Rigid	Rigid	Free	Rigid	Free	Rigid
H49	B60	End	Rigid	Rigid	Free	Rigid	Free	Rigid

C.1.6 Point support on member

Name	Type	Coor System	Pos x Orig	dx Rep (n)	X	Y	Z	Rx	Ry	Rz
Support 1	Standard	Rela GCS	0.500 From end	1	Rigid	Rigid	Rigid	Rigid	Rigid	Rigid

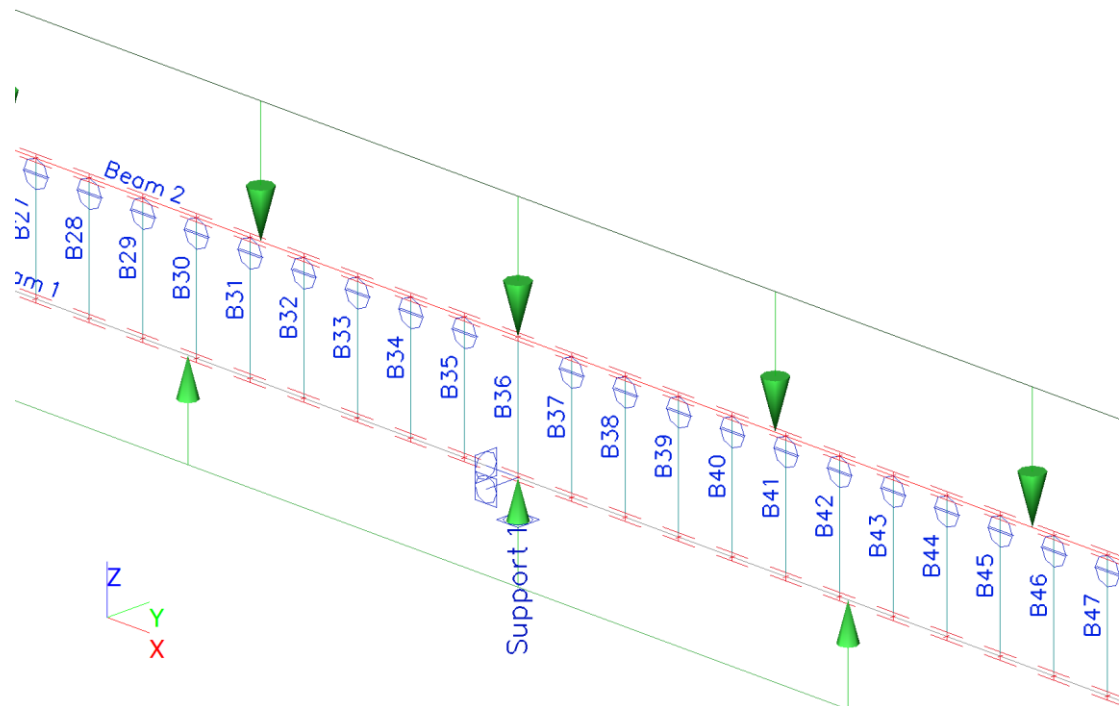


Fig. C-5: Support in analysis model

C.1.7 Loads

Name	Member	Type	Dir	Value - P ₁ [kN/m]	Pos x ₁ [mm]	Coor	Orig	Ecc ey [mm]
	Load case	System	Distribution	Value - P ₂ [kN/m]	Pos x ₂ [mm]	Loc		Ecc ez [mm]
Load 1	Beam 1	Force	Z	252	0.0	Abso	From start	0.0
	LC1	GCS	Uniform		30800.0	Length		0.0
Load 2	Beam 2	Force	Z	-324	0.000	Rela	From start	0.0
	LC1	GCS	Uniform		1.000	Length		0.0

C.2 Results of study

For some values of for the material E_{mod} 'added stiffness' the deformations are calculated. The results are summarized in the graph below.

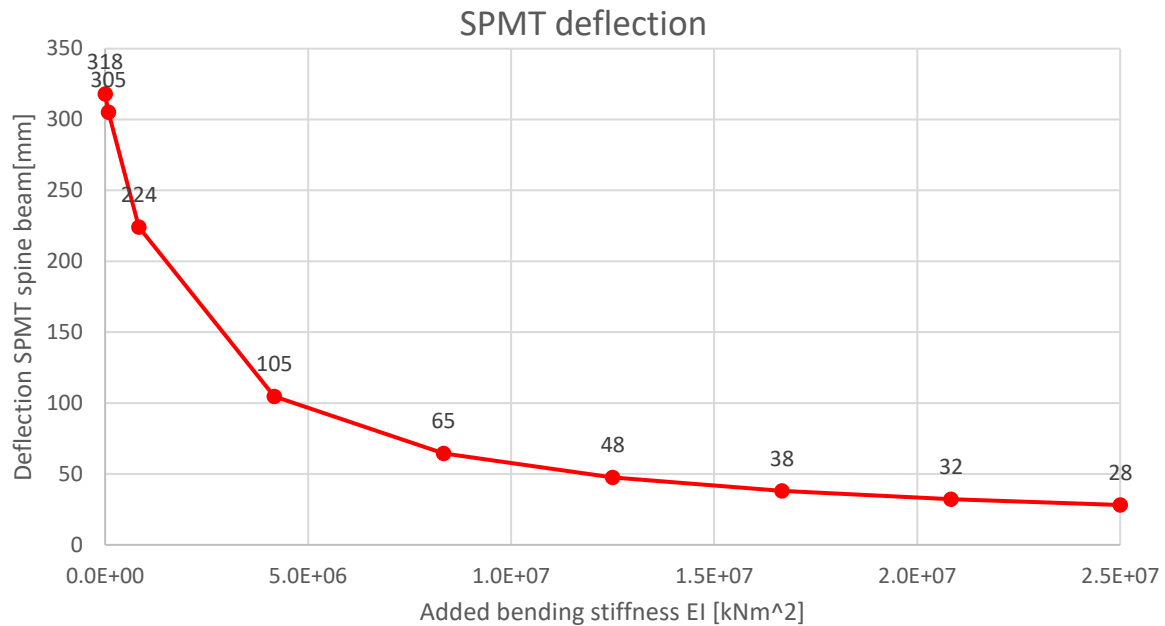


Fig. C-6: Deflection of SPMT spine beam for different stiffnesses of additional beam

Notice that for the added bending stiffness EI the elastic modulus E_{mod} is added to the second moment of area of the beam $I = 8.33 \cdot 10^{-2} \text{ mm}^4$.

C.2.1 Deformation plots

For some results the deformation plots are shown below. Note that all the figures show scaled deformations.

Added stiffness $E_{mod} = 0 \text{ GPa} \rightarrow$ added stiffness of 0 kNm^2

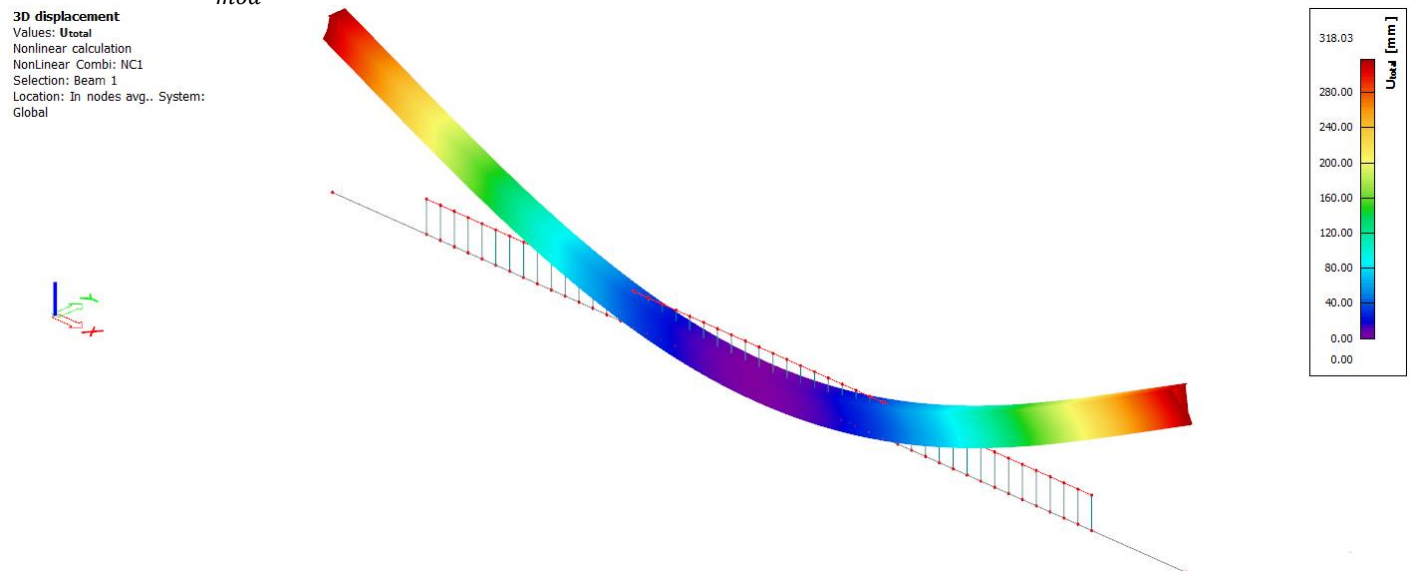


Fig. C-7: Deformation plot for $E_{mod} = 0 \text{ GPa}$

Added stiffness $E_{mod} = 10 \text{ GPa} \rightarrow$ added stiffness of $8.33 \cdot 10^5 \text{ kNm}^2$

3D displacement
Values: U_{total}
Nonlinear calculation
NonLinear Combi: NC1
Selection: All
Location: In nodes avg.. System:
Global

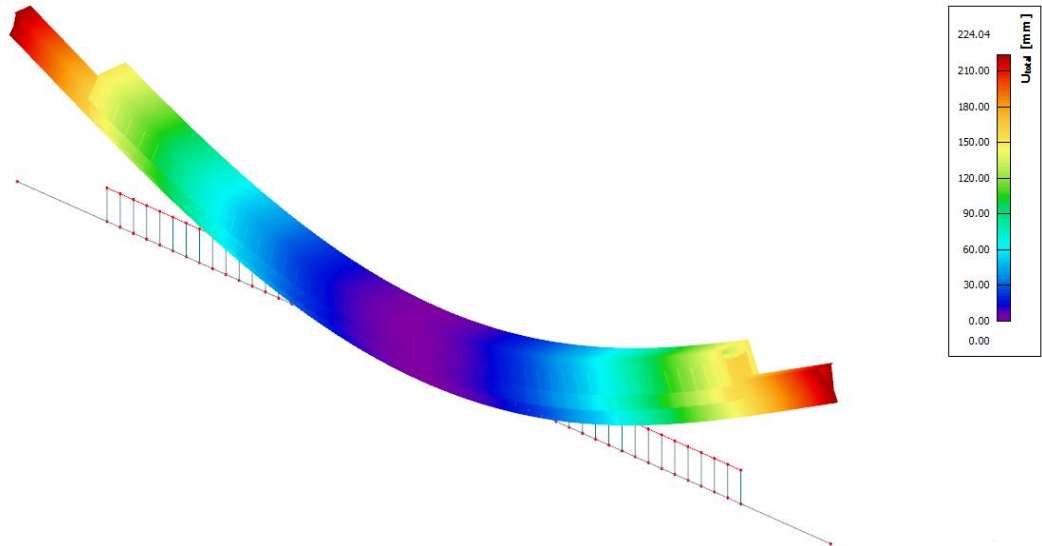


Fig. C-8: Deformation plot for $E_{mod} = 10 \text{ GPa}$

Added stiffness $E_{mod} = 100 \text{ GPa} \rightarrow$ added stiffness of $8.33 \cdot 10^6 \text{ kNm}^2$

3D displacement
Values: U_{total}
Nonlinear calculation
NonLinear Combi: NC1
Selection: All
Location: In nodes avg.. System:
Global

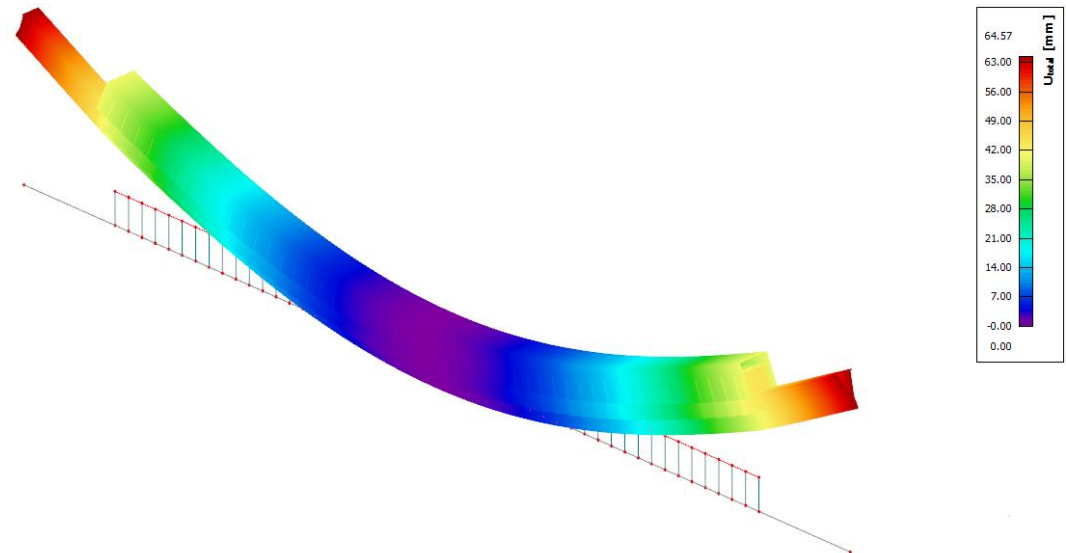


Fig. C-9: Deformation plot for $E_{mod} = 100 \text{ GPa}$

Added stiffness $E_{mod} = \infty$ (only spine beam deflection shown)

3D displacement
Values: U_{total}
Nonlinear calculation
NonLinear Combi: NC1
Selection: Beam 1
Location: In nodes avg.. System:
Global

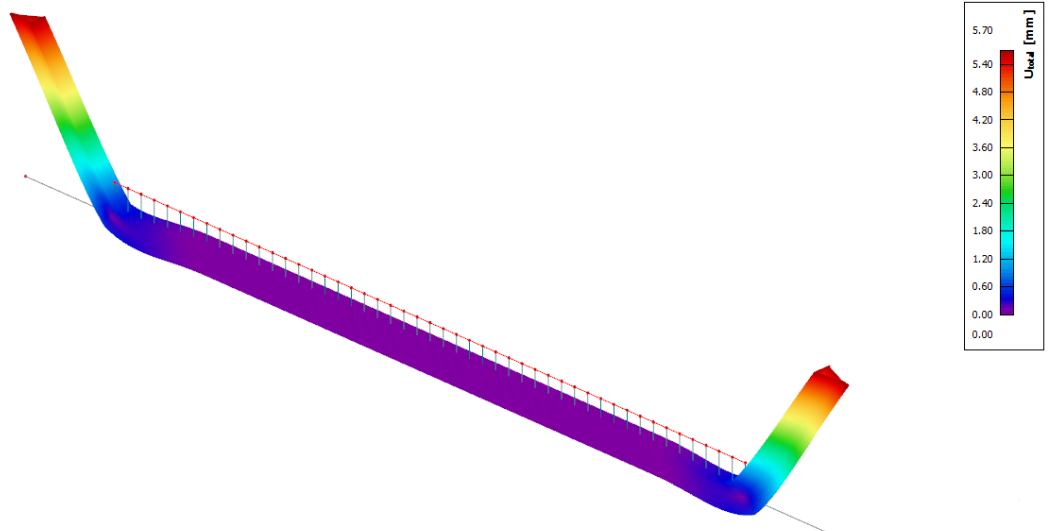


Fig. C-10: Deformation plot for $E_{mod} = \infty$

C.2.2 Stress plots

For some results equivalent Von Misses stresses in the spine beam are shown below

Added

3D stress
 Values: σ_E
 Nonlinear calculation
 Class: ULS
 Selection: Beam 1
 Location: In nodes avg. on macro.
 System: LCS mesh element
 Principal magnitudes

stiffness

$E_{mod} = 0 \text{ GPa}$

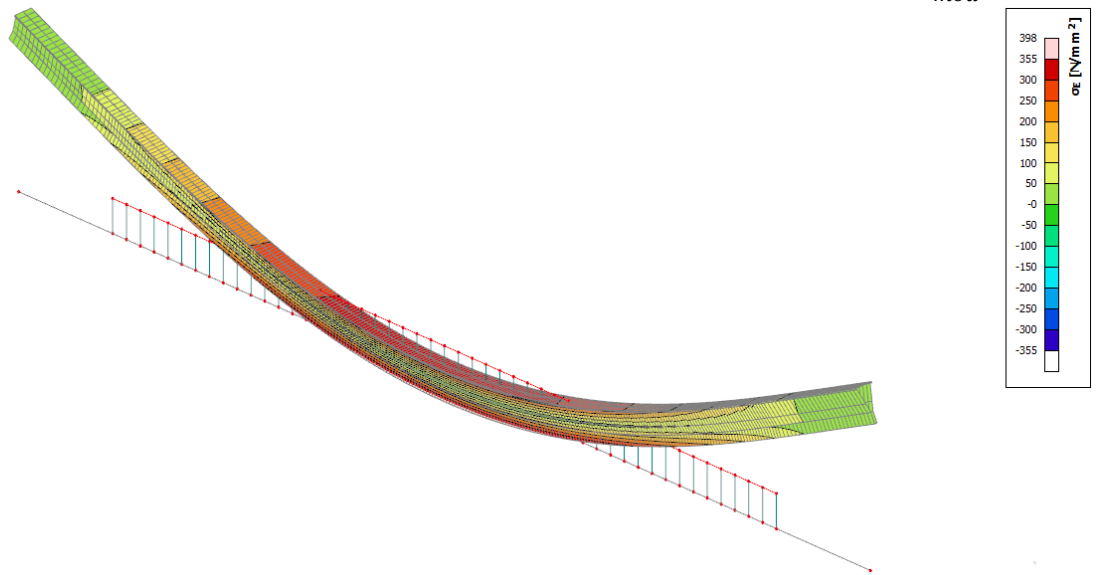


Fig. C-11: Equivalent von misses stress plot for $E_{mod} = 0 \text{ GPa}$

Added stiffness $E_{mod} = 10 \text{ GPa}$

3D stress
 Values: σ_E
 Nonlinear calculation
 Class: ULS
 Selection: Beam 1
 Location: In nodes avg. on macro.
 System: LCS mesh element
 Principal magnitudes

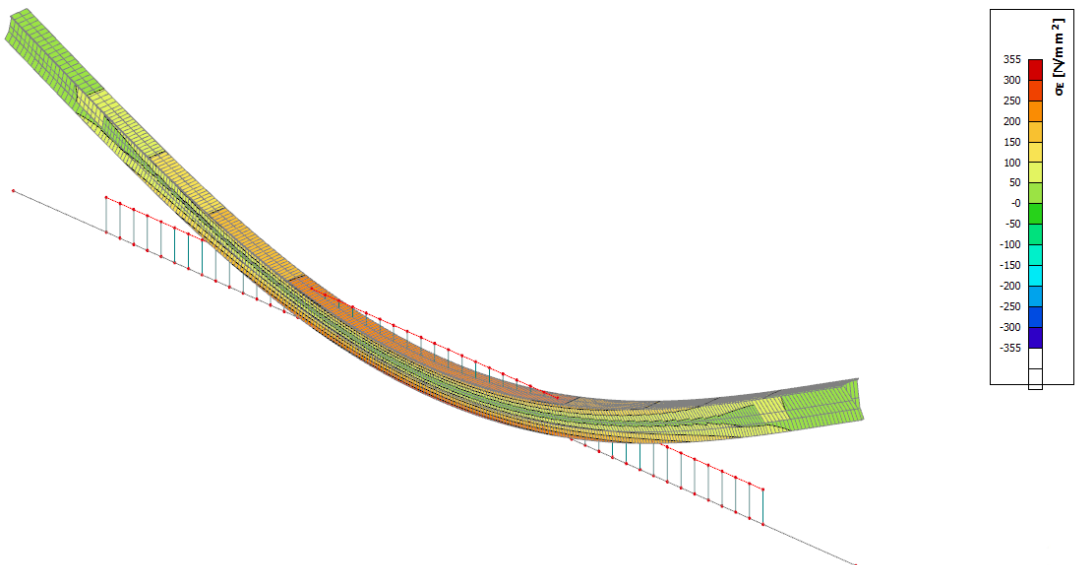
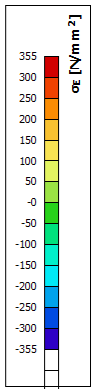
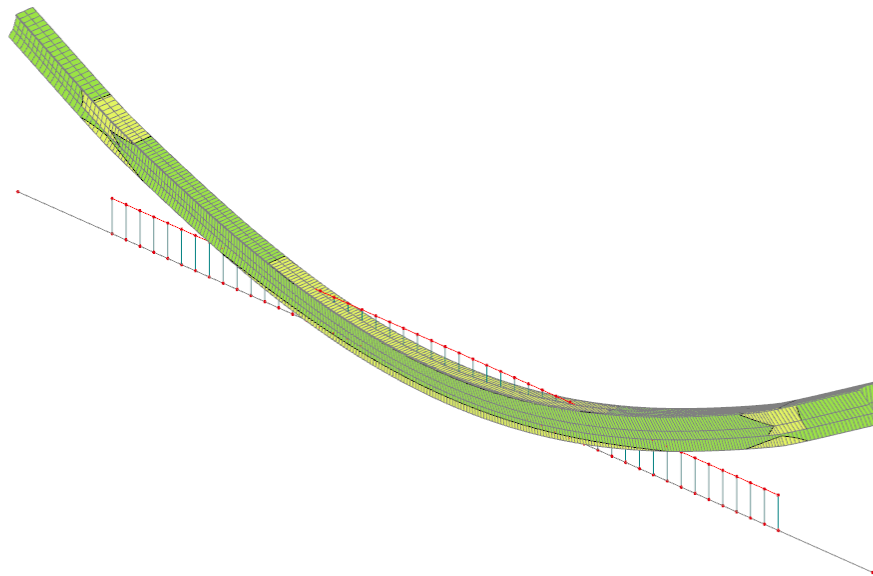


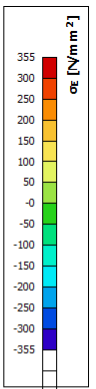
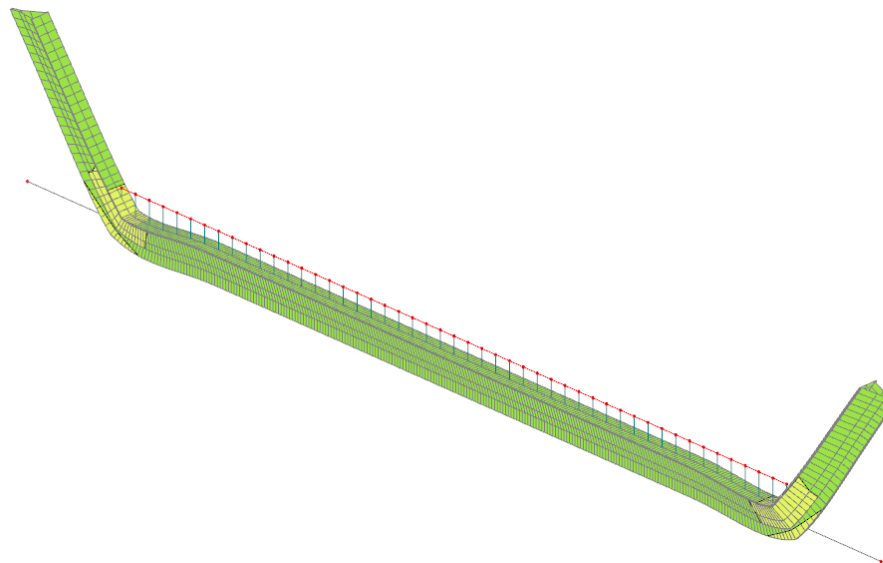
Fig. C-12: Equivalent von misses stress plot for $E_{mod} = 10 \text{ GPa}$

Added stiffness $E_{mod} = 100 \text{ GPa}$

3D stress
Values: σ_E
Nonlinear calculation
Class: ULS
Selection: Beam 1
Location: In nodes avg. on macro.
System: LCS mesh element
Principal magnitudes

Fig. C-13: Equivalent von mises stress plot for $E_{mod} = 100 \text{ GPa}$ Added stiffness $E_{mod} = \infty$

3D stress
Values: σ_E
Nonlinear calculation
Class: ULS
Selection: Beam 1
Location: In nodes avg. on macro.
System: LCS mesh element
Principal magnitudes

Fig. C-14: Equivalent von mises stress plot for $E_{mod} = \infty$

D Cable stack mass and dimensions

The following dimensions are defined to calculate the mass of the entire cable stack

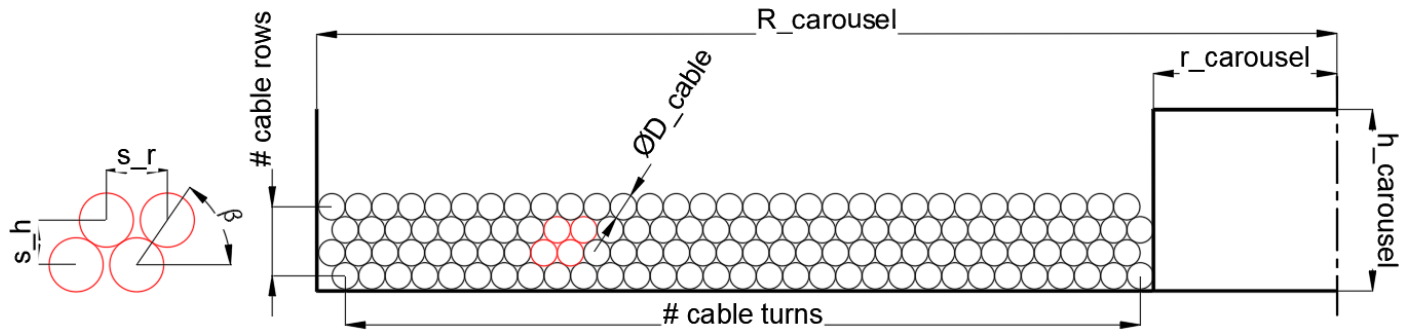


Fig. D-1: Triangular distributed load outer carousel frame and forces on one cable

The number of cable turns for each row can be calculated by

$$\# \text{ cable turns} = \text{rounddown} \left(\frac{R_{\text{carousel}} - r_{\text{carousel}} - 0.5 D_{\text{cable}}}{D_{\text{cable}}} \right) \quad (D-1)$$

It is assumed that the remaining space between the cables on a single row is equally distributed over the space between each turn s_r

$$s_r = \frac{R_{\text{carousel}} - r_{\text{carousel}} - D_{\text{cable}} \cdot (\# \text{ cable turns} + 0.5)}{\# \text{ cable turns} - 0.5} + D_{\text{cable}} \quad (D-2)$$

The height between each row s_h can now be calculated by

$$s_h = \sqrt{D_{\text{cable}}^2 - (s_r/2)^2} \quad (D-3)$$

The number of rows that fit in the height h_{carousel} is given by

$$\# \text{ cable rows} = \text{rounddown} \left(\frac{h_{\text{carousel}} - D_{\text{cable}}}{s_h} \right) + 1 \quad (D-4)$$

For the total number of cable cross sections in the cross section of the carousel we can multiply the number of cables turns per row by the number of rows. The average circumference of a single cable turn is approximated by

$$L_{\text{ct,avg}} = \pi \cdot (r_{\text{carousel}} + R_{\text{carousel}}) \quad (D-5)$$

With formula (2-1) from chapter 2.1.2 it follows that the cable mass μ_{cable} is related to the cable diameter D_{cable} by

$$\mu_{\text{cable}} = 1.18 \cdot 10^{-3} D_{\text{cable}}^2 + 1.28 \cdot 10^{-1} D_{\text{cable}} \quad (D-6)$$

Finally, the mass of the entire cable stack is given by

$$m_{\text{stack}} = \mu_{\text{cable}} \cdot \# \text{ cable turns} \cdot \# \text{ cable rows} \cdot L_{\text{ct,avg}} \quad (D-7)$$

E Comparison CCS and current method

For the comparison between the current method and the CCS, two topics are considered, namely time and costs.

Time

The effective time needed for the cable transportation with the CCS and the current method are compared to each other in Table E-7. The effective time is the time for the transport of the cable where mobilization and preparation of all other equipment, vessels and others is not included.

Table E-7: Overview duration of operations during cable transport

Operation	CCS	Current method	Description
Cable transfer	+/-	--	CCS is significant less because 2 transfers are needed instead of 4
Carousel transfer	+	/	Only applicable to CCS
Storage on transshipment hub	+	+	Expected to be comparable
Storage on manufacturer quay	+	+	Expected to be comparable
Sea transport	-	--	Expected to be better for the CCS as a more efficient location for the transshipment hub can be used

In Table E-7 the time duration is defined as, very time consuming = "--", time consuming = "-", medium time consuming = "+/-", not very time consuming = "+", negligible time compared to other operation = "++" or not applicable = "/". The operations which must be fulfilled for both transportation methods and the results in Table E-7 are described below:

- *Cable transfer*: For the cable transfer the entire cable capacity must be spooled from one carousel to another carousel. As the CCS has the same spool rate as the conventional carousels, there is no difference in time between the effective spooling time with a conventional carousel or the CCS. However, the CCS is expected to need more preparation time as the SPMTs need to be mobilized and lift the carousel, while a conventional carousel is already fixed on a drive system. A large part of the total effective time for the cable transport is due to the cable transfers. The main benefit of the CCS is that only two cable transfers are needed and thus the total effective transport time due to cable transfers is significantly reduced.
- *Carousel transfer*: A carousel transfer is only applicable to the CCS. The effective time of the carousel transfer from quay to vessel or vessel to quay is mainly dependent on the vessel stability. The effective time of the carousel transfer, including lifting the carousel and setting the carousel down, is estimated to be less than 1 day. This is significantly shorter than a cable transfer. For the carousel transfer preparation, mobilization, and demobilization of SPMTs and equipment is needed but this is not included in the effective time.
- *Storage*:
 - o *Transshipment hub*: At the transshipment hub the cable waits to be picked up by the cable installation vessel. The storage on the transshipment hub is different for every cable transportation project and dependent on multiple parameters. For the transportation method with the CCS there are more possibilities for a transshipment hub as only a quay is needed and not a location with a carousel. This allows more efficient locations to be used and can result in a lower waiting time of the cable on the transshipment hub.
 - o *Manufacturer quay*: At the manufacturer quay the cable waits to be picked up by the transportation vessel. It is expected that the waiting time for both the CCS and the current transportation method is comparable. For the CCS it is however possible to transport the carousel to another part of the manufacturer quay where longer storage is possible. For the current transportation method, it is desired that that cable has a short waiting time as it occupies a carousel on the manufacturer quay which is needed for the next project.

- *Sea transport:* The sea transport includes the time to transport the cable from the manufacturer quay to the transshipment hub. This is assumed to be the same for both the CCS and the current method of transport. It must be noticed that for the CCS more options are available for the transshipment hub and thus the route can be shorter than the route of the current transportation method.

Costs

The costs of the cable transportation with the CCS and the current method are compared to each other in Table E-8.

Table E-8: Overview equipment and quays costs comparison

Operation	CCS	Current method	Description
Manufacturer quay	+/-	-	CCS allows cheaper storage on the manufacturer quay
Transshipment hub	+/-	-	CCS allows cheaper storage on the transshipment hub
Transport vessel	+/-	-	CCS allows a cheaper transport vessel to be used
Cable installation vessel	--	--	Comparable
Carousel(s)	-	+/-	CCS is an expensive solution
SPMTs	-	/	SPMTs are expensive
Ro-Ro ramp	+	/	Only applicable to CCS
Other operational equipment	+	+	Expected to be comparable

In Table E-8, the costs are defined as, very high costs = "--", high costs = "-", medium costs = "+/-", low costs = "+", very low costs "++" or not applicable = "/". The needed equipment and quays for both transportation methods are described below:

- *Manufacturer quay:* CCS storage on the manufacturer quay is less expensive because it can be stored on any place where the ground is strong enough. For the current method a carousel must be hired on the manufacturer quay.
- *Transshipment hub:* CCS storage on the transshipment hub is less expensive because the CCS can be stored at any location where the ground is strong enough. For the current transportation methods, a location with a carousel must be found. The flexibility of the CCS storage also allows
- *Transport vessel:* For the CCS a less expensive vessel can be used as only a large and strong enough deck is needed. For the current transportation method, also a carousel on the vessel is needed.
- *Cable installation vessel:* For both transportation method the same cable installation vessel can be used.
- *Carousel(s):* The CCS is a more expensive carousel than used for the current transportation methods
- *SPMT:* For the CCS SPMTs are needed, which are also expensive.
- *Ro-Ro ramp:* For the CCS carousel transfer a Ro-Ro ramp is needed
- *Other operational equipment:* For both the CCS and the current transportation method addition equipment is needed such as cranes, tensioners, and cable guiding. The costs are expected to be comparable for both transportation methods.

F Cable analysis

In this appendix the selected cable from section 5.1 will be analyzed. A few layers are neglected because of their influence such that the new input is selected as in Table F-1, where the used materials are given in Table F-2.

Table F-1: Input for cable analysis

Layer	Component	Layer thickness	Outer diameter	Material
1 (core)	Conductor	15.0	30.0	Copper
2 (core)	Insulation	23.0	76.0	Polyethylene
3 (core)	Load sheath	/	/	
4	Filler	/	163.75	Polyethylene
5	Inner sheath	3.625	171.0	Polyethylene
6	Amour	5.5	182.0	steel
7	Outer sheath	4.0	190.0	Polyethylene

Table F-2: Materials for cable analysis

Material	Poisson's ratio $[\nu]$	Elastic modulus $[GPa]$	Density $[kg/m^3]$
Copper	0.34	110	8900
Steel	0.30	200	7800
Polyethylene	0.42	1.10	950

Model for simulations

For the simulations of the stiffnesses a FEM model with a length of 1m has been developed for the selected cable as shown in Fig. F-1.

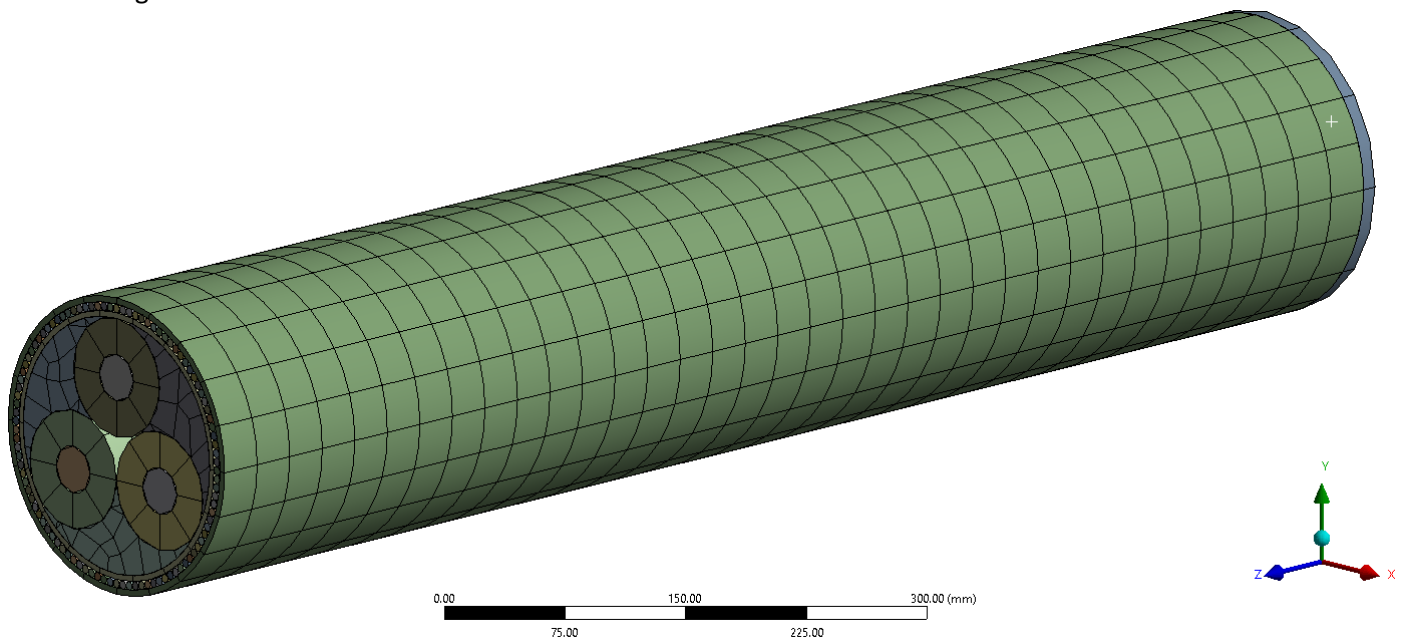


Fig. F-1: Cable FEM model

The cross-sectional view of the model is shown in Fig. F-2.

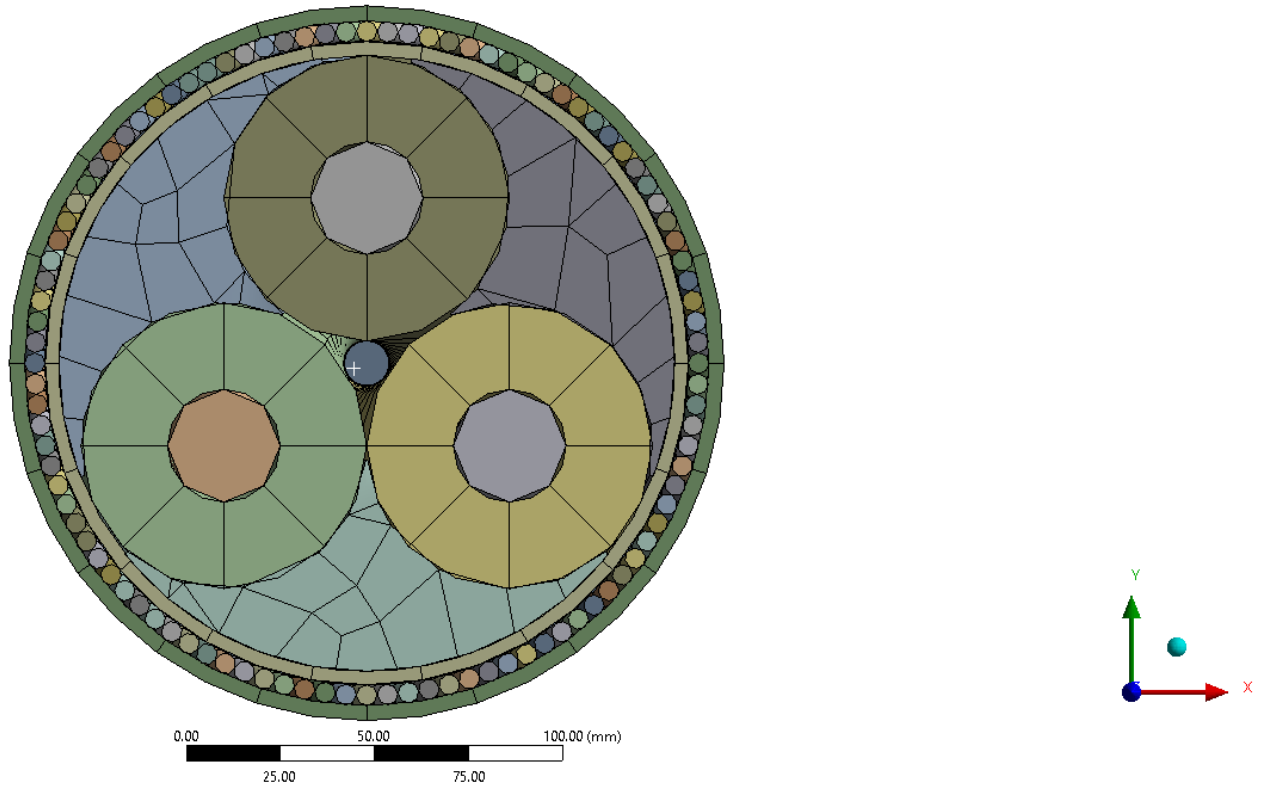


Fig. F-2: Cross sectional view of cable FEM model

All layers, except the inner and outer sheath, are twisted (as a helix) at an angle of 360° over 1m, as shown in Fig. F-3, where some parts are hidden.

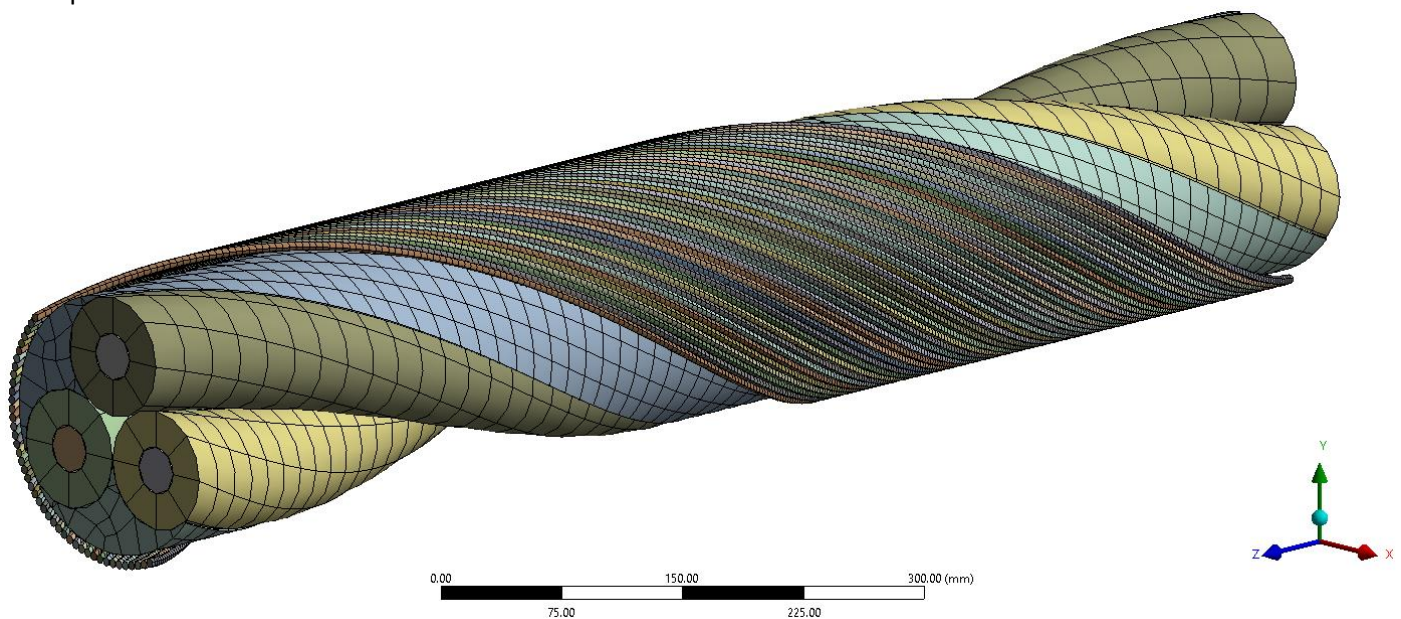


Fig. F-3: Cable FEM model with some hidden layers

The material properties, layers and layer thicknesses are used as defined in Table F-1 and Table F-2. For the mesh, quadratic elements have been used for more accurate results. Because most layers have one element through the thickness, full integration has been used. For the mesh size:

- Armor wires: 100 mm characteristic size ('hard behavior' of the mesh)
- Polymer filler: 16.5 mm characteristic size ('hard behavior' of the mesh)
- Copper core: 50 mm characteristic size ('hard behavior' of the mesh)
- Not listed above: 60 mm characteristic size

The following contacts are defined:

- Armor wire and armor wire
- Conductor and isolation
- Isolation and filler
- Filler and inner sheath
- Isolation and isolation
- Isolation and inner sheath
- Armor wire and inner sheath
- Armor wire and outer sheath

Boundary conditions and contact types are specified for each stiffness study separately and will be discussed in the corresponding section.

F.1 Axial stiffness

The results from section F.1 for the selected cable are shown in Table F-3.

Table F-3: Results axial stiffness

Description	Simulation no.	Abbreviation	Value	Unit
Calculated elastic modulus		$E_{cable,axial}$	25.9	GPa
Elastic modulus FEM: bonded contact	1, 2	$E_{cable,axial}$	21.3	GPa
Elastic modulus FEM: internal friction neglected	3	$E_{cable,axial}$	21.0	GPa
Elastic modulus FEM: both internal friction and wire – wire contact neglected	4	$E_{cable,axial}$	5.26	GPa
Elastic modulus FEM: no separation contact	5	$E_{cable,axial}$	6.19	GPa

F.1.1 Calculation

Considering the elongation δ_i of each layer i , the assumed compatibility condition states that $\delta_i = \delta$. In other words, each layer has the same elongation δ . Due to the reasons below, it is assumed that the normal force is distributed over all layers:

- Friction between layers transfers the normal force to the other layers
- The main loads on the cable are acceleration loads (which works on all the layers) and transverse / radial loads which are transferred as compression forces on each layer to normal force in the cable in all layers

How normal force over the entire cable is distributed over the layers depends on the stiffness of each layer. If the normal force is assumed to be constant it follows that

$$\delta_i = \frac{N_i L}{E_i A_i} = \delta = \frac{L \sum N_i}{E_{cable,axial} A} \quad (F-1)$$

, where A is the total cross-sectional area of the cable, A_i the cross-sectional area of each layer, E_i the elastic modulus of the material of the corresponding layer and $E_{cable,axial}$ is the axial elastic modulus of the cable. It follows that $E_{cable,axial}$ can be calculated by

$$E_{axial} = \frac{\sum_i E_i A_i}{A} = \frac{\sum_i E_i A_i}{\pi R^2} \quad (F-2)$$

For all layers i and cable radius R . There areas and elastic moduli of all layers are given in Table F-4.

Table F-4: Areas and elastic moduli for all layers in the selected cable

Layer	Component	E-modulus [GPa]	Area per core [m ²]	Area [m ²]
1	Conductor	110	7.07E-04	2.12E-03
2	Insulation	1.1	3.83E-03	1.15E-02
3	Load sheath (neglected)	10	/	/
4	Filler	1.1	/	7.45E-03

5	Inner sheath	1.1	/	1.91E-03
6	Amour	200	/	2.38E-03
7	Outer sheath	1.1	/	2.34E-03

With a diameter of 190mm, the cable has a total area (all layers + gabs) of $0.028m^2$. The resulting axial stiffness of the selected cable is given in Table F-5.

Table F-5: Calculation axial stiffness of selected cable

Description	Abbreviation	Value	Unit
Calculated elastic modulus	$E_{cable,axial}$	25.9	GPa

F.1.2 Simulations

The result from Table F-5 will be verified by FEM simulations with the model shown in Fig. F-1.

Boundary conditions

The boundary conditions for the simulations are shown in Fig. F-4.

- A Force: $1.e+005$ N
- B Compression Only Support
- C Fixed Support

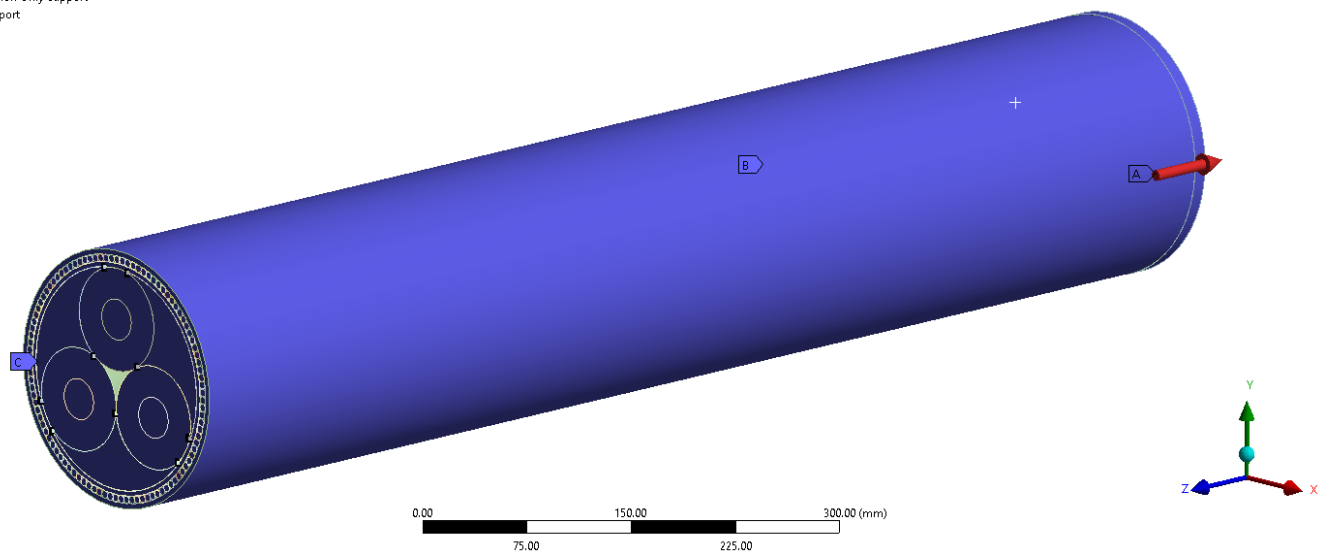


Fig. F-4: Boundary conditions simulations axial stiffness

The different types of boundary conditions denoted by the numbers A, B and C in Fig. F-4 are described below.

- A. A load will be applied to a plate connected to all layers. This plate has a large stiffness to enforce that all layers have the same elongation. The plate is shown in Fig. F-5.

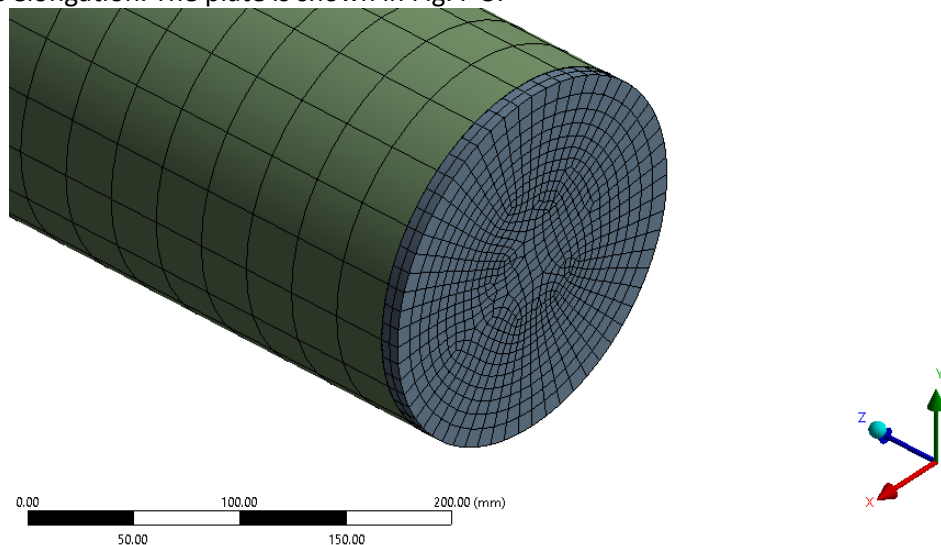


Fig. F-5: Plate connected to all layers to enforce same elongation for each layer

- B. Compression only support on outer layer. This will make the simulation more stable, and it will improve the convergence
- C. Fixed boundary to all layers

Contacts

Multiple simulations are done with different contacts between all layers. Contacts are specified for each corresponding simulation.

Stiffness determination

For multiple contacts a force F will be applied, and the deformation δ will be checked. The stiffness of the cable can then be determined by

$$E_{cable,axial} = \frac{FL}{\delta A} \quad (F-3)$$

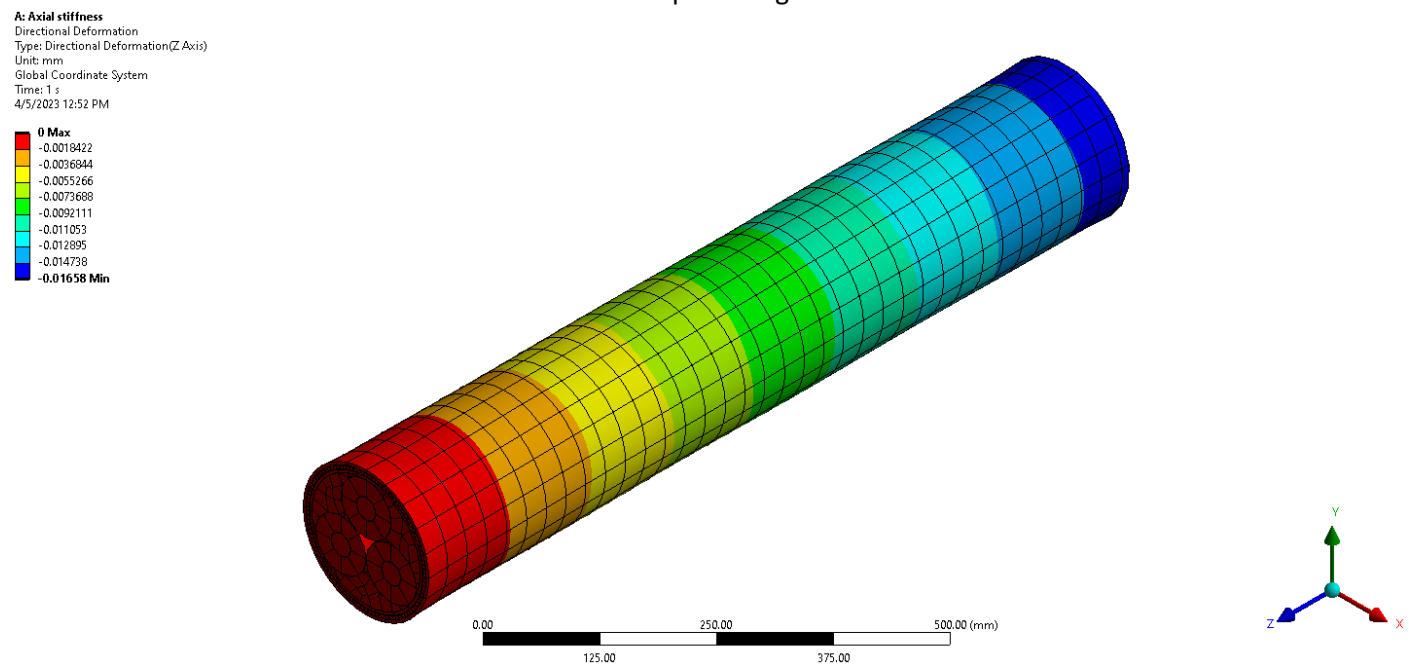
, with $A = 0.028m^2$ the cross-sectional area of the cable and $L = 1m$ the length of the cable. Below the results of the simulations are discussed. Note that the figures show scaled deformations.

Simulation 1

This simulation has the following characteristics:

- All contacts are bonded
- Applied load is $10kN$

The results are shown in the deformation in z direction plot in Fig. F-6.



Simulation 2

This simulation has the following characteristics:

- All contacts are bonded
- Applied load is $100kN$

The results are shown in the deformation in z direction plot in Fig. F-7.

A: Axial stiffness
 Directional Deformation
 Type: Directional Deformation(Z Axis)
 Unit: mm
 Global Coordinate System
 Time: 1 s
 4/5/2023 1:41 PM

0 Max
 -0.018422
 -0.036844
 -0.055266
 -0.073688
 -0.09211
 -0.11053
 -0.12895
 -0.14738
-0.1658 Min

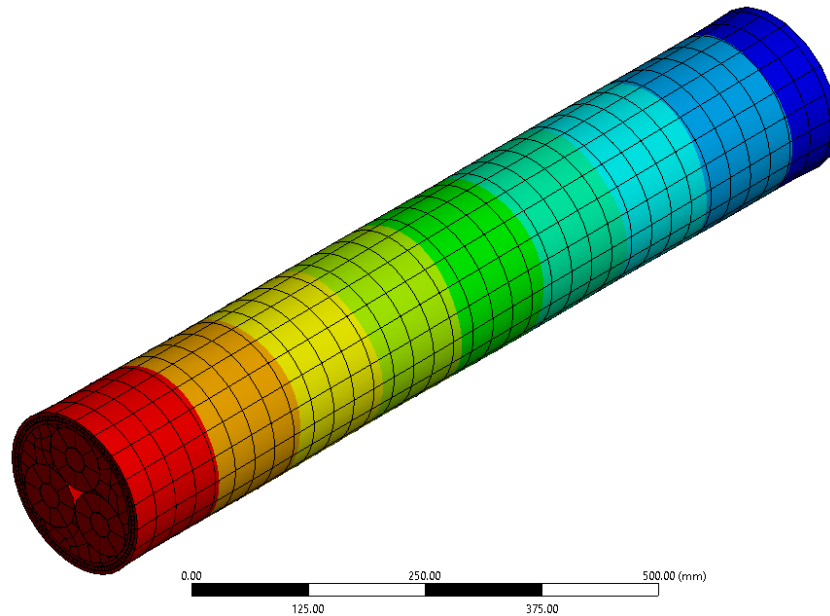


Fig. F-7: Results simulation 2, deformation in z direction plot

Simulation 3

This simulation has the following characteristics:

- Conductor and isolation no separation contact
- Isolation and filler no separation contact
- Filler and inner sheath no separation contact
- Insulation and isolation no separation contact
- Insulation and inner sheath no separation contact
- Other contacts are bonded
- Applied load is $100kN$

The results are shown in the deformation in z direction plot in Fig. F-8.

A: Axial stiffness
 Directional Deformation
 Type: Directional Deformation(Z Axis)
 Unit: mm
 Global Coordinate System
 Time: 1 s
 4/5/2023 2:30 PM

0.00018253 Max
 -0.018501
 -0.037194
 -0.055867
 -0.07455
 -0.093234
 -0.11192
 -0.1306
 -0.14928
-0.16797 Min

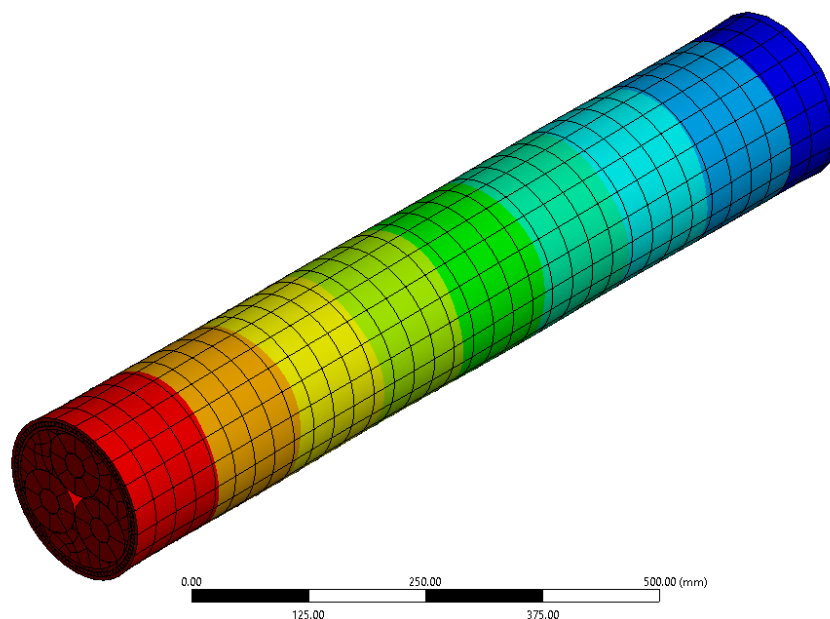


Fig. F-8: Results simulation 3, deformation in z direction plot

Simulation 4

This simulation has the following characteristics:

- Conductor and isolation no separation contact
- Isolation and filler no separation contact
- Filler and inner sheath no separation contact
- Insulation and isolation no separation contact
- Insulation and inner sheath no separation contact
- Wire and wire contact is neglected
- Other contacts are bonded
- Applied load is $100kN$

The results are shown in the deformation in z direction plot in Fig. F-9.

A: Axial stiffness
 Directional Deformation
 Type: Directional Deformation(Z Axis)
 Unit: mm
 Global Coordinate System
 Time: 1 s
 Max: 0.015046
 Min: -0.67206
 5/24/2023 10:24 AM

0.015046
 -0.061299
 -0.13764
 -0.21399
 -0.29033
 -0.36668
 -0.44302
 -0.51937
 -0.59571
 -0.67206

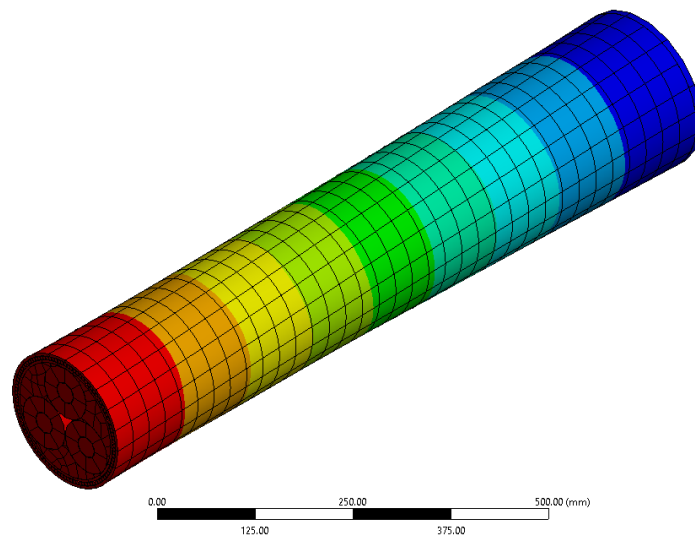


Fig. F-9: Results simulation 4, deformation in z direction plot

Simulation 5

This simulation has the following characteristics:

- All contacts are no separation
- Applied load is $100kN$

The results are shown in the deformation in z direction plot in Fig. F-10.

A: Axial stiffness
 Directional Deformation
 Type: Directional Deformation(Z Axis)
 Unit: mm
 Global Coordinate System
 Time: 1 s
 Max: 0.018798
 Min: -0.57006
 5/24/2023 12:54 PM

0.018798
 -0.046631
 -0.11206
 -0.17749
 -0.24292
 -0.30895
 -0.37377
 -0.43392
 -0.50463
 -0.57006

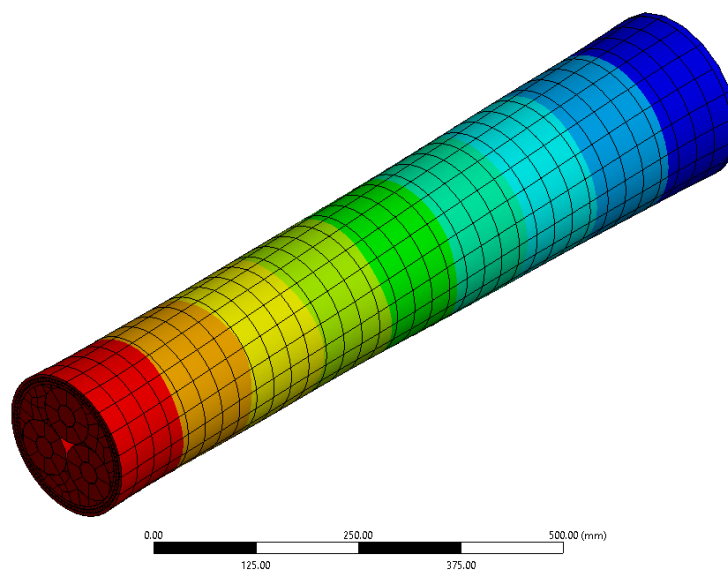


Fig. F-10: Results simulation 5, deformation in z direction plot

F.2 Bending stiffness

The results from section F.2 for the selected cable are shown in Table F-3.

Table F-6: Results bending stiffness

Description	Simulation no.	Abbreviation	Value	Unit
Bending stiffness FEM simulation, no separation contact	1	$(EI)_{cable}$	44.7	kNm^2
Bending stiffness FEM simulation bonded contact	2	$(EI)_{cable}$	2150	kNm^2
Calculated bending stiffness free layers		$(EI)_{cable}$	37.8	kNm^2
Calculated bending stiffness fixed layers		$(EI)_{cable}$	1804	kNm^2

F.2.1 Calculation

For the calculation of the bending stiffness there are two cases: the layers are fixed to each other, and the layers are not fixed to each other. For the first case the bending stiffness of the cable can be determined by the summation of the stiffness of all components with respect to the neutral axis

$$((EI)_{cable})_{fixed} = \sum E_i I_{i,x} \quad (F-4)$$

, with elastic modulus E_i of each component and $I_{i,x}$ the second moment of area around the neutral axis of the cable. The second moment of area around the neutral axis of a component can be calculated by the parallel axis theorem

$$I_{i,x} = I_{i,x'} + A_i d_i^2 \quad (F-5)$$

, with area of the layer A_i , second moment of area around the component's neutral axis $I_{i,x'}$ and the distance d_i of the neutral axis of the cable to the neutral axis of the component.

$$((EI)_{cable})_{free} = \sum E_i I_{i,x} \quad (F-6)$$

The second moment of area around the neutral axis of each component (free) and the second moment of area around the neutral axis of the cable for each layer can be seen in Table F-7.

Table F-7: Bending stiffness of each component

Layer	Component	E-modulus E_i [GPa]	I (free) [m^4]	I (fixed) [m^4]
1	Conductor	110	$1.19 \cdot 10^{-7}$	$2.42 \cdot 10^{-6}$
2	Insulation	1.1	$4.79 \cdot 10^{-6}$	$1.72 \cdot 10^{-5}$
3	Load sheath (neglected)	10	/	/
4	Filler	1.1	/	/
5	Inner sheath	1.1	$6.68 \cdot 10^{-6}$	$6.68 \cdot 10^{-6}$
6	Amour	200	$4.49 \cdot 10^{-9}$	$7.50 \cdot 10^{-6}$
7	Outer sheath	1.1	$1.01 \cdot 10^{-5}$	$1.01 \cdot 10^{-5}$

For the second moment of area of all layers, the filler and the space between the armor cores are neglected. The results are shown in Table F-8.

Table F-8: Calculated bending stiffness of selected cable

Description	Abbreviation	Value	Unit
Calculated bending stiffness free layers	$((EI)_{cable})_{free}$	37.8	kNm^2
Calculated bending stiffness fixed layers	$((EI)_{cable})_{fixed}$	1804	kNm^2

F.2.2 Simulation

The result from Table F-8 will be verified by FEM simulations with the model shown in Fig. F-1.

Boundary conditions

The boundary conditions for the simulations are shown in Fig. F-4.

B: bending stiffness
Static Structural 2
Time: 1. s
5/24/2023 1:09 PM

A: Force: 100. N
B: Fixed Support

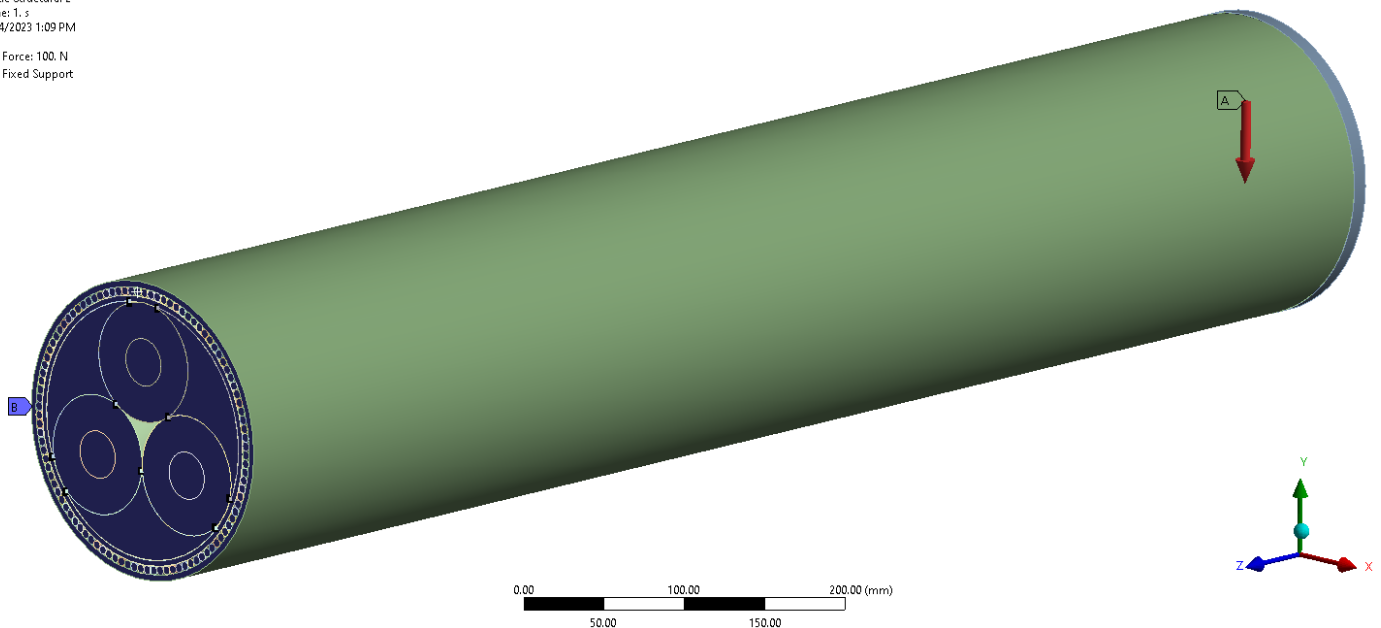


Fig. F-11: Boundary conditions simulations axial stiffness

The different types of boundary conditions denoted by the numbers A and B in Fig. F-4 are described below.

- A. A load will be applied to a plate connected to all layers. This plate has a large stiffness to enforce that all layers have the same elongation. The plate is shown in Fig. F-5.

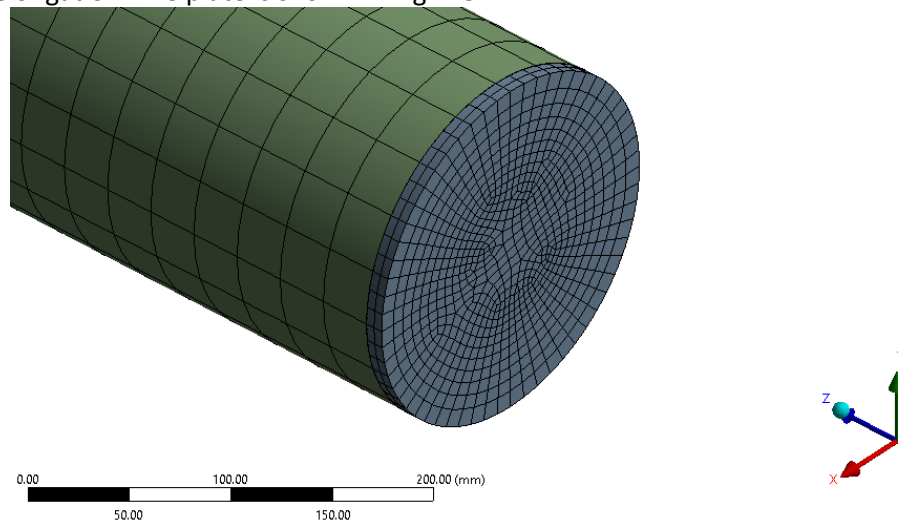


Fig. F-12: Plate connected to all layers to enforce same elongation for each layer

- B. Fixed boundary to all layers

Contacts

Multiple simulations are done with different contacts between all layers. Contacts are specified for each corresponding simulation.

Stiffness determination

For multiple contacts a force F will be applied, and the deformation δ will be checked. The stiffness of the cable can then be determined by elementary beam theory [46] by

$$(EI)_{cable} = \frac{FL^3}{3\delta} \quad (F-7)$$

, with $A = 0.028m^2$ the cross-sectional area of the cable and $L = 1m$ the length of the cable. Below the results of the simulations are discussed. Note that the figures show scaled deformations.

Simulation 1

This simulation has the following characteristics:

- All contacts are no separation
- Applied load is $100N$

The results are shown in the deformation in y direction plot in Fig. F-10.

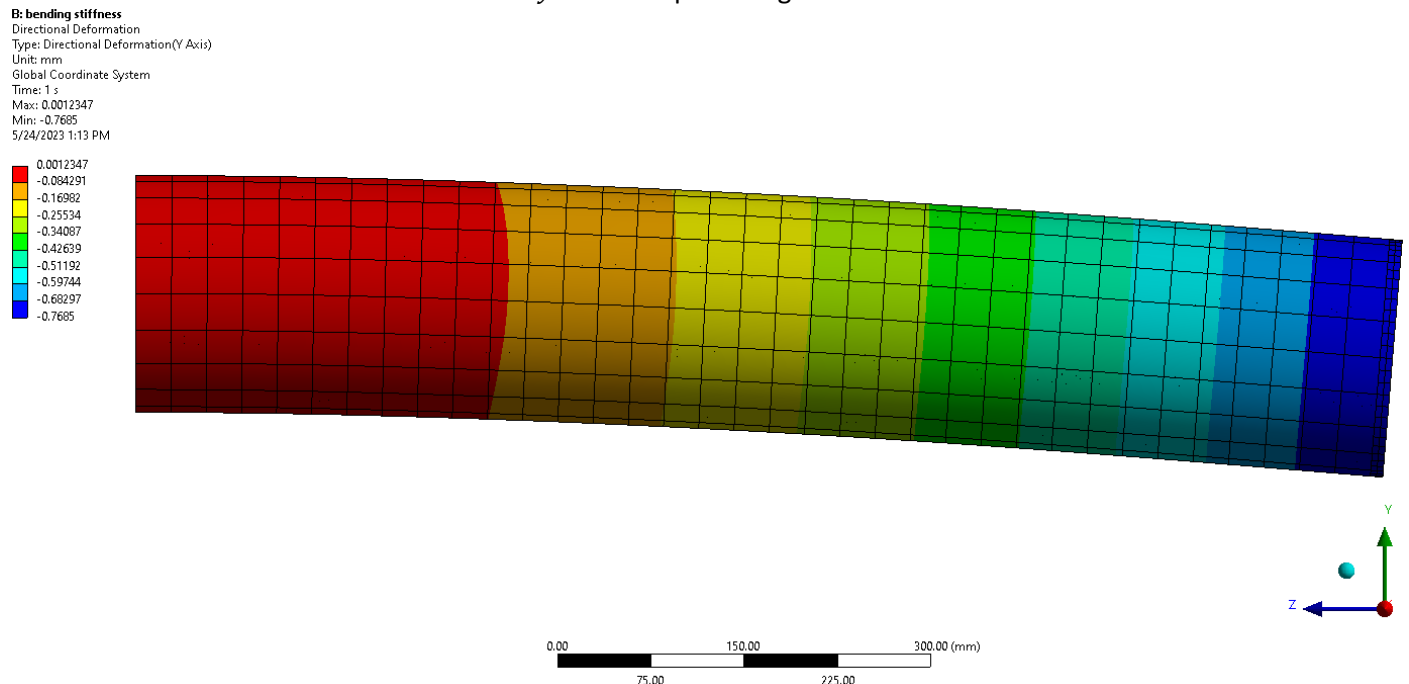


Fig. F-13: Results simulation 5, deformation in y direction plot

Simulation 2

This simulation has the following characteristics:

- All contacts are bonded
- Applied load is $100N$

The results are shown in the deformation in y direction plot in Fig. F-10.

B: bending stiffness

Directional Deformation
 Type: Directional Deformation(Y Axis)
 Unit: mm
 Global Coordinate System
 Time: 1 s
 Max: 3.5666e-6
 Min: -0.015973
 5/24/2023 1:25 PM

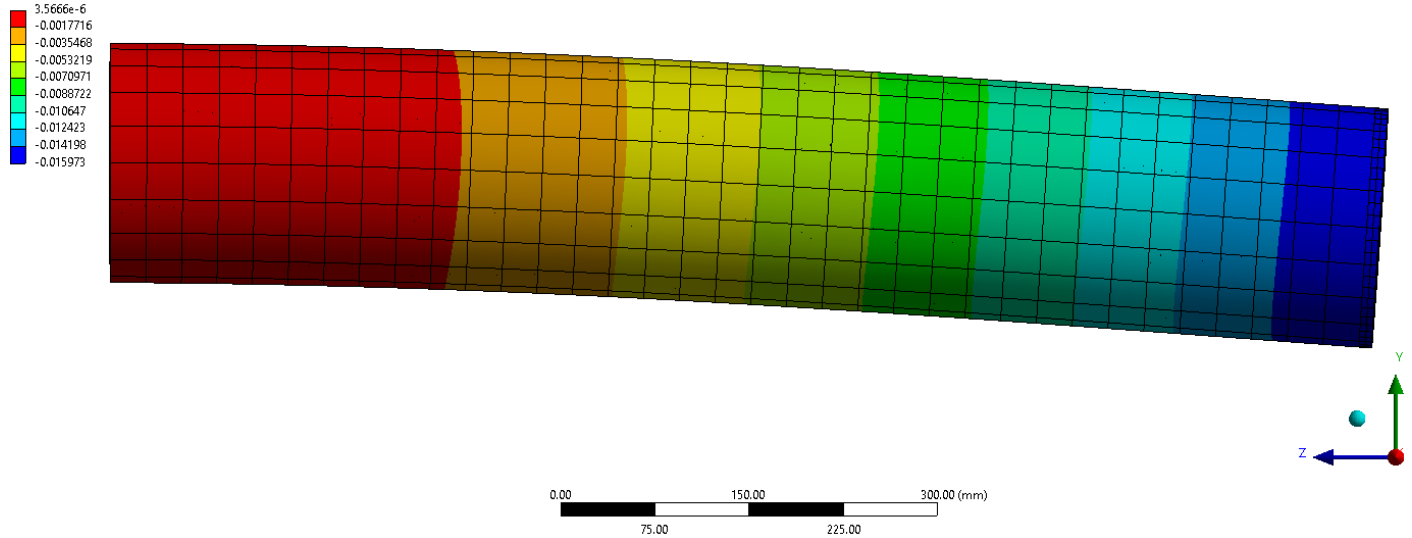


Fig. F-14: Results simulation 5, deformation in y direction plot

F.3 Radial stiffness

For the radial stiffness only FEM simulations have been executed to determine the displacement Δw under loading F as defined in Figure 5-6. Results of the simulations for the loading described in section 5.1 are given in Table F-9.

Table F-9: Simulated deformation of cable under radial loading

Description	Abbreviation	Value	Unit
Displacement FEM simulation no separation contact	Δw	0.0052	mm
Displacement FEM simulation bonded contact	Δw	0.0096	mm

Boundary conditions

The boundary conditions for the simulations are shown in Fig. F-4.

C: Static Structural
 Static Structural
 Time: 1 s
 5/24/2023 2:46 PM

- [A] Displacement
- [B] Displacement 2
- [C] Force: 8790. N
- [D] Force 2: 8790. N

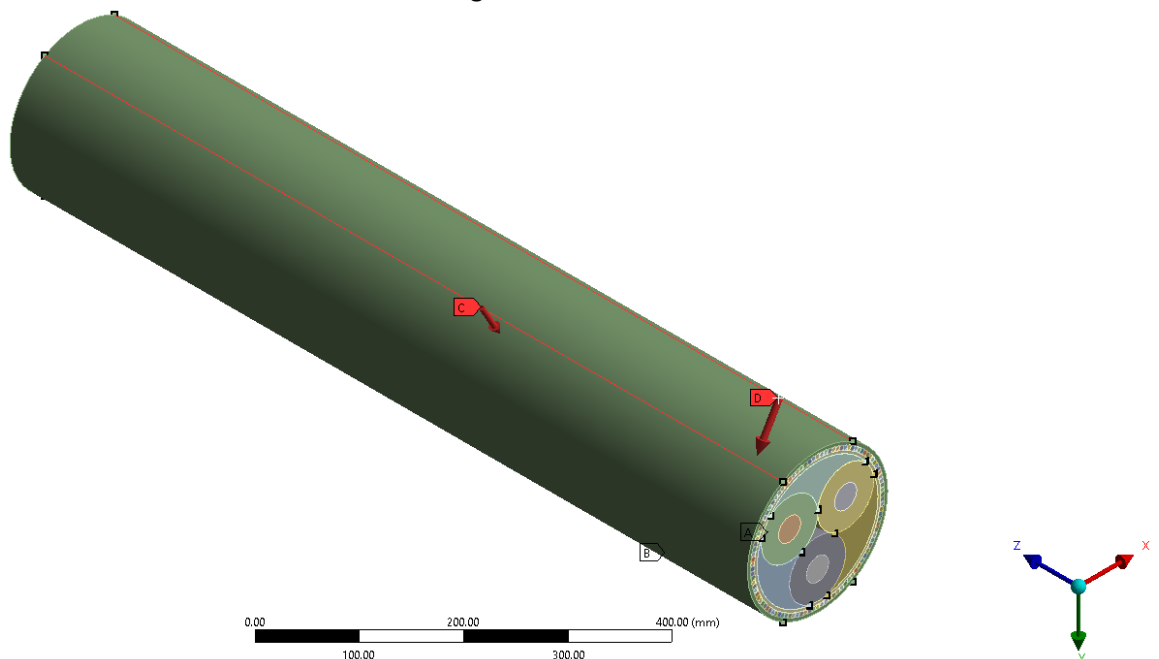


Fig. F-15: Boundary conditions simulations axial stiffness

The different types of boundary conditions denoted by the numbers A, B, C and D in Fig. F-4 are described below.

- A. Zero displacement in all directions over entire edge
- B. Zero displacement in all directions over entire edge
- C. Force of 8790N uniformly distributed over entire edge under angle of 60°
- D. Force of 8790N uniformly distributed over entire edge under angle of 60°

Contacts

Multiple simulations are done with different contacts between all layers. Contacts are specified for each corresponding simulation. Below the results of the simulations are discussed. Note that the figures show scaled deformations.

Simulation 1

This simulation has the following characteristics:

- All contacts are no separation
- $F = 8790N$

The results are shown in the deformation in y direction plot in Fig. F-10.

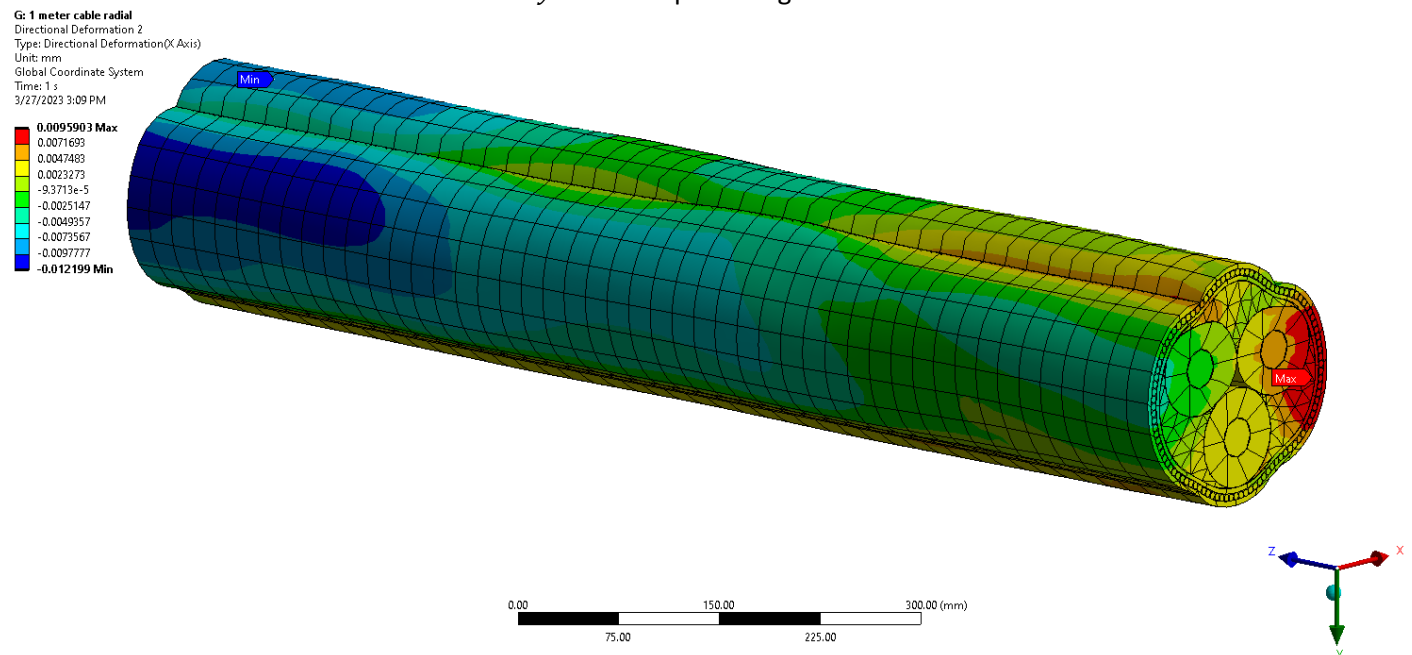


Fig. F-16: Results simulation 5, deformation in y direction plot

Simulation 2

This simulation has the following characteristics:

- All contacts are bonded
- $F = 8790N$

The results are shown in the deformation in x direction plot in Fig. F-10.

G: 1 meter cable radial
Directional Deformation 2
Type: Directional Deformation(X Axis)
Unit: mm
Global Coordinate System
Time: 1 s
3/27/2023 3:19 PM

0.0052021 Max
0.0040598
0.0029176
0.0017753
0.00063302
-0.00050924
-0.0016515
-0.0027938
-0.003936
-0.0050783 Min

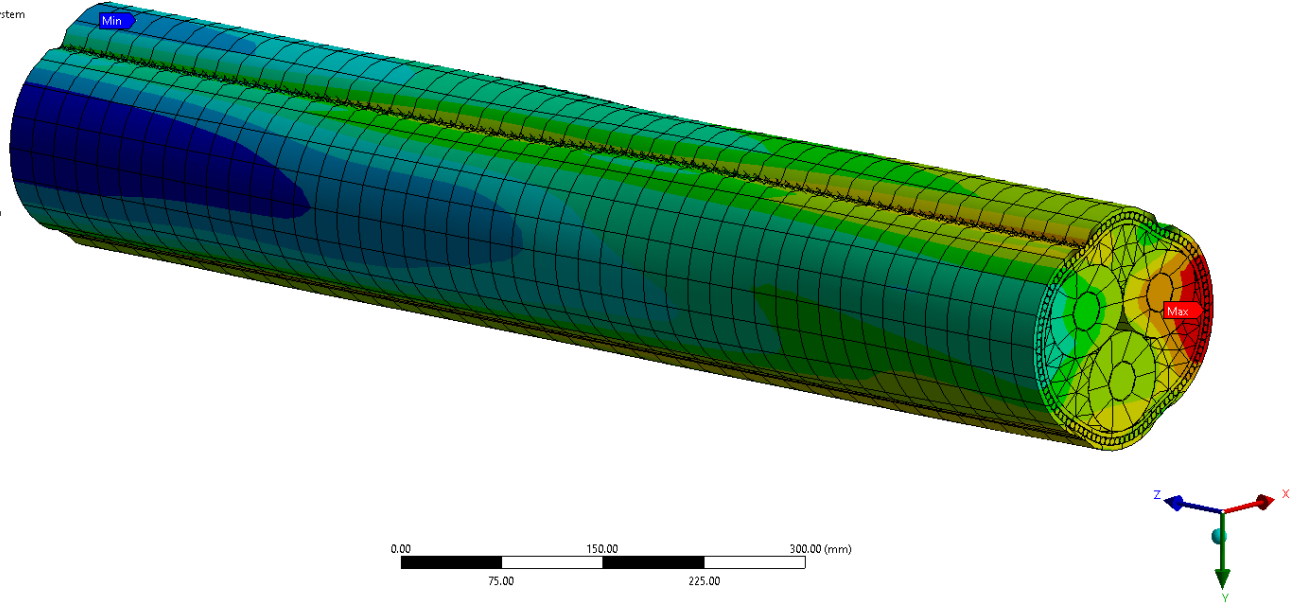

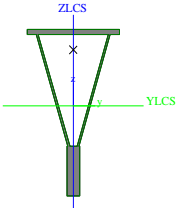

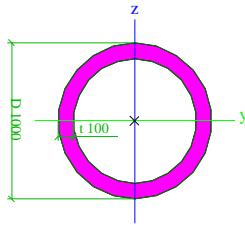



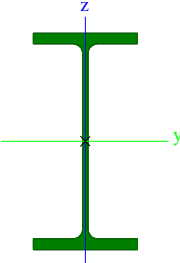
Fig. F-17: Results simulation 5, deformation in x direction plot


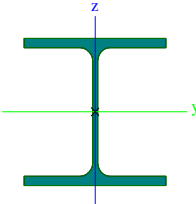
G Setup selection study

G.1 General input

G.1.1 Cross sections

CS31 - SPMT G4 - General CSS			
Type	General cross-section		
Shape type	Thick-walled		
Item material	S 690		
Fabrication	general		
Colour			
Flexural buckling y-y, Flexural buckling z-z	d		d
A [mm²]	6.285e+04		
A _y [mm²], A _z [mm²]	5.974e+04		2.689e+04
A _L [m²/m], A _D [m²/m]	2.9398e+00		4.8904e+00
C _{y,UCS} [mm], C _{z,UCS} [mm]	-1		45
I _{y,LCS} [mm⁴], I _{z,LCS} [mm⁴]	9.362e+09		9.673e+08
I _{yz,LCS} [mm⁴]	1.088e+07		
α [deg]	-0.07		
I _y [mm⁴], I _z [mm⁴]	9.362e+09		9.673e+08
i _y [mm], i _z [mm]	386		124
W _{el,y} [mm³], W _{el,z} [mm³]	1.664e+07		3.221e+06
W _{pl,y} [mm³], W _{pl,z} [mm³]	2.256e+07		5.784e+06
M _{pl,y,+} [Nmm], M _{pl,y,-} [Nmm]	1.40e+10		1.40e+10
M _{pl,z,+} [Nmm], M _{pl,z,-} [Nmm]	3.60e+09		3.60e+09
d _y [mm], d _z [mm]	-1		347
I _t [mm⁴], I _w [mm⁶]	1.071e+09		9.840e+12
β _y [mm], β _z [mm]	-649		4
Picture			
CS105 - DUMMY			
Type	Tube		
Detailed	1000; 100		
Shape type	Thick-walled		
Item material	S 355		
Fabrication	general		
Colour			
Flexural buckling y-y, Flexural buckling z-z	d		d
A [mm²]	2.827e+05		
A _y [mm²], A _z [mm²]	1.921e+05		1.921e+05
A _L [m²/m], A _D [m²/m]	3.1414e+00		5.6546e+00
C _{y,UCS} [mm], C _{z,UCS} [mm]	500		500
α [deg]	0.00		
I _y [mm⁴], I _z [mm⁴]	2.898e+10		2.898e+10
i _y [mm], i _z [mm]	320		320
W _{el,y} [mm³], W _{el,z} [mm³]	5.796e+07		5.796e+07
W _{pl,y} [mm³], W _{pl,z} [mm³]	8.133e+07		8.133e+07
M _{pl,y,+} [Nmm], M _{pl,y,-} [Nmm]	2.89e+10		2.89e+10
M _{pl,z,+} [Nmm], M _{pl,z,-} [Nmm]	2.89e+10		2.89e+10
d _y [mm], d _z [mm]	0		0
I _t [mm⁴], I _w [mm⁶]	5.709e+10		2.335e+02
β _y [mm], β _z [mm]	0		0
Picture			
Floor beam 1			

Type	HEB600	
Formcode	1 - I section	
Shape type	Thin walled	
Item material	S 355	
Fabrication	rolled	
Colour		
Flexural buckling y-y, Flexural buckling z-z	a	b
A [mm ²]	2.700e+04	
A _y [mm ²], A _z [mm ²]	1.756e+04	9.419e+03
A _L [m ² /m], A _D [m ² /m]	2.3200e+00	2.3224e+00
C _{y,UCS} [mm], C _{z,UCS} [mm]	150	300
α [deg]	0.00	
I _y [mm ⁴], I _z [mm ⁴]	1.710e+09	1.353e+08
i _y [mm], i _z [mm]	252	71
W _{el,y} [mm ³], W _{el,z} [mm ³]	5.701e+06	9.020e+05
W _{pl,y} [mm ³], W _{pl,z} [mm ³]	6.425e+06	1.391e+06
M _{pl,y,+} [Nmm], M _{pl,y,-} [Nmm]	2.28e+09	2.28e+09
M _{pl,z,+} [Nmm], M _{pl,z,-} [Nmm]	4.94e+08	4.94e+08
d _y [mm], d _z [mm]	0	0
I _t [mm ⁴], I _w [mm ⁶]	6.672e+06	1.097e+13
β _y [mm], β _z [mm]	0	0
Picture		

Floor beam 2		
Type	HEB300	
Formcode	1 - I section	
Shape type	Thin walled	
Item material	S 355	
Fabrication	rolled	
Colour		
Flexural buckling y-y, Flexural buckling z-z	b	c
A [mm ²]	1.491e+04	
A _y [mm ²], A _z [mm ²]	1.096e+04	3.544e+03
A _L [m ² /m], A _D [m ² /m]	1.7300e+00	1.7314e+00
C _{y,UCS} [mm], C _{z,UCS} [mm]	150	150
α [deg]	0.00	
I _y [mm ⁴], I _z [mm ⁴]	2.517e+08	8.563e+07
i _y [mm], i _z [mm]	130	76
W _{el,y} [mm ³], W _{el,z} [mm ³]	1.678e+06	5.709e+05
W _{pl,y} [mm ³], W _{pl,z} [mm ³]	1.869e+06	8.701e+05
M _{pl,y,+} [Nmm], M _{pl,y,-} [Nmm]	6.64e+08	6.64e+08
M _{pl,z,+} [Nmm], M _{pl,z,-} [Nmm]	3.09e+08	3.09e+08
d _y [mm], d _z [mm]	0	0
I _t [mm ⁴], I _w [mm ⁶]	1.850e+06	1.688e+12
β _y [mm], β _z [mm]	0	0
Picture		

Explanations of symbols	
A	Area
A _y	Shear Area in principal y-direction - Calculated by 2D FEM analysis
A _z	Shear Area in principal z-direction - Calculated by 2D FEM analysis

Explanations of symbols	
A_L	Circumference per unit length
A_D	Drying surface per unit length
$C_{Y,UCS}$	Centroid coordinate in Y-direction of Input axis system
$C_{Z,UCS}$	Centroid coordinate in Z-direction of Input axis system
$I_{Y,LCS}$	Second moment of area about the YLCS axis
$I_{Z,LCS}$	Second moment of area about the ZLCS axis
$I_{YZ,LCS}$	Product moment of area in the LCS system
α	Rotation angle of the principal axis system
I_y	Second moment of area about the principal y-axis
I_z	Second moment of area about the principal z-axis
i_y	Radius of gyration about the principal y-axis
i_z	Radius of gyration about the principal z-axis
$W_{el,y}$	Elastic section modulus about the principal y-axis
$W_{el,z}$	Elastic section modulus about the principal z-axis
$W_{pl,y}$	Plastic section modulus about the principal y-axis
$W_{pl,z}$	Plastic section modulus about the principal z-axis
$M_{pl,y,+}$	Plastic moment about the principal y-axis for a positive M_y moment
$M_{pl,y,-}$	Plastic moment about the principal y-axis for a negative M_y moment
$M_{pl,z,+}$	Plastic moment about the principal z-axis for a positive M_z moment
$M_{pl,z,-}$	Plastic moment about the principal z-axis for a negative M_z moment
d_y	Shear center coordinate in principal y-direction measured from the centroid - Calculated by 2D FEM analysis
d_z	Shear center coordinate in principal z-direction measured from the centroid - Calculated by 2D FEM analysis
I_t	Torsional constant - Calculated by 2D FEM analysis
I_w	Warping constant - Calculated by 2D FEM analysis
β_y	Mono-symmetry constant about the principal y-axis
β_z	Mono-symmetry constant about the principal z-axis

G.1.2 Materials

Name	ρ [t/m ³]	E_{mod} [MPa]	G_{mod} [MPa]	F_y [N/mm ²]	F_u [N/mm ²]
S 690	7.9	2.1000e+05	8.0769e+04	622	770
S 355	7.9	2.1000e+05	8.0769e+04	355	510

G.2 Setup 1

G.2.1 Model

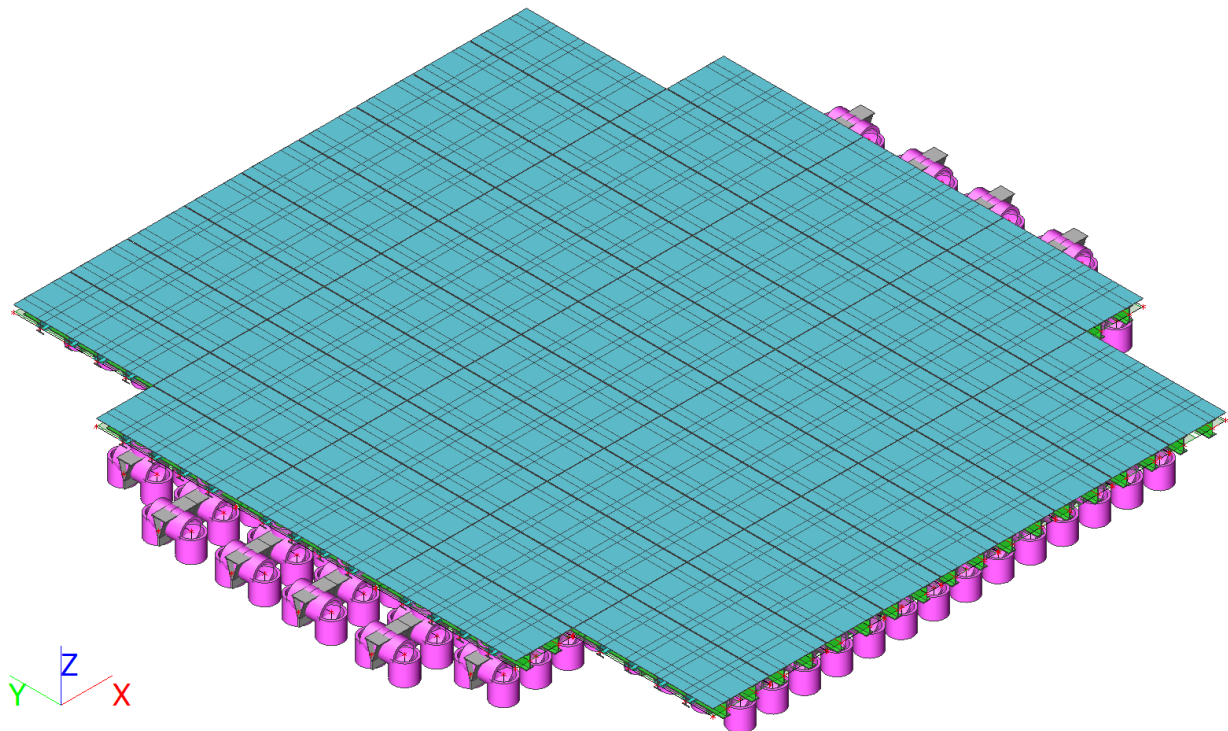


Fig. G-1: Setup 1 model

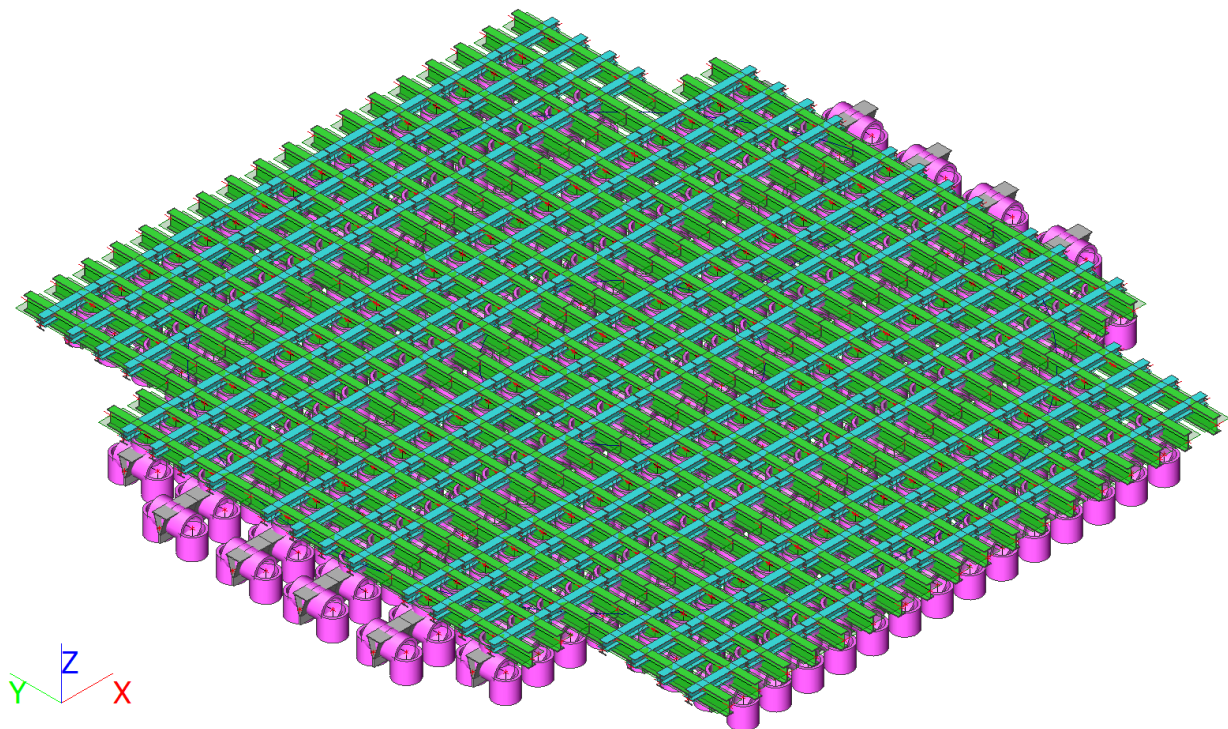


Fig. G-2: Setup 1 model with hidden plates

Name	Type, detailed	Item material	Colour
CS31 - SPMT G4 - General CSS	General cross-section	S 690	
CS105 - DUMMY	Tube, 1000; 100	S 355	
Floor beam 1	HEB600	S 355	
Floor beam 2	HEB300	S 355	

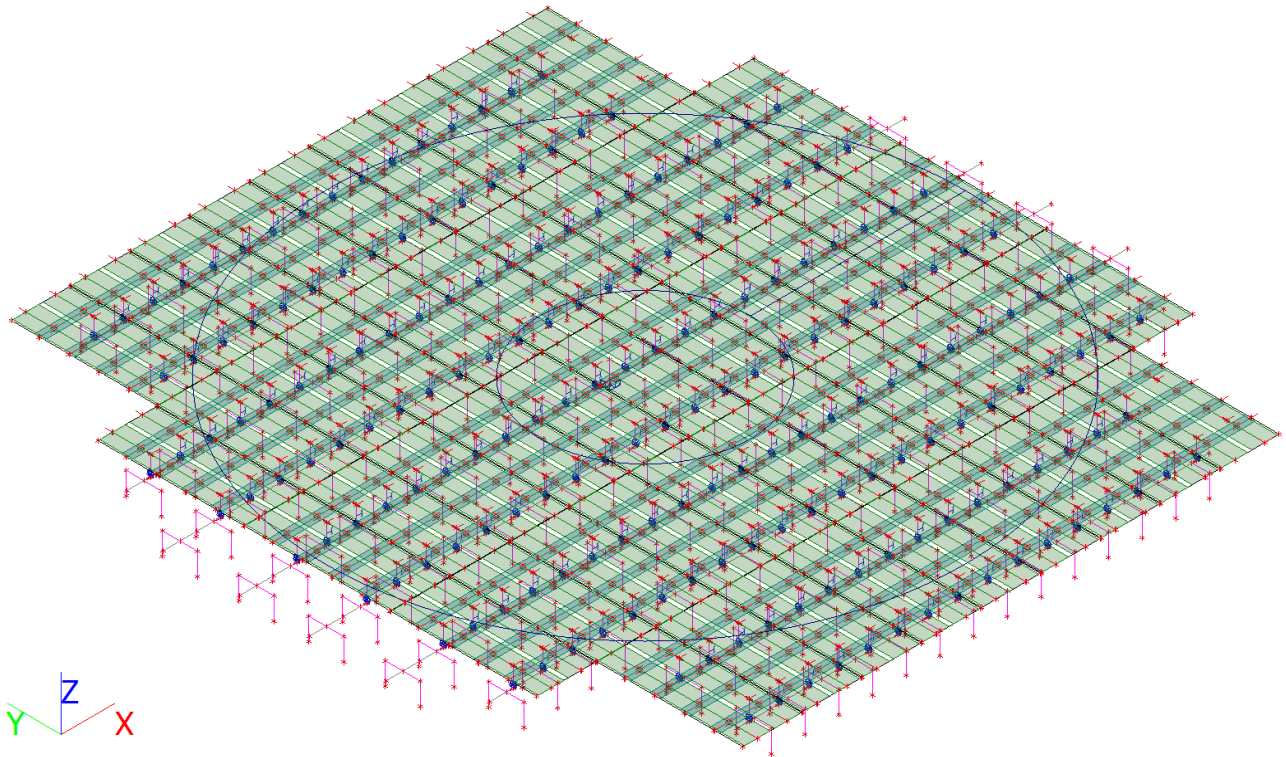


Fig. G-3: Setup 1 analytical model

G.2.2 Loads

Load cases

Name	Description	Action type	Load group	X	Y	Z
	Spec	Load type		[kN]	[kN]	[kN]
LC1	Self-weight	Permanent	LG1	0	0	-2451
		Standard				
LC2	SPMT axle Z	Permanent	LG1	0	0	51502
		Standard				
LC3	Cable load z	Permanent	LG1	0	0	-49008
		Standard				

Load combinations

Name	Description	Type	Load cases	Coeff. [-]
NC1	SLS	Serviceability	LC1 - Self weight	1.00
			LC2 - SPMT axle Z	1.00
			LC3 - Cable load z	1.00

G.2.3 Results

Resultant of reactions
Nonlinear calculation
NonLinear Combi: NC1
Extreme: Global
Selection: All
System: Global

x	y	z	Case	R _x	R _y	R _z	M _x	M _y	M _z
[mm]	[mm]	[mm]		[kN]	[kN]	[kN]	[kNm]	[kNm]	[kNm]
0.0	1450.0	-800.0	NC1	0	0	-42	61	6	0

3D displacement; u_z

Values: **u_z**
Nonlinear calculation
NonLinear Combi: NC1
Selection: All
Location: In nodes avg.. System:
Global

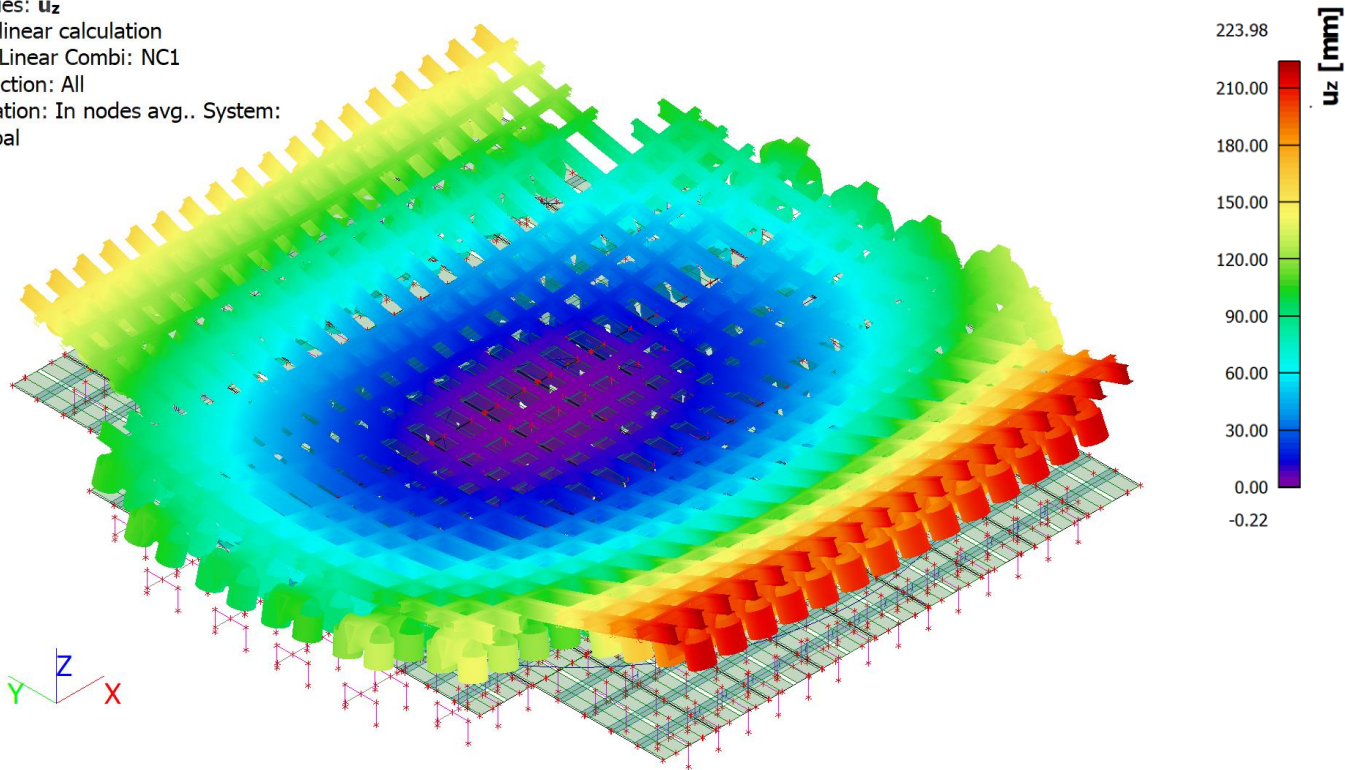


Fig. G-4: Setup 1 deformation in z direction

G.3 Setup 11.2

G.3.1 Model

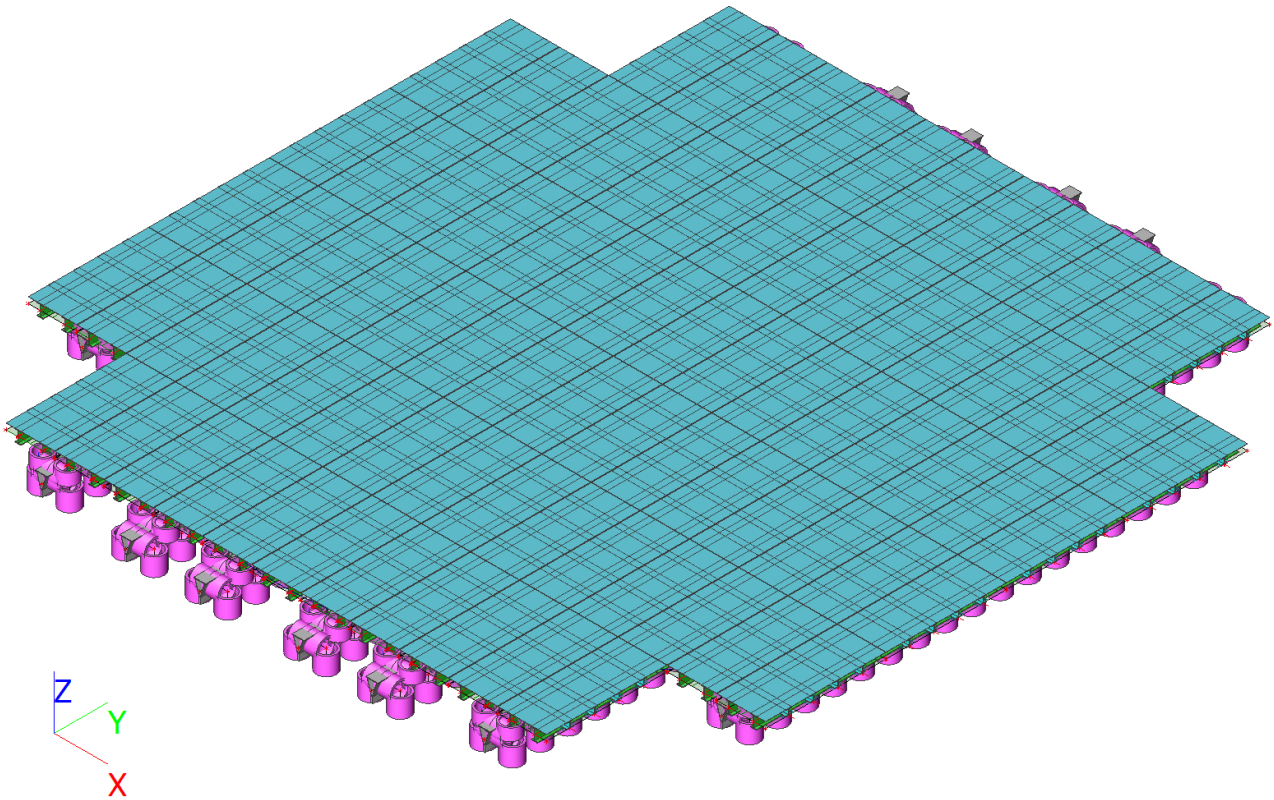


Fig. G-5: Setup 11.2 model

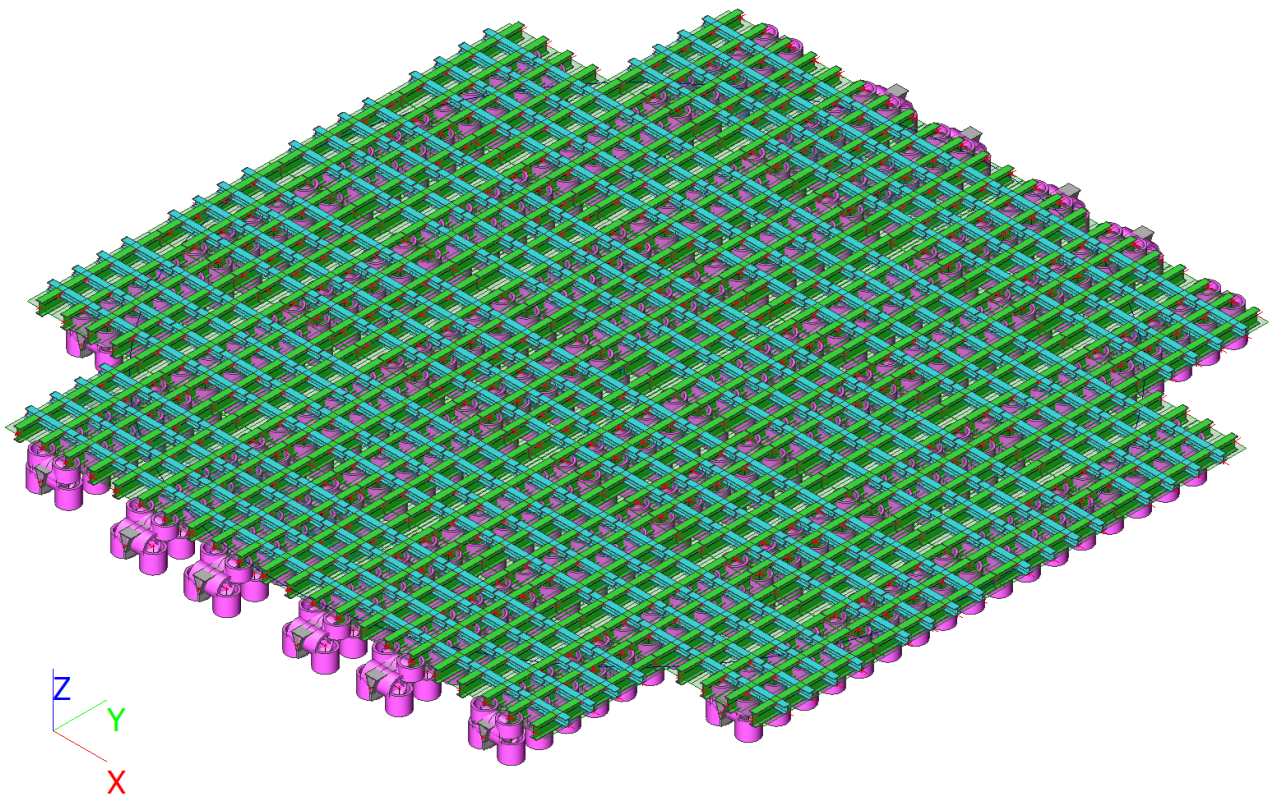


Fig. G-6: Setup 11.2 model with plates hidden

Name	Type, detailed	Item material	Colour
CS31 - SPMT G4 - General CSS	General cross-section	S 690	
CS105 - DUMMY	Tube, 1000; 100	S 355	
Floor beam 1	HEB600	S 355	
Floor beam 2	HEB300	S 355	

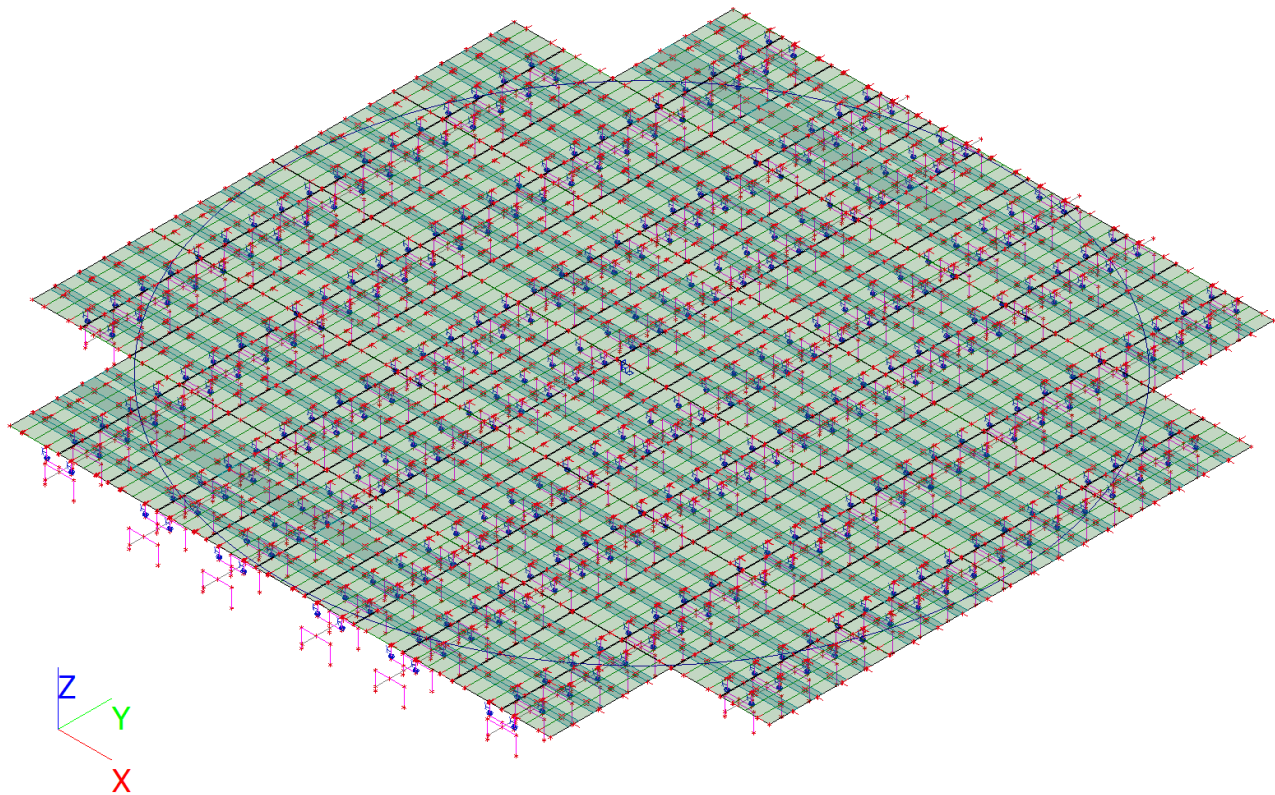


Fig. G-7: Setup 11.2 analytical model

G.3.2 Loads

Load cases

Name	Description	Action type	Load group	X	Y	Z
	Spec	Load type		[kN]	[kN]	[kN]
LC1	Self-weight	Permanent	LG1	0	0	-3941
		Standard				
LC2	SPMT axle Z	Permanent	LG1	0	0	52991
		Standard				
LC3	Cable load z	Permanent	LG1	0	0	-49011
		Standard				

Load combinations

Name	Description	Type	Load cases	Coeff. [-]
NC1	SLS	Serviceability	LC1 - Self weight	1.00
			LC2 - SPMT axle Z	1.00
			LC3 - Cable load z	1.00

G.3.3 Results

Resultant of reactions

Nonlinear calculation
NonLinear Combi: NC1
Extreme: Global
Selection: All
System: Global

x	y	z	Case	R _x	R _y	R _z	M _x	M _y	M _z
[mm]	[mm]	[mm]		[kN]	[kN]	[kN]	[kNm]	[kNm]	[kNm]
-620.0	10.0	0.0	NC1	0	0	-40	39	11	0

Values: u_z
Nonlinear calculation
NonLinear Combi: NC1
Selection: All
Location: In nodes avg.. System:
Global

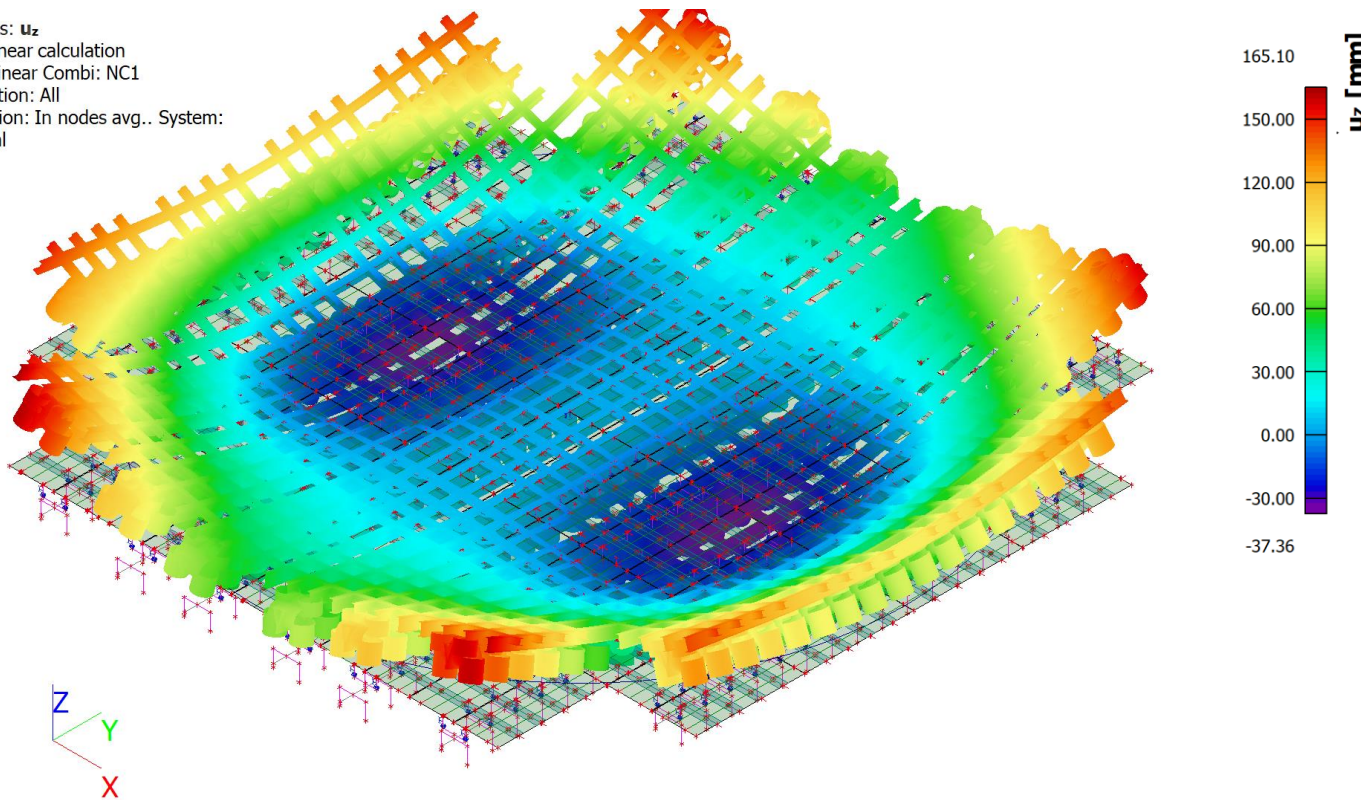


Fig. G-8: Setup 11.2 deformation in z direction

G.4 Setup 9.1

G.4.1 Model

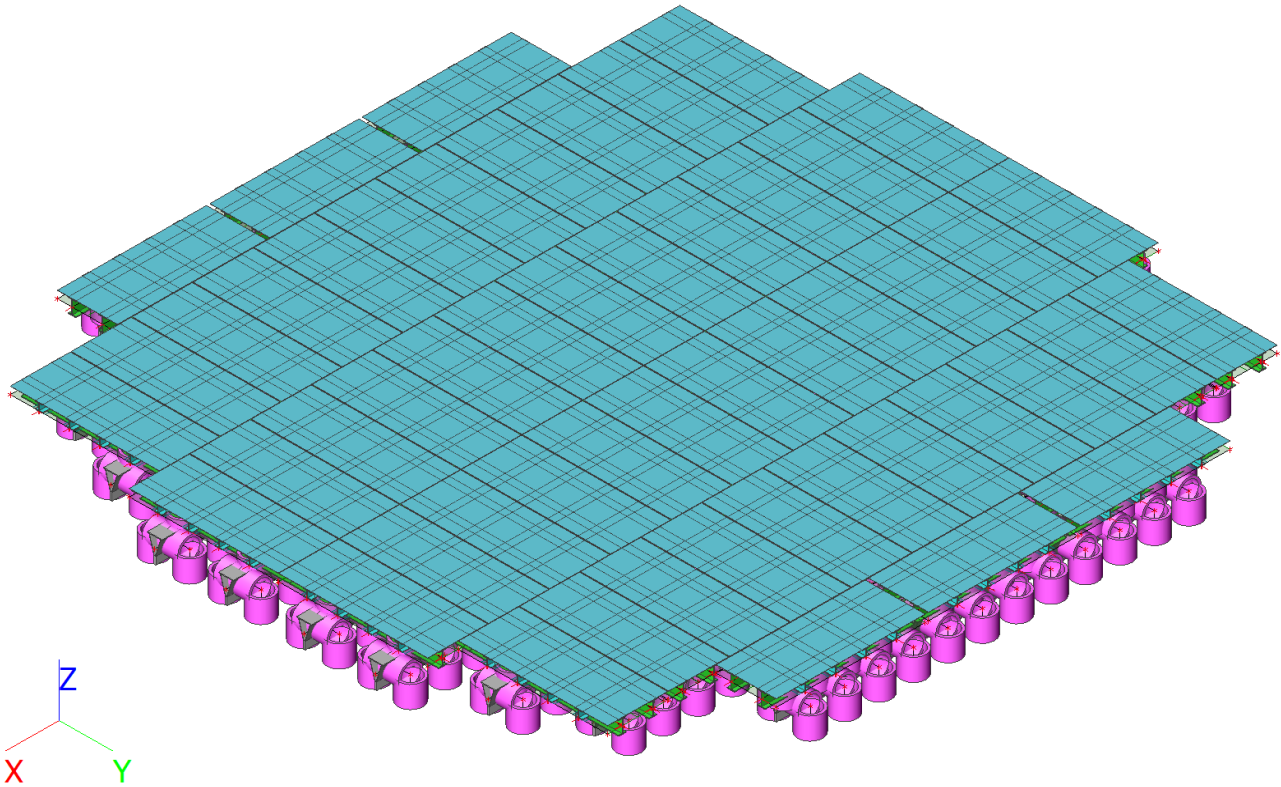


Fig. G-9: Setup 9.1 model

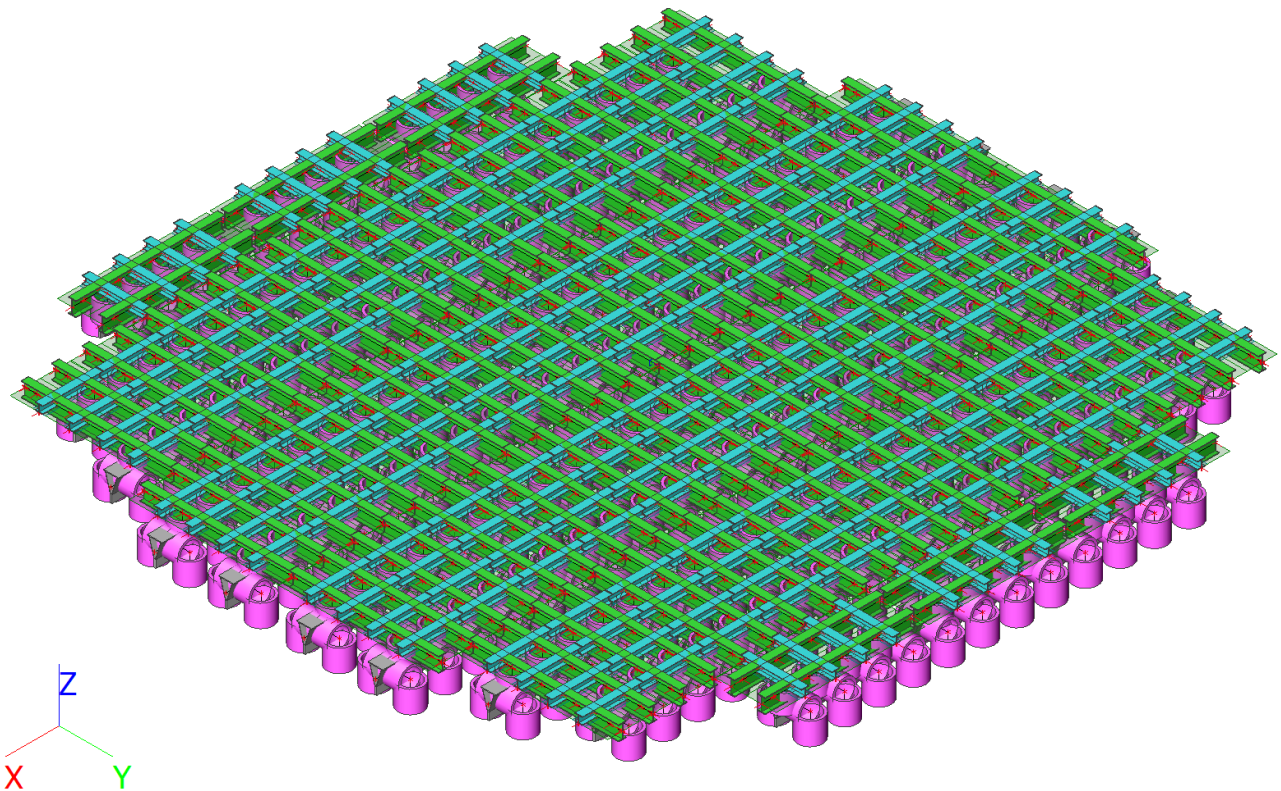


Fig. G-10: Setup 9.1 model with plates hidden

Name	Type, detailed	Item material	Colour
CS31 - SPMT G4 - General CSS	General cross-section	S 690	
CS105 - DUMMY	Tube, 1000; 100	S 355	
Floor beam 1	HEB600	S 355	
Floor beam 2	HEB300	S 355	

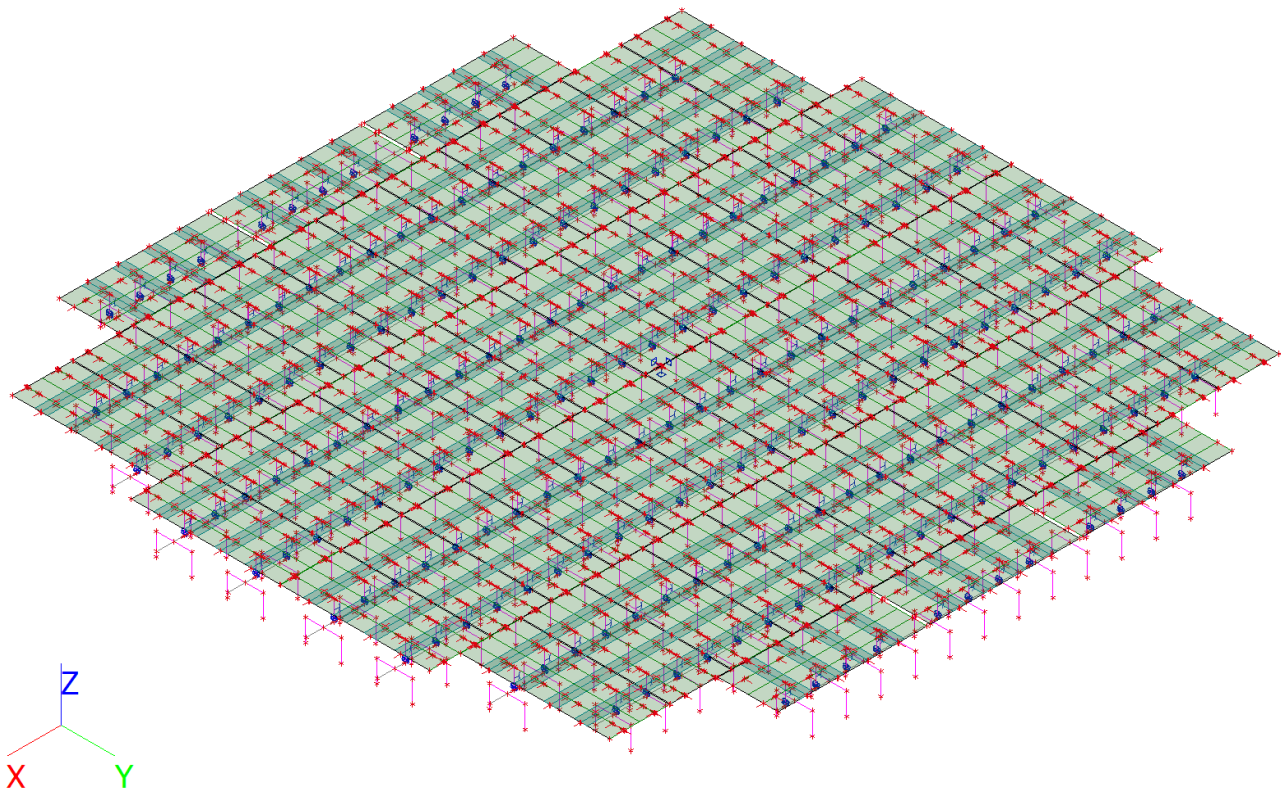


Fig. G-11: Setup 9.1 analytical model

G.4.2 Loads

Load cases

Name	Description	Action type	Load group	X	Y	Z
	Spec	Load type		[kN]	[kN]	[kN]
LC1	Self-weight	Permanent	LG1	0	0	-2499
		Standard				
LC2	SPMT axle Z	Permanent	LG1	0	0	51549
		Standard				
LC3	Cable load z	Permanent	LG1	0	0	-49014
		Standard				

Load combinations

Name	Description	Type	Load cases	Coeff. [-]
NC1	SLS	Serviceability	LC1 - Self weight	1.00
			LC2 - SPMT axle Z	1.00
			LC3 - Cable load z	1.00

G.4.3 Results

Resultant of reactions

Nonlinear calculation
NonLinear Combi: NC1
Extreme: Global
Selection: All
System: Global

x	y	z	Case	R _x	R _y	R _z	M _x	M _y	M _z
[mm]	[mm]	[mm]		[kN]	[kN]	[kN]	[kNm]	[kNm]	[kNm]
-620.0	10.0	0.0	NC1	0	0	-36	1	18	0

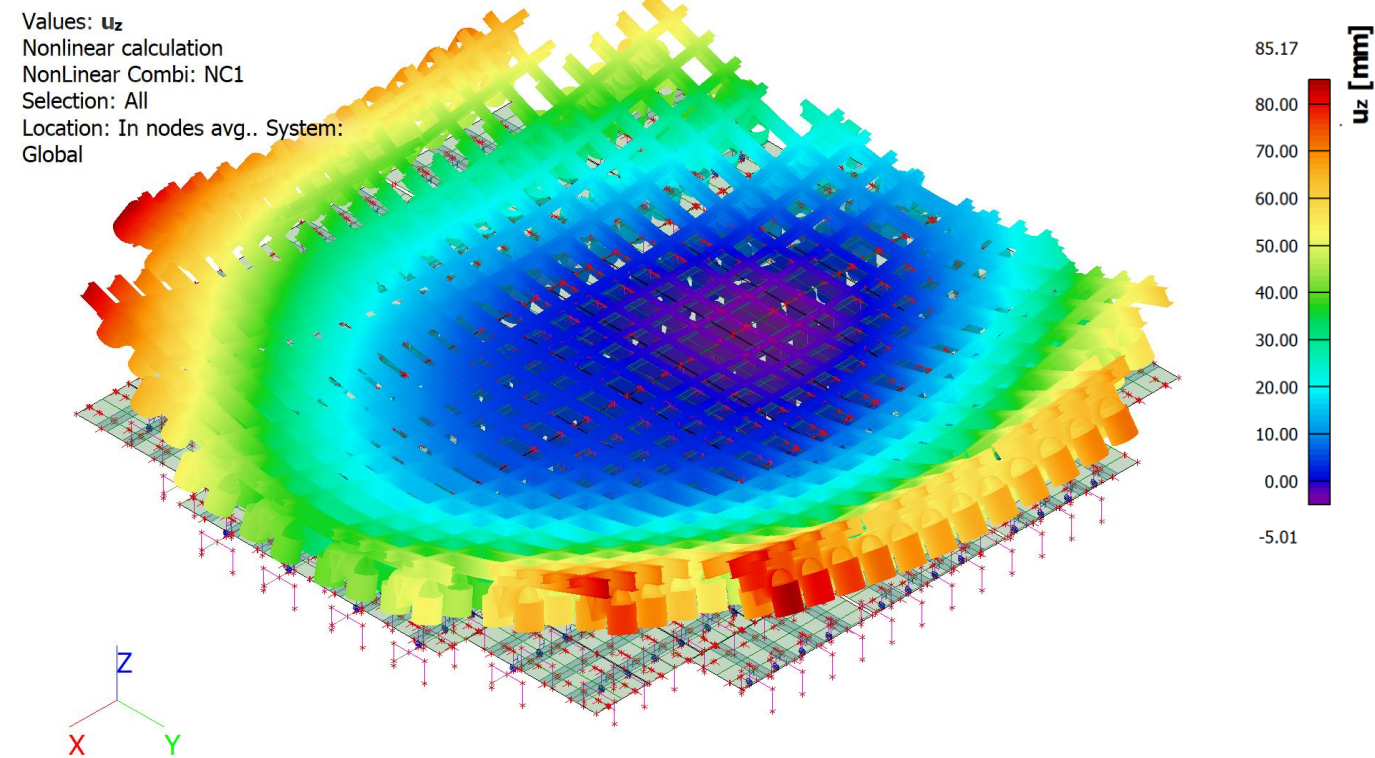


Fig. G-12: Setup 9.1 deformation in z direction

H Analysis of elaborated concept

H.1 Model description

H.1.1 Overview

Structural model

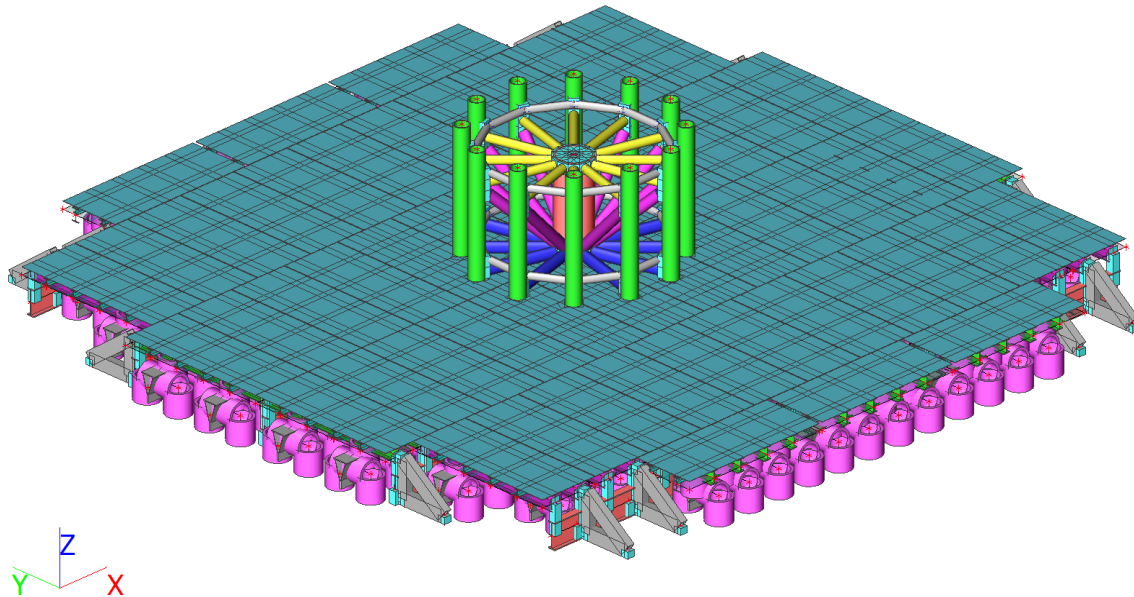


Fig. H-1: Elaborated model with SPMTs and sea fastening

Analysis model

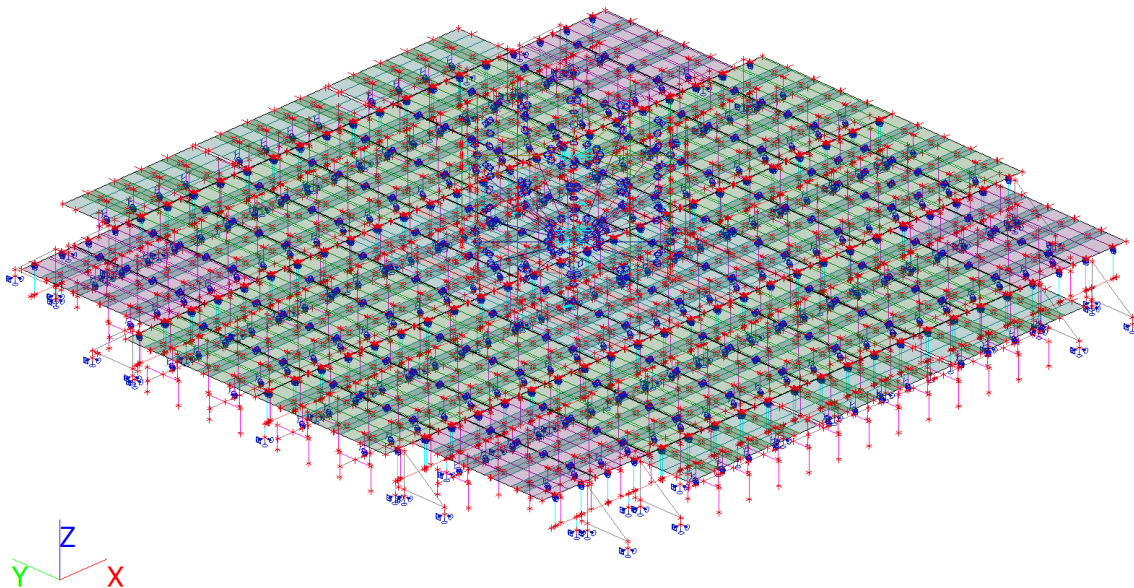


Fig. H-2: Elaborated analytical model with SPMTs and sea fastening

H.1.2 Structure

Inner frame

1. Analysis model

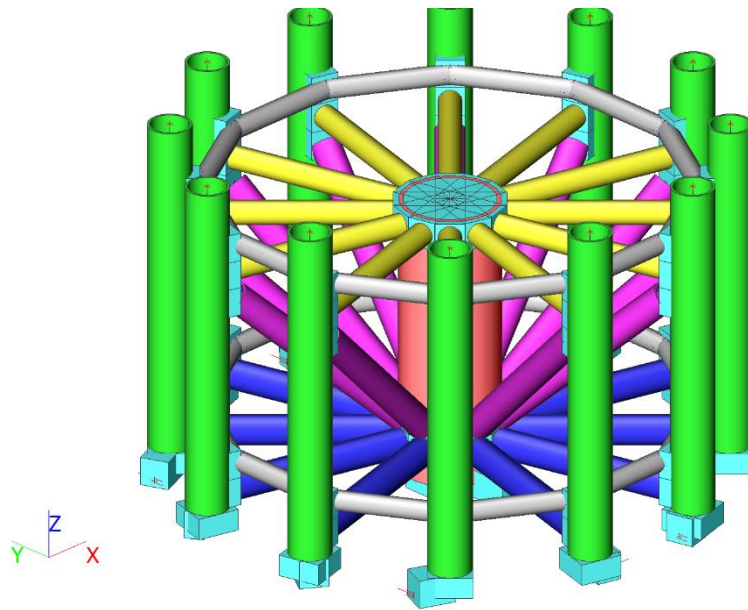


Fig. H-3: Elaborated concept inner frame model

2. Analysis model

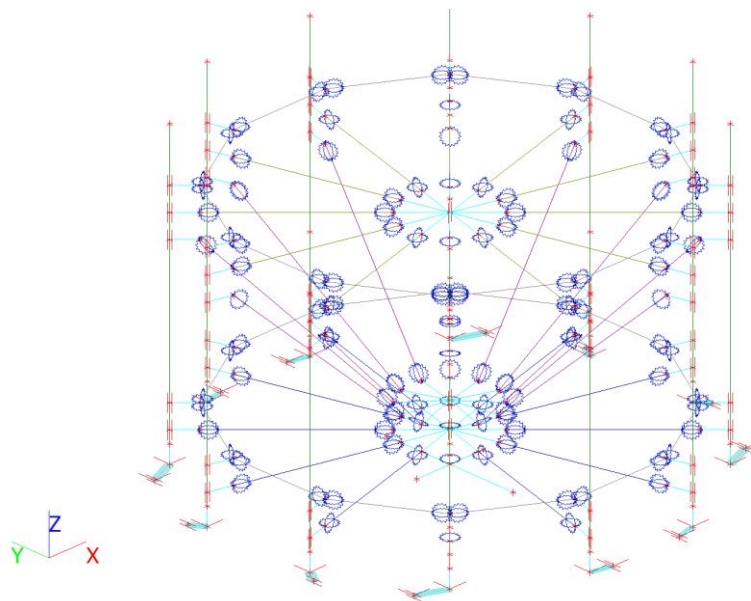
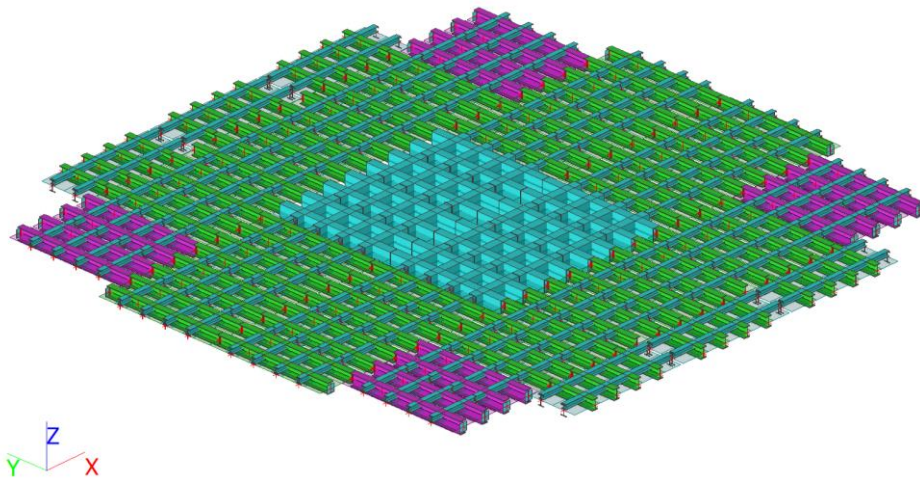
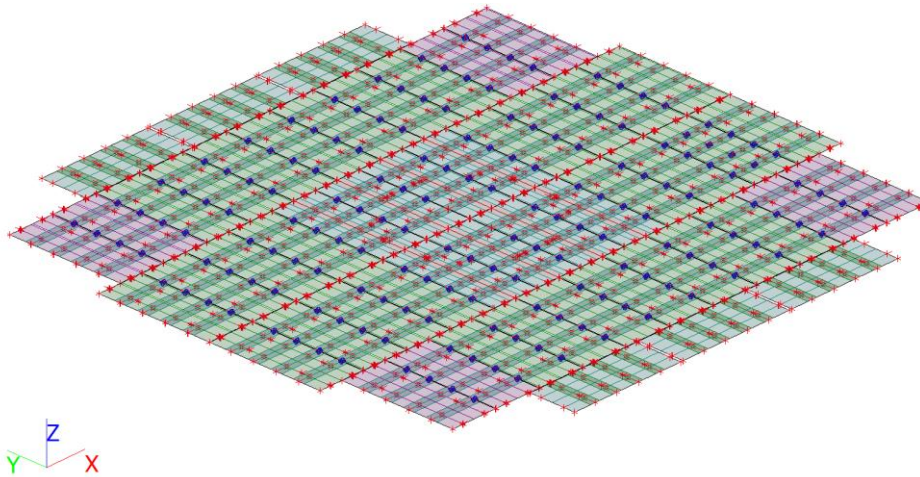


Fig. H-4 Elaborated concept analytical model

3. Cross-sections

Name	Type	Item material	Colour
Inner frame - Column 1	Tube (600; 35)	S 355	Green
Inner frame - Core	Tube (1370. 60)	S 355	Red
Inner frame - Brace 1	CHSCF406.4/20.0	S 355	Blue
Inner frame - Brace 2	CHS406.4/25.0	S 355	Purple
Inner frame - Brace 3	CHS323.9/20.0	S 355	Yellow
Inner frame - Brace 4	CHS273.0/16.5	S 355	Grey
Inner frame - DUMMY	Rectangle (400; 400)	DUMMY	Cyan
Inner frame - DUMMY 2	Rectangle (600; 600)	DUMMY	Light Blue

Floor**1. Analysis model / Steel data***Fig. H-5: Elaborated concept floor model***2. Analysis model / Steel data***Fig. H-6: Elaborated concept floor analytical model***3. Cross-sections**

Name	Type	Item material	Colour
Floor - Beam 1	HEB500	S 355	Green
Floor - Beam 2	HEB240	S 355	Teal
Floor - Beam 3	HEB600	S 355	Purple
Floor - Beam 4	HEB400	S 355	Red
Floor - Beam 5	RHS600/400/28.0	S 355	Dark Teal
Floor - DUMMY	Rectangle (400; 400)	DUMMY	Cyan

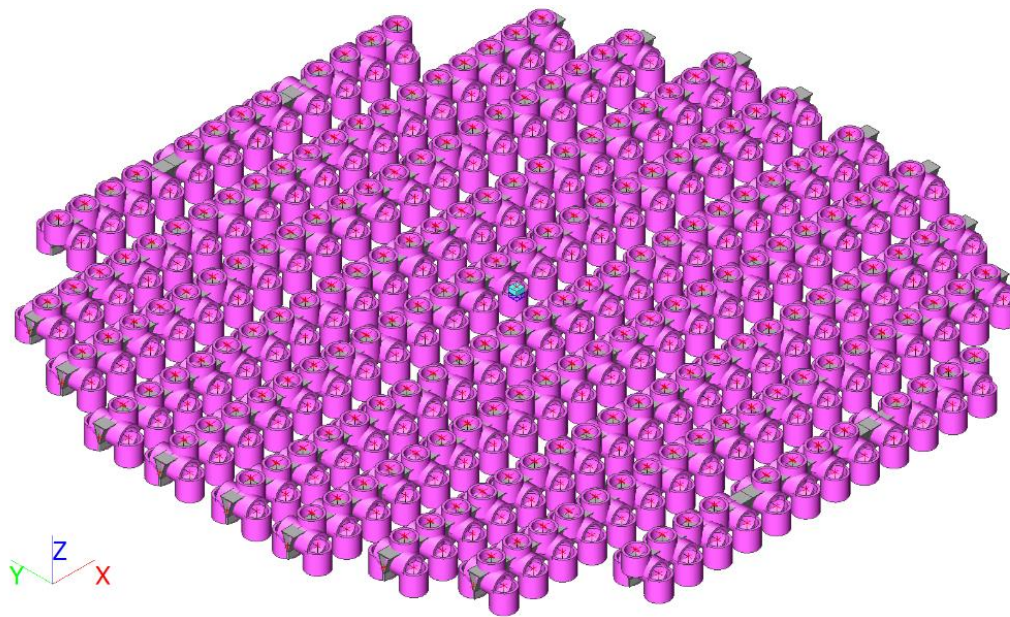
SPMT group**1. Analysis model / Steel data**

Fig. H-7: Elaborated concept SPMT setup model

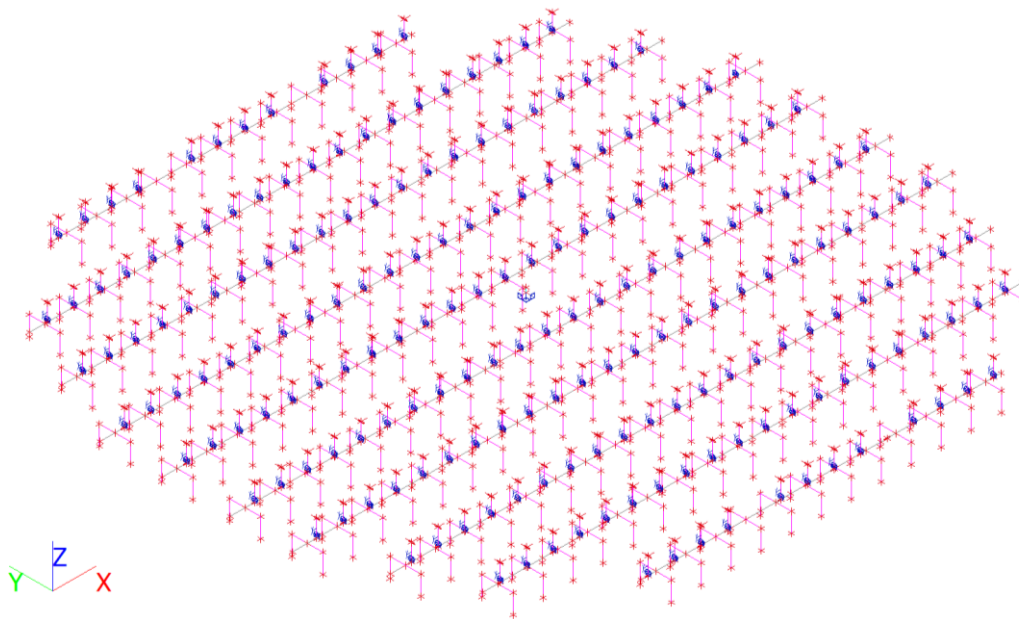
2. Analysis model / Steel data

Fig. H-8: Elaborated concept SPMT analytical model

3. Cross-sections

Name	Type	Item material	Colour
Detailed			
SPMT - Spine beam	General cross-section	S 690	■
SPMT - DUMMY	Tube 1000; 100	S 355	■
Floor - DUMMY	Rectangle 400; 400	DUMMY	■

Sea fastening

1. Analysis model / Steel data

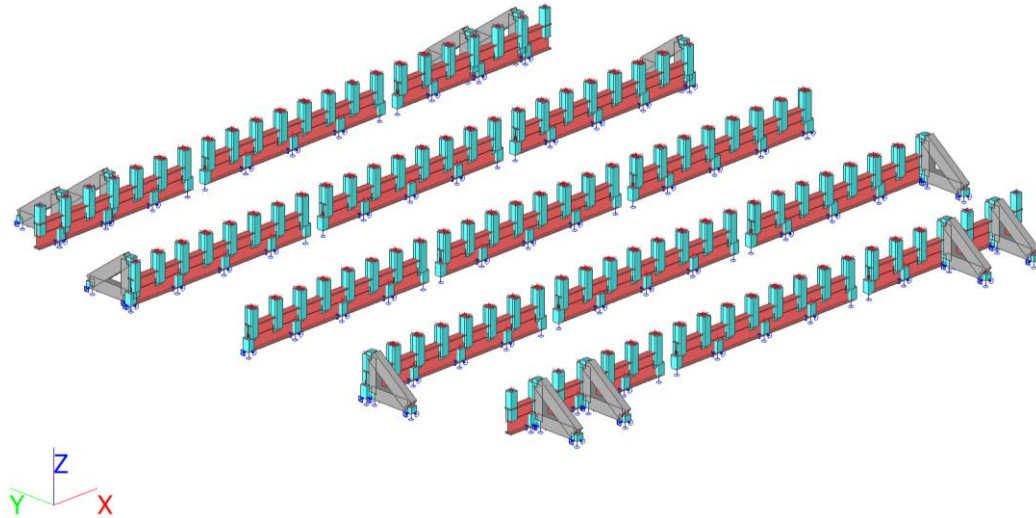


Fig. H-9: Elaborated concept sea fastening model

2. Analysis model / Steel data

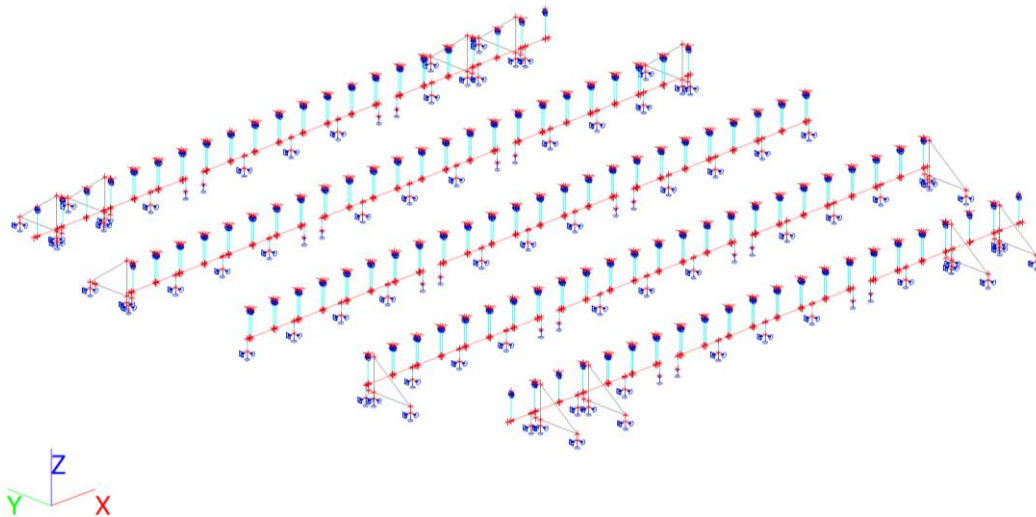



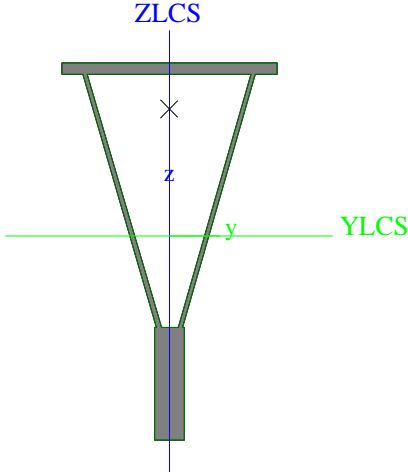
Fig. H-10: Elaborated concept sea fastening analytical model

3. Cross-sections


Name	Type	Item material	Colour
Sea fastening - DUMMY	Detailed		
	Rectangle	DUMMY	
	300; 300		
Sea fastening - Beam 1	HEB1000	S 355	
Sea fastening - Beam 2	RHS500/300/16.0	S 355	

H.1.3 Cross-sections

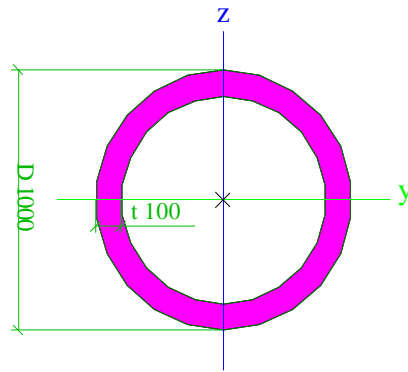
SPMT - Spine beam

Type	General cross-section	
Shape type	Thick-walled	
Item material	S 690	
Fabrication	general	
Colour		
Flexural buckling y-y, Flexural buckling z-z	d	d
A [mm ²]	6.285e+04	
A _y [mm ²], A _z [mm ²]	5.974e+04	2.689e+04
A _L [m ² /m], A _D [m ² /m]	2.9398e+00	4.8904e+00
C _{y,UCS} [mm], C _{z,UCS} [mm]	-1	45
I _{y,UCS} [mm ⁴], I _{z,UCS} [mm ⁴]	9.362e+09	9.673e+08
I _{yz,UCS} [mm ⁴]	1.088e+07	
α [deg]	-0.07	
I _y [mm ⁴], I _z [mm ⁴]	9.362e+09	9.673e+08
i _y [mm], i _z [mm]	386	124
W _{el,y} [mm ³], W _{el,z} [mm ³]	1.664e+07	3.221e+06
W _{pl,y} [mm ³], W _{pl,z} [mm ³]	2.256e+07	5.784e+06
M _{pl,y,+} [Nmm], M _{pl,y,-} [Nmm]	1.40e+10	1.40e+10
M _{pl,z,+} [Nmm], M _{pl,z,-} [Nmm]	3.60e+09	3.60e+09
d _y [mm], d _z [mm]	-1	347
I _t [mm ⁴], I _w [mm ⁶]	1.071e+09	9.840e+12
β _y [mm], β _z [mm]	-649	4
Picture		


SPMT - DUMMY

Type	Tube	
Detailed	1000; 100	
Shape type	Thick-walled	
Item material	S 355	
Fabrication	general	
Colour		
Flexural buckling y-y, Flexural buckling z-z	d	d
A [mm ²]	2.827e+05	
A _y [mm ²], A _z [mm ²]	1.921e+05	1.921e+05
A _L [m ² /m], A _D [m ² /m]	3.1414e+00	5.6546e+00
C _{y,UCS} [mm], C _{z,UCS} [mm]	500	500
α [deg]	0.00	
I _y [mm ⁴], I _z [mm ⁴]	2.898e+10	2.898e+10
i _y [mm], i _z [mm]	320	320
W _{el,y} [mm ³], W _{el,z} [mm ³]	5.796e+07	5.796e+07
W _{pl,y} [mm ³], W _{pl,z} [mm ³]	8.133e+07	8.133e+07
M _{pl,y,+} [Nmm], M _{pl,y,-} [Nmm]	2.89e+10	2.89e+10
M _{pl,z,+} [Nmm], M _{pl,z,-} [Nmm]	2.89e+10	2.89e+10
d _y [mm], d _z [mm]	0	0
I _t [mm ⁴], I _w [mm ⁶]	5.709e+10	2.335e+02
β _y [mm], β _z [mm]	0	0

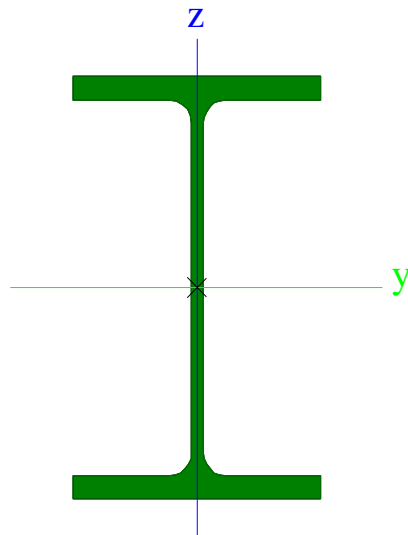
Picture




Floor - Beam 1

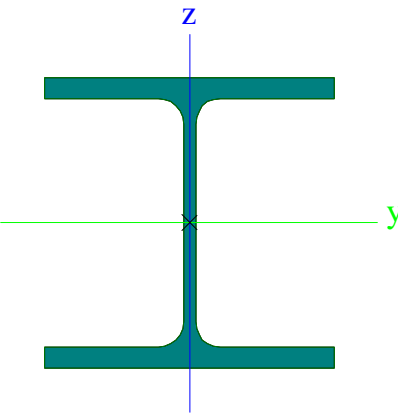
Type	HEB500	
Formcode	1 - I section	
Shape type	Thin walled	
Item material	S 355	
Fabrication	rolled	
Colour		
Flexural buckling y-y, Flexural buckling z-z	a	b
A [mm ²]	2.386e+04	
A _y [mm ²], A _z [mm ²]	1.616e+04	7.490e+03
A _L [m ² /m], A _D [m ² /m]	2.1300e+00	2.1244e+00
c _{y,UCS} [mm], c _{z,UCS} [mm]	150	250
α [deg]	0.00	
I _y [mm ⁴], I _z [mm ⁴]	1.072e+09	1.262e+08
i _y [mm], i _z [mm]	212	73
W _{el,y} [mm ³], W _{el,z} [mm ³]	4.287e+06	8.416e+05
W _{pl,y} [mm ³], W _{pl,z} [mm ³]	4.815e+06	1.292e+06
M _{pl,y,+} [Nmm], M _{pl,y,-} [Nmm]	1.71e+09	1.71e+09
M _{pl,z,+} [Nmm], M _{pl,z,-} [Nmm]	4.59e+08	4.59e+08
d _y [mm], d _z [mm]	0	0
I _t [mm ⁴], I _w [mm ⁶]	5.384e+06	7.018e+12
β _y [mm], β _z [mm]	0	0

Picture




Floor - Beam 2

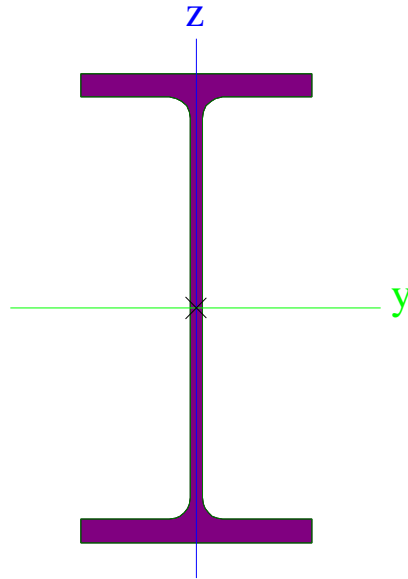
Type	HEB240	
Formcode	1 - I section	
Shape type	Thin walled	
Item material	S 355	
Fabrication	rolled	
Colour		
Flexural buckling y-y, Flexural buckling z-z	b	c
A [mm ²]	1.060e+04	
A _y [mm ²], A _z [mm ²]	7.822e+03	2.554e+03

A_L [m ² /m], A_D [m ² /m]	1.3800e+00	1.3838e+00
$c_{Y,UCS}$ [mm], $c_{Z,UCS}$ [mm]	120	120
α [deg]	0.00	
I_y [mm ⁴], I_z [mm ⁴]	1.126e+08	3.923e+07
i_y [mm], i_z [mm]	103	61
$W_{el,y}$ [mm ³], $W_{el,z}$ [mm ³]	9.383e+05	3.269e+05
$W_{pl,y}$ [mm ³], $W_{pl,z}$ [mm ³]	1.053e+06	4.984e+05
$M_{pl,y,+}$ [Nmm], $M_{pl,y,-}$ [Nmm]	3.74e+08	3.74e+08
$M_{pl,z,+}$ [Nmm], $M_{pl,z,-}$ [Nmm]	1.77e+08	1.77e+08
d_y [mm], d_z [mm]	0	0
I_t [mm ⁴], I_w [mm ⁶]	1.027e+06	4.869e+11
β_y [mm], β_z [mm]	0	0
Picture		


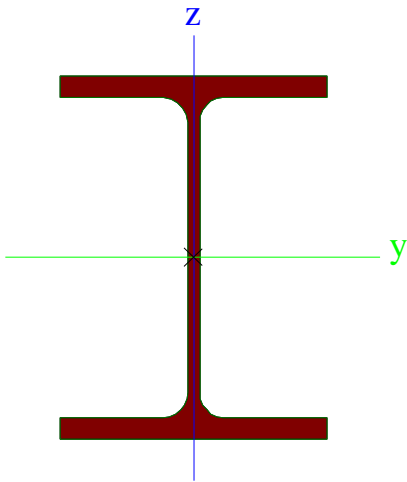
Floor - Beam 3

Type	HEB600	
Formcode	1 - I section	
Shape type	Thin walled	
Item material	S 355	
Fabrication	rolled	
Colour		
Flexural buckling y-y, Flexural buckling z-z	a	b
A [mm ²]	2.700e+04	
A_y [mm ²], A_z [mm ²]	1.756e+04	9.419e+03
A_L [m ² /m], A_D [m ² /m]	2.3200e+00	2.3224e+00
$c_{Y,UCS}$ [mm], $c_{Z,UCS}$ [mm]	150	300
α [deg]	0.00	
I_y [mm ⁴], I_z [mm ⁴]	1.710e+09	1.353e+08
i_y [mm], i_z [mm]	252	71
$W_{el,y}$ [mm ³], $W_{el,z}$ [mm ³]	5.701e+06	9.020e+05
$W_{pl,y}$ [mm ³], $W_{pl,z}$ [mm ³]	6.425e+06	1.391e+06
$M_{pl,y,+}$ [Nmm], $M_{pl,y,-}$ [Nmm]	2.28e+09	2.28e+09
$M_{pl,z,+}$ [Nmm], $M_{pl,z,-}$ [Nmm]	4.94e+08	4.94e+08
d_y [mm], d_z [mm]	0	0
I_t [mm ⁴], I_w [mm ⁶]	6.672e+06	1.097e+13
β_y [mm], β_z [mm]	0	0

Picture


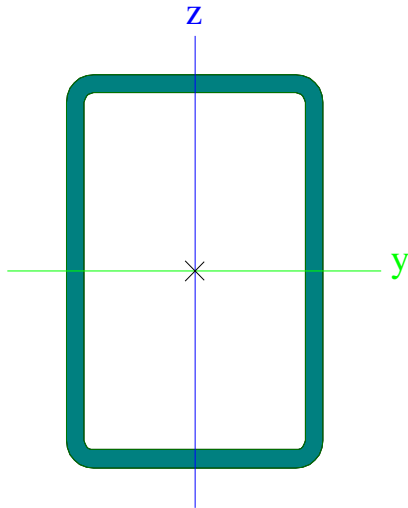



Floor - Beam 4

Type	HEB400	
Formcode	1 - I section	
Shape type	Thin walled	
Item material	S 355	
Fabrication	rolled	
Colour		
Flexural buckling y-y, Flexural buckling z-z	a	b
A [mm ²]	1.978e+04	
A _y [mm ²], A _z [mm ²]	1.387e+04	5.648e+03
A _L [m ² /m], A _D [m ² /m]	1.9300e+00	1.9264e+00
c _{y,UCS} [mm], c _{z,UCS} [mm]	150	200
α [deg]	0.00	
I _y [mm ⁴], I _z [mm ⁴]	5.768e+08	1.082e+08
i _y [mm], i _z [mm]	171	74
W _{el,y} [mm ³], W _{el,z} [mm ³]	2.884e+06	7.213e+05
W _{pl,y} [mm ³], W _{pl,z} [mm ³]	3.232e+06	1.104e+06
M _{pl,y,+} [Nmm], M _{pl,y,-} [Nmm]	1.15e+09	1.15e+09
M _{pl,z,+} [Nmm], M _{pl,z,-} [Nmm]	3.92e+08	3.92e+08
d _y [mm], d _z [mm]	0	0
I _t [mm ⁴], I _w [mm ⁶]	3.557e+06	3.817e+12
β _y [mm], β _z [mm]	0	0
Picture		

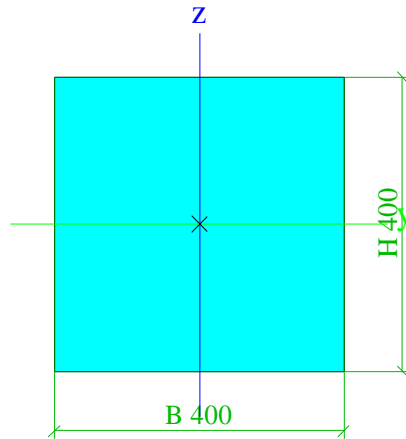
Floor - Beam 5

Type	RHS600/400/28.0	
Formcode	2 - Rectangular hollow section	


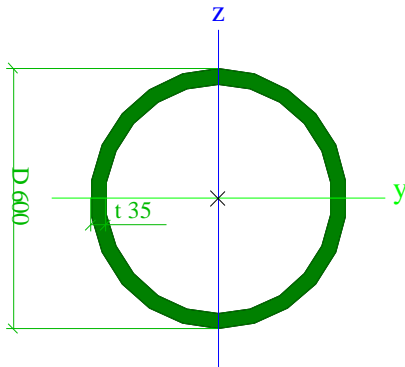
Shape type	Thin walled	
Item material	S 355	
Fabrication	rolled	
Colour		
Flexural buckling y-y, Flexural buckling z-z	a	a
A [mm²]	5.080e+04	
A _y [mm²], A _z [mm²]	2.060e+04	3.090e+04
A _L [m²/m], A _D [m²/m]	1.9276e+00	3.6794e+00
c _{y,UCS} [mm], c _{z,UCS} [mm]	200	300
α [deg]	0.00	
I _y [mm⁴], I _z [mm⁴]	2.467e+09	1.303e+09
i _y [mm], i _z [mm]	220	160
W _{el,y} [mm³], W _{el,z} [mm³]	8.224e+06	6.517e+06
W _{pl,y} [mm³], W _{pl,z} [mm³]	1.015e+07	7.641e+06
M _{pl,y,+} [Nmm], M _{pl,y,-} [Nmm]	3.60e+09	3.60e+09
M _{pl,z,+} [Nmm], M _{pl,z,-} [Nmm]	2.71e+09	2.71e+09
d _y [mm], d _z [mm]	0	0
I _t [mm⁴], I _w [mm⁶]	2.700e+09	6.720e+13
β _y [mm], β _z [mm]	0	0
Picture		

Floor - DUMMY		
Type	Rectangle	
Detailed	400; 400	
Shape type	Thick-walled	
Item material	DUMMY	
Fabrication	general	
Colour		
Flexural buckling y-y, Flexural buckling z-z	d	d
A [mm²]	1.600e+05	
A _y [mm²], A _z [mm²]	1.335e+05	1.335e+05
A _L [m²/m], A _D [m²/m]	1.6000e+00	1.6000e+00
c _{y,UCS} [mm], c _{z,UCS} [mm]	200	200
α [deg]	0.00	
I _y [mm⁴], I _z [mm⁴]	2.133e+09	2.133e+09
i _y [mm], i _z [mm]	115	115
W _{el,y} [mm³], W _{el,z} [mm³]	1.067e+07	1.067e+07
W _{pl,y} [mm³], W _{pl,z} [mm³]	1.600e+07	1.600e+07
M _{pl,y,+} [Nmm], M _{pl,y,-} [Nmm]	5.68e+09	5.68e+09
M _{pl,z,+} [Nmm], M _{pl,z,-} [Nmm]	5.68e+09	5.68e+09
d _y [mm], d _z [mm]	0	0
I _t [mm⁴], I _w [mm⁶]	3.594e+09	5.166e+11
β _y [mm], β _z [mm]	0	0


Picture

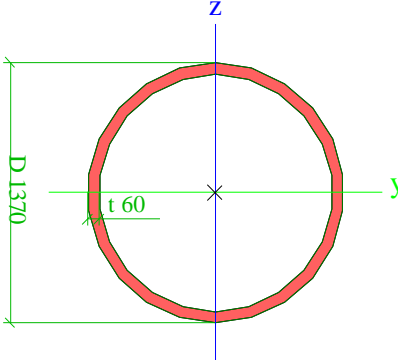



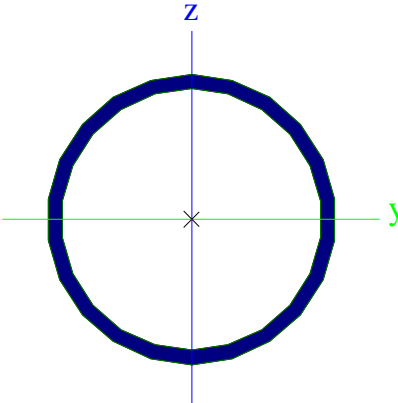
Inner frame - Column 1


Type	Tube	
Detailed	600; 35	
Shape type	Thick-walled	
Item material	S 355	
Fabrication	general	
Colour		
Flexural buckling y-y, Flexural buckling z-z	d	d
A [mm ²]	6.212e+04	
A _y [mm ²], A _z [mm ²]	4.147e+04	4.147e+04
A _L [m ² /m], A _D [m ² /m]	1.8849e+00	3.5498e+00
C _{y,UCS} [mm], C _{z,UCS} [mm]	300	300
α [deg]	0.00	
I _y [mm ⁴], I _z [mm ⁴]	2.488e+09	2.488e+09
i _y [mm], i _z [mm]	200	200
W _{el,y} [mm ³], W _{el,z} [mm ³]	8.295e+06	8.295e+06
W _{pl,y} [mm ³], W _{pl,z} [mm ³]	1.119e+07	1.119e+07
M _{pl,y,+} [Nmm], M _{pl,y,-} [Nmm]	3.97e+09	3.97e+09
M _{pl,z,+} [Nmm], M _{pl,z,-} [Nmm]	3.97e+09	3.97e+09
d _y [mm], d _z [mm]	0	0
I _t [mm ⁴], I _w [mm ⁶]	4.784e+09	8.834e+02
β _y [mm], β _z [mm]	0	0
Picture		

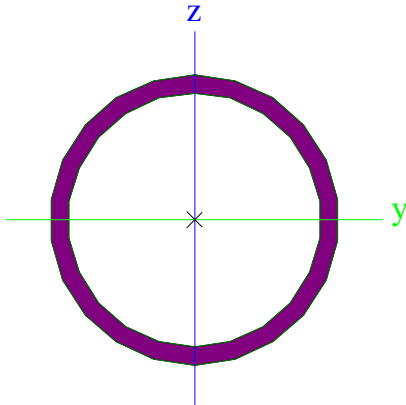
Inner frame - Core


Type	Tube	
Detailed	1370; 60	
Shape type	Thick-walled	
Item material	S 355	
Fabrication	general	
Colour		
Flexural buckling y-y, Flexural buckling z-z	d	d
A [mm ²]	2.469e+05	
A _y [mm ²], A _z [mm ²]	1.651e+05	1.651e+05
A _L [m ² /m], A _D [m ² /m]	4.3038e+00	8.2306e+00
C _{y,UCS} [mm], C _{z,UCS} [mm]	685	685
α [deg]	0.00	
I _y [mm ⁴], I _z [mm ⁴]	5.308e+10	5.308e+10

i_y [mm], i_z [mm]	464	464
$W_{el,y}$ [mm ³], $W_{el,z}$ [mm ³]	7.749e+07	7.749e+07
$W_{pl,y}$ [mm ³], $W_{pl,z}$ [mm ³]	1.030e+08	1.030e+08
$M_{pl,y,+}$ [Nmm], $M_{pl,y,-}$ [Nmm]	3.66e+10	3.66e+10
$M_{pl,z,+}$ [Nmm], $M_{pl,z,-}$ [Nmm]	3.66e+10	3.66e+10
d_y [mm], d_z [mm]	0	0
I_t [mm ⁴], I_w [mm ⁶]	1.040e+11	1.203e+02
β_y [mm], β_z [mm]	0	0
Picture		

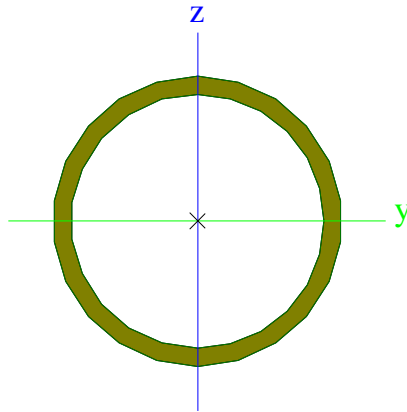
Inner frame - Brace 1		
Type	CHSCF406.4/20.0	
Formcode	3 - Circular hollow section	
Shape type	Thin walled	
Item material	S 355	
Fabrication	cold formed	
Colour		
Flexural buckling y-y, Flexural buckling z-z	c	c
A [mm ²]	2.430e+04	
A_y [mm ²], A_z [mm ²]	1.546e+04	1.546e+04
A_L [m ² /m], A_D [m ² /m]	1.2800e+00	2.4277e+00
$C_{Y,UCS}$ [mm], $C_{Z,UCS}$ [mm]	203	203
α [deg]	0.00	
I_y [mm ⁴], I_z [mm ⁴]	4.543e+08	4.543e+08
i_y [mm], i_z [mm]	137	137
$W_{el,y}$ [mm ³], $W_{el,z}$ [mm ³]	2.236e+06	2.236e+06
$W_{pl,y}$ [mm ³], $W_{pl,z}$ [mm ³]	2.942e+06	2.942e+06
$M_{pl,y,+}$ [Nmm], $M_{pl,y,-}$ [Nmm]	1.06e+09	1.06e+09
$M_{pl,z,+}$ [Nmm], $M_{pl,z,-}$ [Nmm]	1.06e+09	1.06e+09
d_y [mm], d_z [mm]	0	0
I_t [mm ⁴], I_w [mm ⁶]	9.086e+08	2.434e-20
β_y [mm], β_z [mm]	0	0
Picture		

Inner frame - Brace 2		
Type	CHS406.4/25.0	
Formcode	3 - Circular hollow section	
Shape type	Thin walled	
Item material	S 355	
Fabrication	rolled	
Colour		


Flexural buckling y-y, Flexural buckling z-z	a	a
A [mm²]	3.000e+04	
A _y [mm²], A _z [mm²]	1.907e+04	1.907e+04
A _L [m²/m], A _D [m²/m]	1.2800e+00	2.3963e+00
c _{y,UCS} [mm], c _{z,UCS} [mm]	203	203
α [deg]	0.00	
I _y [mm⁴], I _z [mm⁴]	5.470e+08	5.470e+08
i _y [mm], i _z [mm]	135	135
W _{el,y} [mm³], W _{el,z} [mm³]	2.692e+06	2.692e+06
W _{pl,y} [mm³], W _{pl,z} [mm³]	3.584e+06	3.584e+06
M _{pl,y,+} [Nmm], M _{pl,y,-} [Nmm]	1.29e+09	1.29e+09
M _{pl,z,+} [Nmm], M _{pl,z,-} [Nmm]	1.29e+09	1.29e+09
d _y [mm], d _z [mm]	0	0
I _t [mm⁴], I _w [mm⁶]	1.094e+09	1.906e-20
β _y [mm], β _z [mm]	0	0
Picture		

Inner frame - Brace 3		
Type	CHS323.9/20.0	
Formcode	3 - Circular hollow section	
Shape type	Thin walled	
Item material	S 355	
Fabrication	rolled	
Colour		
Flexural buckling y-y, Flexural buckling z-z	a	a
A [mm²]	1.910e+04	
A _y [mm²], A _z [mm²]	1.216e+04	1.216e+04
A _L [m²/m], A _D [m²/m]	1.0200e+00	1.9094e+00
c _{y,UCS} [mm], c _{z,UCS} [mm]	162	162
α [deg]	0.00	
I _y [mm⁴], I _z [mm⁴]	2.214e+08	2.214e+08
i _y [mm], i _z [mm]	108	108
W _{el,y} [mm³], W _{el,z} [mm³]	1.367e+06	1.367e+06
W _{pl,y} [mm³], W _{pl,z} [mm³]	1.821e+06	1.821e+06
M _{pl,y,+} [Nmm], M _{pl,y,-} [Nmm]	6.56e+08	6.56e+08
M _{pl,z,+} [Nmm], M _{pl,z,-} [Nmm]	6.56e+08	6.56e+08
d _y [mm], d _z [mm]	0	0
I _t [mm⁴], I _w [mm⁶]	4.428e+08	8.689e-21
β _y [mm], β _z [mm]	0	0

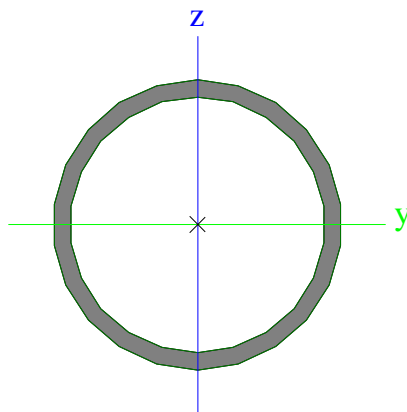
Picture



Inner frame - Brace 4

Type	CHS273.0/16.0	
Formcode	3 - Circular hollow section	
Shape type	Thin walled	
Item material	S 355	
Fabrication	rolled	
Colour		
Flexural buckling y-y, Flexural buckling z-z	a	a
A [mm ²]	1.290e+04	
A _y [mm ²], A _z [mm ²]	8.224e+03	8.224e+03
A _L [m ² /m], A _D [m ² /m]	8.5800e-01	1.6147e+00
c _{y,UCS} [mm], c _{z,UCS} [mm]	137	137
α [deg]	0.00	
I _y [mm ⁴], I _z [mm ⁴]	1.071e+08	1.071e+08
i _y [mm], i _z [mm]	91	91
W _{el,y} [mm ³], W _{el,z} [mm ³]	7.840e+05	7.840e+05
W _{pl,y} [mm ³], W _{pl,z} [mm ³]	1.041e+06	1.041e+06
M _{pl,y,+} [Nmm], M _{pl,y,-} [Nmm]	3.76e+08	3.76e+08
M _{pl,z,+} [Nmm], M _{pl,z,-} [Nmm]	3.76e+08	3.76e+08
d _y [mm], d _z [mm]	0	0
I _t [mm ⁴], I _w [mm ⁶]	2.141e+08	5.332e-21
β _y [mm], β _z [mm]	0	0

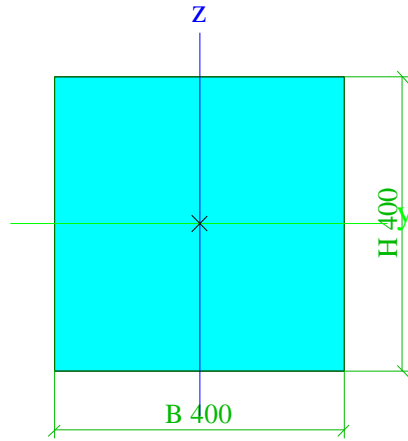
Picture




Inner frame - DUMMY

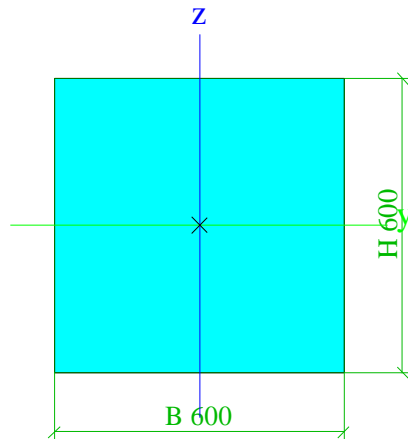
Type	Rectangle	
Detailed	400; 400	
Shape type	Thick-walled	
Item material	DUMMY	
Fabrication	general	
Colour		
Flexural buckling y-y, Flexural buckling z-z	d	d
A [mm ²]	1.600e+05	
A _y [mm ²], A _z [mm ²]	1.335e+05	1.335e+05
A _L [m ² /m], A _D [m ² /m]	1.6000e+00	1.6000e+00
c _{y,UCS} [mm], c _{z,UCS} [mm]	200	200
α [deg]	0.00	

I_y [mm ⁴], I_z [mm ⁴]	2.133e+09	2.133e+09
i_y [mm], i_z [mm]	115	115
$W_{el,y}$ [mm ³], $W_{el,z}$ [mm ³]	1.067e+07	1.067e+07
$W_{pl,y}$ [mm ³], $W_{pl,z}$ [mm ³]	1.600e+07	1.600e+07
$M_{pl,y,+}$ [Nmm], $M_{pl,y,-}$ [Nmm]	5.68e+09	5.68e+09
$M_{pl,z,+}$ [Nmm], $M_{pl,z,-}$ [Nmm]	5.68e+09	5.68e+09
d_y [mm], d_z [mm]	0	0
I_t [mm ⁴], I_w [mm ⁶]	3.594e+09	5.166e+11
β_y [mm], β_z [mm]	0	0
Picture		




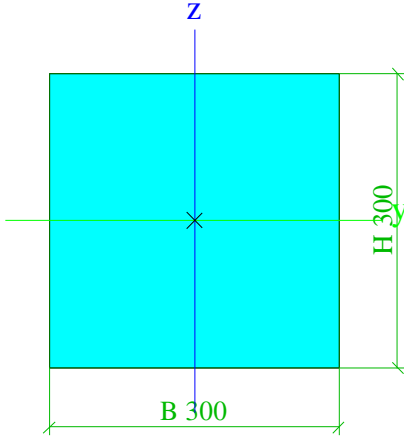
Inner frame - DUMMY 2

Type	Rectangle	
Detailed	600; 600	
Shape type	Thick-walled	
Item material	DUMMY	
Fabrication	general	
Colour		
Flexural buckling y-y, Flexural buckling z-z	d	d
A [mm ²]	3.600e+05	
A_y [mm ²], A_z [mm ²]	3.004e+05	3.004e+05
A_L [m ² /m], A_D [m ² /m]	2.4000e+00	2.4000e+00
$c_{y,UCS}$ [mm], $c_{z,UCS}$ [mm]	300	300
α [deg]	0.00	
I_y [mm ⁴], I_z [mm ⁴]	1.080e+10	1.080e+10
i_y [mm], i_z [mm]	173	173
$W_{el,y}$ [mm ³], $W_{el,z}$ [mm ³]	3.600e+07	3.600e+07
$W_{pl,y}$ [mm ³], $W_{pl,z}$ [mm ³]	5.400e+07	5.400e+07
$M_{pl,y,+}$ [Nmm], $M_{pl,y,-}$ [Nmm]	1.92e+10	1.92e+10
$M_{pl,z,+}$ [Nmm], $M_{pl,z,-}$ [Nmm]	1.92e+10	1.92e+10
d_y [mm], d_z [mm]	0	0
I_t [mm ⁴], I_w [mm ⁶]	1.819e+10	5.833e+12
β_y [mm], β_z [mm]	0	0
Picture		




Sea fastening - DUMMY

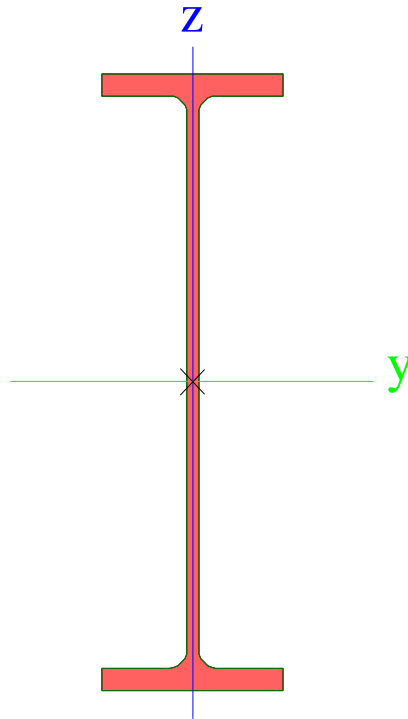
Type	Rectangle	
------	-----------	--

Detailed	300; 300	
Shape type	Thick-walled	
Item material	DUMMY	
Fabrication	general	
Colour		
Flexural buckling y-y, Flexural buckling z-z	d	d
A [mm ²]	9.000e+04	
A _y [mm ²], A _z [mm ²]	7.509e+04	7.509e+04
A _L [m ² /m], A _D [m ² /m]	1.2000e+00	1.2000e+00
C _{y,UCS} [mm], C _{z,UCS} [mm]	150	150
α [deg]	0.00	
I _y [mm ⁴], I _z [mm ⁴]	6.750e+08	6.750e+08
i _y [mm], i _z [mm]	87	87
W _{el,y} [mm ³], W _{el,z} [mm ³]	4.500e+06	4.500e+06
W _{pl,y} [mm ³], W _{pl,z} [mm ³]	6.750e+06	6.750e+06
M _{pl,y+} [Nmm], M _{pl,y-} [Nmm]	2.40e+09	2.40e+09
M _{pl,z+} [Nmm], M _{pl,z-} [Nmm]	2.40e+09	2.40e+09
d _y [mm], d _z [mm]	0	0
I _t [mm ⁴], I _w [mm ⁶]	1.137e+09	9.114e+10
β _y [mm], β _z [mm]	0	0
Picture		


Sea fastening - Beam 1

Type	HEB1000	
Formcode	1 - I section	
Shape type	Thin walled	
Item material	S 355	
Fabrication	rolled	
Colour		
Flexural buckling y-y, Flexural buckling z-z	a	b
A [mm ²]	4.000e+04	
A _y [mm ²], A _z [mm ²]	2.228e+04	1.904e+04
A _L [m ² /m], A _D [m ² /m]	3.1100e+00	3.1103e+00
C _{y,UCS} [mm], C _{z,UCS} [mm]	150	500
α [deg]	0.00	
I _y [mm ⁴], I _z [mm ⁴]	6.447e+09	1.628e+08
i _y [mm], i _z [mm]	401	64
W _{el,y} [mm ³], W _{el,z} [mm ³]	1.289e+07	1.085e+06
W _{pl,y} [mm ³], W _{pl,z} [mm ³]	1.486e+07	1.716e+06
M _{pl,y+} [Nmm], M _{pl,y-} [Nmm]	5.28e+09	5.28e+09
M _{pl,z+} [Nmm], M _{pl,z-} [Nmm]	6.09e+08	6.09e+08
d _y [mm], d _z [mm]	0	0
I _t [mm ⁴], I _w [mm ⁶]	1.254e+07	3.764e+13
β _y [mm], β _z [mm]	0	0

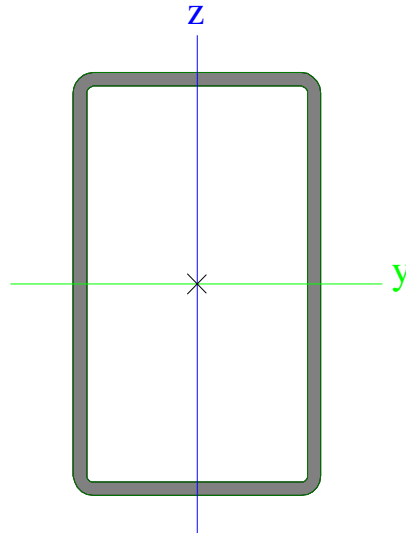
Picture



Sea fastening - Beam 2

Type	RHS500/300/16.0	
Formcode	2 - Rectangular hollow section	
Shape type	Thin walled	
Item material	S 355	
Fabrication	rolled	
Colour		
Flexural buckling y-y, Flexural buckling z-z	a	a
A [mm ²]	2.430e+04	
A _y [mm ²], A _z [mm ²]	9.048e+03	1.508e+04
A _L [m ² /m], A _D [m ² /m]	1.5600e+00	3.0168e+00
c _{y,UCS} [mm], c _{z,UCS} [mm]	150	250
α [deg]	0.00	
I _y [mm ⁴], I _z [mm ⁴]	8.178e+08	3.677e+08
i _y [mm], i _z [mm]	183	123
W _{el,y} [mm ³], W _{el,z} [mm ³]	3.271e+06	2.451e+06
W _{pl,y} [mm ³], W _{pl,z} [mm ³]	3.965e+06	2.781e+06
M _{pl,y,+} [Nmm], M _{pl,y,-} [Nmm]	1.41e+09	1.41e+09
M _{pl,z,+} [Nmm], M _{pl,z,-} [Nmm]	9.87e+08	9.87e+08
d _y [mm], d _z [mm]	0	0
I _t [mm ⁴], I _w [mm ⁶]	8.033e+08	1.200e+13
β _y [mm], β _z [mm]	0	0

Picture



Explanations of symbols	
A	Area
A_y	Shear Area in principal y-direction - Calculated by 2D FEM analysis
A_z	Shear Area in principal z-direction - Calculated by 2D FEM analysis
A_L	Circumference per unit length
A_D	Drying surface per unit length
$C_{Y,UCS}$	Centroid coordinate in Y-direction of Input axis system
$C_{Z,UCS}$	Centroid coordinate in Z-direction of Input axis system
$I_{Y,LCS}$	Second moment of area about the YLCS axis
$I_{Z,LCS}$	Second moment of area about the ZLCS axis
$I_{YZ,LCS}$	Product moment of area in the LCS system
α	Rotation angle of the principal axis system
I_y	Second moment of area about the principal y-axis
I_z	Second moment of area about the principal z-axis
i_y	Radius of gyration about the principal y-axis
i_z	Radius of gyration about the principal z-axis
$W_{el,y}$	Elastic section modulus about the principal y-axis
$W_{el,z}$	Elastic section modulus about the principal z-axis
$W_{pl,y}$	Plastic section modulus about the principal y-axis
$W_{pl,z}$	Plastic section modulus about the principal z-axis
$M_{pl,y,+}$	Plastic moment about the principal y-axis for a positive M_y moment
$M_{pl,y,-}$	Plastic moment about the principal y-axis for a negative M_y moment
$M_{pl,z,+}$	Plastic moment about the principal z-axis for a positive M_z moment
$M_{pl,z,-}$	Plastic moment about the principal z-axis for a negative M_z moment
d_y	Shear center coordinate in principal y-direction measured from the centroid - Calculated by 2D FEM analysis
d_z	Shear center coordinate in principal z-direction measured from the centroid - Calculated by 2D FEM analysis
I_t	Torsional constant - Calculated by 2D FEM analysis
I_w	Warping constant - Calculated by 2D FEM analysis
β_y	Mono-symmetry constant about the principal y-axis
β_z	Mono-symmetry constant about the principal z-axis

H.1.4 Materials

Steel EC3

Name	ρ [t/m ³]	E mod [MPa]	Poisson - nu	F_y [N/mm ²]	F_u [N/mm ²]
S 690	7.9	2.1000e+05	0.3	622	770
S 355	7.9	2.1000e+05	0.3	355	510
DUMMY	0.0	2.1000e+05	0.3	1000	1000

H.1.5 Load cases

Name	Description	Action type	Load group	Sum load X	Sum load Y	Sum load Z
	Spec	Load type		[kN]	[kN]	[kN]
LC1	Self-weight - Floor and Carousel	Permanent	LG1	0	0	-4095
		Standard				
LC2	SPMT support	Permanent	LG1	0	0	52320
		Standard				
LC3	Payload	Permanent	LG1	0	0	-49014
		Standard				
LC4	Self-weight - Sea fastening	Permanent	LG2	0	0	-501
		Standard				
LC5	Pitch - Self weight	Permanent	LG2	789	0	0
		Standard				
LC6	Pitch - Self weight grillage	Permanent	LG2	100	0	0
		Standard				
LC7	Pitch - Payload	Permanent	LG2	10000	0	0
		Standard				
LC8	Roll - Self weight	Permanent	LG2	0	2048	0
		Standard				
LC9	Roll - Self weight grillage	Permanent	LG2	0	251	0
		Standard				
LC10	Roll - Payload	Permanent	LG2	0	25000	0
		Standard				

H.1.6 Nonlinear combinations

Name	Description	Type	Load cases	Coeff. [-]
NC1 - SPMT	SLS	Serviceability	LC1 - Self weight - Floor and Carousel	1.00
			LC2 - SPMT support	1.00
			LC3 - Payload	1.00
NC2 - SPMT	ULS	Ultimate	LC1 - Self weight - Floor and Carousel	1.50
			LC2 - SPMT support	1.50
			LC3 - Payload	1.50
NC1	SLS	Serviceability	LC1 - Self weight - Floor and Carousel	0.76
			LC3 - Payload	0.69
			LC4 - Self weight - Sea fastening	0.76
			LC5 - Pitch - Self weight	1.00
			LC6 - Pitch - Self weight grillage	1.00
			LC7 - Pitch - Payload	1.00
			LC8 - Roll - Self weight	0.00
			LC9 - Roll - Self weight grillage	0.00
			LC10 - Roll - Payload	0.00
NC2	SLS	Serviceability	LC1 - Self weight - Floor and Carousel	0.76
			LC3 - Payload	0.69
			LC4 - Self weight - Sea fastening	0.76
			LC5 - Pitch - Self weight	0.00
			LC6 - Pitch - Self weight grillage	0.00
			LC7 - Pitch - Payload	0.00
			LC8 - Roll - Self weight	1.00
			LC9 - Roll - Self weight grillage	1.00
			LC10 - Roll - Payload	1.00
NC3	SLS	Serviceability	LC1 - Self weight - Floor and Carousel	1.44
			LC3 - Payload	1.31
			LC4 - Self weight - Sea fastening	1.44
			LC5 - Pitch - Self weight	1.00
			LC6 - Pitch - Self weight grillage	1.00
			LC7 - Pitch - Payload	1.00
			LC8 - Roll - Self weight	0.00

Name	Description	Type	Load cases	Coeff. [-]
NC4	SLS	Serviceability	LC9 - Roll - Self weight grillage	0.00
			LC10 - Roll - Payload	0.00
			LC1 - Self weight - Floor and Carousel	1.44
			LC3 - Payload	1.31
			LC4 - Self weight - Sea fastening	1.44
			LC5 - Pitch - Self weight	0.00
			LC6 - Pitch - Self weight grillage	0.00
			LC7 - Pitch - Payload	0.00
			LC8 - Roll - Self weight	1.00
			LC9 - Roll - Self weight grillage	1.00
NC5	ULS	Ultimate	LC10 - Roll - Payload	1.00
			LC1 - Self weight - Floor and Carousel	1.15
			LC3 - Payload	1.04
			LC4 - Self weight - Sea fastening	1.15
			LC5 - Pitch - Self weight	1.65
			LC6 - Pitch - Self weight grillage	1.65
			LC7 - Pitch - Payload	1.50
			LC8 - Roll - Self weight	0.00
			LC9 - Roll - Self weight grillage	0.00
			LC10 - Roll - Payload	0.00
NC6	ULS	Ultimate	LC1 - Self weight - Floor and Carousel	1.15
			LC3 - Payload	1.04
			LC4 - Self weight - Sea fastening	1.15
			LC5 - Pitch - Self weight	0.00
			LC6 - Pitch - Self weight grillage	0.00
			LC7 - Pitch - Payload	0.00
			LC8 - Roll - Self weight	1.65
			LC9 - Roll - Self weight grillage	1.65
			LC10 - Roll - Payload	1.50
NC7	ULS	Ultimate	LC1 - Self weight - Floor and Carousel	2.15
			LC3 - Payload	1.96
			LC4 - Self weight - Sea fastening	2.15
			LC5 - Pitch - Self weight	1.65
			LC6 - Pitch - Self weight grillage	1.65
			LC7 - Pitch - Payload	1.50
			LC8 - Roll - Self weight	0.00
			LC9 - Roll - Self weight grillage	0.00
			LC10 - Roll - Payload	0.00
NC8	ULS	Ultimate	LC1 - Self weight - Floor and Carousel	2.15
			LC3 - Payload	1.96
			LC4 - Self weight - Sea fastening	2.15
			LC5 - Pitch - Self weight	0.00
			LC6 - Pitch - Self weight grillage	0.00
			LC7 - Pitch - Payload	0.00
			LC8 - Roll - Self weight	1.65
			LC9 - Roll - Self weight grillage	1.65
			LC10 - Roll - Payload	1.50

H.2 Results SPMT transport without grillage frame

H.2.1 SLS

Reactions

Nonlinear calculation
NonLinear Combi: NC1 - SPMT
System: Global
Extreme: Global
Selection: All
Nodal reactions

Name	Case	R _x [kN]	R _y [kN]	R _z [kN]	M _x [kNm]	M _y [kNm]	M _z [kNm]
Sn96/N40609	NC1 - SPMT	0	0	-36	1	-4	0

3D displacement; U_{total}

Values: **U_{total}**
Nonlinear calculation
NonLinear Combi: NC1 - SPMT
Selection: All
Location: In nodes avg.. System:
Global

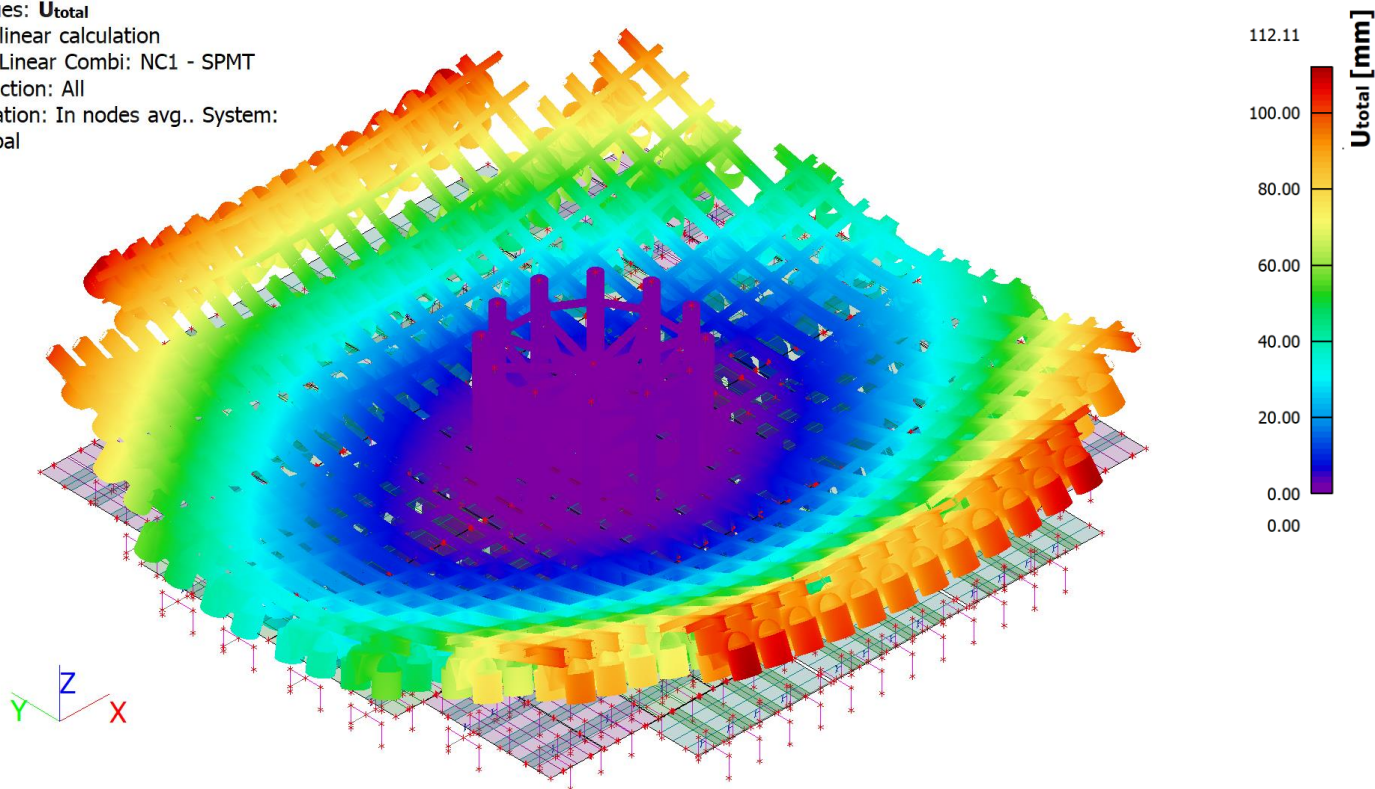


Fig. H-11: Elaborated concept SPMT transport, total deformation

3D displacement; u_z

Values: u_z
Nonlinear calculation
NonLinear Combi: NC1 - SPMT
Selection: All
Location: In nodes avg.. System:
Global

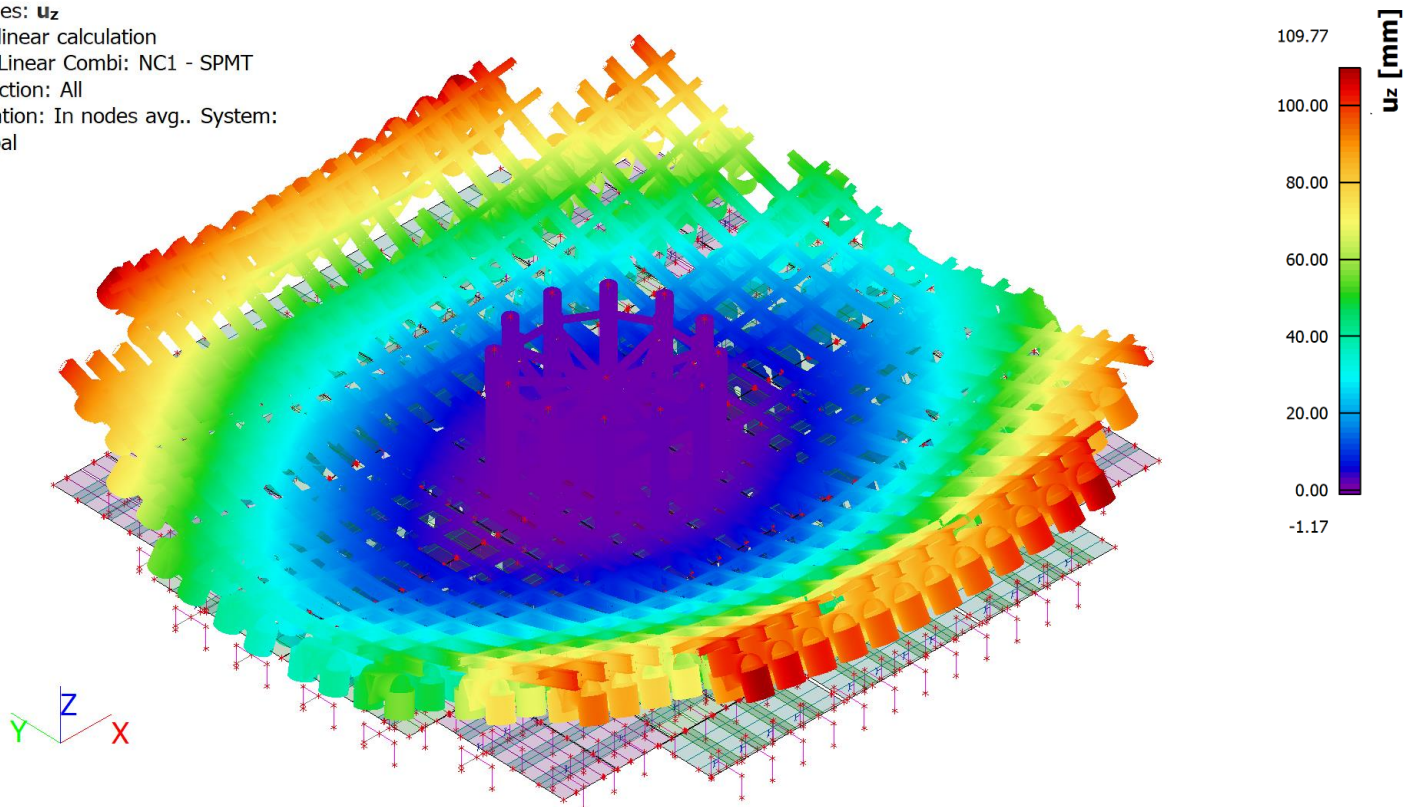


Fig. H-12: Elaborated concept SPMT transport, deformation in z direction

H.2.2 ULS

Reactions

Nonlinear calculation
 NonLinear Combi: NC2 - SPMT
 System: Global
 Extreme: Global
 Selection: All
 Nodal reactions

Name	Case	R _x [kN]	R _y [kN]	R _z [kN]	M _x [kNm]	M _y [kNm]	M _z [kNm]
Sn96/N40609	NC2 - SPMT	0	0	-54	1	-7	0

EC-EN 1993 Steel check ULS; Overall check, Inner frame

Values: **UC_{Overall}**
 Nonlinear calculation
 NonLinear Combi: NC2 - SPMT
 Coordinate system: Principal
 Extreme 1D: Member
 Selection: All

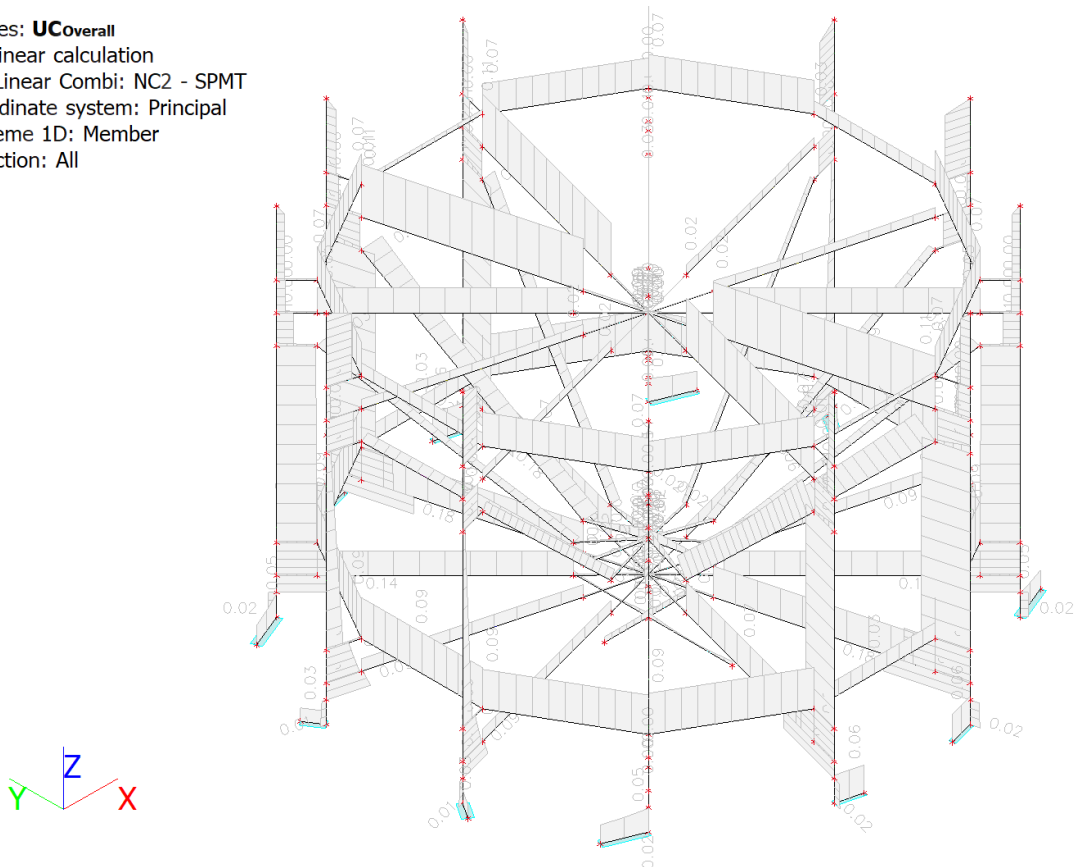


Fig. H-13: Elaborated concept overall SPMT transport ULS unity checks inner frame

EC-EN 1993 Steel check ULS, Inner frame

Nonlinear calculation
 NonLinear Combi: NC2 - SPMT
 Coordinate system: Principal
 Extreme 1D: Global
 Selection: All
 Filter: Layer = Inner frame
 There are 2 warnings on selected members. 2 of them are shown.
 Overall Unity Check

Name	dx [mm]	Case	Cross-section	Material	UC _{Overall} [-]	UC _{Sec} [-]	UC _{Stab} [-]	E/W/N
B25952	0.0	NC2 - SPMT	Inner frame - Column 1 - Tube (600; 35)	S 355	0.18	0.17	0.18	W2, W9

E/W/N	Present on members
W2	B25833, B25861, B25874, B25887, B25952
W9	B25833, B25861, B25874, B25887, B25952

EC-EN 1993 Steel check ULS; Overall check, Floor

Values: **UC_{Overall}**
Nonlinear calculation
NonLinear Combi: NC2 - SPMT
Coordinate system: Principal
Extreme 1D: Member
Selection: All

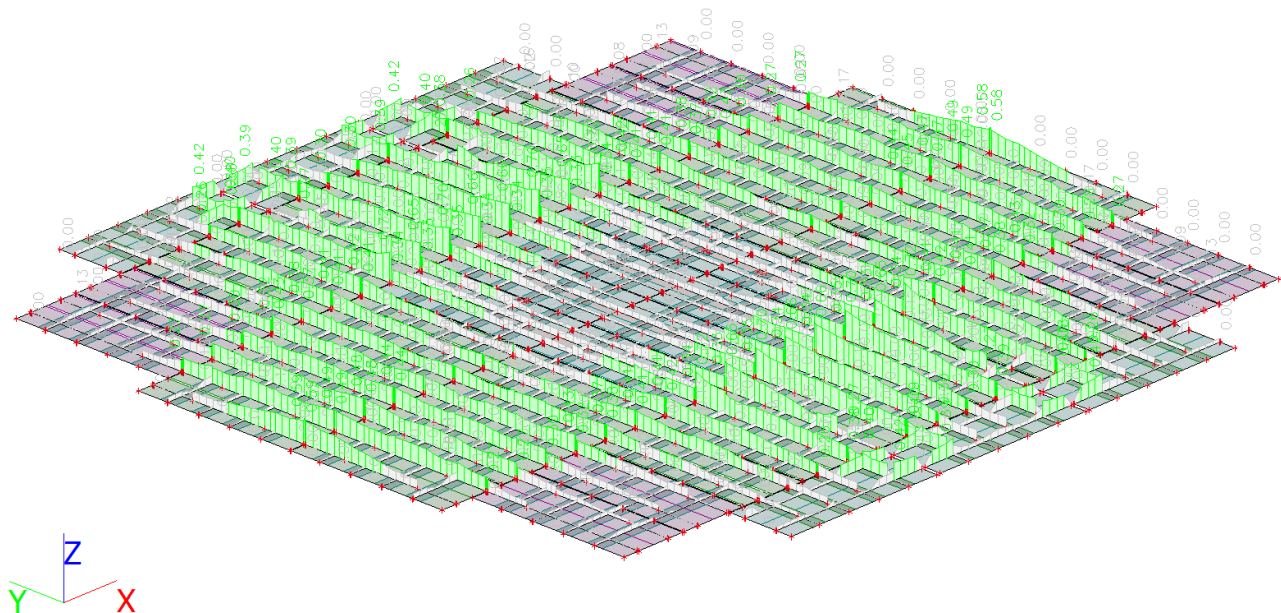


Fig. H-14: Elaborated concept overall SPMT transport ULS unity checks floor

2.2.5. EC-EN 1993 Steel check ULS, Floor

Nonlinear calculation
NonLinear Combi: NC2 - SPMT
Coordinate system: Principal
Extreme 1D: Global
Selection: All
Filter: Layer = Floor
Overall Unity Check

Name	dx [mm]	Case	Cross-section	Material	UC _{Overall} [-]	UC _{Sec} [-]	UC _{Stab} [-]
B23877	0.0	NC2 - SPMT	Floor - Beam 1 - HEB500	S 355	0.72	0.72	0.00

2.2.6. EC-EN 1993 Steel check ULS; Overall check, SPMT group

Values: **UC_{Overall}**
 Nonlinear calculation
 NonLinear Combi: NC2 - SPMT
 Coordinate system: Principal
 Extreme 1D: Member
 Selection: All

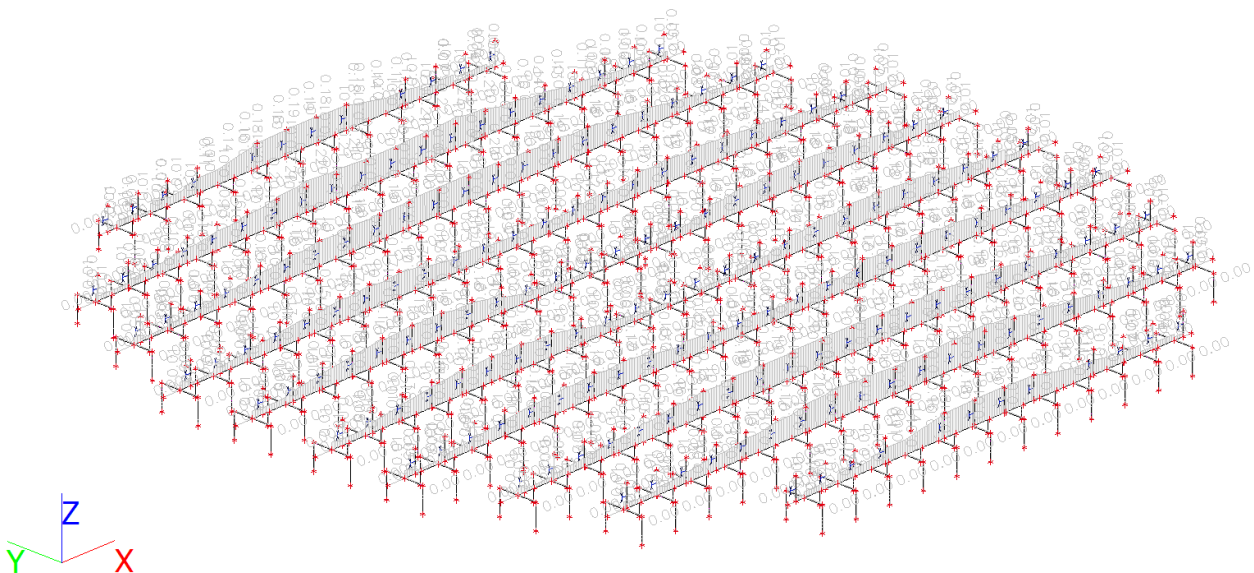


Fig. H-15: Elaborated concept overall SPMT transport ULS unity checks inner frame

Nonlinear calculation
 NonLinear Combi: NC2 - SPMT
 Coordinate system: Principal
 Extreme 1D: Global
 Selection: All
 Filter: Layer = SPMT group
 There are 2 warnings on selected members. 2 of them are shown.
 Overall Unity Check

Name	dx [mm]	Case	Cross-section	Material	UC _{Overall} [-]	UC _{Sec} [-]	UC _{Stab} [-]	E/W/N
B27157	300.0+	NC2 - SPMT	SPMT - Spine beam - General cross-section	S 690	0.23	0.23	0.00	W2, W9

E/W/N	Present on members
W2	B26272, B26273, B26277, B26278, B26284, B26290, B26296, B26302, B26308, B26311, B26317, B26428, B26434, B26437, B26569, B26848, B26860, B26866, B26998, B27124, B27157
W9	B26272, B26273, B26277, B26278, B26284, B26290, B26296, B26302, B26308, B26311, B26317, B26428, B26434, B26437, B26569, B26848, B26860, B26866, B26998, B27124, B27157

H.3 Results Sea transport

H.3.1 SLS

3D displacement; U_{total}

Values: U_{total}
Nonlinear calculation
NonLinear Combi: NC1
Selection: All
Location: In nodes avg.. System:
Global

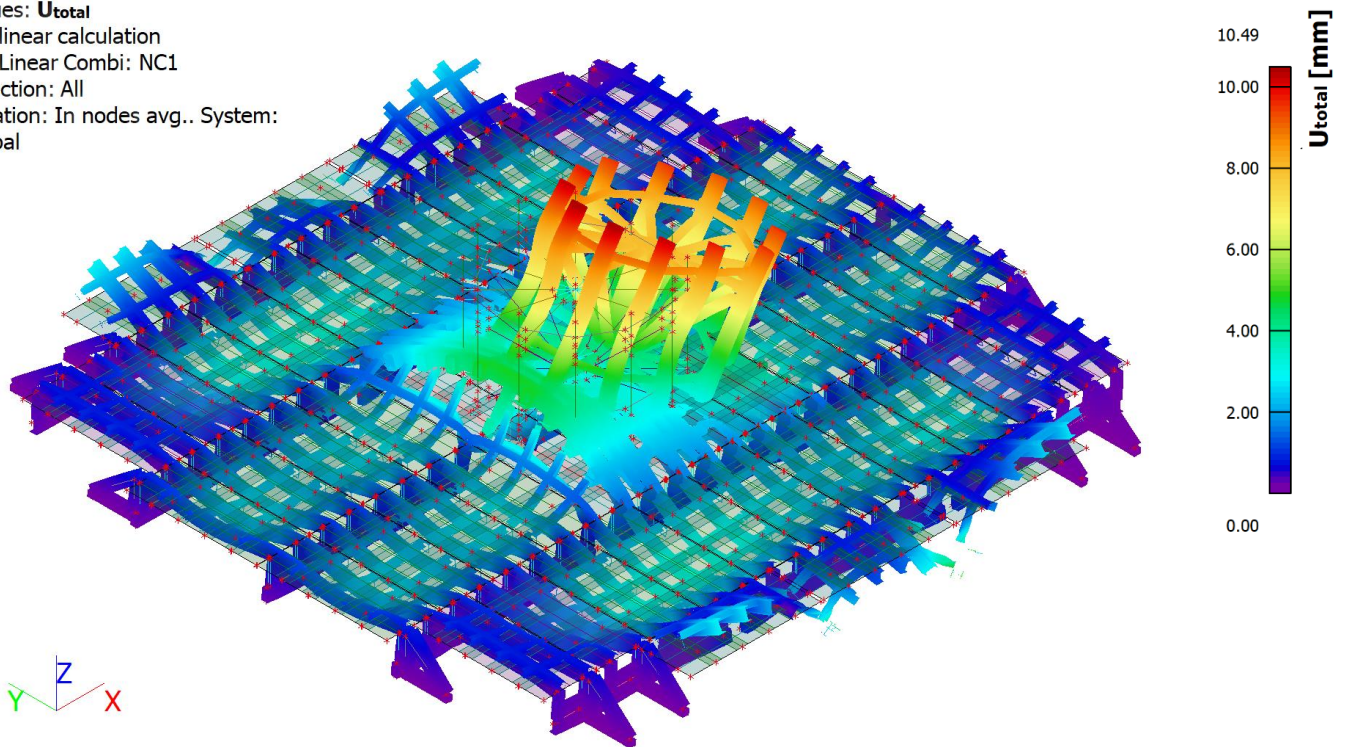


Fig. H-16: Elaborated concept Sea transport SLS load combination 1, total deformation

3D displacement; U_{total}

Values: U_{total}
Nonlinear calculation
NonLinear Combi: NC2
Selection: All
Location: In nodes avg.. System:
Global

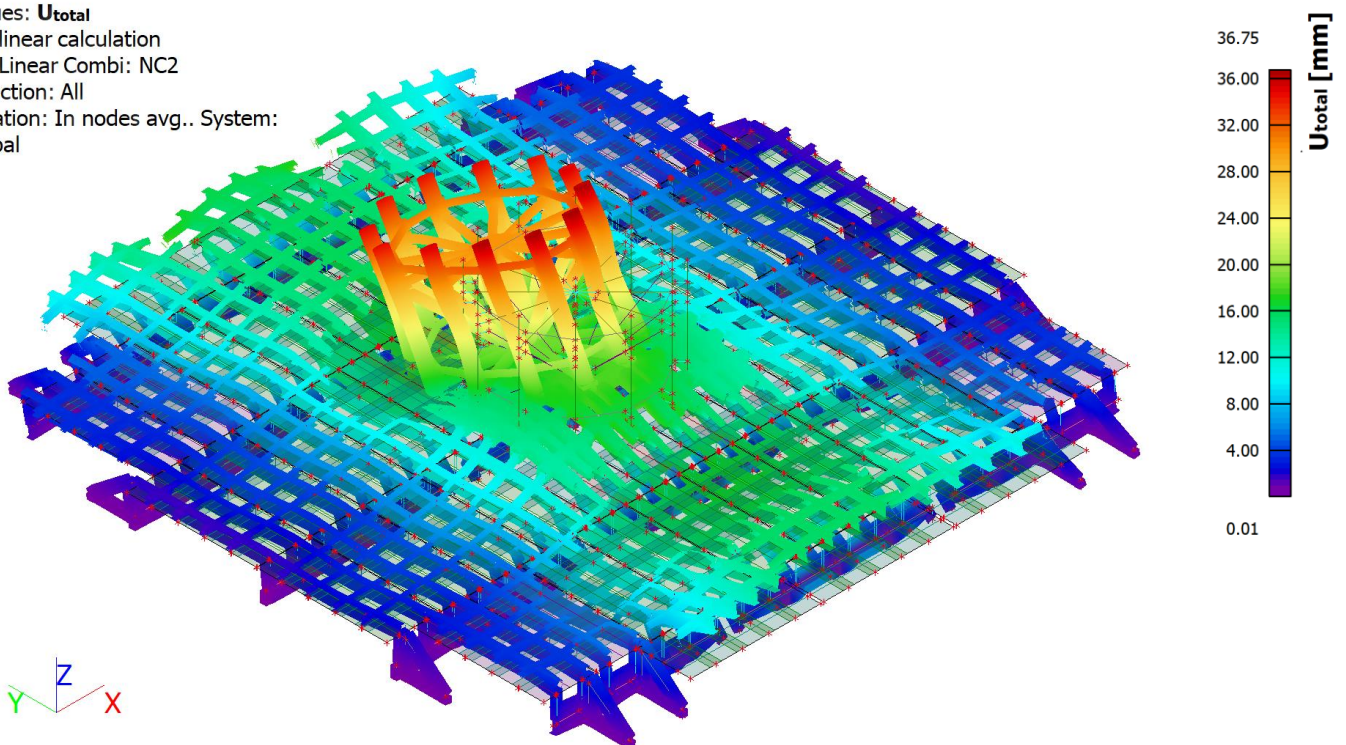


Fig. H-17: Elaborated concept Sea transport SLS load combination 2, total deformation

3D displacement; U_{total}

Values: U_{total}

Nonlinear calculation

NonLinear Combi: NC3

Selection: All

Location: In nodes avg.. System:

Global

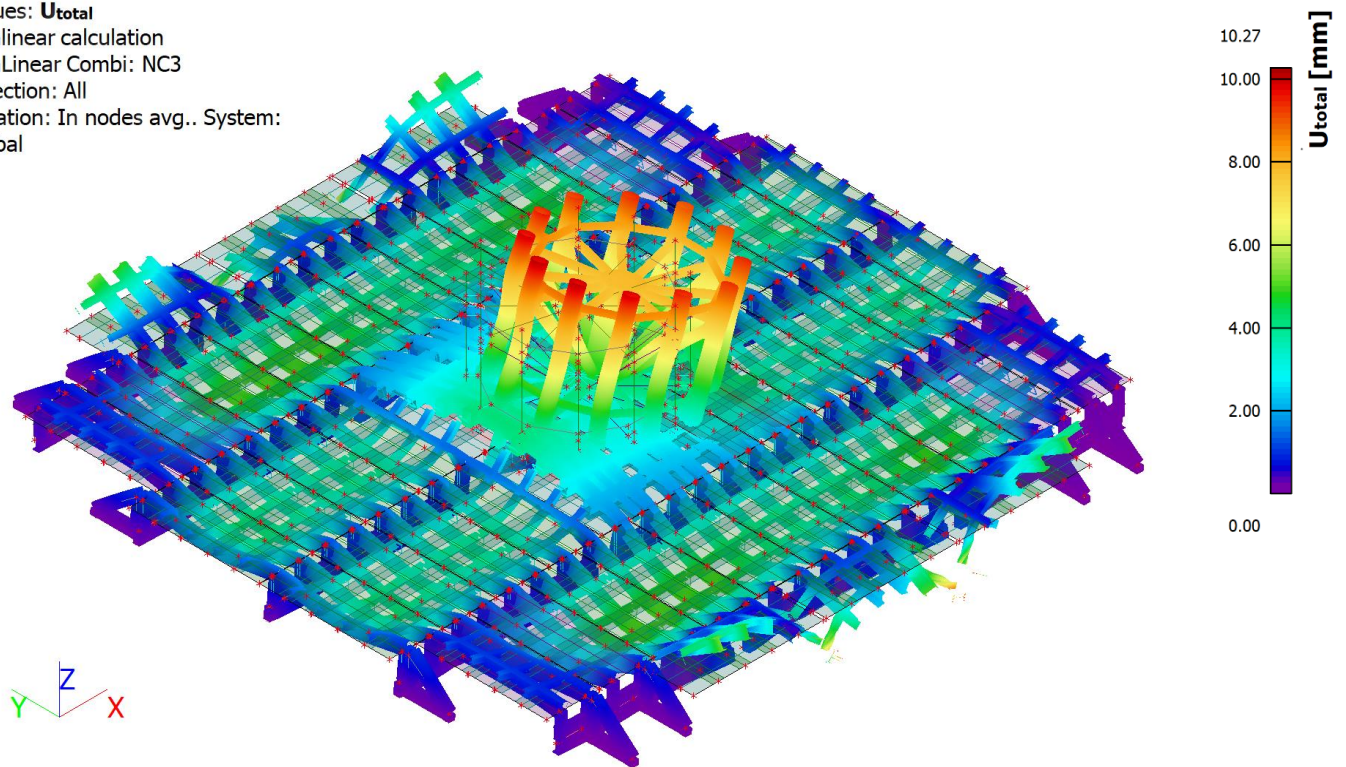


Fig. H-18: Elaborated concept Sea transport SLS load combination 3, total deformation

3D displacement; U_{total}

Values: U_{total}

Nonlinear calculation

NonLinear Combi: NC4

Selection: All

Location: In nodes avg.. System:

Global

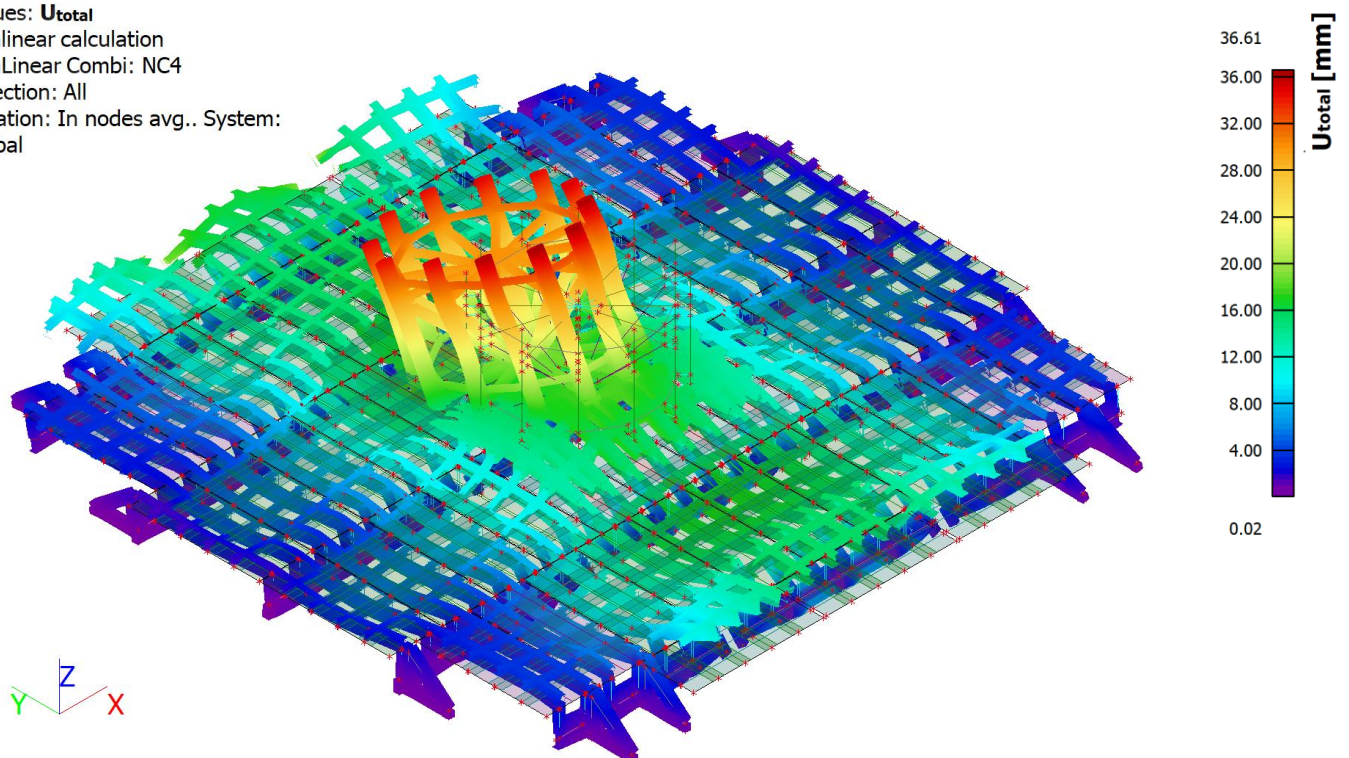


Fig. H-19: Elaborated concept Sea transport SLS load combination 4, total deformation

EC-EN 1993 Steel check ULS; Overall check

Values: **UC_{Overall}**
Nonlinear calculation
Class: ULS
Coordinate system: Principal
Extreme 1D: Member
Selection: All
Filter: Layer = Grillage frame

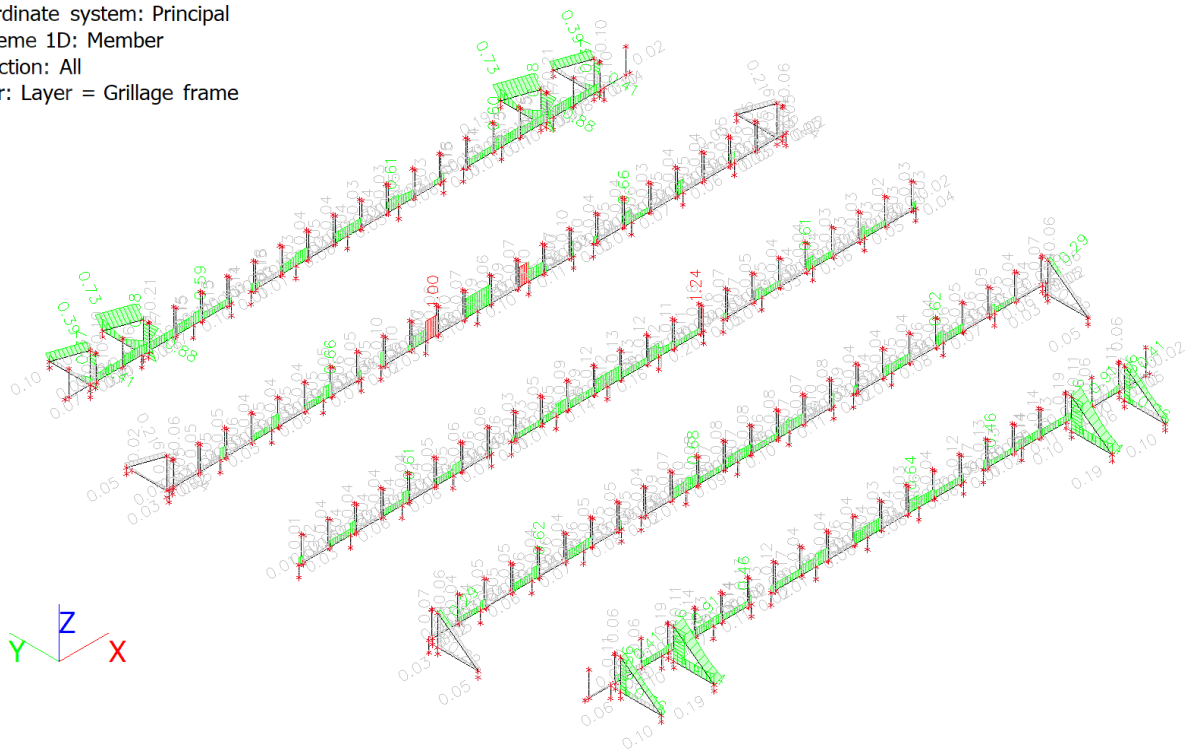


Fig. H-21: Elaborated concept sea transport ULS overall unity check sea fastening

EC-EN 1993 Steel check ULS

Nonlinear calculation
Class: ULS
Coordinate system: Principal
Extreme 1D: Global
Selection: All
Filter: Layer = Sea fastening
Overall Unity Check

Name	dx [mm]	Case	Cross-section	Material	UC _{Overall} [-]	UC _{Sec} [-]	UC _{stab} [-]
B25818	0.0	NC7	Sea fastening - Beam 1 - HEB1000	S 355	1.24	1.24	0.97

EC-EN 1993 Steel check ULS; Overall check

Values: **UC_{Overall}**
Nonlinear calculation
Class: ULS
Coordinate system: Principal
Extreme 1D: Member
Selection: All
Filter: Layer = Inner frame

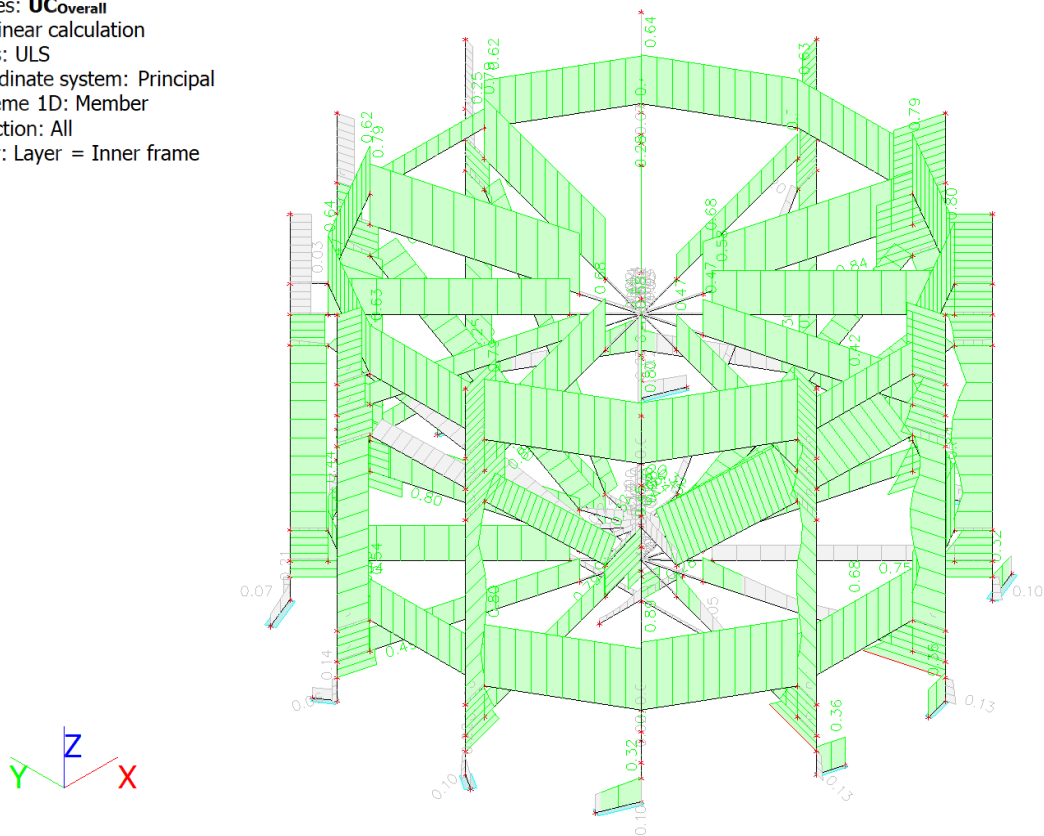


Fig. H-22: Elaborated concept sea transport ULS overall unity check inner frame

EC-EN 1993 Steel check ULS

Nonlinear calculation
Class: ULS
Coordinate system: Principal
Extreme 1D: Global
Selection: All
Filter: Layer = Inner frame
There are 2 warnings on selected members. 2 of them are shown.
Overall Unity Check

Name	dx [mm]	Case	Cross-section	Material	UC _{Overall} [-]	UC _{Sec} [-]	UC _{Stab} [-]	E/W/N
B25965	0.0	NC6	Inner frame - Column 1 - Tube (600; 35)	S 355	1.01	1.01	0.00	W2, W9

E/W/N	Present on members
W2	B25833, B25845, B25874, B25926, B25952, B25965
W9	B25833, B25845, B25874, B25926, B25952, B25965

I Load distribution study

I.1.1 Model description

To determine the load distribution of the payload on the carousel under accelerations, a FEM model has been elaborated, as shown in Fig. I-1.

Geometry
4/7/2023 3:16 PM

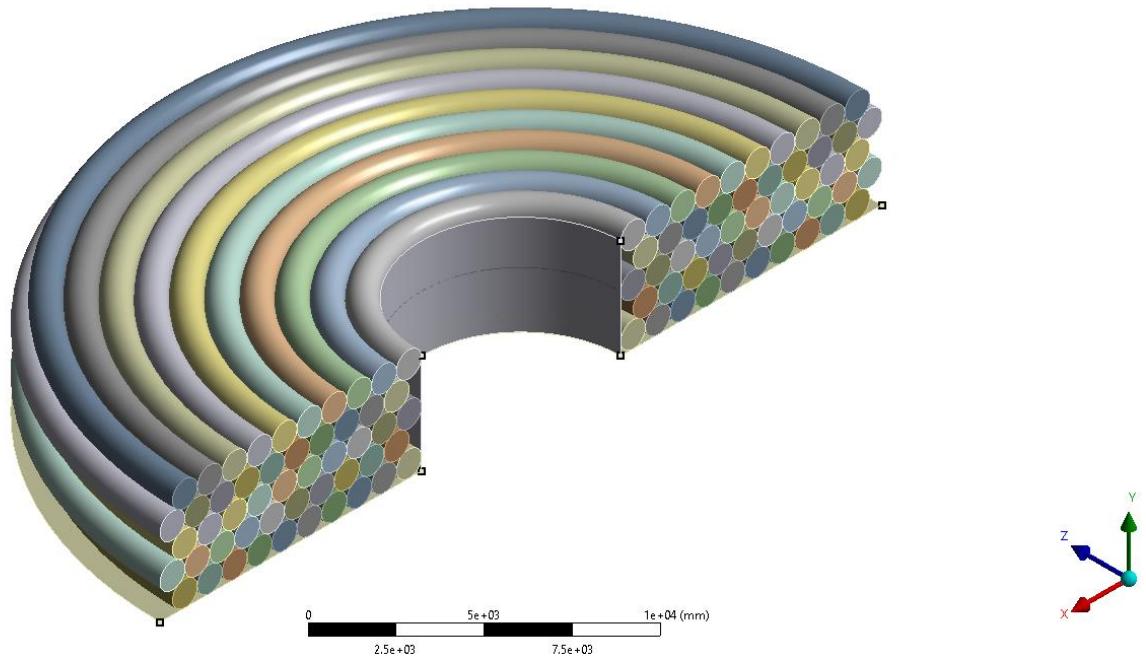


Fig. I-1: Load distribution FEM model

Symmetry region

Symmetry has been used in the model to simplify the analysis. The symmetry region is shown in Fig. I-2.

Symmetry Region 2
4/7/2023 3:16 PM
A Symmetry Region
B Symmetry Region 2

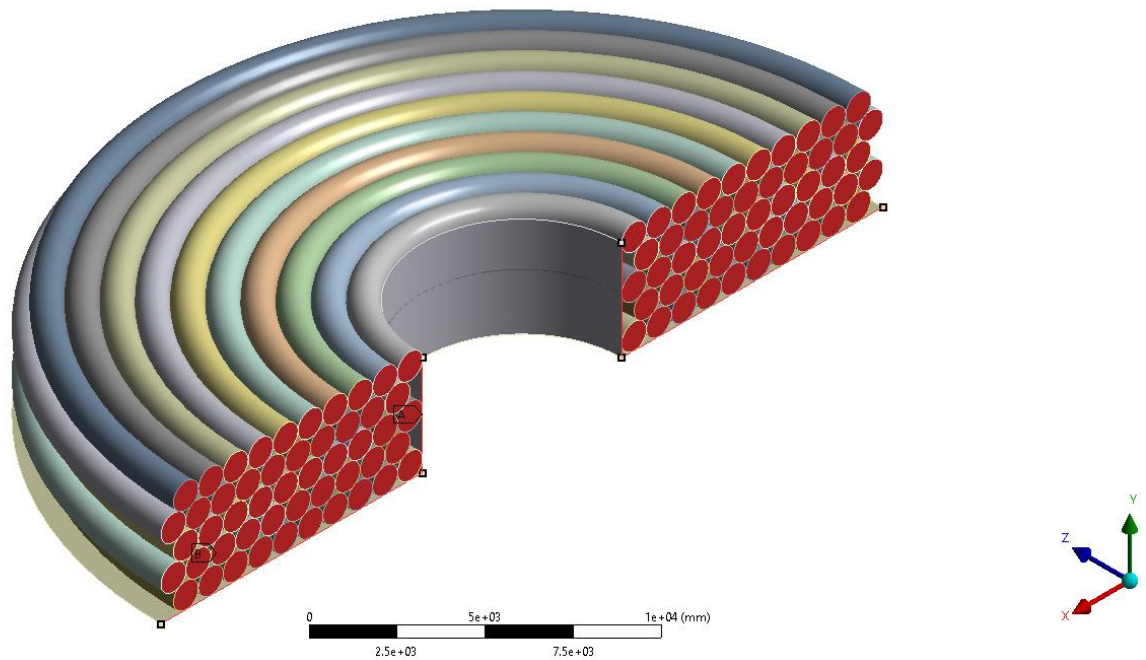


Fig. I-2: Symmetry region in FEM model

Contacts

The following contact types have been defined:

- Cable – floor contact (Fig. I-3)
- Cable – inner wall contact (Fig. I-4)
- Cable – cable horizontal contact (Fig. I-5)
- Cable – cable other contacts (Fig. I-6)

All contacts are defined for each specific simulation in Table I-1.

Frictional - Component16\Solid1 To Component52\Surface 2
4/7/2023 3:17 PM

- Frictional - Component1\Solid1 To Component52\Surface 2 (Contact Bodies)
- Frictional - Component1\Solid1 To Component52\Surface 2 (Target Bodies)
- Frictional - Component2\Solid1 To Component52\Surface 2 (Contact Bodies)
- Frictional - Component2\Solid1 To Component52\Surface 2 (Target Bodies)
- Frictional - Component3\Solid1 To Component52\Surface 2 (Contact Bodies)
- Frictional - Component3\Solid1 To Component52\Surface 2 (Target Bodies)
- Frictional - Component4\Solid1 To Component52\Surface 2 (Contact Bodies)
- Frictional - Component4\Solid1 To Component52\Surface 2 (Target Bodies)
- Frictional - Component5\Solid1 To Component52\Surface 2 (Contact Bodies)
- Frictional - Component5\Solid1 To Component52\Surface 2 (Target Bodies)

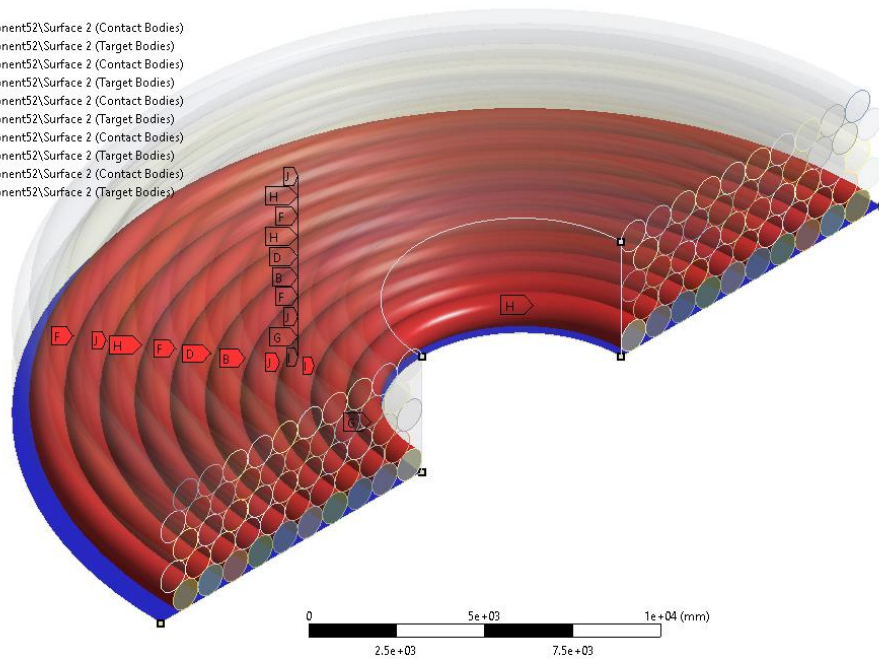


Fig. I-3: Cable – floor contact

Frictionless - Component41\Solid1 To Component51\Surface 1
4/7/2023 3:18 PM

- Frictionless - Component16\Solid1 To Component51\Surface 1 (Contact Bodies)
- Frictionless - Component16\Solid1 To Component51\Surface 1 (Target Bodies)
- Frictionless - Component23\Solid1 To Component51\Surface 1 (Contact Bodies)
- Frictionless - Component23\Solid1 To Component51\Surface 1 (Target Bodies)
- Frictionless - Component41\Solid1 To Component51\Surface 1 (Contact Bodies)
- Frictionless - Component41\Solid1 To Component51\Surface 1 (Target Bodies)

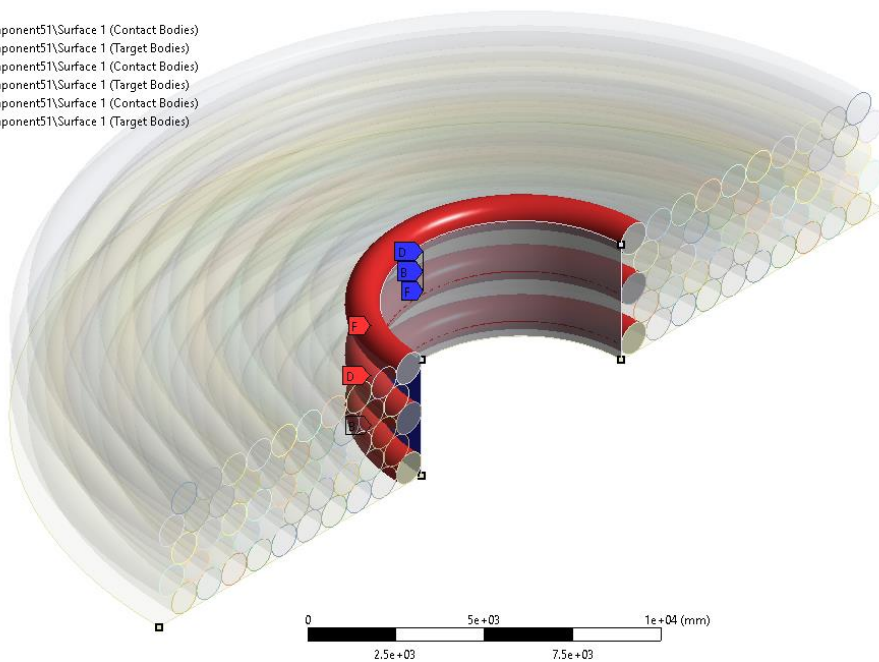


Fig. I-4: Cable – inner wall contact

Frictionless - Component41\Solid1 To Component42\Solid1
4/7/2023 3:18 PM

- Frictionless - Component41\Solid1 To Component42\Solid1 (Contact Bodies)
- Frictionless - Component41\Solid1 To Component42\Solid1 (Target Bodies)

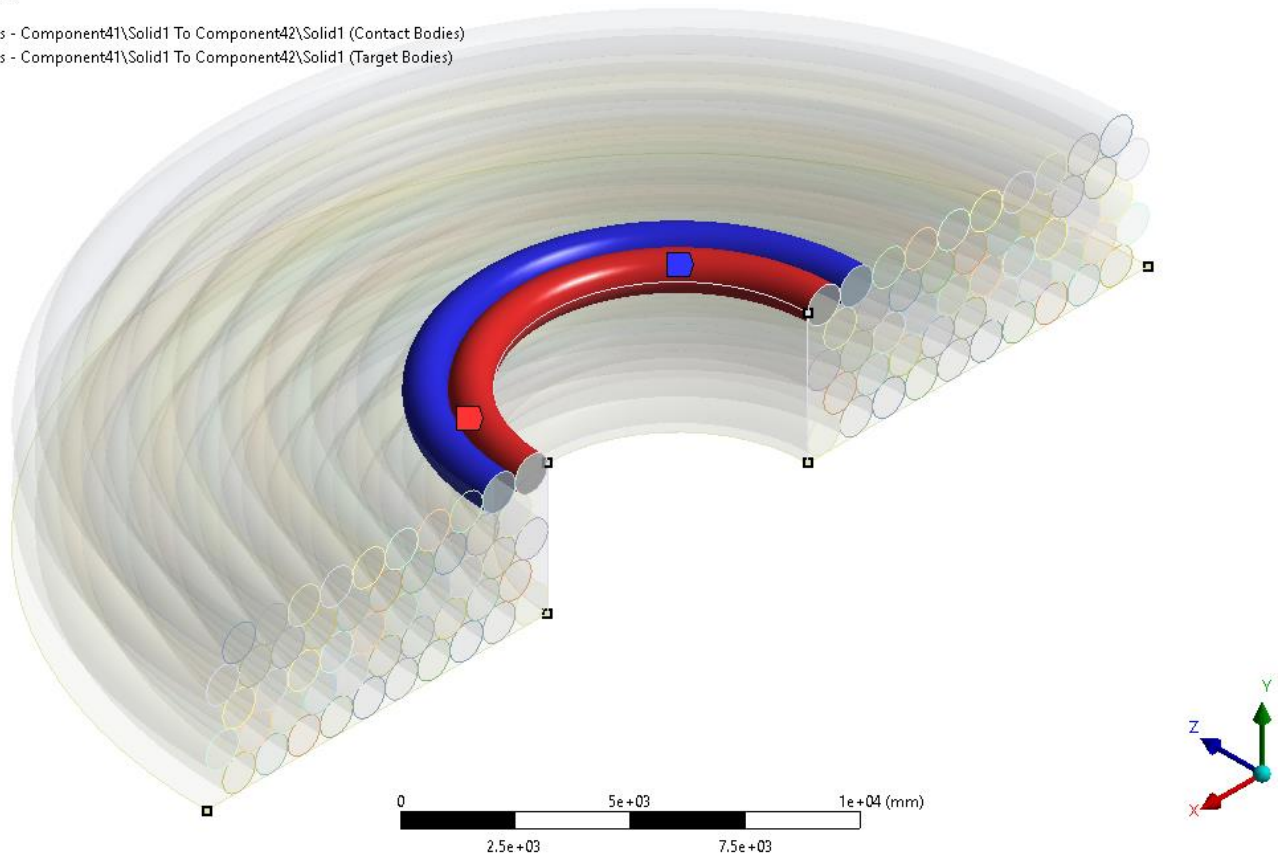


Fig. I-5: Cable – cable horizontal contact

No Separation - Component39\Solid1 To Component48\Solid1
4/7/2023 3:19 PM

- No Separation - Component39\Solid1 To Component48\Solid1 (Contact Bodies)
- No Separation - Component39\Solid1 To Component48\Solid1 (Target Bodies)

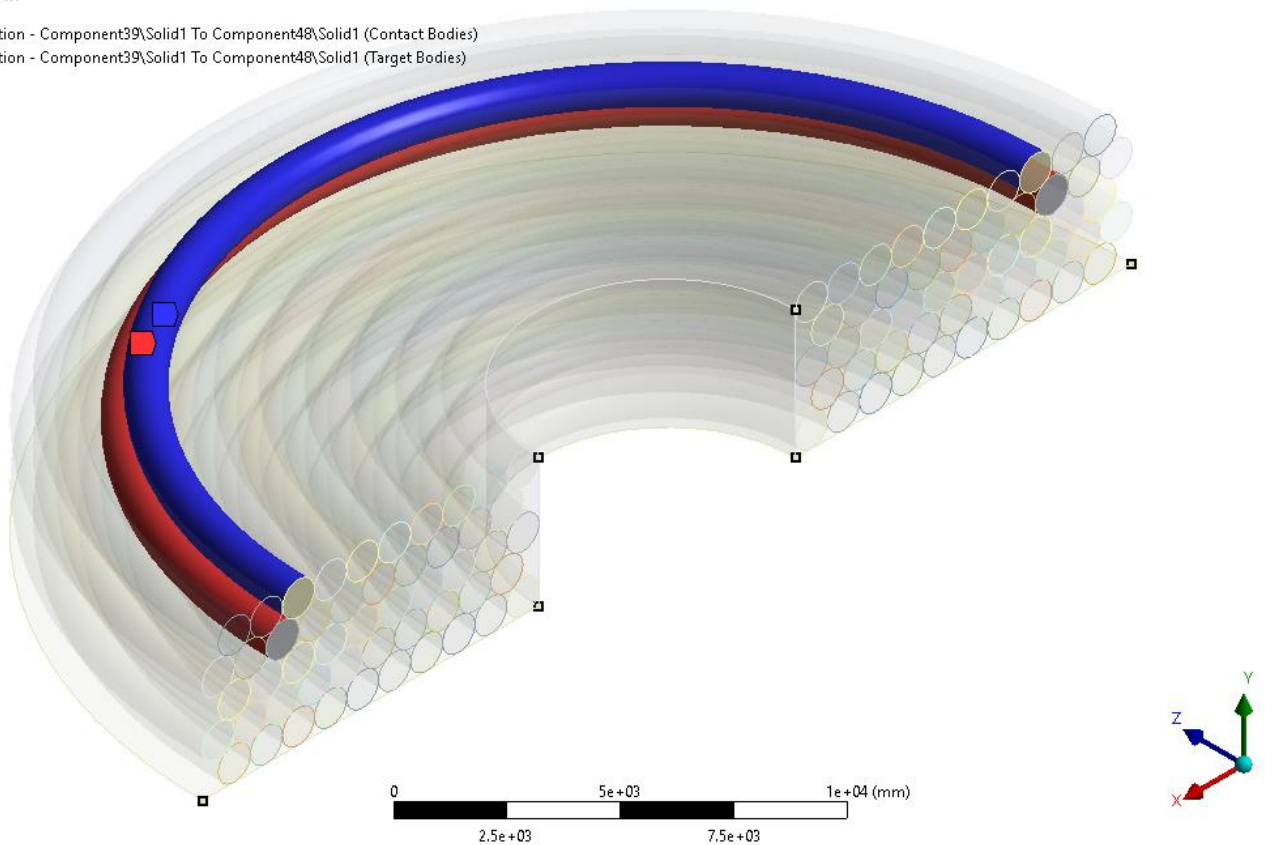


Fig. I-6: Cable – cable other contacts

Mesh

For the cable a quadratic brick mesh with reduced integration and a standard size of 400mm has been used. The floor and inner wall are modelled with quadratic quad plate elements with a standard size of 200mm. The final mesh is shown in Fig. I-7.

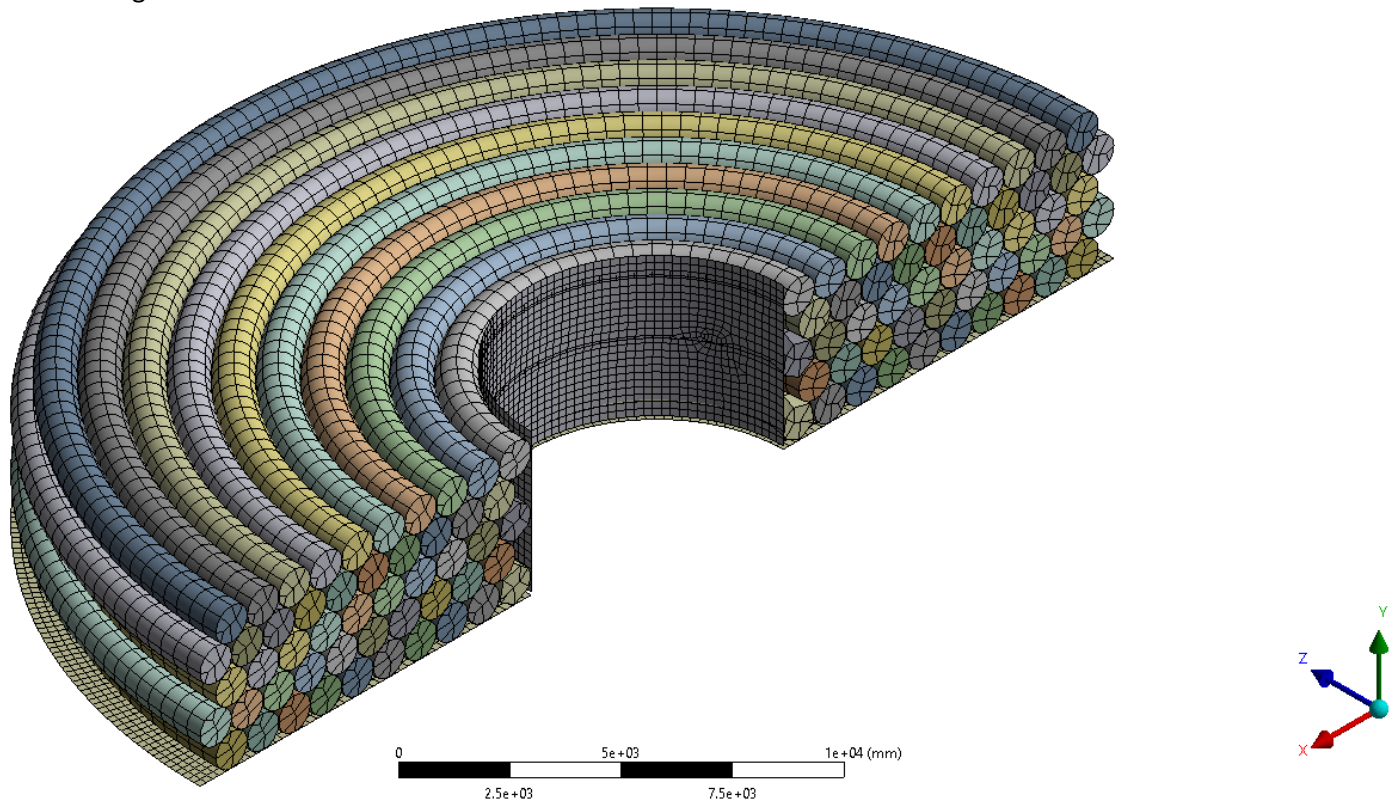


Fig. I-7: Mesh of FEM calculation model

Supports and loads

For the simulation both the floor and inner wall are fixed. Furthermore, an acceleration of -9.81m/s^2 in Y direction and 5m/s^2 in x direction have been applied to the model. The supports and the acceleration are shown in Fig. I-8.

B: Static Structural

Static Structural

Time: 1. s

4/7/2023 3:21 PM

- Fixed Support
- Fixed Support 2
- Acceleration: 11011 mm/s²

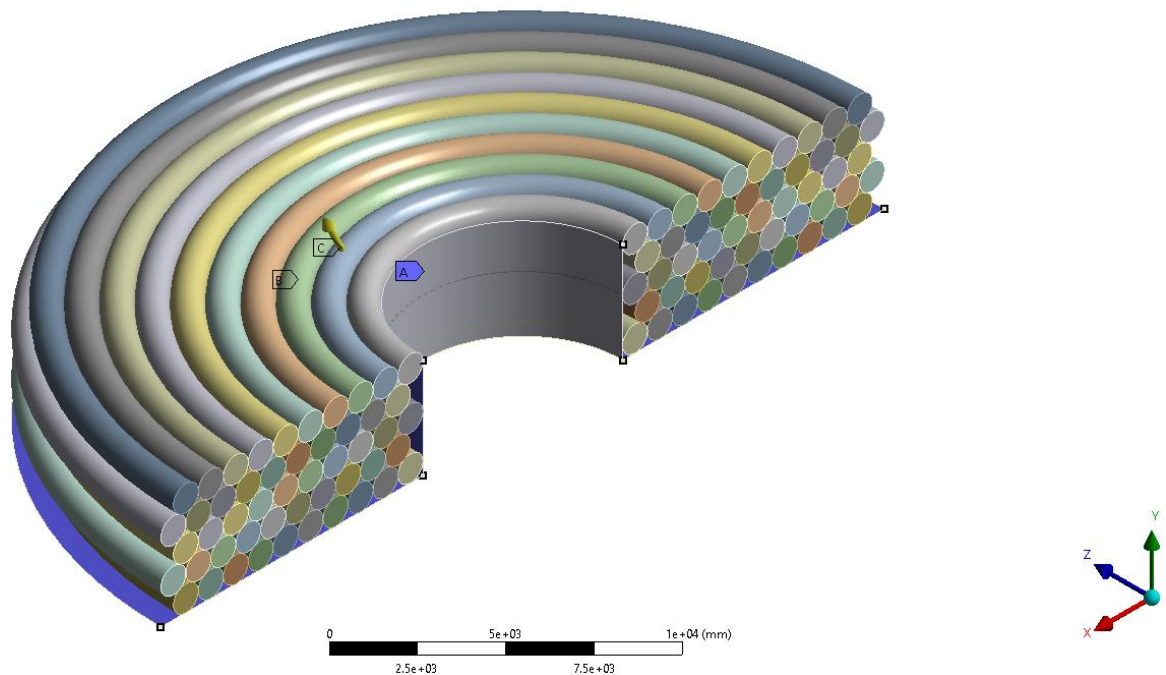


Fig. I-8: Supports and acceleration for simulation

I.1.2 Input

Multiple simulations have been executed with different inputs regarding the contacts and the elastic modulus of the cable material. The input per simulation is shown in Table I-1.

Table I-1: Simulation input

Simulation	Cable - floor	Cable - wall	Cable – cable horizontal	Cable – cable others	Elastic modulus cable	Poisson’s ratio cable	
	[friction coefficient / contact type]				[GPa]	[\]	
1	0.2 / Pressure only	0.2 / Pressure only	0.2 / Pressure only	∞ / Bonded	1	0.4	
2		0.0 / Pressure only			0.0 / Pressure only	1	0.4
3						1	0.4
4		0.2 / Pressure only	0.2 / Pressure only		5	0.4	
5				0 / Bonded	5	0.4	
6	0.1 / Pressure only				5	0.4	

I.1.3 Results

The results of the simulations corresponding to the input defined in Table I-1 is summarized in Table I-2. In Table I-2 the total deformation of the cable stack and the resultant reaction on the floor and on the inner frame are shown. The plots of the deformation and the contact pressures for each simulation are shown in section I.1.4.

Table I-2: Simulation output

#	Maximum deformation [mm]	Inner frame reaction (Rx, Ry, Rz) [N]			Floor reaction (Rx, Ry, Rz) [N]		
1	12.918	5.0824e+006	20858	3.7963e+006	7.3883e+006	2.4467e+007	2.321e+005
2	13.231	5.0543e+006	23.242	4.2138e+006	7.4124e+006	2.4487e+007	2.1821e+005
3	13.256	5.0593e+006	23.254	4.2032e+006	7.408e+006	2.4486e+007	2.0392e+005
4	2.0594	7.7698e+006	-29093	5.451e+006	4.6943e+006	2.4518e+007	-40186
5	15.435	7.9827e+006	-4.195e+005	7.0035e+006	4.4525e+006	2.4945e+007	28708
6	20.348	1.0641e+007	-8.0313e+005	8.8089e+006	2.1583e+006	2.5102e+007	-1.0165e+005

I.1.4 Plots of results

Simulation 1

B: Static Structural
Total Deformation
Type: Total Deformation
Unit: mm
Time: 1 s
Max: 12.918
Min: 0
4/19/2023 12:28 PM

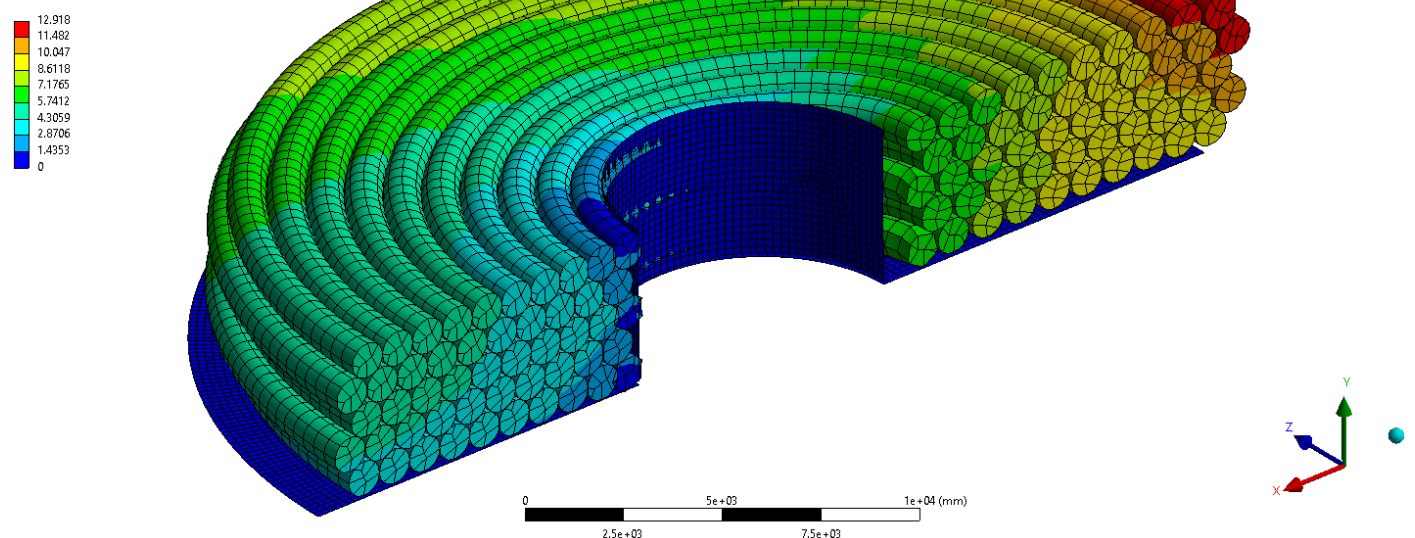


Fig. I-9: Simulation 1, deformation

B: Static Structural
Pressure
Type: Pressure
Unit: MPa
Time: 1 s
Max: 2.6828
Min: 0
4/19/2023 12:31 PM

2.6828
2.3847
2.0866
1.7885
1.4904
1.1924
0.89426
0.59618
0.29809
0

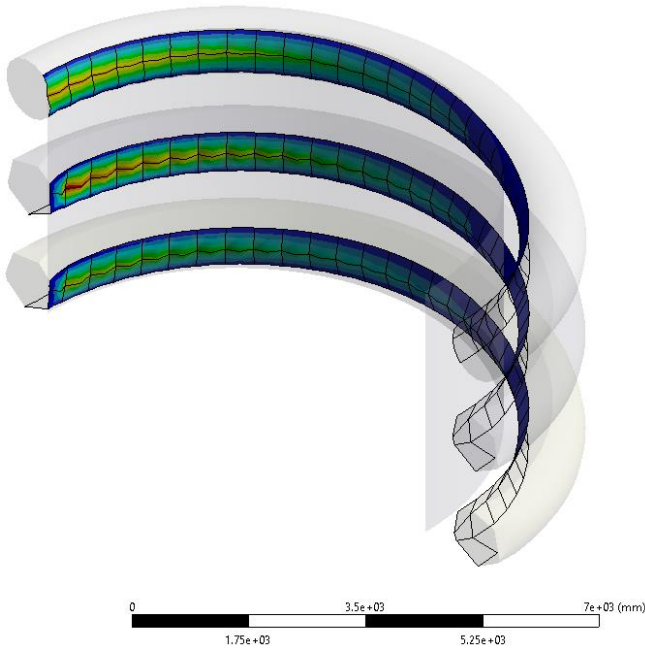


Fig. I-10: Simulation 1, pressure distribution on inner frame

B: Static Structural
Frictional Stress
Type: Frictional Stress
Unit: MPa
Time: 1 s
Max: 0.16722
Min: 0
4/19/2023 12:31 PM

0.16722
0.14864
0.13006
0.11148
0.092901
0.074321
0.055741
0.03716
0.01858
0

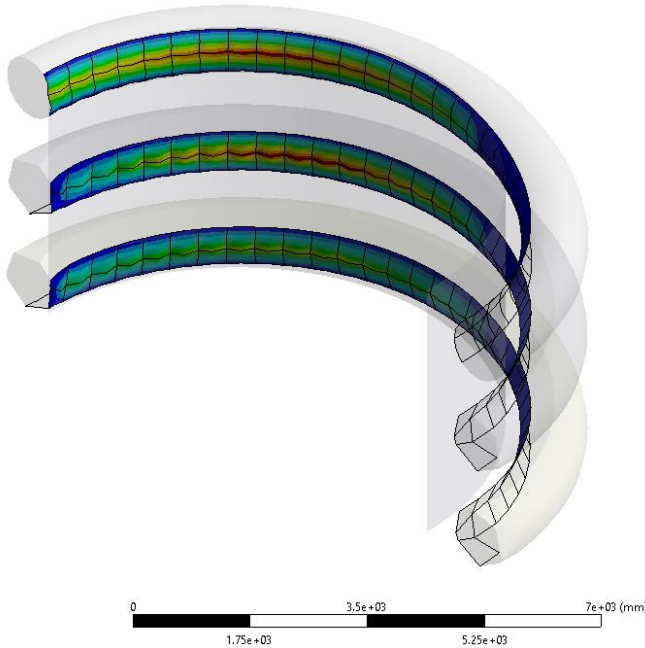


Fig. I-11: Simulation 1, friction distribution on inner frame

B: Static Structural

Pressure
Type: Pressure
Unit: MPa
Time: 1 s
Max: 0.57879
Min: 0
4/19/2023 12:33 PM

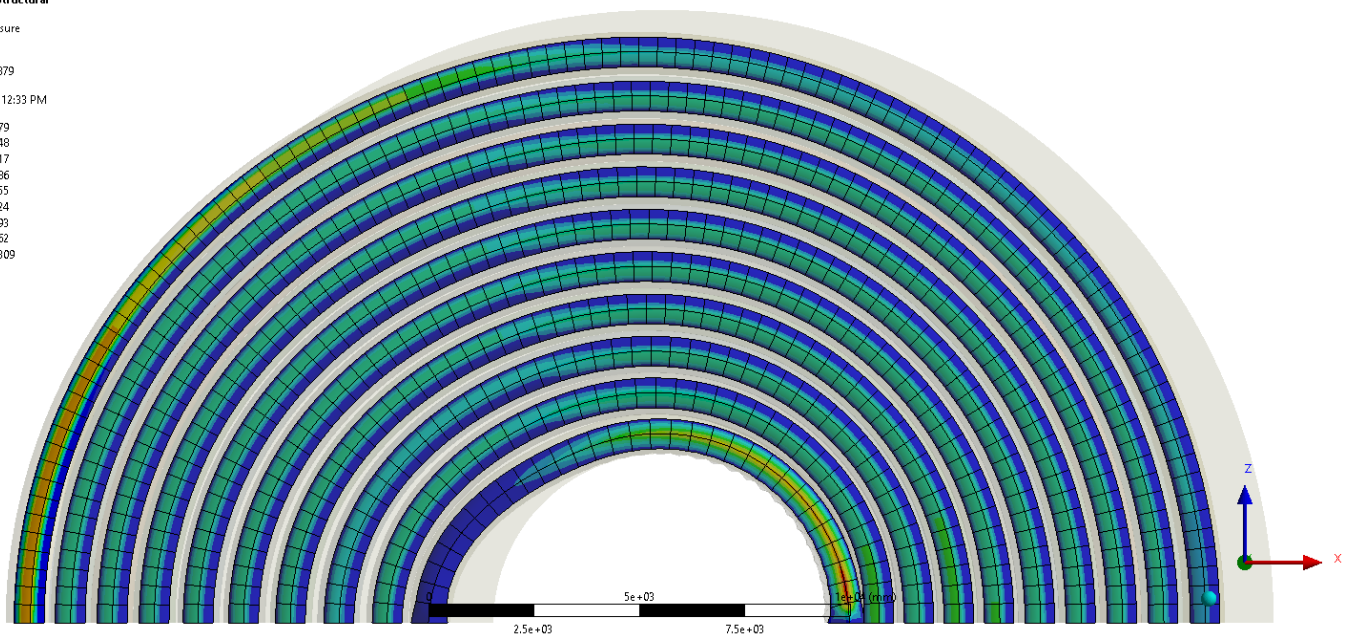
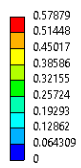


Fig. I-12: Simulation 1, pressure distribution on floor

B: Static Structural

Frictional Stress
Type: Frictional Stress
Unit: MPa
Time: 1 s
Max: 0.096989
Min: 0
4/19/2023 12:33 PM

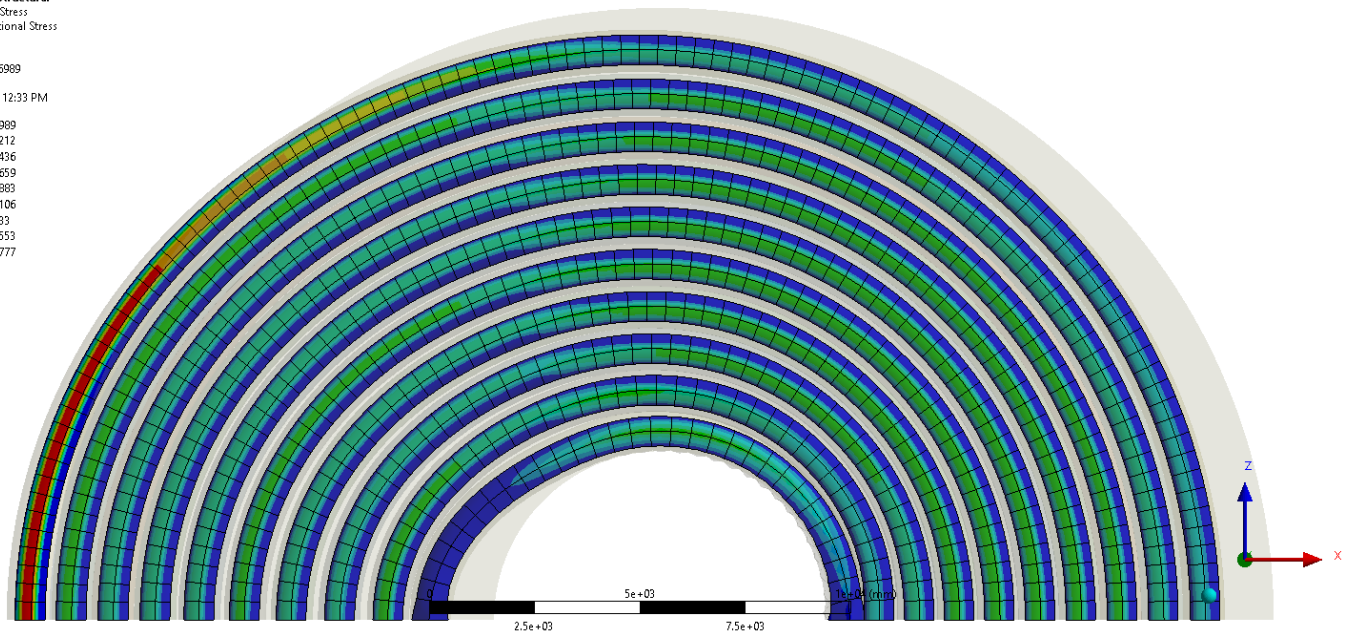
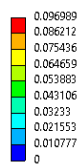
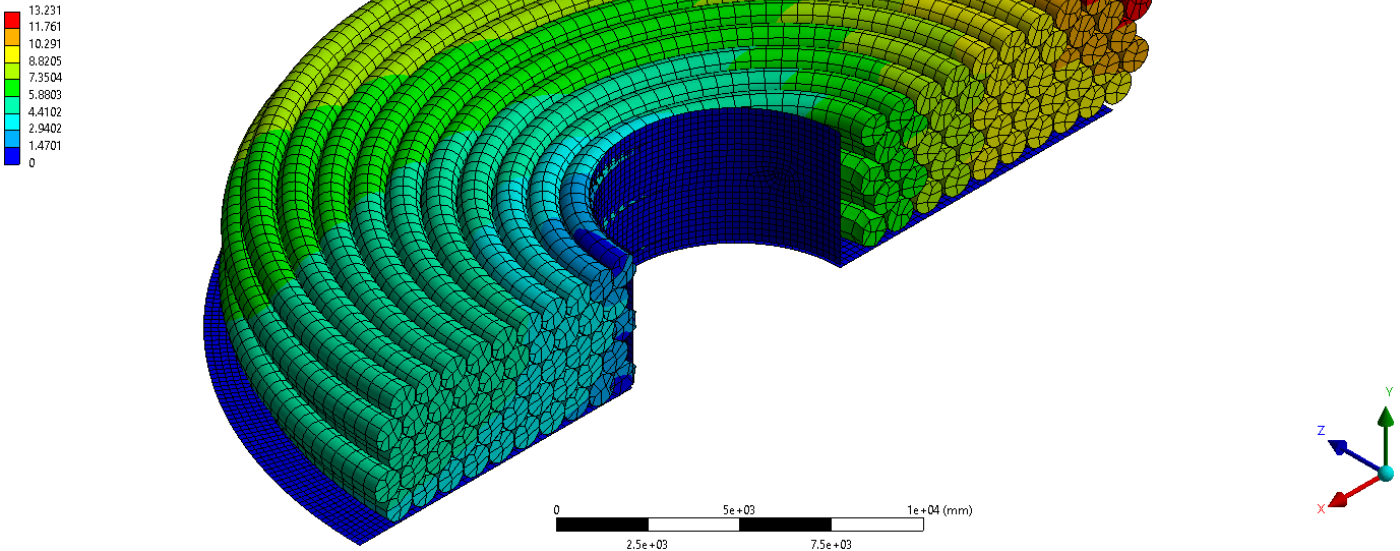


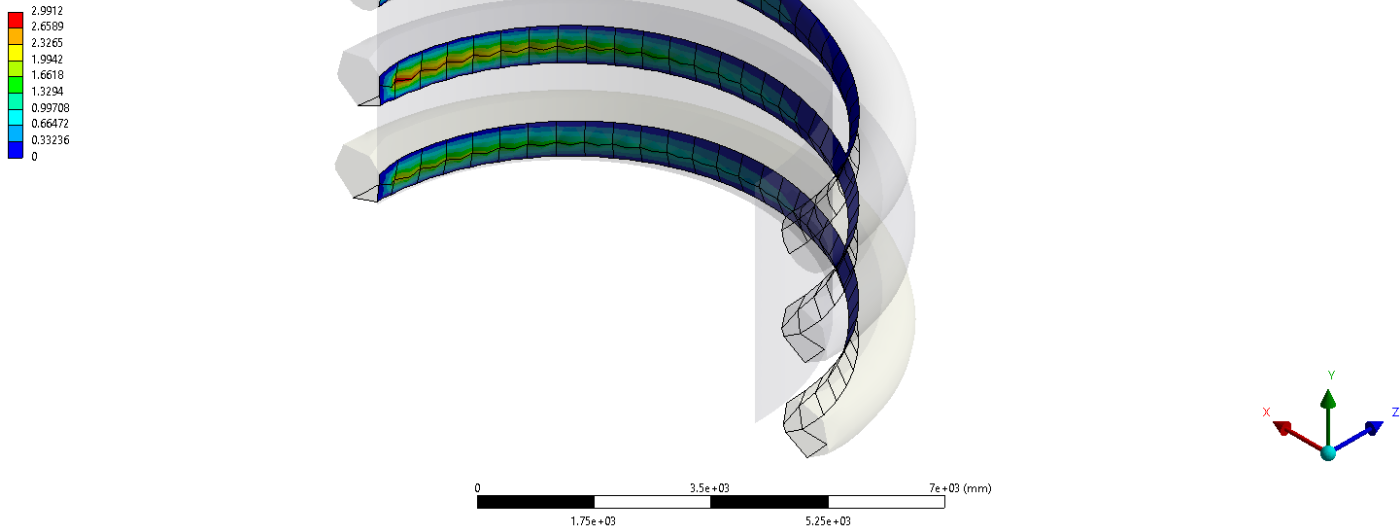
Fig. I-13: Simulation 1, friction distribution on floor

Simulation 2

B: Static Structural
Total Deformation
Type: Total Deformation
Unit: mm
Time: 1 s
Max: 13.231
Min: 0
4/19/2023 12:50 PM



B: Static Structural
Pressure
Type: Pressure
Unit: MPa
Time: 1 s
Max: 2.9912
Min: 0
4/19/2023 12:52 PM



B: Static Structural

Pressure
Type: Pressure
Unit: MPa
Time: 1 s
Max: 0.66027
Min: 0
4/19/2023 12:51 PM

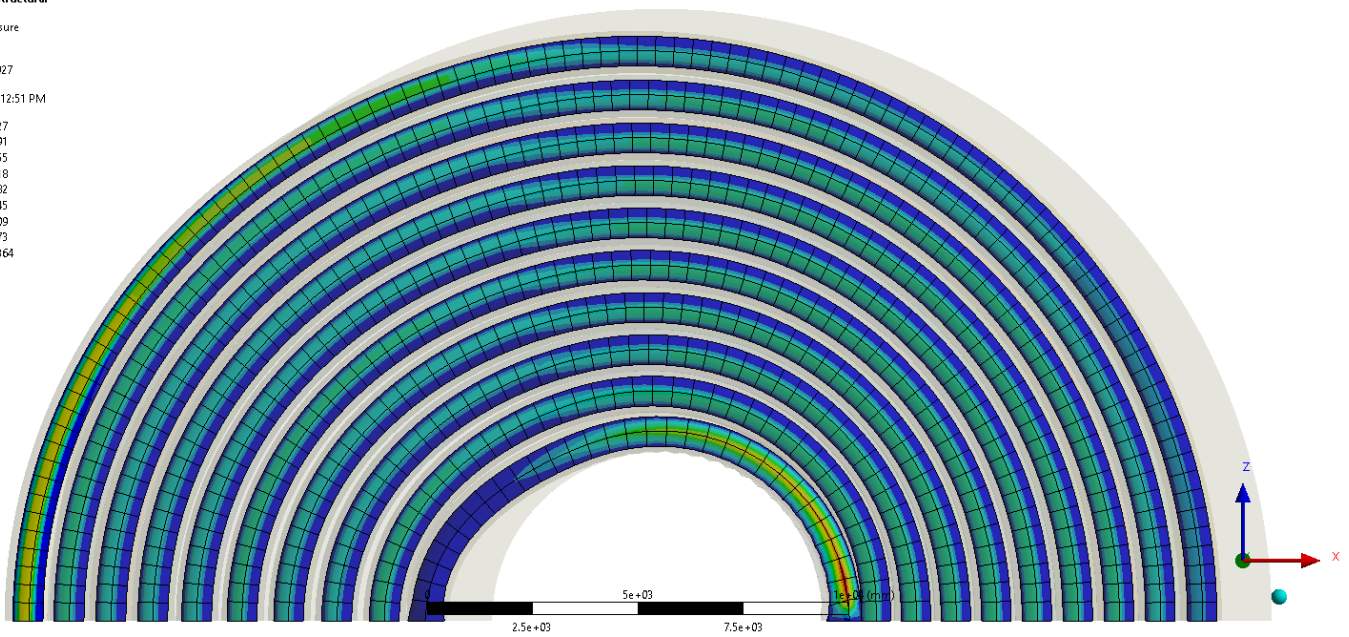
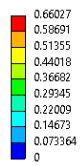


Fig. I-16: Simulation 2, pressure distribution on inner frame

B: Static Structural

Frictional Stress
Type: Frictional Stress
Unit: MPa
Time: 1 s
Max: 0.096886
Min: 0
4/19/2023 12:51 PM

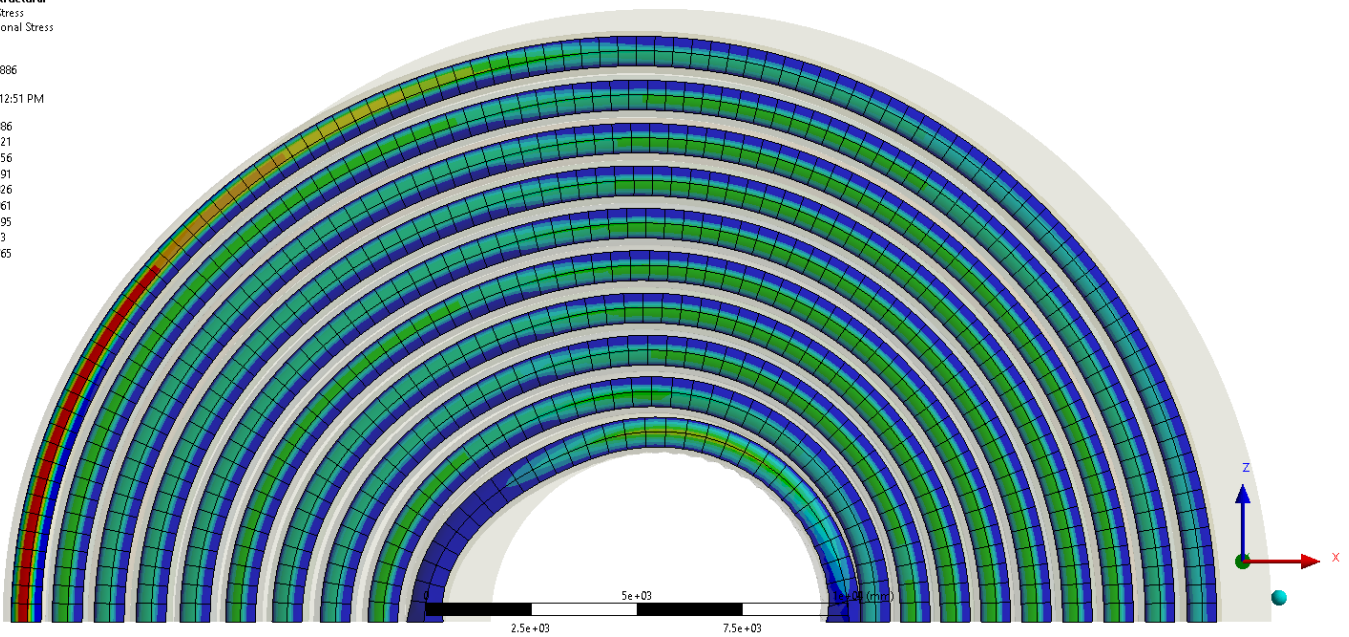
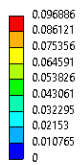


Fig. I-17: Simulation 2, friction distribution on floor

Simulation 3

B: Static Structural
Total Deformation
Type: Total Deformation
Unit: mm
Time: 1 s
Max: 13.256
Min: 0
4/19/2023 11:47 AM

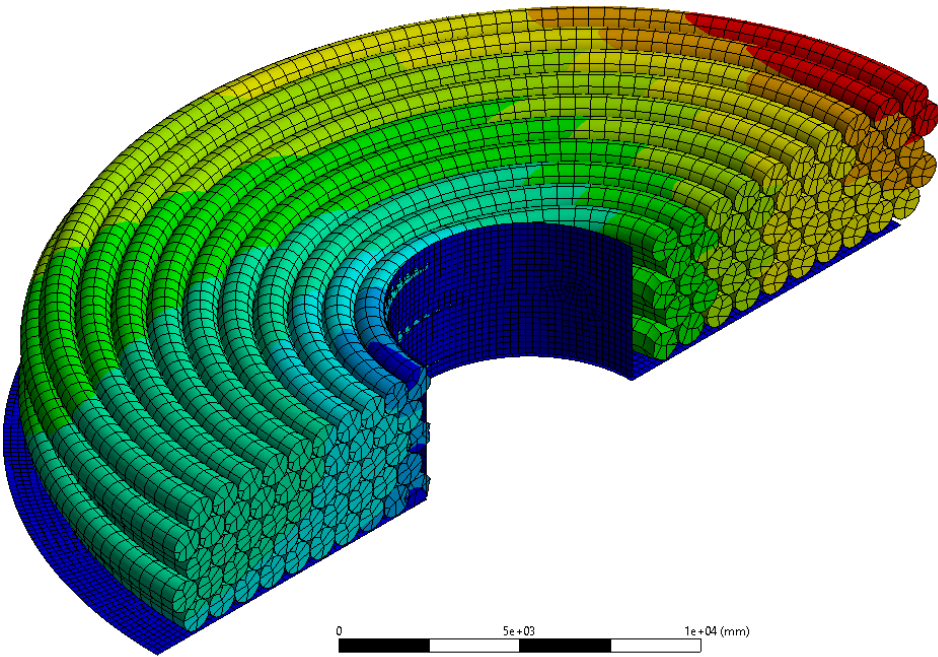
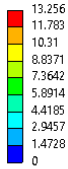


Fig. I-18: Simulation 3, deformation

B: Static Structural
Pressure
Type: Pressure
Unit: MPa
Time: 1 s
Max: 3.0119
Min: 0
4/19/2023 11:51 AM

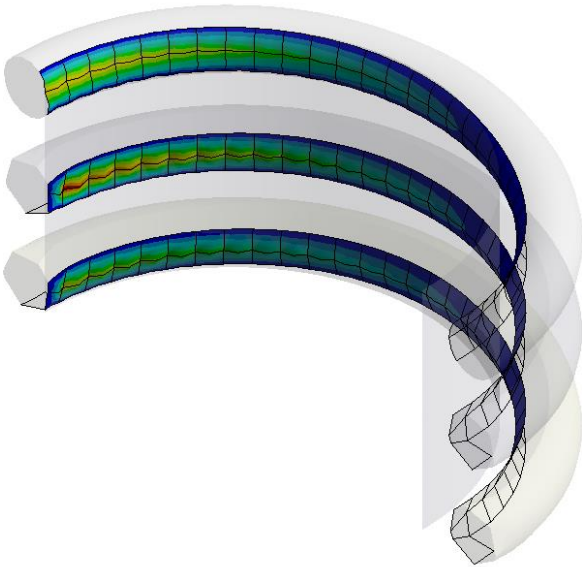
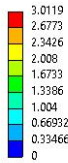


Fig. I-19: Simulation 3, pressure distribution on inner frame

B: Static Structural

Pressure
Type: Pressure
Unit: MPa
Time: 1 s
Max: 0.65546
Min: 0
4/19/2023 11:48 AM

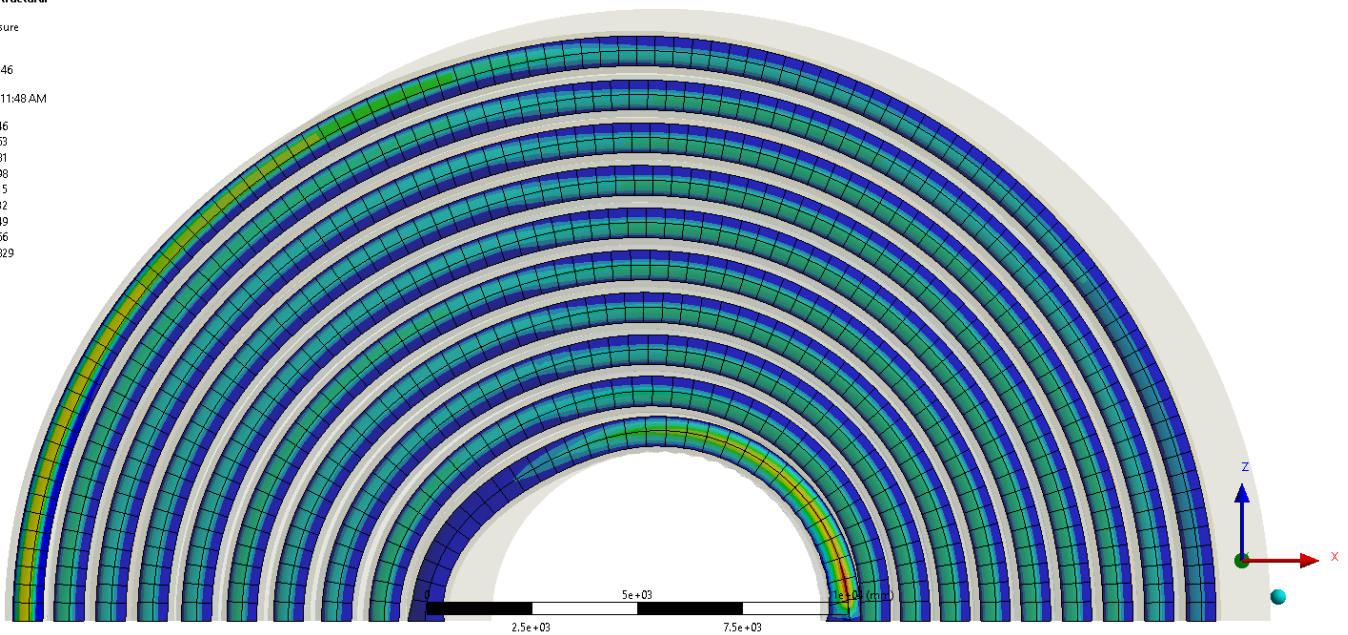
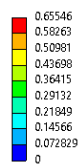


Fig. I-20: Simulation 3, pressure distribution on floor

B: Static Structural

Frictional Stress
Type: Frictional Stress
Unit: MPa
Time: 1 s
Max: 0.096716
Min: 0
4/19/2023 11:49 AM

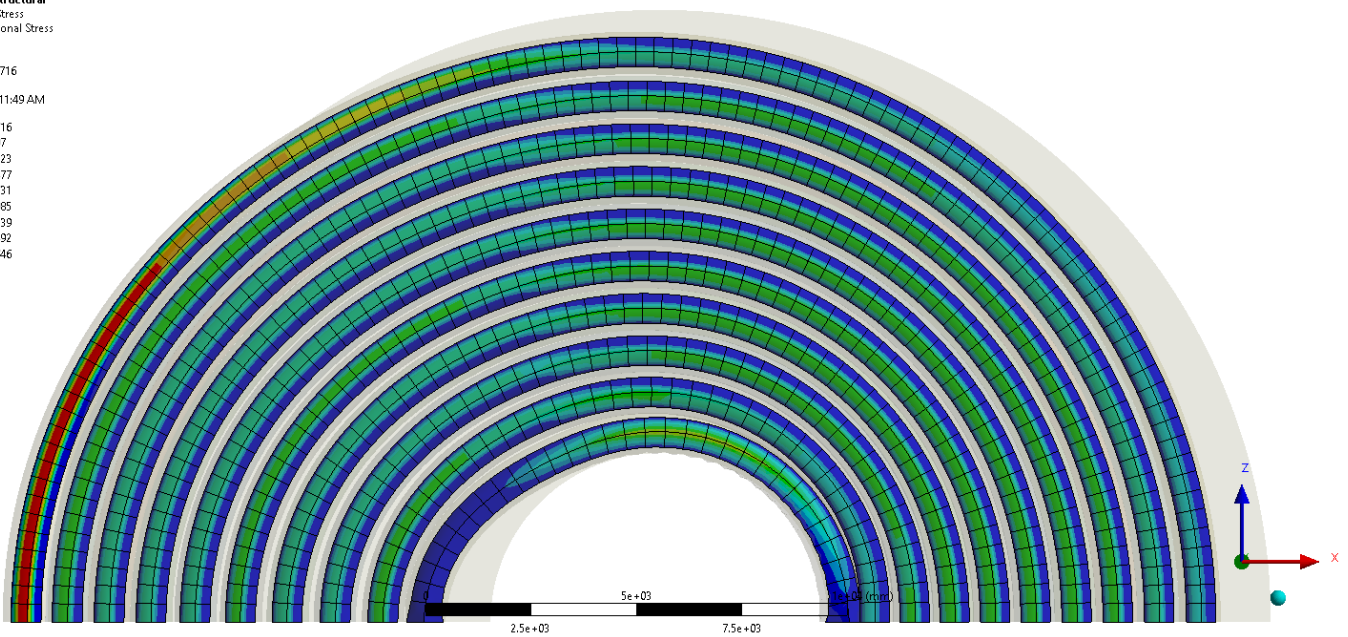
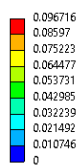


Fig. I-21: Simulation 3, friction distribution on floor

Simulation 4

B: Load distribution model with symmetry

Total Deformation
Type: Total Deformation
Unit: mm
Time: 1 s
Max: 2.0594
Min: 0
5/25/2023 12:00 PM

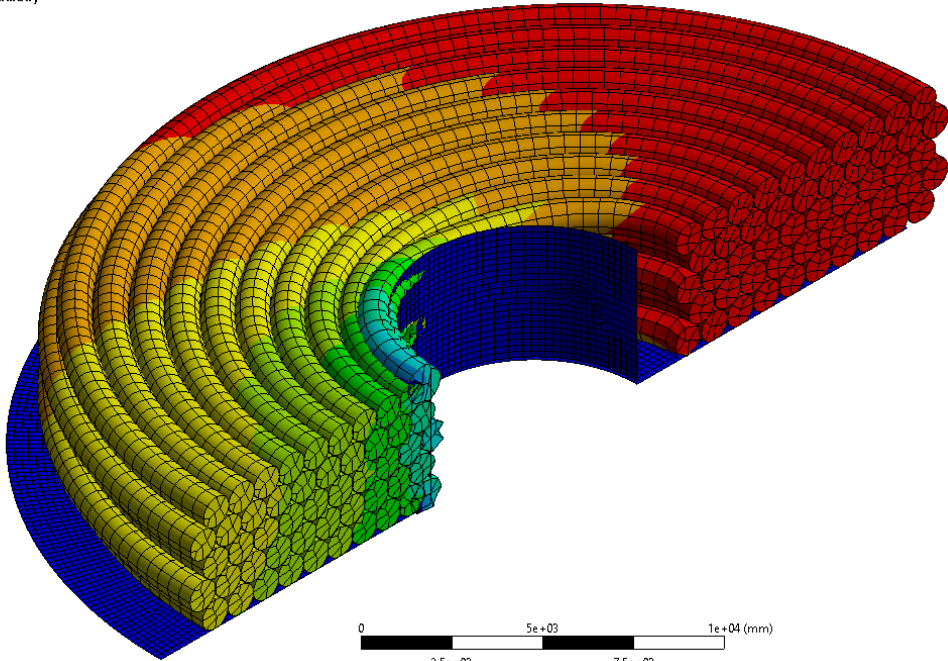
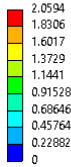


Fig. I-22: Simulation 4, deformation

B: Load distribution model with symmetry

Pressure
Type: Pressure
Unit: MPa
Time: 1 s
Max: 5.9505
Min: 0
5/25/2023 12:03 PM

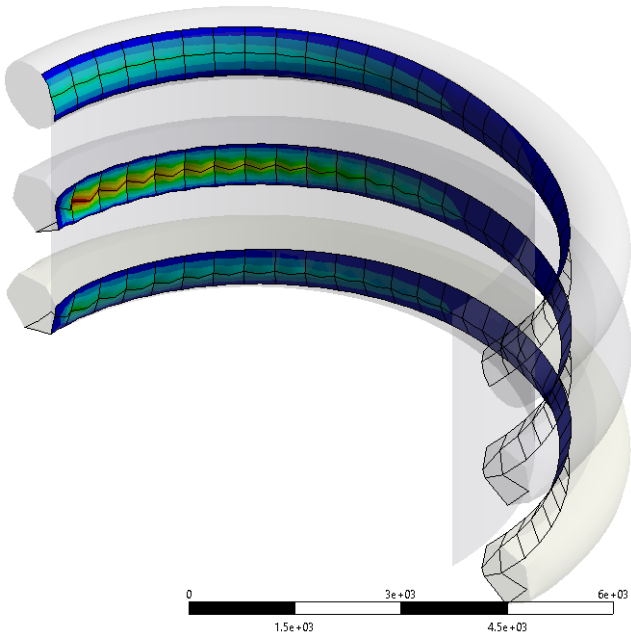
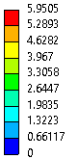


Fig. I-23: Simulation 4, pressure distribution on inner frame

B: Load distribution model with symmetry
Frictional Stress
Type: Frictional Stress
Unit: MPa
Time: 1 s
Max: 0.15401
Min: 0
5/25/2023 12:04 PM

0.15401
0.1369
0.11978
0.10267
0.08556
0.068448
0.051336
0.034224
0.017112
0

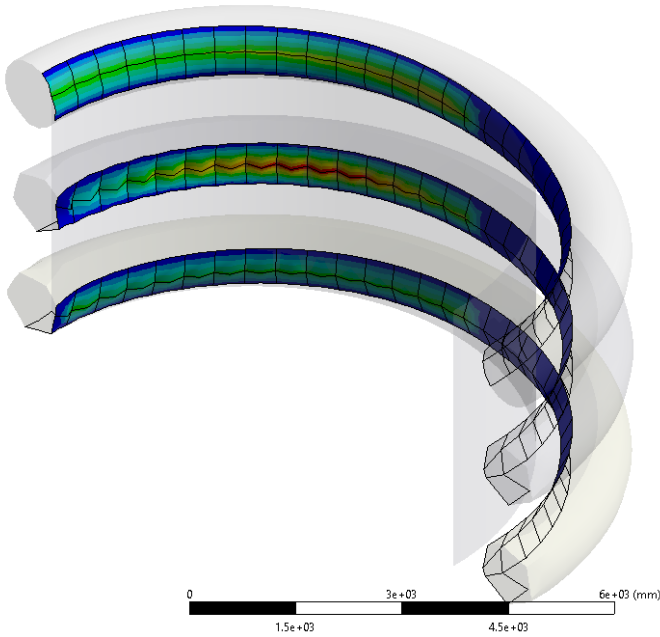


Fig. I-24: Simulation 4, friction distribution on inner frame

B: Load distribution model with symmetry
Pressure
Type: Pressure
Unit: MPa
Time: 1 s
Max: 1.4693
Min: 0
5/25/2023 12:02 PM

1.4693
1.306
1.1428
0.9795
0.81625
0.653
0.48975
0.3265
0.16325
0

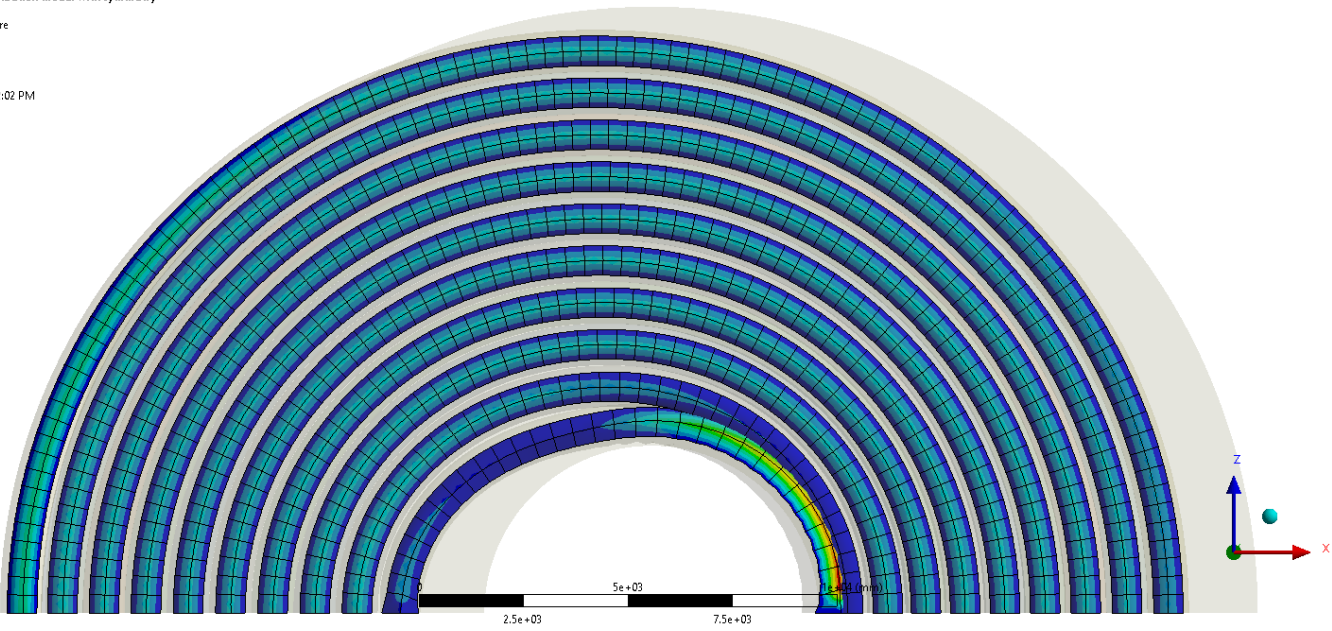
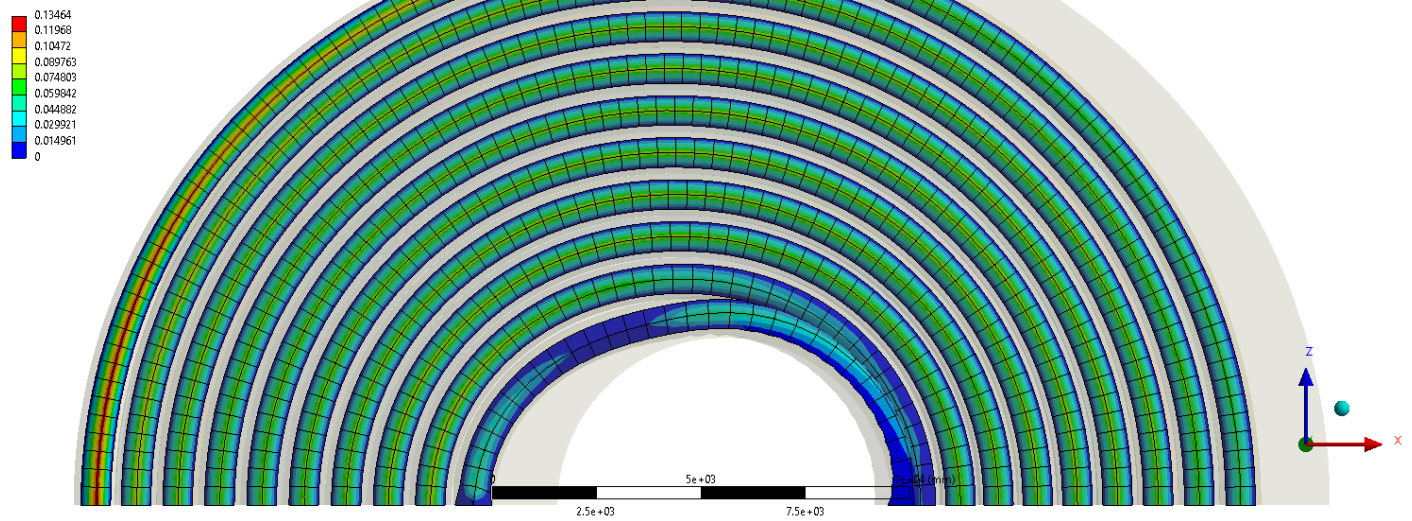


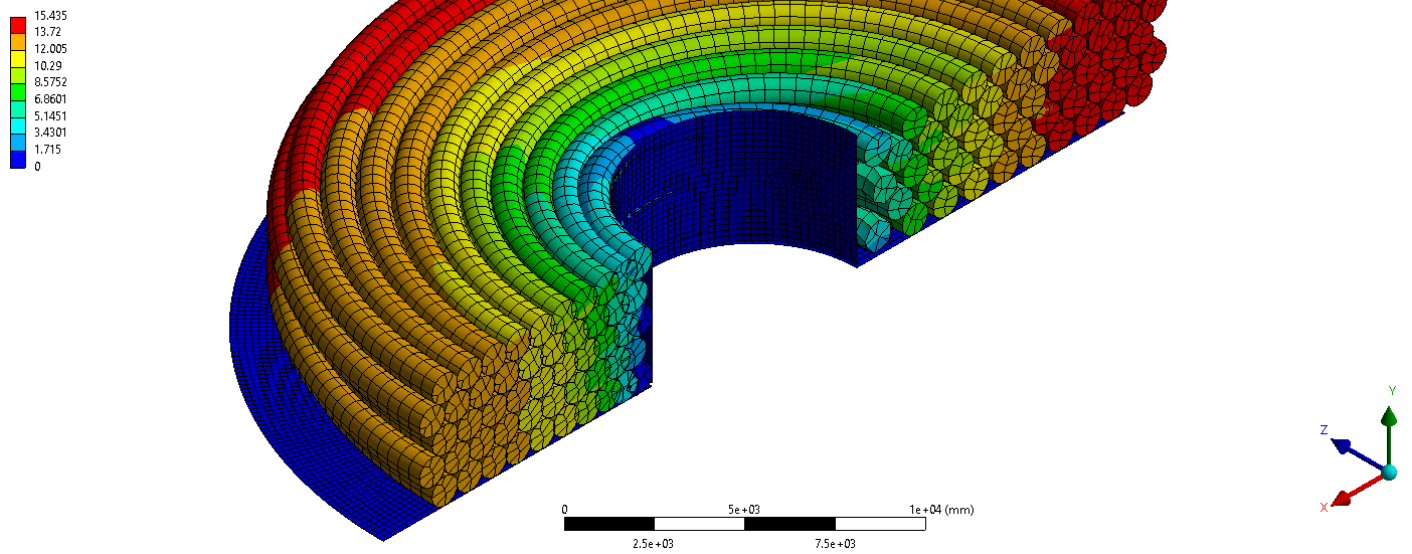
Fig. I-25: Simulation 4, pressure distribution on floor

B: Load distribution model with symmetry

Frictional Stress
Type: Frictional Stress
Unit: MPa
Time: 1 s
Max: 0.13464
Min: 0
5/25/2023 12:02 PM

**Simulation 5****B: Load distribution model with symmetry**

Total Deformation
Type: Total Deformation
Unit: mm
Time: 1 s
Max: 15.435
Min: 0
5/25/2023 2:08 PM



B: Load distribution model with symmetry

Pressure
Type: Pressure
Unit: MPa
Time: 1 s
Max: 6.0653
Min: 0
5/25/2023 2:15 PM

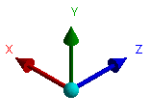
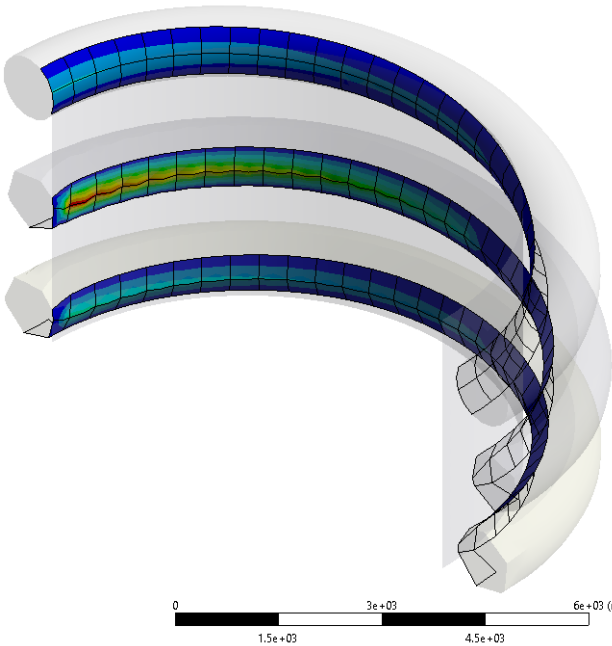
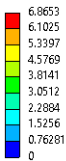


Fig. I-28: Simulation 5, pressure distribution on inner frame

B: Load distribution model with symmetry

Frictional Stress
Type: Frictional Stress
Unit: MPa
Time: 1 s
Max: 0.38868
Min: 0
5/25/2023 2:15 PM

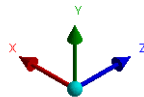
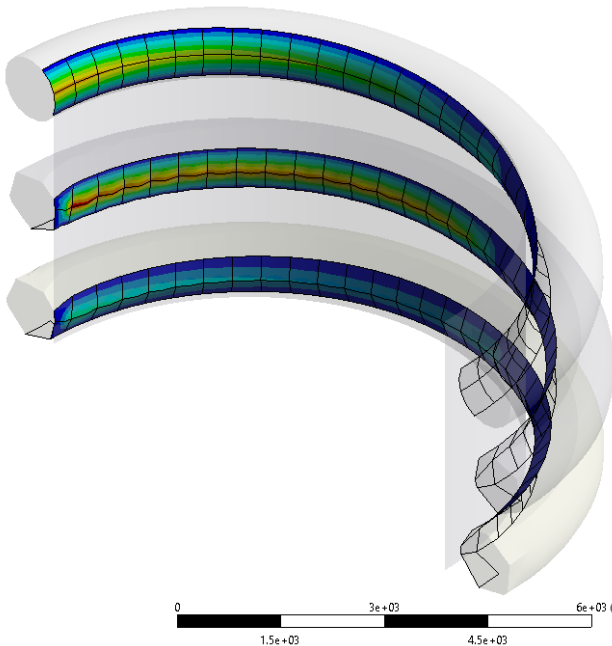
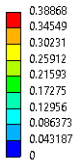


Fig. I-29: Simulation 5, friction distribution on inner frame

B: Load distribution model with symmetry

Pressure
Type: Pressure
Unit: MPa
Time: 1 s
Max: 2.925
Min: 0
5/25/2023 2:16 PM

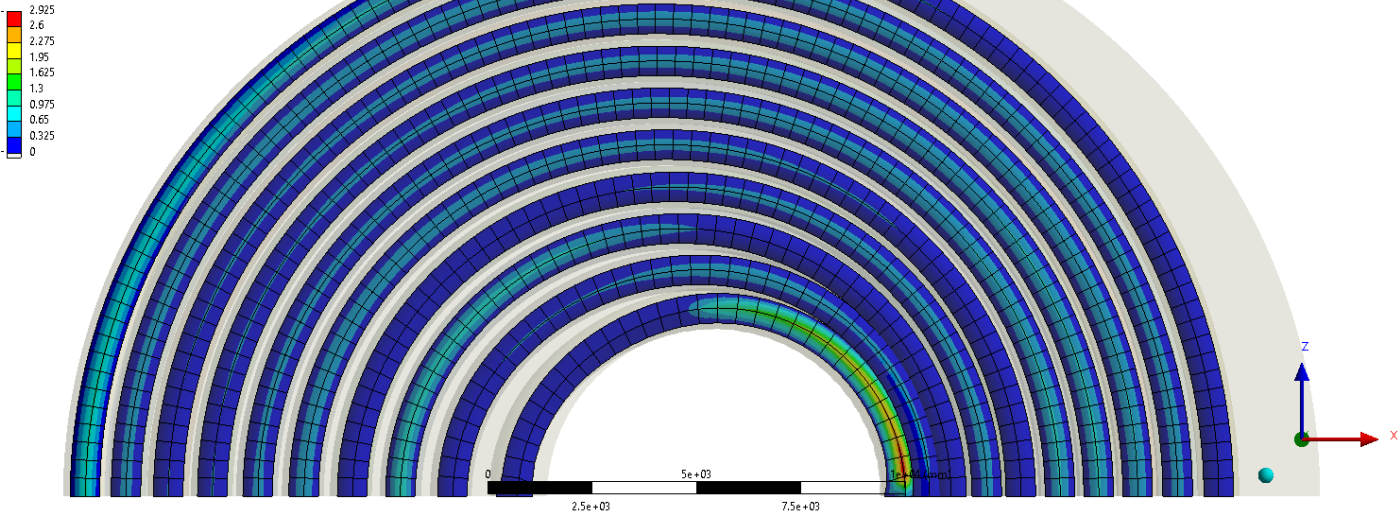


Fig. I-30: Simulation 5, pressure distribution on floor

B: Load distribution model with symmetry

Frictional Stress
Type: Frictional Stress
Unit: MPa
Time: 1 s
Max: 0.21155
Min: 0
5/25/2023 2:16 PM

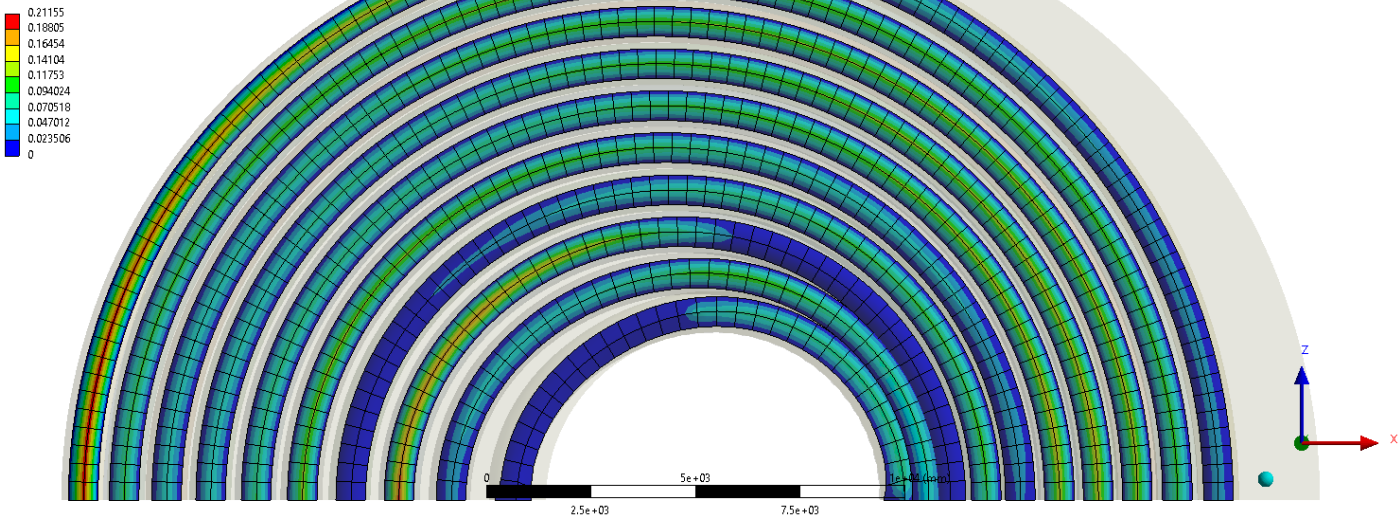


Fig. I-31: Simulation 5, friction distribution on floor

Simulation 6

B: Load distribution model with symmetry
Total Deformation
Type: Total Deformation
Unit: mm
Time: 1 s
Max: 20.348
Min: 0
5/25/2023 3:23 PM

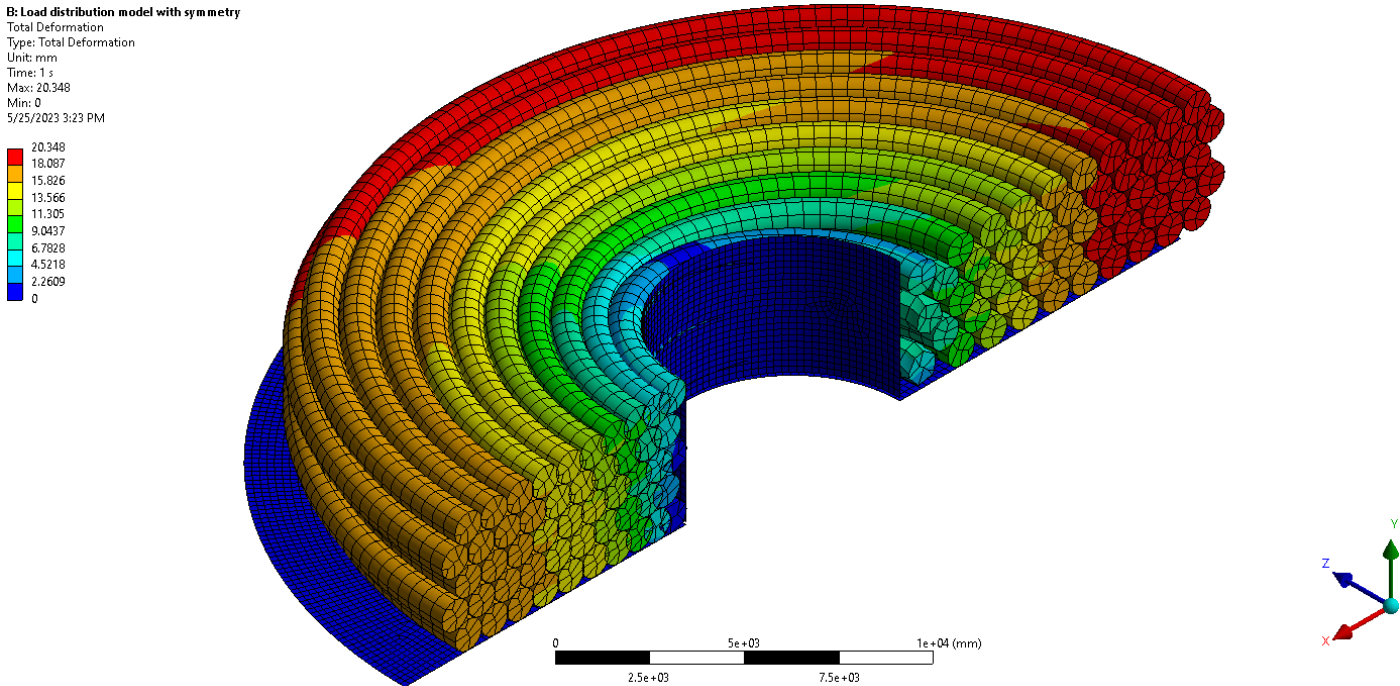


Fig. I-32: Simulation 6, deformation

B: Load distribution model with symmetry
Pressure
Type: Pressure
Unit: MPa
Time: 1 s
Max: 8.8238
Min: 0
5/25/2023 3:27 PM

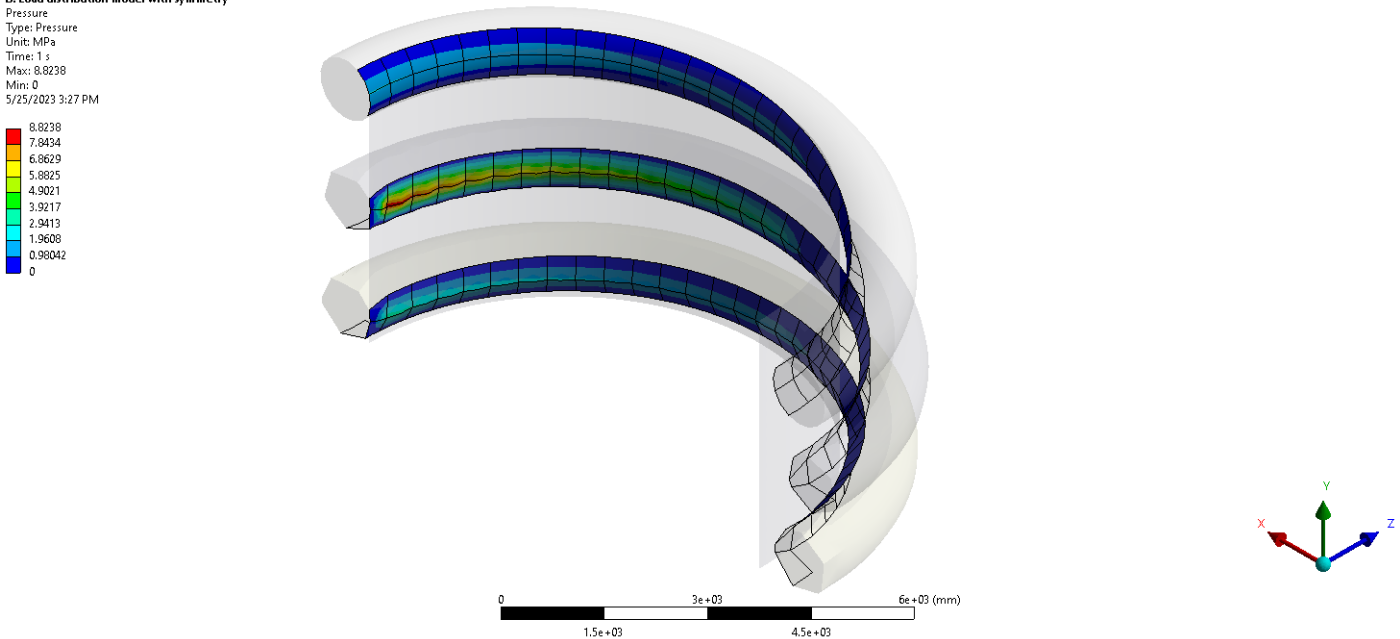


Fig. I-33: Simulation 6, pressure distribution on inner frame

B: Load distribution model with symmetry

Frictional Stress
Type: Frictional Stress
Unit: MPa
Time: 1 s
Max: 1.7648
Min: 0
5/25/2023 3:27 PM

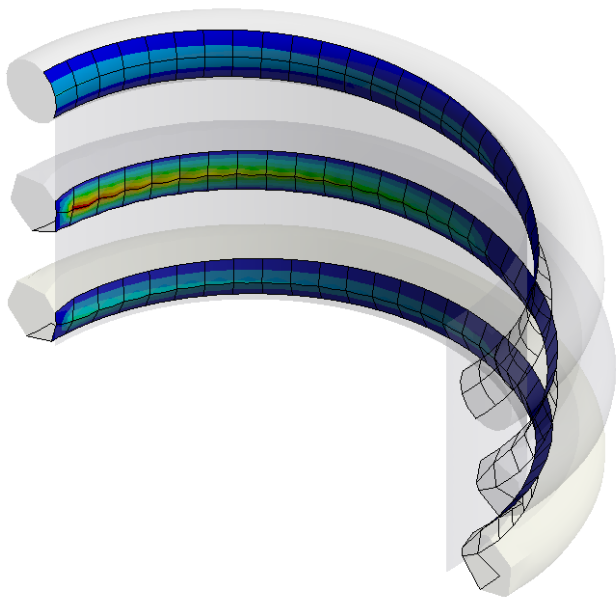
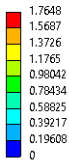


Fig. I-34: Simulation 6, friction distribution on inner frame

B: Load distribution model with symmetry

Pressure
Type: Pressure
Unit: MPa
Time: 1 s
Max: 3.4868
Min: 0
5/25/2023 3:26 PM

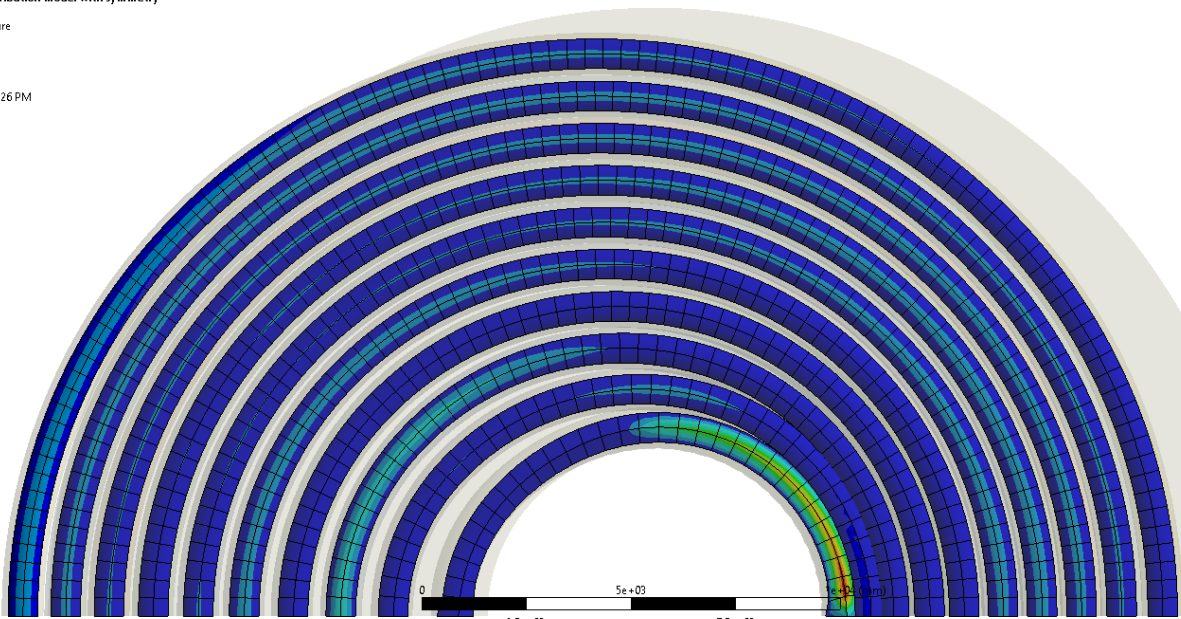
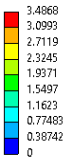


Fig. I-35: Simulation 6, pressure distribution on floor

B: Load distribution model with symmetry

Frictional Stress
Type: Frictional Stress
Unit: MPa
Time: 1 s
Max: 0.34868
Min: 0
5/25/2023 3:26 PM

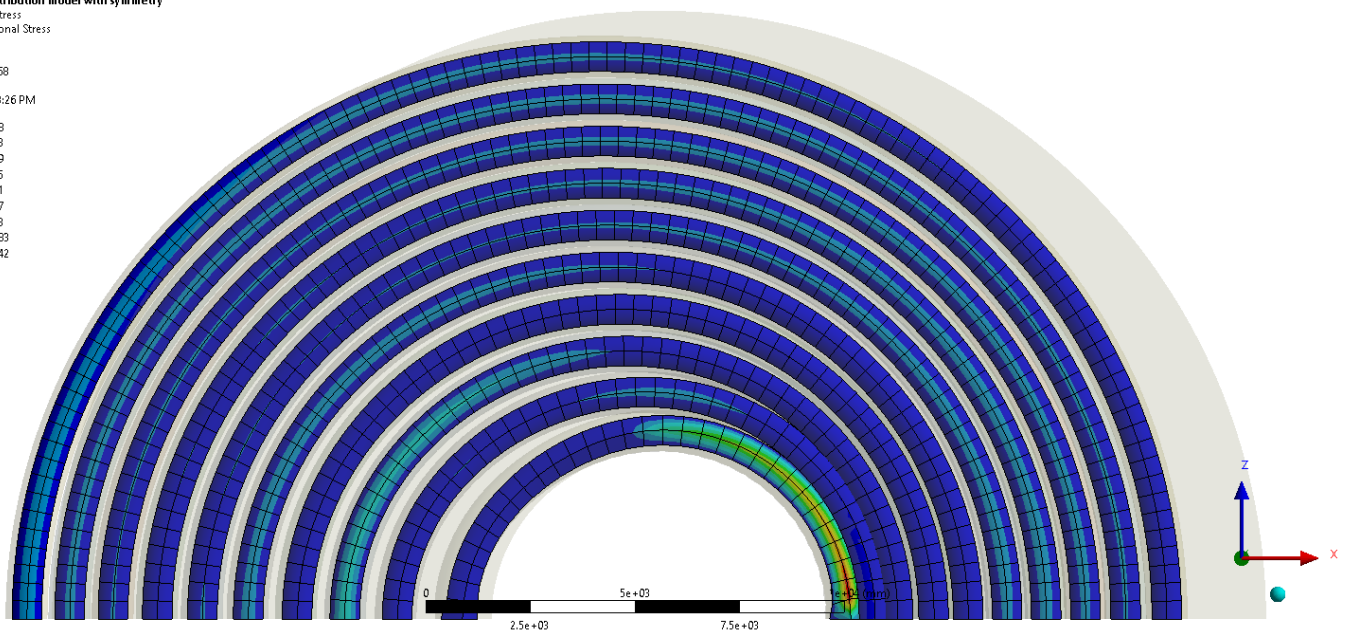
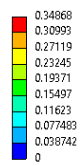


Fig. I-36: Simulation 6, friction distribution on floor